Charles University
Faculty of Science

Study programme: Physical Geography and Geoecology

RNDr. Tomáš Uxa

Past and Present Permafrost and Active-Layer Phenomena as Indicators of Late Quaternary Environmental Changes

Minulé a současné charakteristiky a formy vázané na permafrost a činnou vrstvu jako indikátory pozdně kvartérních změn přírodního prostředí

Doctoral dissertation

Supervisor: RNDr. Marek Křížek, Ph.D.

Praha 2020

I declare that I compiled this doctoral dissertation independently and that I properly cited all the utilized information sources and literature. Neither the thesis nor any of its substantial parts has not been submitted to obtain the same or other academic degree.

Prohlašuji, že jsem tuto disertační práci vypracoval samostatně a že jsem řádně citoval všechny použité informační zdroje a literaturu. Tato práce ani žádná její podstatná část nebyla předložena k získání stejného nebo jiného akademického titulu.

9 June 2020, Praha

Contents

Acknowledgements

First of all, I would like to express my sincere thanks to Dr. Marek Křížek who introduced me to periglacial geomorphology and awakened my passion for this discipline, spent an immeasurable amount of time accompanying me to the field, debating scientific problems, co-authoring publications, and supervising the thesis. Huge thanks also go to Dr. Jan Šafanda who took me under his wings at the Institute of Geophysics of the Czech Academy of Sciences, which gave me a chance to develop my career within an established scientific institution and finish the thesis. My gratitude also belongs to Mgr. Peter Mida, Dr. David Krause, and Dr. Filip Hrbáček for a large amount of time spent in the field or preparing joint publications, which also contributed substantially to my scientific as well as personal growth. However, thanks also go to other co-authors, Doc. Zbyněk Engel, Dr. Filip Hartvich, Dr. hab. Marek Kasprzak, Dr. Petr Tábořík, Dr. Adrzej Traczkyk, and Doc. Václav Treml, and many others who helped me in any way during my studies. Last but not least, I would also like to thank my family and my girlfriend for their constant support and endless patience.

The research was made possible thanks to the permissions of the Krkonoše National Park, the Jeseníky Protected Landscape Area, and the Tatra Mountains National Park administrations to conduct field work in strictly protected areas. The Czech Polar Research Infrastructure allowed investigations in present-day permafrost environments in terms of field work in the northern Billefjorden, Svalbard archipelago, and work with data obtained on James Ross Island, eastern Antarctic Peninsula region. Finally, the research would also not be possible without a direct financial support of the Charles University Grant Agency, projects GAUK 674512 and GAUK 1312214; the Czech Science Foundation, project GA17-21612S; and the Charles University, one-year specific academic research projects SVV 265212, SVV 267202, SVV 260078, SVV 260203, SVV 260307, and SVV 260438.

Poděkování

Nejdříve bych chtěl vyjádřit svůj upřímný dík Dr. Marku Křížkovi, který mě přivedl k periglaciální geomorfologii a probudil ve mně vášeň pro tuto vědní disciplínu, strávil se mnou nesmírné množství času v terénu, diskutováním nad vědeckými otázkami, přípravou společných publikací a vedením disertační práce. Velké poděkování patří rovněž Dr. Janu Šafandovi, který mě vzal pod svá křídla na Geofyzikálním ústavu AV ČR, čímž mi dal šanci rozvíjet kariéru v zázemí etablované vědecké instituce a dokončit disertační práci. Můj vděk náleží také Mgr. Peteru Midovi, Dr. Davidu Krausemu a Dr. Filipu Hrbáčkovi za velké množství času stráveného v terénu či přípravou společných publikací, což rovněž významně přispělo k mému vědeckému i osobnímu růstu. Dík však patří i dalším spoluautorům, Doc. Zbyňku Engelovi, Dr. Filipu Hartvichovi, Dr. hab. Marku Kasprzakovi, Dr. Petru Táboříkovi, Dr. Adrzeji Traczkykovi a Doc. Václavu Tremlovi, a mnoha dalším, kteří mi během studia jakkoli pomohli. V neposlední řadě bych také rád poděkoval své rodině a partnerce za jejich neutuchající podporu a nekonečnou trpělivost.

Výzkum byl umožněn díky povolení správ Krkonošského národního parku, Chráněné krajinné oblasti Jeseníky a Tatranského národného parku provádět terénní práce v přísně chráněných oblastech. Česká polární výzkumná infrastruktura umožnila výzkum v oblastech současného výskytu permafrostu v podobě terénních prací v severním Billefjordenu na souostroví Špicberky a práce s daty získanými na ostrově Jamese Rosse v regionu východního Antarktického poloostrova. Výzkum by rovněž nebylo možné uskutečnit bez přímé finanční podpory Grantové agentury Univerzity Karlovy, projektů GAUK 674512 a GAUK 1312214; Grantové agentury České republiky, projektu GA17-21612S; a Univerzity Karlovy, jednoletých projektů specifického vysokoškolského výzkumu SVV 265212, SVV 267202, SVV 260078, SVV 260203, SVV 260307 a SVV 260438.

Abstract

Late Quaternary has seen numerous major permafrost expansions and retreats associated with alternating glacial and interglacial periods as well as stadials and interstadials, the research of which is necessary to understand the past environmental evolution, but also provides useful analogues for its present-day and future behaviour. However, observations of permafrost and active-layer phenomena are still limited, and sometimes misleading, even in many present-day permafrost regions, and naturally less comprehensive evidence is available from areas where permafrost existed in the past.

The thesis provides comprehensive information on the distribution and morphology of mostly relict patterned ground and rock glaciers in the High Sudetes Mts. and in the Western and High Tatra Mts., respectively, which are the most widespread permafrost features that occur in these Central European mountain ranges situated north of the Alps. It shows that the landforms are closely related to increased severity of climates and/or sparser vegetation at higher elevations and as such they attest to the environmental conditions, which prevailed there towards the end of the Last Glacial Period to the early Holocene, but also to their current states. Similar elevation trends in the pattern morphology are also documented for active sorted patterned ground in the Svalbard archipelago. Nonetheless, these patterns may also have been forming throughout the Holocene and as such they are not in equilibrium with present-day climate conditions, also considering the excessively thick active layer caused by recent climate warming, which has occurred in most permafrost regions in the Northern Hemisphere. It thus calls for a broader use of the pattern morphology, established at the time of its initiation, in palaeo-environmental reconstructions. However, not all present-day permafrost regions are currently experiencing its degradation as observations from the Antarctic Peninsula region indicate that active layer has been cooling and thinning there in recent years.

Conclusively, the thesis provides insights into the past and present dynamics of the examined regions, which documents that permafrost and active-layer phenomena are valuable measures of Late Quaternary environmental changes, but it also has notable methodological and genetic implications as well as relevance to concepts of permafrost landscape evolution.

Keywords: permafrost, active layer, patterned ground, rock glacier, High Sudetes Mts., Western and High Tatra Mts., Svalbard archipelago, Antarctic Peninsula region, Late Quaternary

Abstrakt

V pozdním kvartéru došlo v důsledku střídání glaciálních a interglaciálních období i stadiálů a interstadiálů k četným rozšířením a ústupům permafrostu, jehož výzkum je nezbytný pro pochopení vývoje přírodního prostředí v minulosti, ale poskytuje cenné informace i z hlediska jeho současné a budoucí dynamiky. Pozorování charakteristik a forem vázaných na permafrost a činnou vrstvu jsou však stále nedostatečná a někdy také zavádějící i v mnoha oblastech se současným výskytem permafrostu a mnohem méně informací je k dispozici z regionů, kde se permafrost nacházel v minulosti.

Disertační práce poskytuje ucelené informace o rozšíření a morfologii převážně reliktních strukturních půd a kamenných ledovců ve Vysokých Sudetech a Západních a Vysokých Tatrách, jež jsou nejrozšířenějšími formami vázanými na permafrost, které se v těchto středoevropských pohořích severně od Alp vyskytují. Je ukázáno, že tyto tvary reliéfu mají těsnou vazbu na zvyšující se drsnost klimatických podmínek a ubývání vegetace směrem do vyšších nadmořských výšek a jako takové svědčí o přírodních podmínkách, které zde panovaly ke konci posledního glaciálu a na počátku holocénu, jakož i o jejich současném stavu. Obdobné výškové trendy v morfologii strukturních půd jsou dokumentovány také pro aktivní tříděné strukturní půdy na souostroví Špicberky. I tyto tvary se však mohly vyvíjet v průběhu celého holocénu a jako takové nejsou v rovnováze se současnými klimatickými podmínkami, i s ohledem na neúměrně mocnou činnou vrstvu způsobenou recentním oteplováním klimatu, k němuž došlo ve většině oblastí s výskytem permafrostu na severní polokouli. Z toho důvodu práce nabádá k širšímu využití morfologie strukturních půd, utvořené v období jejich vzniku, pro paleoenvironmentální rekonstrukce. Nicméně ne ve všech oblastech se současným výskytem permafrostu aktuálně dochází k jeho degradaci, jelikož pozorování z regionu Antarktického poloostrova indikují, že v posledních letech zde docházelo ke snižování teploty a mocnosti činné vrstvy.

Závěrem lze konstatovat, že disertační práce přispěla k lepšímu pochopení minulé i současné dynamiky zkoumaných oblastí, což ukazuje, že charakteristiky a formy vázané na permafrost a činnou vrstvu jsou cennými indikátory pozdně kvartérních změn přírodního prostředí. Výsledky však mají také značný metodický a genetický aspekt, jakož i význam pro obecné koncepty vývoje oblastí s výskytem permafrostu.

Klíčová slova: permafrost, činná vrstva, strukturní půdy, kamenný ledovec, Vysoké Sudety, Západní a Vysoké Tatry, Špicberky, Antarktický poloostrov, pozdní kvartér

List of publications included in the thesis

The thesis summarizes results of seven papers published in well-recognized international Web-of-Science-indexed journals that are attached as its Supplements.

Paper I	Křížek, M., Krause, D., **Uxa, T.**, Engel, Z., Treml, T., Traczyk, A. (2019). Patterned ground above the alpine timberline in the High Sudetes, Central Europe. *Journal of Maps*, 15(2), 563–569. https://doi.org/10.1080/17445647.2019.1636890 Author's contribution (10 %): data collection, manuscript and maps editing.
Paper II	Křížek, M., **Uxa, T.** (2013). Morphology, Sorting and Microclimates of Relict Sorted Polygons, Krkonoše Mountains, Czech Republic. *Permafrost and Periglacial Processes*, 24(4), 313–321. https://doi.org/10.1002/ppp.1789 Author's contribution (50 %): data collection, GIS and statistical analyses, interpretation of results, drawing of figures, and manuscript co-writing.
Paper III	**Uxa, T.**, Křížek, M., Krause, D., Hartvich, F., Tábořík, P., Kasprzak, M. (2019). Comment on 'Geophysical approach to the study of a periglacial blockfield in a mountain area (Ztracené kameny, Eastern Sudetes, Czech Republic)' by Stan *et al.* (2017). *Geomorphology*, 328(1 March 2019), 231–237. https://doi.org/10.1016/j.geomorph.2018.10.010 Author's contribution (30 %): data collection, extensive literature search, statistical analyses, (re)interpretation of results, drawing of a figure, manuscript writing, and correspondence with the journal.
Paper IV	**Uxa, T.**, Mida, P. (2017). Rock Glaciers in the Western and High Tatra Mountains, Western Carpathians. *Journal of Maps*, 13(2), 844–857. https://doi.org/10.1080/17445647.2017.1378136 Author's contribution (80 %): data collection, extensive literature search, GIS and statistical analyses, interpretation of results, drawing of figures, map compiling, manuscript writing, and correspondence with the journal.
Paper V	**Uxa, T.**, Mida, P., Křížek, M. (2017). Effect of Climate on Morphology and Development of Sorted Circles and Polygons. *Permafrost and Periglacial Processes*, 28(4), 663–674. https://doi.org/10.1002/ppp.1949 Author's contribution (70 %): data collection, sample analysis, extensive literature search, GIS and statistical analyses, interpretation of results, drawing of figures, manuscript writing, and correspondence with the journal.
Paper VI	**Uxa, T.** (2017). Discussion on 'Active Layer Thickness Prediction on the Western Antarctic Peninsula' by Wilhelm *et al.* (2015). *Permafrost and Periglacial Processes*, 28(2), 493–498. https://doi.org/10.1002/ppp.1888 Author's contribution (100 %).
Paper VII	Hrbáček, F., **Uxa, T.** (2020). The evolution of a near-surface ground thermal regime and modeled active-layer thickness on James Ross Island, Eastern Antarctic Peninsula, in 2006–2016. *Permafrost and Periglacial Processes*, 31(1), 141–155. https://doi.org/10.1002/ppp.2018 Author's contribution (50 %): measurements of ground thermal properties, active-layer thickness modelling, extensive literature search, interpretation of results, manuscript co-writing.

1 Introduction

The term *permafrost* refers to a layer of ground (soil, sediment, or rock and any incorporated materials, but excluding glacier ice, icings, or sea ice) at some depth beneath the surface, the temperature of which remains at or below 0 °C for at least two consecutive years (van Everdingen, 2005). This means that it is defined purely on the basis of temperature and as such it is essentially a physical state, which has no explicit material expression; moisture in the form of ice or water may or may not be present (Dobiński, 2011). Mostly, however, moisture occurs in various amounts and comprises its significant component that is responsible for its characteristic behaviour and processes related to water–ice transitions (French, 2017; Ballantyne, 2018). Grounds hosting permafrost have a negative energy balance that is broadly governed by climate and locally modulated by other factors, such as topography, ground physical properties, hydrology, snow cover, vegetation, or heat flux from the Earth's interior, the complex interactions of which control the surface and subsurface thermal regime and thus also the permafrost extent, thickness as well as temporal dynamics (Riseborough *et al.*, 2008; Burn, 2013).

Globally, it is estimated that permafrost underlies *ca.* 19.1–24.7 million km^2 (14–19 %) of the exposed land surfaces (that is, excluding regions covered by glaciers and perennial snow, or offshore areas) mainly in polar, sub-polar, and alpine regions of the Northern Hemisphere having markedly negative mean annual air temperature (MAAT) (Zhang *et al.*, 2008; Gruber, 2012; Obu *et al.*, 2019a,b,c). It extends almost continuously (>90 % areal coverage; Brown *et al.*, 1997) and reaches a depth of up to hundreds of meters to over one and a half kilometres in the coldest non-glacierized areas, such as in Canadian Arctic or Siberia (Figure 1), where MAAT is less than *ca.* −8 to −6 °C (Brown, 1960; Brown & Péwé, 1973; King, 1986), but even there it is normally absent at the ground surface as it is superimposed by up to several meters thick zone termed as the *active layer* where temperature seasonally rises above 0 °C and the thickness of which mainly depends on summer temperature conditions (Burn, 1998; Bonnaventure & Lamoureux, 2013). Generally, permafrost coverage and thickness tend to decline towards lower latitudes and lower elevations as the climate becomes milder, while the active layer tends to thicken until it eventually equals the freezing depth at the permafrost–seasonal frost boundary. However, the latter cannot be simply delineated by a single borderline because it is affected by a number of other regional- and local-scale variables. Instead, it is rather

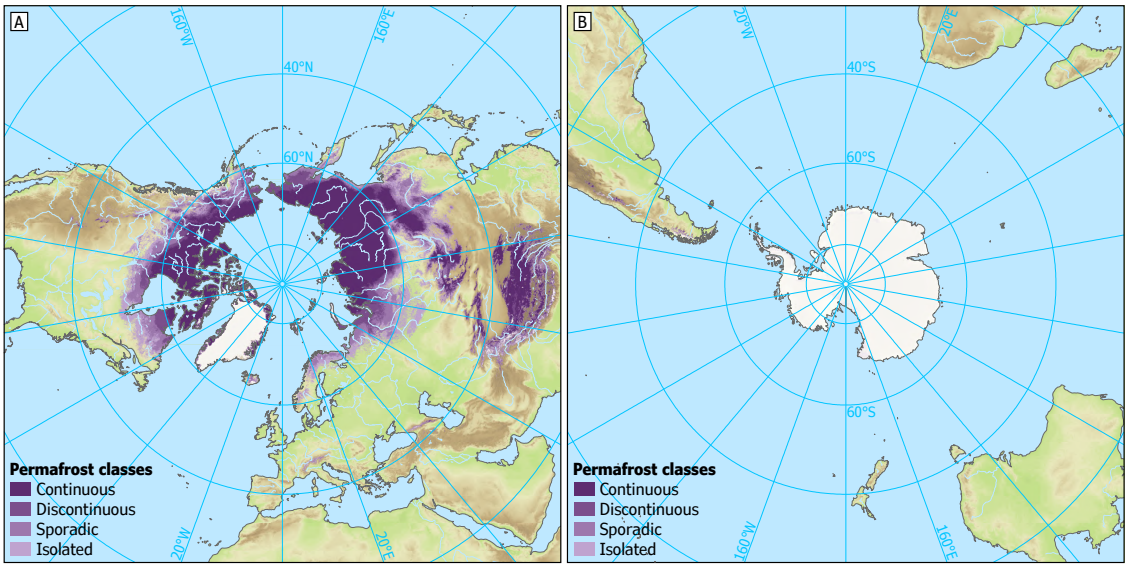

Figure 1. Present-day distribution of continuous (>90 % areal coverage), discontinuous (50–90 % areal coverage), sporadic (10–50 % areal coverage), and isolated permafrost (<10 % areal coverage) in the (A) Northern and (B) Southern Hemisphere based on Obu *et al.* (2019a,b,c). Note the contrast between the two hemispheres; even the most extensive permafrost occurrences in the Southern Hemisphere, situated in Antarctica and the Andes, are almost invisible in the hemispheric scale. Topography is based on the Global Multi-resolution Terrain Elevation Data 2010 dataset (Amatulli *et al.*, 2018) and global-scale shapefiles available at Natural Earth (https://www.naturalearthdata.com).

a transition area that spans over extensive regions underlain by discontinuous to sporadic permafrost (50–90 to 10–50 % areal coverage, respectively; Brown *et al.*, 1997), which is interspersed with seasonally frozen ground (Figure 1), and where MAAT commonly attains *ca.* −6 to −1 °C (Brown, 1960; Brown & Péwé, 1973; Péwé, 1983; King, 1986). Seasonally frozen ground mostly dominates in warmer locations because MAAT usually tends to be slightly lower than mean annual ground surface temperature due to the buffering effects of snow and vegetation (Smith & Riseborough, 2002), although some environmental settings, such as those of debris covers or long-lasting snow fields, may, under favourable circumstances, host isolated permafrost patches even under MAAT well above zero (e.g. Delaloye & Lambiel, 2005; Wicky & Hauck, 2017).

Nonetheless, permafrost is not invariable and everlasting, as its name might suggest, but in reality it is among the Earth system components that are most sensitive to climate forcings (Riseborough *et al.*, 2008; Burn, 2013). Indeed, the Quaternary has seen numerous major permafrost expansions and retreats associated with alternating glacial and interglacial periods as well as stadials and interstadials. For instance, it is estimated that the maximum permafrost extent of the Last Glacial Period (LGP) achieved up to *ca.* 40 % larger area than at present in the Northern Hemisphere (Figure 2) (Lindgren *et al.*, 2016). This so-called Last Permafrost Maximum (LPM) occurred under cold and dry climate conditions 25–17 ka (Vandenberghe *et al.*, 2014) and is thus believed to be slightly asynchronous with the period of maximum ice-sheet volume (Last Glacial Maximum [LGM]) taking place 26.5–19 ka (*sensu* Clark *et al.*, 2009). The last major permafrost expansion occurred in the Younger Dryas (12.9–11.7 ka), but then it degraded rapidly and has largely retreated to its current extent at the latest during the early Holocene (Vandenberghe, 2001). However, it is now dramatically declining in most present-day permafrost regions due to recent climate warming (Harris *et al.*, 2009; Romanovsky *et al.*, 2010; Biskaborn *et al.*, 2019).

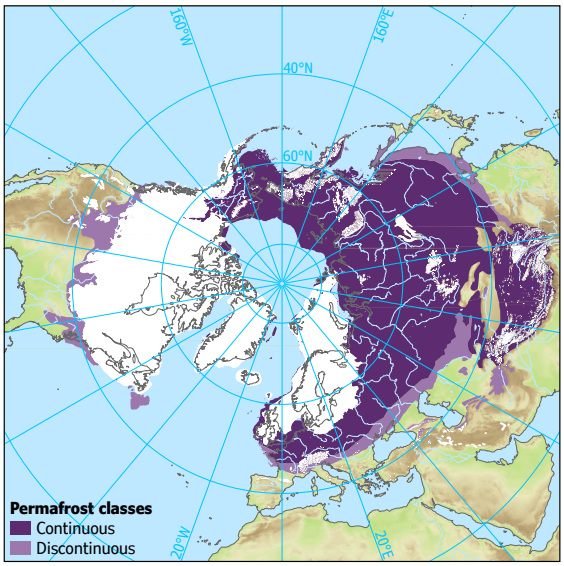

Figure 2. Maximum Last Glacial extent of continuous (>90 % areal coverage) and discontinuous permafrost (50–90 % areal coverage) and ice sheets in the Northern Hemisphere including the exposed sea shelves based on Lindgren *et al.* (2016) and Ehlers *et al.* (2011). Present-day topography is based on the Global Multi-resolution Terrain Elevation Data 2010 dataset (Amatulli *et al.*, 2018) and global-scale shapefiles available at Natural Earth (https://www.naturalearthdata.com).

1.1 Permafrost features

Seasonal and annual temperature variations within the uppermost permafrost and especially recurrent freezing and thawing of the active layer stimulate numerous thermally- and gravity-induced processes, mostly related to water–ice volume changes, that cause frost weathering, ground deformations, and/or mass displacements, which, if acting long enough, result in the development of a variety of distinctive landforms

and subsurface structures that are collectively termed as *permafrost features*. Some of them typically arise during periods of permafrost aggradation, while others develop at its steady states or during its degradation, and all this takes place within certain ranges of climate and environmental settings. During these phases, they also usually tend to change their morphology and/or internal structure to some extent as they respond to newly established conditions and as such they can signal various stages of permafrost evolution, which has important environmental and engineering implications for present-day permafrost regions. However, as many permafrost features can survive and retain some of their attributes long after the permafrost has disappeared, they also enable to reasonably infer its former extent and dynamics or the thickness of the active layer as well as to estimate the MAAT thresholds at the time of their formation, which is indispensable for reconstructions of climate and environmental history in past permafrost regions where other palaeo-records may frequently be poorly preserved (Washburn, 1980; Matsuoka, 2011; Ballantyne, 2018). Permafrost and active-layer phenomena can thus provide important insights into how the system is evolving (Bonnaventure & Lamoureux, 2013).

Some of the most common features in present-day permafrost regions are various kinds of *patterned ground* and *rock glaciers*, which, along with their distinctive surface morphology and frequently large dimensions, predetermines them to be among the best and most abundantly preserved features in former permafrost environments as well. As such, patterned ground and rock glaciers are well suited for exploring past and present permafrost extents and associated temperature conditions in lowlands and mountains having smooth slopes or in rugged terrains of high-alpine areas, respectively, where they usually occur (Barsch, 1996; Ballantyne, 2018).

1.1.1 Patterned ground

Patterned ground is a collective term for level or moderately sloping surfaces exhibiting strikingly regular patterning, typically in the form of decimetres to several meters wide circles, polygons, nets, labyrinths, stripes, or steps (Figure 3), which develop through mass displacements driven by recurrent freezing and thawing of the ground, and thus the patterns also extend a few centimetres to over a meter in depth, thereby building complex three-dimensional structures (Washburn, 1979; Warburton, 2013; Ballantyne, 2013, 2018). Most classifications distinguish between sorted patterns (Figure 3A, B, D, E), which are usually characterized by predominantly fine cells surrounded by raised or depressed stony borders, and non-sorted patterns (Figure 3C, F), which are defined by micro-topography and/or vegetation structures (Washburn, 1956; Ballantyne, 2013, 2018). Active sorted patterns having a diameter over 1–2 m are com-

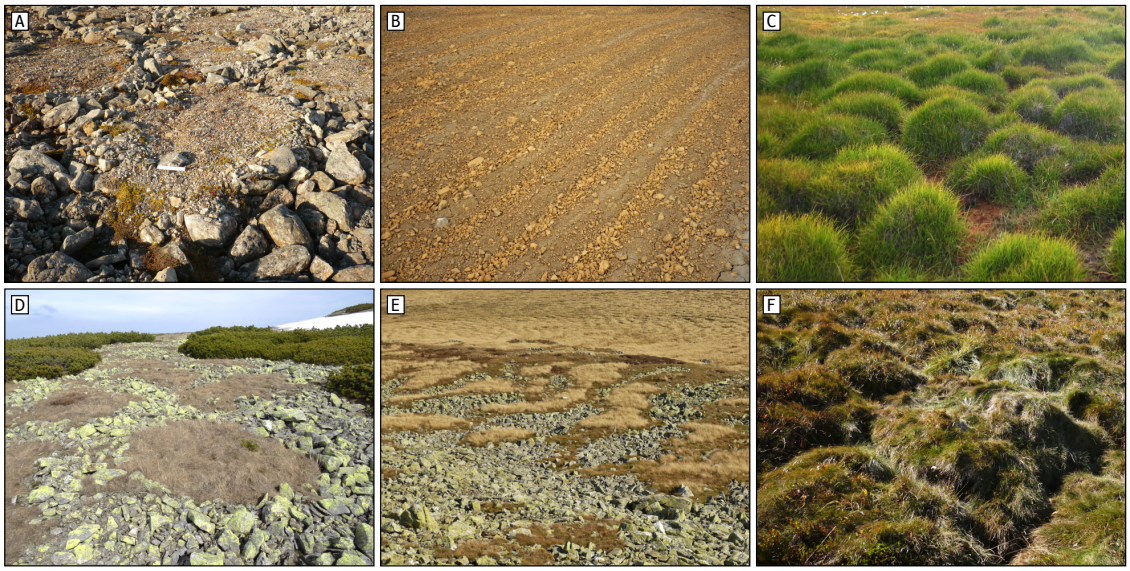

Figure 3. Active (A) sorted polygons, (B) sorted stripes, and (C) earth hummocks in the Svalbard archipelago and their (D, E) relict to (F) semi-active counterparts in the High Sudetes Mts.

monly associated with permafrost conditions and MAAT <−6 to −4 °C, while smaller patterns are mostly considered to form within seasonally frozen ground and under MAAT of *ca.* −2 to 5 °C (Goldthwait, 1976; Washburn, 1980; Grab, 2002; Ballantyne, 2018). Similarly, active non-sorted patterns also frequently develop in permafrost environments, but many of them probably do not necessarily require permafrost for their formation. Unfortunately, their MAAT thresholds are poorly known, but generally they occur where MAAT is less than *ca.* 3 to 5 °C (Grab, 2005; Ballantyne, 2013, 2018). Large-scale patterns, particularly those defined by boulders, can survive long after their activity has ceased (e.g. Winkler *et al.*, 2016, 2020), even under vegetation cover (occasionally including trees) and well-developed soil profiles (Figure 3D, E). On the other hand, small-scale patterns have limited preservation potential and usually perish rapidly (Ballantyne & Harris, 1994).

1.1.2 Rock glaciers

Rock glaciers are tens of meters to kilometres long tongue- or lobate-shaped landforms (Figure 4) resulting from downslope creeping of ice-rich debris masses that commonly form in high-alpine environments having MAAT <−2 °C (e.g. Barsch, 1996; Berthling, 2011; Kääb, 2013). Source material for their formation usually comes from above-situated talus slopes, producing so-called talus rock glaciers (Figure 4B, D) that do not substantially extend down to the valley bottoms, or from glacigenic materials, giving rise to so-called debris rock glaciers (Figure 4A) that form more extensive deposits on the valley floors (Barsch, 1996). Most rock glaciers exhibit characteristic surface morphology consisting of up to tens of meters high steep frontal and lateral slopes enclosing rugged upper surface with a sequence of longitudinal and/or transversal ridges and furrows (Figure 4A, C) that emerge due to the compression of the debris-ice mixture associated with the rock-glacier flow, closely resembling lava streams (Kääb, 2013). Given their mostly large dimensions and because the debris usually predominates, rock glaciers are able to retain much of their morphology long after

Figure 4. Active (A) debris (photo: Martin Frauenfelder / CC BY-SA 3.0) and (B) talus rock glaciers in the Alps and the Svalbard archipelago, respectively, and relict (C) debris–talus and (D) talus rockglaciers in the Western and High Tatra Mts.

the ground ice inside has completely thawed (Hughes *et al.*, 2003), and thus they can be frequently identified even in a relict state and under dense vegetation cover (e.g. Colucci *et al.*, 2016; Kellerer-Pirklbauer *et al.*, 2016). Active and inactive (collectively referred to as intact) rock glaciers represent important components of mountain cryosphere because they typically contain substantial volumes of ground ice and as such they act as long-term stores of water, even in arid or semi-arid regions (e.g. Brenning, 2005; Azócar & Brenning, 2010; Millar *et al.*, 2013). On the other hand, relict rock glaciers have no ground ice inside, but they indicate permafrost existence and MAAT <-2 °C in the past (e.g. Barsch, 1996; Kääb, 2013). Some rock glaciers may look superficially relict while containing isolated ground-ice patches, and these have been tentatively referred to as pseudo-relict rock glaciers (Kellerer-Pirklbauer, 2008), but the term has not yet been widely accepted (e.g. Kääb, 2013; Jones *et al.*, 2019), and thus the standard terminology, distinguishing between active and inactive ($\sim$intact) and relict rock glaciers (*sensu* Barsch, 1996), is used hereafter.

1.2 Motivation

Most present-day permafrost regions have experienced one of the globally fastest temperature rises over the past few decades (Harris *et al.*, 2009; Romanovsky *et al.*, 2010; Biskaborn *et al.*, 2019), which has triggered permafrost degradation and active-layer thickening over large areas, and it is expected to continue and affect wider areas in the near future (Chadburn *et al.*, 2017). As a result, this will also highly impact landscape and ecosystem dynamics, hydrological and biogeochemical cycling, and/or human infrastructure throughout permafrost regions (e.g. Ping *et al.*, 2015; Hjort *et al.*, 2018; Lafrenière & Lamoureux, 2019). Besides, carbon emissions released due to the permafrost decay are believed to further accelerate the warming through a positive feedback mechanism, which is likely to bring even more dramatic changes that may have globally significant repercussions (Schuur *et al.*, 2015). Notwithstanding the uncertainties in the current permafrost projections, it is assumed that its future areal losses under the most extreme climate-warming scenarios could reach the same order of magnitude as in the post-LPM period (cf. Lindgren *et al.*, 2016; Chadburn *et al.*, 2017). The Late Quaternary permafrost and climate evolution can thus be seen as an analogy to what is happening now in most present-day permafrost regions because of the climate warming and as such it can tell us what its consequences might be. Research of permafrost and active-layer phenomena is thus necessary to assess the Late Quaternary climate and landscape dynamics across both past and present-day permafrost regions, to forecast their future changes as well as to improve the adaptation strategies to counter the negative impacts of associated environmental adjustments. However, it is of the utmost importance for non-permafrost regions as well because many of the changes are likely to have global consequences.

Yet, despite considerable efforts, observations are still either lacking or limited, and sometimes misleading, even in many present-day permafrost regions, and naturally less comprehensive evidence is available from areas where permafrost existed in the past as numerous permafrost features have completely disappeared or have degraded so that they are difficult to identify at present. The latter situation is also partly due to hitherto imprecisely known controls on the development of many permafrost features (see Section 1.1), which is why numerous scientists have considered them to be poor indicators of any specific conditions, and it has hindered their more extensive research. Consequently, the information remains sketchy and far from conclusive in many aspects as local or regional permafrost and active-layer dynamics may substantially differ from those at continental or global scales.

It is true for many Central European, mostly past permafrost areas north of the Alps where the most momentous palaeo-permafrost and active-layer research has so far been done in lowlands using various wedge-like structures, cryoturbations, or pingo scars (e.g. Isarin, 1997; Huijzer & Vandenberghe, 1998; Czudek, 2005; Vandenberghe *et al.*, 2014; Lindgren *et al.*, 2016), while the investigations have been much less intense in uplands, such as in the High Sudetes Mts. or in the Western and High Tatra Mts. (e.g. Traczyk & Migoń, 2000; Křížek, 2007, 2016; Rączkowska, 2007; Krzemień & Kłapyta, 2017/2018), where local glaciations have particularly been explored (e.g. Engel, 1997; Křížek *et al.*, 2012; Engel *et al.*, 2014;

Zasadni & Kłapyta, 2014; Makos, 2015; Kłapyta & Zasadni, 2017/2018). Knowledge of the distribution and morphology of even the most common permafrost features, patterned ground and rock glaciers, respectively, has thus been far from exhaustive there, which is also partly because these mountain ranges stretch along the Czech–Polish and Slovak–Polish border, respectively, and hence they have long been studied separately on both sides, which has historical reasons as well. Besides, numerous information has been published in local, non-English journals and as such it has remained largely hidden to the international permafrost community. Definitely, more attention has been paid to present-day activity of seasonal-frost features in the High Sudetes Mts. (e.g. Sekyra & Sekyra, 1995; Křížek *et al.*, 2010; Křížek, 2016) and to potential present-day permafrost occurrences in the Western and High Tatra Mts. (e.g. Dobiński, 2005; Kędzia, 2015; Krzemień & Kłapyta, 2017/2018).

Similarly, most investigations in present-day permafrost regions, such as in the interior areas of the Svalbard archipelago or in the eastern Antarctic Peninsula region, have addressed particularly past (e.g. Svendsen & Mangerud, 1997; Landvik *et al.*, 1998; Ó Cofaigh *et al.*, 2014) and present-day (de)glaciation (e.g. Rachlewicz *et al.*, 2007; Małecki, 2016; Davies *et al.*, 2012; Engel *et al.*, 2012, 2018) and paraglacial response to it (e.g. Ewertowski & Tomczyk, 2015; Strzelecki *et al.*, 2017; Ruiz-Fernández *et al.*, 2019), while research of permafrost and active-layer phenomena has long been rather limited there, which is also due to their remoteness resulting in high financial and logistics costs (e.g. Humlum *et al.*, 2003; Juliussen *et al.*, 2010; Hrbáček *et al.*, 2019a). No detailed observations of patterned ground have thus been available from the central Spitsbergen, and have been completely absent from higher elevations throughout the Svalbard archipelago, while no analysis of the long-term active-layer behaviour and its drivers has been available from the eastern Antarctic Peninsula region (Hrbáček *et al.*, 2019a), but the information remains very limited from around the Peninsula as most monitoring sites were set up there after the International Polar Year 2007–2009 (Vieira *et al.*, 2010).

1.3 Objectives

The main objective of the thesis is thus to obtain new primary data on some of the poorly investigated permafrost and active-layer phenomena in mostly past permafrost landscapes of selected Central European mountain ranges situated north of the Alps as well as in present-day permafrost environments of the Svalbard archipelago and the Antarctic Peninsula region where most of the Czech permafrost and active-layer research has taken place in recent years. Specifically, research of mostly past permafrost landscapes is mainly oriented on the comprehensive cross-border mapping and analysis of the distribution and morphology of the most widespread permafrost features that occur there, that is, patterned ground and rock glaciers, and their interpretation in terms of past and potential present-day permafrost occurrences and associated temperature conditions (Paper I, Paper II, Paper III, and Paper IV). Research of present-day permafrost regions is mainly focused on the analysis of the distribution and morphology of patterned ground, their developmental rates, chronology, and relation to present-day environmental conditions, which have implications for reconstructions of past permafrost environments (Paper V). Also, it concentrates on the long-term monitoring and modelling of the thermal regime and thickness of the active layer, which is critical for assessing the regional contrasts of climate-change impacts on this important component of the cryosphere (Paper VI and Paper VII). Beside the new or amended information about the past and present permafrost and climate evolution in the study areas and putting it into broader research and/or regional contexts that complement the mosaic of existing knowledge, it also seeks to develop and/or implement novel observation procedures and methods as well as to bring new perspectives that increase the reputation of past and present permafrost and active-layer phenomena as indicators of Late Quaternary environmental changes.

2 Study areas

The research targeted past permafrost landscape of the High Sudetes Mts. (Paper I, Paper II, and Paper III) and a currently marginal permafrost area of the Western and High Tatra Mts. (Paper IV), Central Europe, as well as present-day permafrost environments of the northern Billefjorden, Svalbard archipelago (Paper V), and James Ross Island, eastern Antarctic Peninsula region (Paper VII), the environmental settings of which (Figure 5) are briefly described in this chapter. Despite Paper VI is localized on Amsler Island, western Antarctic Peninsula region (Figure 5E), its environmental setting is not specifically characterized here because it is basically a technical paper that demonstrates some common problems of active-layer and permafrost modelling through the reanalysis of another study. Collectively, these areas cover a wide range of climate conditions that form a transition between past and present permafrost environments.

Figure 5. Location of the study areas in the (A) Northern and (B) Southern Hemisphere, and their positions (orange rectangles) within the (C) Central Europe, (D) Svalbard archipelago, and (E) Antarctic Peninsula region. Global topography (A, B) is based on the Global Multi-resolution Terrain Elevation Data 2010 dataset (Amatulli *et al.*, 2018) and global-scale shapefiles available at Natural Earth (https://www.naturalearthdata.com). Regional maps are based on other data obtained from the (C) CGIAR Consortium for Spatial Information (http://srtm.csi.cgiar.org/srtmdata), (D) Norwegian Polar Institute (https://geodata.npolar.no), and (E) Antarctic Digital Database (https://www.add.scar.org).

2.1 High Sudetes Mts.

The High Sudetes Mts. consist of three isolated mountain ranges, the Krkonoše Mts., Králický Sněžník Mts., and the Hrubý Jeseník Mts., that are situated along the border of the Czech Republic and Poland (Figure 5C). They are characterized by extensive summit plateaus of low relief at *ca.* 1300–1450 m asl, with mostly gentle hills and saddles rising up to 100–150 m above, which are dissected by deep valleys.

Their highest summits are Mt. Sněžka (1603 m asl), Mt. Králický Sněžník (1424 m asl), and Mt. Praděd (1491 m asl), respectively. Geology mostly consists of Upper Proterozoic and Palaeozoic crystalline rocks that are covered by various Quaternary sediments (Chlupáč *et al.*, 2011). The mountains faced much colder climates during the Pleistocene glaciations, which gave rise to numerous permafrost features particularly on the summit plateaus (Traczyk & Migoń, 2000; Křížek, 2007, 2016), whereas up to several tens of valleys exhibit a glacier remodelling (Králík & Sekyra, 1969; Šebesta & Treml, 1976; Engel, 1997; Křížek *et al.*, 2012; Engel *et al.*, 2014). The last major glaciation phase took place during the LGM (Engel *et al.*, 2014) when the MAAT depression was estimated to be −10.3 to −6.7 °C as compared to the present (Heyman *et al.*, 2013), and glaciers receded intermittently until the Younger Dryas (Engel *et al.*, 2014). Most permafrost features are believed to have developed and/or been last active towards the end of the LGP (Traczyk & Migoń, 2000; Traczyk, 2004), but some seasonal-frost features are thought to have been active throughout the Holocene (Sekyra & Sekyra, 1995; Křížek, 2007; Křížek *et al.*, 2010). The MAAT was 1.2 °C at Mt. Sněžka in 1981–2010 (Migała *et al.*, 2016), but it has been increasing at an average rate of 0.023 °C a^{-1}. The mean annual precipitation (MAP) there was 1186 mm in 1961–2017 (Pińskwar *et al.*, 2019). However, it somewhat decreases to the east as continentality increases. Snow cover is commonly <1.5–2.0 m thick, though it can be only a few centimetres at wind-exposed sites to over 10 m at leeward locations (Harčarik, 2002; Janásková, 2006; Hejcman *et al.*, 2006). No present-day permafrost occurrences have been documented, but it existed there during the colder periods of the Quaternary (Kociánová, 2002; Czudek, 2005; Křížek, 2016). Spruce forests prevail below the tree line that is at *ca.* 1250–1300 m asl (Treml & Migoń, 2015). Higher elevations host alpine meadows with dwarf shrubs and sparse vegetation-free surfaces.

2.2 Western and High Tatra Mts.

The Western and High Tatra Mts. are *ca.* 42 and 26 km, respectively, long mountain ranges located in the northernmost area of the Carpathian arc and stretching longitudinally along the border of Slovakia and Poland (Figure 5C). They reach the maximum elevations of 2248 and 2655 m asl at the summit of Bystrá and Gerlachovský štít, respectively. Geology of the mountain ranges is dominated by Palaeozoic crystalline rocks that are overlaid by thrust sheets of Mesozoic sedimentary rocks on the northern sides. Valley slopes and floors are rich in Quaternary deposits (Nemčok *et al.*, 1994; Jurewicz, 2007). Glaciations recurrently occurred during the cold phases of the Pleistocene and resulted in typical alpine-type topography with numerous cirques, U-shaped valleys and distinct moraine ridges (e.g. Zasadni & Kłapyta, 2014; Makos, 2015; Kłapyta & Zasadni, 2017/2018). Glaciers reached their last maximum extent during the LGM when the MAAT reduction probably attained *ca.* −12 to −11 °C as compared to the present, then readvanced several times until the Younger Dryas, presumably experiencing the MAAT depression of *ca.* −7 to −6 °C, and finally disappeared at the Pleistocene–Holocene transition (Makos, 2015; Kłapyta & Zasadni, 2017/2018) when most rock glaciers probably developed as well (Kotarba, 2007; Zasadni *et al.*, 2020). Currently, the climatic snowline occurs at *ca.* 2500–2600 and 2700–2800 m asl on northern and southern slopes, respectively (Zasadni & Kłapyta, 2009), and the mountains host no glaciers; only perennial snowfields and firn-ice patches can be found at high-elevated and well-shaded locations (Gądek, 2014). The MAAT was −3.4 °C at Lomnický štít (2635 m asl) in 1981–2010 (Slovak Hydrometeorological Institute) and it has been increasing at an average rate of 0.023 °C a^{-1} since 1961 (Pribullová *et al.*, 2013). The MAP there amounted 1653 mm (Slovak Hydrometeorological Institute), but precipitation generally tends to decrease eastwards as air masses mainly come from the west (Niedźwiedź, 1992). Snow cover is normally <2–3 m thick at the highest elevations (Niedźwiedź, 1992), but high spatial variability occurs because of rugged terrain, which causes little snow on steep rock walls or wind-exposed surfaces, while much thicker, frequently avalanche-nourished accumulations develop at the foot of the slopes or in topographic depressions. Discontinuous permafrost has been estimated to occur above 1930±150–200 m asl (Dobiński, 1997, 2004, 2005), mostly within less irradiated blocky covers promoting internal air circulation (Gądek & Kędzia, 2008). The

thickness of permafrost and active layer is estimated at *ca.* 0.5–25 and 0.5–6 m, respectively (Dobiński *et al.*, 1996, 2008; Mościcki & Kędzia, 2001; Gądek & Grabiec, 2008). Vegetation mostly consists of spruce forests below the tree line that is situated at *ca.* 1550–1715 m asl (Plesník, 1971; Švajda *et al.*, 2011). The areas above it are dominated by alpine meadows and dwarf shrubs that are increasingly being replaced by vegetation-free surfaces towards higher elevations.

2.3 Northern Billefjorden

The northern Billefjorden is located in the central part of Spitsbergen, the largest island of the Svalbard archipelago (Figure 5D). Geology of the area mostly consists of Precambrian crystalline rocks and Palaeozoic sedimentary rocks that are extensively covered by various Quaternary deposits (Dallmann *et al.*, 2004). The region was largely covered by the Late Weichselian ice sheet (Landvik *et al.*, 1998), which started to recede 12.3 ka (Mangerud *et al.*, 1992). Local glaciers had retreated close to their present-day extent by the end of the Pleistocene (Baeten *et al.*, 2010) and further declined in the early and mid-Holocene, but readvanced again around 3 ka and particularly during the Little Ice Age (Landvik *et al.*, 1998), which terminated there in the early 20th century (Svendsen & Mangerud, 1997; Isaksson *et al.*, 2005). Since then, air temperatures have increased substantially, which has led to rapid glacier retreat (Rachlewicz *et al.*, 2007; Małecki, 2016). The MAAT was −5.1 °C near sea level at Svalbard Airport, 50–60 km to the south, in 1981–2010 (Nordli *et al.*, 2014), but the northern Billefjorden exhibits somewhat larger air temperature amplitudes and up to 1 °C lower MAAT based on local short-term studies (Rachlewicz & Styszyńska, 2007; Láska *et al.*, 2012). The MAP is estimated at *ca.* 200 mm (Hagen *et al.*, 1993). Snow cover is <0.30 m thick on ice-bound fjord and 0.6–1.2 m in valleys, but strong winds may locally produce much thicker snowdrifts (Strzelecki *et al.*, 2017). Continuous permafrost underlies extensive non-glacierized areas (Humlum *et al.*, 2003) and can be <100 m thick near coasts to >500 m in mountains (Liestøl, 1976). Active-layer thickness commonly reaches 0.30–1.60 m, and in diamictons occasionally up to 2.5 m (Gibas *et al.*, 2005; Rachlewicz & Szczuciński, 2008; Láska *et al.*, 2010). Active layer has been thickening at a rate of *ca.* 0.01–0.03 m a^{-1} since the 1990s in central Svalbard and it is expected to continue along with the climate warming (Etzelmüller *et al.*, 2011). Vegetation is limited and mostly occurs near sea level (Prach *et al.*, 2012).

2.4 James Ross Island

James Ross Island is the largest island in the northeastern coast of the Antarctic Peninsula (Figure 5E). Glaciers cover *ca.* 75 % of its *ca.* 2600 km^2, but only a few occur on its northernmost tip, the Ulu Peninsula, where >300 km^2 of land has been exposed since 12.9±1.2 ka (Nývlt *et al.*, 2014) that is one of the largest glacier-free areas within the region and most research activities on the island have thus been taking place there. Geology of the peninsula is dominated by Neogene volcanic rocks, which form flat-topped mesas, and Cretaceous sedimentary rocks in lowlands, which are covered by Neogene and Quaternary sediments of various origins (Mlčoch *et al.*, 2019). The MAAT was −7.0 °C at sea level near the Johann Gregor Mendel Station in 2005–2015, but it tended to decrease (Ambrožová & Láska, 2016) due to regional climate cooling that began around 2000 and replaced the major warming of the second half of 20th century (Turner *et al.*, 2016; Oliva *et al.*, 2017). The MAP is estimated at 300–500 mm of which most falls as snow that is largely redistributed by strong winds and commonly reaches <0.30–0.50 m on flat surfaces (Hrbáček *et al.*, 2016) and much thicker accumulations around topographic depressions or obstacles (Kňažková *et al.*, 2020). Glacier-free surfaces are underlain by continuous permafrost (Bockheim *et al.*, 2013), the thickness of which has been estimated to be *ca.* 3.4 m on coastal marine terraces to >67 m in lower-lying inland areas (Fukuda *et al.*, 1992; Borzotta & Trombotto, 2004). Active-layer thickness usually attains *ca.* 0.50–1.45 m (Borzotta & Trombotto, 2004; Hrbáček *et al.*, 2017, 2019a,b), but its temporal dynamics has been unknown. Vegetation is sparse and mostly concentrates in moist and nutrient-rich areas (Nývlt *et al.*, 2016).

3 Data and methods

Numerous methods were employed for data collection and analysis, of which most were done by the author himself to the extents indicated for individual publications (see List of publications included in the thesis). These included (*i*) terrain and/or remotely-sensed mapping of past and present sorted and non-sorted patterns as well as rock glaciers; (*ii*) determining their topographic attributes from digital elevation models; (*iii*) and measuring their surface as well as subsurface morphology and internal structure *in situ* or using aerial photographs and digital elevation models; (*iv*) collecting ground samples and determining their physical properties, such as texture, bulk density, moisture content, thermal conductivity, or volumetric heat capacity; (*v*) measuring air and ground temperatures; (*vi*) active-layer thickness modelling using analytical solutions; (*vii*) interpreting geophysical measurements; (*viii*) statistical analysis; (*ix*) extensive literature searching aimed at putting results into broader research and/or regional contexts; (*x*) and interpreting and synthesizing of results. The GIS works were done in ArcGIS 10 (Environmental Systems Research Institute), whereas the computations were mostly elaborated in STATISTICA 9 (StatSoft) and Mathcad 14 (Parametric Technology Corporation). Please note that all the data and methods used are detailed in the publications themselves (see Supplements) and are thus not thoroughly described here.

4 Overview of publications

This chapter provides a condensed summary of the key results and findings of the seven papers included in the thesis, which were all published in well-recognized international Web-of-Science-indexed journals, namely *Journal of Maps* (Paper I and Paper IV), *Permafrost and Periglacial Processes* (Paper II, Paper V, Paper VI, and Paper VII), and *Geomorphology* (Paper III).

4.1 Paper I

Křížek, M., Krause, D., **Uxa, T.**, Engel, Z., Treml, T., Traczyk, A. (2019). Patterned ground above the alpine timberline in the High Sudetes, Central Europe. *Journal of Maps*, 15(2), 563–569. https://doi.org/10.1080/17445647.2019.1636890

This paper presents the very first comprehensive cross-border map of mostly relict patterned ground in the sub-alpine belt of the Krkonoše Mts., Králický Sněžník Mts., and the Hrubý Jeseník Mts., Czech Republic and Poland (50°01′–50°47′ N, 15°30′–17°16′ E, 1260–1555 m asl), based on detailed field mapping aided by aerial-photography surveying mostly aimed at refining the delineated patterned-ground areas. The map depicts sorted polygons, sorted nets, sorted circles, sorted stripes, earth hummocks, peat hummocks, and non-sorted stripes, which are situated at elevations of *ca.* 1260–1555 m asl and cover a total area of 5.23 km^2 that accounts for 11.4 % of the entire mapped region.

Sorted patterns represent 94.6 % of the total patterned-ground area and, except for sorted circles, they occur in all the three mountain ranges. Most sorted polygons reside summit locations of the Krkonoše Mts. (90.4%), and thus they attain the highest elevations, of 1475–1550 m asl, of all the sorted patterns, but rest in rather level terrains commonly having 2–4° and comprise as low as 2.6 % of the total area of the sorted patterns. Sorted nets arise at somewhat lower elevations, of 1382–1462 m asl, and slightly less inclined surfaces, of 1–3°, but embody 37.6 % of the sorted patterns and tend to form large networks. Sorted stripes are the most common of the sorted patterns (59.8 %) and cover extensive areas that commonly border with those of the sorted polygons or nets, but they are situated at the same or lower elevations, of 1385–1457 m asl, and on steeper slopes, of 4–8°. Sorted circles show up only at two tiny patches at the Modré sedlo Saddle (1510 m asl) and Mt. Luční hora (1555 m asl), the Krkonoše Mts., and miniature patterns also arise occasionally at one spot at Mt. Keprník (1423 m asl), the Hrubý Jeseník Mts., but the latter features are constantly being damaged by tourists.

Non-sorted patterns constitute as little as 5.4 % of the total patterned-ground area and are unevenly distributed as well. Earth hummocks occur exclusively in the Hrubý Jeseník Mts., whereas peat hummocks

exist only in the Krkonoše Mts. They reside small sites characterised by gentle slopes and flats, of 4–7 and 0–2°, respectively, located at elevations of 1417–1461 and 1422–1433 m asl. Non-sorted stripes are the most widespread of the non-sorted patterns (69.2 %) and occur in both the Krkonoše Mts. and the Hrubý Jeseník Mts., but arise on steeper slopes, of 4–11°, and at slightly lower elevations, of 1376–1425 m asl, than the hummocks. No non-sorted patterns have been observed in the Králický Sněžník Mts.

Obviously, the most symmetrical sorted and non-sorted patterns, such as sorted polygons and circles or peat and earth hummocks, tend to be situated at higher elevations, whereas the least symmetrical features, such as sorted and non-sorted stripes, usually occupy lower elevations. It largely mirrors the distribution of slope inclinations within the region, but at the same time it indicates former existence of a typical mountain patterned-ground zonation there (cf. Harris, 1982; Niessen *et al.*, 1992; Hjort & Luoto, 2006; Feuillet *et al.*, 2012) as most of the patterns currently exhibit no or little activity (Křížek, 2007, 2016; Křížek *et al.*, 2010). The transitional gradient, at which the symmetrical patterns decline, whereas the elongated ones become dominant, is *ca.* 4–7°.

The map itself is a helpful requisite for successive detailed patterned-ground surveys and related research as well as other investigations taking place in the region. Besides, it may also serve as a training and/or validation dataset for statistical- or machine-learning-based landform distribution models. Finally, the map is an important basis for environmental planning and nature protection management inside the vulnerable ecosystems of the highest parts of the Krkonoše/Karkonosze Mts. National Parks and the Jeseníky Protected Landscape Area.

4.2 Paper II

Křížek, M., **Uxa, T.** (2013). Morphology, Sorting and Microclimates of Relict Sorted Polygons, Krkonoše Mountains, Czech Republic. *Permafrost and Periglacial Processes*, 24(4), 313–321. https://doi.org/10.1002/ppp.1789

This study details 62 relict large-scale sorted polygons located at Mt. Luční hora in the Krkonoše Mts., Czech Republic (50°43′40″ N, 15°40′57″ E, 1455–1555 m asl), using *in situ* observations, and investigates the influence of past microclimates on their morphology and degree of frost sorting.

The sorted polygons have an average length, width, and height of 1.94, 1.51, and 0.22 m, respectively, and are dominated by tabular clasts having an average *a*-axis size of 0.11 m at the borders and 0.05 m in the interiors. However, the patterns located at higher elevations have significantly smaller diameters and higher height-to-width ratios and are better sorted than the lower-elevated ones. Generally, larger sorted polygons tend to be formed by larger clasts, which probably controls the intra-site variations in the pattern diameters associated with natural heterogeneity in debris size, but it cannot explain their inter-site contrasts because the mean clast size is similar throughout the study area. Smaller diameters of the higher-elevated sorted polygons can be rather attributed to shallower freeze-thaw depth (∼active layer) at the time of their formation caused by lower air temperatures there. Snow cover was also thinner there due to windier conditions, which promoted more numerous freeze-thaw cycles of higher intensity that enhanced frost heaving and resulted in the higher height-to-width ratios of the sorted polygons at higher elevations. However, the latter was also likely related to lower moisture contents due to less snow and intense wind action (*sensu* Van Vliet-Lanoë, 1991).

Smaller sorted polygons and those having higher height-to-width ratios also tend to be better sorted. Besides the contrasting microclimates that still exist today, this is because the distances for clasts to move to the pattern borders are shorter within smaller polygons, and thus the clast movements in them can also be smaller to achieve the same degree of sorting as larger polygons. Likewise, patterns with higher height-to-width ratios have steeper surfaces where the gravity-induced processes, such as frost or needle-ice creep, can accelerate the clast displacements towards the pattern borders (Ballantyne, 1996; Kling, 1997; Matsuoka *et al.*, 2003). Also, it is hypothesized that sorting steadily increases the frost susceptibility of the polygon centres, which in turn intensifies the freeze-thaw processes there and hence further enhances the sorting. Consequently, the pattern development probably involves a positive feedback mechanism between

morphology and frost susceptibility that is driven by microclimates.

The study showed that large-scale sorted polygons are highly sensitive to fine-scale variations in environmental conditions and that these contrasts can be deduced even from the Last Glacial features, which indicates a high palaeo-environmental potential of relict sorted patterns located in flat or convex terrains. Also, it designed a scheme for evaluating their sorting that allows clast measurements using traditional or modern methods (such as terrestrial photogrammetry), modifications of the sampling strategy as well as repetitive surveys within individual sorted patterns and as such it can be easily adapted to be used elsewhere.

4.3 Paper III

Uxa, T., Křížek, M., Krause, D., Hartvich, F., Tábořík, P., Kasprzak, M. (2019). Comment on 'Geophysical approach to the study of a periglacial blockfield in a mountain area (Ztracené kameny, Eastern Sudetes, Czech Republic)' by Stan *et al.* (2017). *Geomorphology*, 328(1 March 2019), 231–237. https://doi.org/10.1016/j.geomorph.2018.10.010

This paper rebuts present-day permafrost existence in the Hrubý Jeseník Mts., Czech Republic, which was suggested by Stan *et al.* (2017) who investigated the internal structure of two blockfields at the Ztracené kameny site (50°00′58″ N, 17°10′29″ E, 1250 m asl) using electrical resistivity tomography and seismic refraction tomography, and interpreted two isolated high-resistivity (>80–100 kΩ m) and high-P-wave-velocity (<2000–3000 m s^{-1}) zones situated in lower-lying sections of the blockfields as permafrost patches that were moreover thought to be of the Pleistocene age. However, this interpretation is of doubtful validity because it mainly relies on ambiguous geophysical data alone that are poorly supported by other and mostly dubious evidence.

The maximum resistivity of the alleged permafrost spots attains or even exceeds the highest values documented for mid-latitude, low-elevation permafrost sites that usually ranged between 5–50 kΩ m and <100 kΩ m (e.g. Kneisel *et al.*, 2000; Delaloye *et al.*, 2003; Stiegler *et al.*, 2014; Popescu *et al.*, 2017); and as such resembles rather massive ice (*sensu* Hauck & Vonder Mühll, 2003). Nonetheless, the latter can hardly occur there because the amount of ground ice tends to be limited in these permafrost-hostile environments situated well below the lower regional permafrost limits. Consistent with that, the maximum P-wave velocity is lower or at the bottom of the range of *ca.* 2000–3500 m s^{-1} commonly associated with mid-latitude, low-elevation permafrost patches (e.g. Kneisel *et al.*, 2000; Gude *et al.*, 2003), and most velocity values rather comply with air-filled layers that usually achieved *ca.* 350–1500 m s^{-1} elsewhere (e.g. Kneisel *et al.*, 2000; Gude *et al.*, 2003; Draebing, 2016). Since the blockfields are dominated by quartz-rich quartzites, which can show resistivity values of up to 10^9 Ω m (Kneisel & Hauck, 2008) and pure quartz even well above 10^{10} Ω m (e.g. Parkhomenko, 1967; Telford *et al.*, 1990), our alternate hypothesis is that the maximum resistivity and P-wave velocity likely relates to the occurrences of solid quartzite bedrock, larger quartzite boulders, quartz veins traversing the blockfields, or locally increased quartz content, which, in combination with air-filled voids, produces geophysical images mimicking permafrost conditions.

Numerous evidence suggests that the latter interpretation should be favoured. So above all, the MAAT there is estimated to be *ca.* 2.9–4.9 °C and the mean near-subsurface temperatures recorded directly at the alleged permafrost spots between 25 May 2017 and 18 May 2018 were as high as 5.3 and 4.8 °C. Besides, the ground temperatures had reached their minima of −7.1 and −7.5 °C before snow cover established at the turn of November–December and then mostly remained above −2 °C throughout the winter. Notwithstanding that, the blockfields have a limited insulation because snow tends to be not thick enough to cover them continuously and usually completely disappears as early as in March–April and then the ground temperatures rise sharply. Symptomatic of rather warm and dry conditions is also the absence of mosses and cryophilic plants, which frequently colonize most mid-latitude, low-elevation permafrost sites (e.g. Delaloye *et al.*, 2003; Gude *et al.*, 2003; Zacharda *et al.*, 2007; Stiegler *et al.*, 2014; Popescu *et al.*, 2017). Lastly, the blockfields have rather low elevation extent of *ca.* 20–65 m, are relatively shallow, of *ca.* <8–12 m, and have straight slopes with no distinct concavities around the alleged permafrost spots, which reduces the potential for internal air circulation and the formation of cold reservoirs in their lower

sections (*sensu* Delaloye *et al.*, 2003; Delaloye & Lambiel, 2005; Morard *et al.*, 2008, 2010; Popescu *et al.*, 2017). Consequently, it is highly improbable that the blockfields contain permafrost under their current environmental settings. Also, the alleged ground-ice patches could hardly be termed as remnants of the Pleistocene permafrost even if actually present because such shallow and tiny permafrost bodies would be impacted by seasonal and interannual air temperature variations, and thus they would have to exist in equilibrium with contemporary climate conditions otherwise they would disappear. True relict permafrost reflects a colder climate in the past and is usually situated tens to hundreds of meters beneath the ground surface where it persists until positive temperatures propagate into its depth level.

Finally, it should be added that geophysics only estimates the subsurface distribution of ground physical properties, and other non-geophysical inputs are thus necessary to support its interpretation. Otherwise, it is almost impossible (Schrott & Sass, 2008).

4.4 Paper IV

Uxa, T., Mida, P. (2017). Rock Glaciers in the Western and High Tatra Mountains, Western Carpathians. *Journal of Maps*, 13(2), 844–857. https://doi.org/10.1080/17445647.2017.1378136

This paper introduces the very first detailed cross-border map of rock glaciers in the Western and High Tatra Mts., Slovakia and Poland (49°06′–49°17′ N, 19°39′–20°15′ E, 1375–2250 m asl), produced through a remotely sensed mapping mostly based on aerial photographs, validated by field checks and previously published reports. The map contains a total of 383 rock glaciers covering a total area of 13.84 km^2, which are supplied by rock material from 51.81 km^2 of their contributing areas. A total rock-glacier-related area thus constitutes 65.65 km^2, which comprises *ca.* 16 % of the area above 1375 m asl where the rock glaciers have their lower limit.

The Western Tatra Mts. host fewer rock glaciers, 183 (*ca.* 48 %), than the High Tatra Mts. where 200 rock glaciers (*ca.* 52 %) were mapped. However, the total rock-glacier area is 0.45 km^2 larger in the Western Tatra Mts., while the total contributing area is 2.60 km^2 more extensive in the High Tatra Mts. Talus rock glaciers predominate in both mountain ranges, with *ca.* 63 and 74 % in the Western Tatra and High Tatra Mts., respectively, but their total area represents only *ca.* 25 and 42 % of all the rock glaciers because debris rock glaciers are substantially larger. The latter also have more extensive contributing areas, which are necessary to supply their voluminous bodies with a sufficient amount of material.

Since both mountain ranges are dominated by granitic rocks, *ca.* 65 and 96 % of the rock glaciers, having a total area of 4.84 and 6.46 km^2, are formed within these substrates in the Western and High Tatra Mts., respectively. More diverse geology of the Western Tatra Mts. gives rise to *ca.* 27 % of rock glaciers (2.00 km^2) consisting of Palaeozoic metamorphic rocks (particularly gneisses and migmatites) and *ca.* 8 % (0.31 km^2) developed within Mesozoic limestones, dolomites, sandstones, shales and quartzites. On the other hand, only 1 and 3 % of the rock glaciers (0.07 and 0.17 km^2) are formed by these materials in the High Tatra Mts. Notably, the Mesozoic limestones, dolomites, sandstones, shales and quartzites host the smallest rock glaciers having the lowest density and specific area in both mountain ranges, which suggests that these substrates are the least favourable for the rock-glacier formation there.

Most rock glaciers are considered as relict; only *ca.* 4 and 25 % are classified as intact in the Western and High Tatra Mts., respectively, comprising a total area of 1.34 km^2. Relict rock glaciers have their average front elevation at 1644±119 and 1731±143 m asl in the Western and High Tatra Mts., respectively, whereas it is at 1812±30 and 2011±92 m asl for the intact ones. However, their lower limits are higher in southern aspects than in northerly exposed places. Intact rock glaciers are mostly smaller landforms of talus type, with *ca.* 86 and 78 % in the Western and High Tatra Mts., respectively, that tend to concentrate in well-shaded cirque locations. Collectively for both mountain ranges, their front elevation is at 1986±109 m asl, which is on average 56 m above the previously proposed average lower discontinuous permafrost boundary of 1930±150–200 m asl based on air temperature data (Dobiński, 1997, 2004, 2005). Given the lowermost relict rock glaciers descend to *ca.* 1400 m asl, the lower boundary of discontinuous permafrost at the

time of their development, presumably taking place at the Pleistocene–Holocene transition (Kotarba, 2007; Zasadni *et al.*, 2020), probably extended to this level, provided that the rock glaciers could have fully developed. Since rock glaciers typically form under the MAAT of <−2 °C (Barsch, 1996), while its present-day value is estimated to be 3.4 °C at this elevation, it suggests that the MAAT decline was at least −5.4 °C. The rock-glacier fronts occur on average *ca.* 400–600 and 100–250 m lower than in the Alps and the Southern Carpathians, respectively, which can be attributed to less precipitation towards the east (*sensu* Onaca *et al.*, 2017), causing thinner snow cover during winter and thus lower ground temperatures (*sensu* Gruber & Haeberli, 2009), as well as to latitudinal temperature decrease (*sensu* Dobiński, 2005).

The map is the most comprehensive rock-glacier inventory for the whole area of the Western and High Tatra Mts. published so far and as such it complements surveys from other European high-alpine regions, such as the Alps, the Pyrenees, the Scandinavian Mts., or the Southern Carpathians, where rock glaciers have been extensively mapped much earlier. However, it must be stressed that the deduced permafrost limits should be understood as tentative because rock glaciers provide a first-order evaluation of potential permafrost distribution, which generally tends to overestimate permafrost extent at places without debris cover. The study is thus rather a starting point for more thorough analyses of rock-glacier distribution, morphology, or chronology as well as modelling of permafrost extents, which can substantially improve the understanding of past and present environmental conditions in the Western and High Tatra Mts. Lastly, the map can be utilized as a basis for environmental planning and nature protection management in the Tatra National Parks.

4.5 Paper V

Uxa, T., Mida, P., Křížek, M. (2017). Effect of Climate on Morphology and Development of Sorted Circles and Polygons. *Permafrost and Periglacial Processes*, 28(4), 663–674. https://doi.org/10.1002/ppp.1949

This paper explores 290 large-scale active sorted circles and polygons located at 16 sites around the Petuniabukta and Adolfbukta bays in the northernmost Billefjorden, central Spitsbergen, Svalbard archipelago (78°40′–78°44′ N, 16°16′–16°56′ E, 28–773 m asl), using *in situ* observations, and investigates their relation to elevation and hypothesizes about their developmental rates, chronology as well as relation to present-day environmental conditions.

Overall, the sorted circles and polygons have a median length, width, and height of 1.80, 1.40, and 0.15 m, respectively, but they occur in two distinct elevation zones, on raised marine and kame terraces below *ca.* 200–250 m asl and on adjacent flat mountain tops and ridges above *ca.* 600 m asl, which are separated by steep pebbly-bouldery talus slopes that are highly unfavourable for any sorted patterns. The higher-elevated patterns have smaller diameters and shallower sorting depths due to thinner freeze-thaw depth (∼active layer) there. On the other hand, their heights and height-to-width ratios are larger probably because of more intense freeze-thaw cycling and better drainage there, which promotes more pronounced up-heaving of the pattern centres than at lower elevations (*sensu* Van Vliet-Lanoë, 1991). Besides, the diameter-to-sorting depth ratios have a median value of 3.57, which is consistent with theoretical models of patterned-ground formation involving circulation mechanisms that suggested values of *ca.* 3.1–3.8 (Ray *et al.*, 1983; Gleason *et al.*, 1986; Hallet & Prestrud, 1986; Peterson & Krantz, 2008) as well as with previous reports for active sorted patterns from elsewhere that showed a median of 3.54. The latter suggests that surface morphology of the patterns allows estimation of the sorting depth, which in turn can be used to reconstruct the former freeze-thaw depths and thus also the temperature conditions associated with relict patterns. Also, literature survey shows that elevation trends in the pattern diameters are opposite in permafrost and seasonally frozen regions, which can be used to distinguish between these contrasting ground thermal states at the time when the patterns developed.

Given the area was largely ice- or at least snow-covered during the LGM (Landvik *et al.*, 1998), the upper age limit of sorted patterns at most sites is probably the Pleistocene–Holocene transition. But since the marine and kame terraces hosting the patterns formed no later than *ca.* 8.7 cal. ka BP (Long *et al.*, 2012),

the sorted circles and polygons have probably been forming throughout most of the Holocene. Notably, large-scale sorted circles and polygons are totally absent inside the Little Ice Age glacier limit despite having favourable conditions and over a century to develop there; only miniature and poorly developed sorted circles rarely occur in these locations. Sorted patterns may thus develop over centennial timescales in this high-Arctic environment that is dominated by a strong seasonal cycle with weak diurnal variations and fewer freeze–thaw cycles, which agrees with present-day movement rates observed for several sorted patterns elsewhere in the Svalbard archipelago (Hallet & Prestrud, 1986; Hallet, 1998; Kääb *et al.*, 2014). This is an order of magnitude longer than for small-scale patterns located in mid-latitude alpine climates (cf. Ballantyne & Matthews, 1982; Haugland, 2006; Feuillet & Mercier, 2012) that themselves form faster owing to their smaller dimensions (*sensu* Paper II), but their sorting is further accelerated by well-developed seasonal and diurnal temperature variations and numerous freeze–thaw cycles.

Finally, the sorted circles and polygons are probably not in equilibrium with current climate conditions because permafrost table occurs well below their sorting depth, which also favours their non-recent origin. On the other hand, it raises questions about the significance of sorted patterns located in present-day permafrost environments under a changing climate.

4.6 Paper VI

Uxa, T. (2017). Discussion on 'Active Layer Thickness Prediction on the Western Antarctic Peninsula' by Wilhelm *et al.* (2015). *Permafrost and Periglacial Processes*, 28(2), 493–498. https://doi.org/10.1002/ppp.1888

This paper responds to the study of Wilhelm *et al.* (2015) who modelled active-layer thickness of 4.7–8.7 m in soils and unconsolidated materials and 11.9–18.6 m in bedrock on Amsler Island, western Antarctic Peninsula region (64°45′48″ S, 64°04′20″ W, 16–67 m asl), using the Stefan (1891) and Kudryavtsev (Kudryavtsev *et al.*, 1977) models, and attributed it to regional climate warming that reached unprecedented rates in the second half of the 20th century and culminated in the late 1990s (Turner *et al.*, 2016; Oliva *et al.*, 2017). Nonetheless, these extremely thick active layers seem to be doubtful as they were mostly not validated against any ground temperature records and, additionally, far exceeded the maximum values of *ca.* 1–2 and 2–6 m, respectively, which have been reported elsewhere in the region (Vieira *et al.*, 2010; Bockheim *et al.*, 2013; Hrbáček *et al.*, 2019b).

Recalculations of the active-layer thickness using the same models and inputs most closely matched the values modelled by Wilhelm *et al.* (2015) when the unfrozen water contents were set close to or equal to the total water contents, that is, when little or no water in the active layer was assumed to undergo phase changes. Under these conditions, the active layer was on average 4.6–8.9 m thick in soils and unconsolidated materials and 10.1–16.5 m in bedrock, which was −0.1 to 0.2 m (−2.1 to 2.3 %) and −2.1 to −1.8 m (−15.1 to −11.3 %), respectively, as compared to the estimates of Wilhelm *et al.* (2015). However, this assumption is far from reality at the non-bedrock sites as these have non-zero water contents, sand or silty sand textures, and winter ground temperatures well below 0 °C. Most of the water in the active layer thus probably experiences phase changes there, which is documented by the presence of zero-curtain periods, that is, isothermal conditions associated with the release or absorption of latent heat during freezing or thawing, respectively. Scenarios that assumed all the water is involved in phase changes showed substantially smaller active-layer thickness of 1.0–2.5 m in soils and unconsolidated materials, which was −6.2 to −3.7 m (−78.7 to −71.3 %) as compared to Wilhelm *et al.* (2015). Definitely, this is much more realistic estimate as it is mostly within the range of values published from other parts of the Antarctic Peninsula region (cf. Vieira *et al.*, 2010; Bockheim *et al.*, 2013; Hrbáček *et al.*, 2019b).

Conclusively, the active-layer thickness modelled by Wilhelm *et al.* (2015) is significantly overestimated because it represents its upper limit that incorrectly assumes little or no latent heat is absorbed during thawing. Hence, it should not be accepted by the scientific community until it is thoroughly revised as it seriously misrepresents the climate state of the region that is among the most important climate change hotspots. Unfortunately, Wilhelm & Bockheim (2017) did not clarify most of the issues in their reply.

Besides, at the time they were undoubtedly aware of their erroneous calculations, they submitted a revised version of an analogous paper that overestimated the active-layer thickness by up to hundreds of percent at several other locations and that was published afterwards (Wilhelm & Bockheim, 2016).

4.7 Paper VII

Hrbáček, F., **Uxa, T.** (2020). The evolution of a near-surface ground thermal regime and modeled active-layer thickness on James Ross Island, Eastern Antarctic Peninsula, in 2006–2016. *Permafrost and Periglacial Processes*, 31(1), 141–155. https://doi.org/10.1002/ppp.2018

This paper examines the temporal dynamics of air temperature and ground temperature at a depth of 5 cm and modelled active-layer thickness using the Stefan and Kudryavtsev models at the Abernethy Flats site, James Ross Island, eastern Antarctic Peninsula region (63°52′53″ S, 57°56′05″ W, 41 m asl), between March 2006 and February 2016, which is among the longest observations of its kind ever published in the region as well as throughout the Antarctica.

The analysis showed that the decadal average of air and ground temperature was −7.3 and −6.1 °C, respectively, and the average modelled active-layer thickness achieved 60 cm. The MAAT increased by an average of 0.10 °C a^{-1} over the study period, whereas the mean annual ground temperature exhibited the opposite tendency of −0.05 °C a^{-1}. However, the air and ground temperature trends were positive only in autumn (March–May), of 0.31 and 0.13 °C a^{-1}, respectively, but they were negative in the other three seasons, of −0.16 to −0.08 °C a^{-1} and −0.20 to −0.13 °C a^{-1}, respectively. Likewise, the active layer tended to thin on average by −1.6 cm a^{-1} because it strongly positively correlated with the summer air and ground temperatures and also showed moderate positive correlations with annual as well as winter temperatures. The active-layer thinning is in line with the analogous rates of −1.6 to −1.5 cm a^{-1} reported from the South Shetland Islands, western Antarctic Peninsula region (Ramos *et al.*, 2017; de Pablo *et al.*, 2018), and can be mainly attributed to declining summer (December–February) temperatures and shortening of the thawing seasons, which started across the whole Antarctic Peninsula region around 2000 (Turner *et al.*, 2016; Oliva *et al.*, 2017). However, the trends should be taken cautiously because all were statistically non-significant at $p < 0.05$. Also, the time series is still too short to capture a climate signal reliably.

The Stefan and Kudryavtsev models reproduced the active-layer thickness with mean absolute errors of 2.6 and 3.4 cm, respectively, while their mean absolute percentage errors were 5.0 and 5.9 %. Such a high accuracy is substantially better than in most previous studies that showed average mean absolute errors of 3.6–58.8 and 2.8–65.7 cm or 6.0–26.1 and 5.8–24.7 %, respectively, which is probably linked to the model enhancements through correction factors (Kurylyk & Hayashi, 2016) and other modifications improving their performance as well as rather homogeneous distribution and low temporal variations of ground physical properties within the active layer. This study is thus the first to provide reasonable and validated active-layer thickness estimates using these analytical models in Antarctica. Given a small number of inputs required by them, it is highly encouraging for calculating the active-layer thickness at other locations as well as its spatial modelling throughout the continent.

5 Discussion, conclusions, and outlook

The thesis brought new insights into some of the poorly investigated permafrost and active-layer phenomena of mostly past permafrost landscapes of selected Central European mountain ranges situated north of the Alps as well as of present-day permafrost environments of the Svalbard archipelago and the Antarctic Peninsula region, the most noteworthy of which are synthesized and shortly discussed below together with potential future research perspectives.

Comprehensive cross-border mapping of mostly relict sorted and non-sorted patterns above the alpine timberline in the High Sudetes Mts., first carried out by Paper I, resulted in one of the few such detailed maps ever published, which depicts the actual areas of the patterned ground and not just its presence or

absence within predefined gridcells of hundreds of meters or kilometres (cf. Niessen *et al.*, 1992; Hjort & Luoto, 2006; Feuillet *et al.*, 2012). It confirmed that the patterns are the most widespread permafrost features that occur there (cf. Křížek, 2007, 2016). Also, it indicated that the most symmetrical patterns, such as sorted polygons and circles or peat and earth hummocks, tend to be situated on flat or gently-inclined surfaces of higher elevations, whereas the least symmetrical ones, such as sorted and non-sorted stripes, usually occur on steeper slopes of lower elevations. Likewise, sorted patterns tend be located at somewhat higher elevations as compared to non-sorted patterns. Generally, it largely mirrors the distribution of slope inclinations within the region that is characterized by extensive summit plateaus surrounded by much steeper slopes, but at the same time it indicates the existence of a typical mountain patterned-ground zonation associated with increased severity of climate conditions and sparser vegetation at higher elevations (cf. Harris, 1982; Niessen *et al.*, 1992; Hjort & Luoto, 2006; Feuillet *et al.*, 2012) towards the end of the LGP when most of the patterns supposedly originated (Sekyra & Sekyra, 1995; Traczyk & Migoń, 2000; Sekyra *et al.*, 2002). Given the patterns extend over a narrow range of elevations of *ca.* 1260–1555 m asl, it implies their high sensitivity to climate and environmental variables as well. Moreover, the latter also translates into the pattern morphology as Paper II revealed that sorted polygons tend to be better developed at higher elevations because of more severe and longer-lasting microclimates suitable for their development there. Specifically, these promoted shallower freeze-thaw depth (∼active layer) and more numerous freeze-thaw cycles of higher intensity, which resulted in polygons having smaller diameters and higher height-to-width ratios as well as better sorting at higher elevations, but were also probably responsible for their partial reactivation and formation of secondary sorting centres during the colder periods of the Holocene. Besides, Paper II suggested that the pattern development probably involves a positive feedback mechanism between morphology and frost susceptibility that is driven by microclimates.

Strikingly, the smaller pattern diameters at higher elevations detected by Paper II for relict sorted polygons in the High Sudetes Mts. are well consistent with those observed by Paper V for active sorted patterns of similar morphology in the northern Billefjorden, Svalbard archipelago, as well as on James Ross Island, eastern Antarctic Peninsula region (Marvánek, 2010), and in other permafrost areas (Kling, 1998). On the other hand, the diameters of active sorted patterns have the opposite tendency in seasonally frozen ground regions (Holness, 2003; Feuillet *et al.*, 2012). Collectively, it suggests that pattern diameters closely relate to the freeze-thaw depth and that their elevation trends within a particular geographical area can indicate whether the patterns developed under permafrost or seasonally frozen ground conditions, or alternatively, at what level the permafrost–seasonal frost boundary was located at that time. Besides, the summary of available diameter-to-sorting depth ratios of circular and polygonal subaerial sorted patterns demonstrated that the ratios tend to cluster between values of *ca.* 3.1–3.8, previously provided by theoretical models of pattern-ground development (Ray *et al.*, 1983; Gleason *et al.*, 1986; Hallet & Prestrud, 1986; Peterson & Krantz, 2008), which indicates that surface size of the patterns might be reasonably used to estimate their sorting depth without the need for laborious and time-consuming excavations. Given the sorting depth is believed to be representative of the freeze-thaw depth and thus also of the temperature conditions at the time of the pattern formation (*sensu* Hallet & Prestrud, 1986; Ballantyne & Harris, 1994), efforts should be made towards palaeo-temperature reconstructions utilizing the sorting depth (∼freeze-thaw depth) as these could provide more reasonable temperature estimates than traditional empirical procedures that build on modern air temperatures associated with active sorted patterns (Ballantyne & Harris, 1994; Ballantyne, 2018). Certainly, the latter can be misleading because Paper V also suggested that many of the patterns examined are probably not in equilibrium with present-day climate conditions and, albeit manifestly active, may have probably been forming throughout the Holocene, that is, under climate conditions that may have substantially differed from those of today (cf. Ballantyne & Harris, 1994; Ballantyne, 2018). Also, the pattern dynamics likely exhibits latitudinal variations because of contrasting insolation budgets that produce distinct thermal regimes, including the number and intensity of freeze-thaw cycles, which is another complication for the traditional reconstruction methods because these have typically utilized active high-latitude patterns as analogues for relict patterns in mid-latitude areas (Ballantyne & Harris, 1994; Ballantyne, 2018).

Given that some of the patterns, such as large-scale sorted polygons and nets, are commonly associated with at least discontinuous permafrost conditions and the MAAT <−6 to −4 °C (Goldthwait, 1976; Washburn, 1980; Grab, 2002; Ballantyne, 2018), their widespread presence in the High Sudetes Mts. attests that permafrost having up to *ca.* 1.5–2 m thick active layer extensively occurred there towards the end of the LGP and that the MAAT decline was at least −8 to −4 °C at that time. Since the latter denotes the minimal MAAT reduction, it is in line with the previously suggested values of *ca.* −12 to −8 °C for the summit areas of the High Sudetes Mts. based on other tentative permafrost evidence and glacier mass-balance modelling (Czudek, 1986; Chmal & Traczyk, 1993; Heyman *et al.*, 2013), but is also well consistent with the average MAAT depressions of at least *ca.* −8 to −4.5 °C indicated by groundwater data and borehole temperature logs in the surrounding lowlands (Šafanda & Rajver, 2001; Zuber *et al.*, 2004; Corcho Alvarado *et al.*, 2011). Currently, however, the mountains most likely host no permafrost as Paper III demonstrated that it is absent even within the high-elevated blockfields, the openwork debris of which usually provides one of the most suitable places for potential permafrost maintenance, but the blockfields have rather low elevation extent and are relatively shallow there, which hinders the development of seasonally reversing, gravity-driven internal air circulation that could insulate their interiors and thus produce negative thermal anomalies as compared to the outside air (*sensu* Delaloye & Lambiel, 2005; Wicky & Hauck, 2017).

On the other hand, Paper IV, which introduced the very first cross-border inventory of rock glaciers for the Western and High Tatra Mts., and as such complemented those from other European high-mountain areas, such as the Alps, the Pyrenees, the Scandinavian Mts., or the Southern Carpathians, suggested that present-day permafrost probably discontinuously occurs there above *ca.* 2000 m asl based on the front elevations of intact rock glaciers, but its level varies locally mainly depending on the slope aspect and surface cover, which is also supported by rare near-subsurface temperature measurements (e.g. Gądek & Kędzia, 2008; Uxa & Mida, 2016, 2017). Obviously, it is slightly above the previously proposed average discontinuous permafrost boundary of 1930 m asl based on the elevation of zero isotherm of MAAT (Dobiński, 1997, 2004, 2005). Of course, the difference can be partly due to distinctive methodologies. However, the earlier estimates (Dobiński, 1997, 2004, 2005) were mostly based on air temperatures from 1985–1989 or 1985–1994 when climate was slightly colder as the MAAT has been increasing there at an average rate of 0.02 °C a^{-1} since the 1960s (Żmudzka, 2011; Pribullová *et al.*, 2013). Such a warming rate would have elevated the zero isotherm level from 1930 m asl to 2003–2039 m asl in 20–30 years, assuming the average temperature lapse rate of 0.0055 °C m^{-1} (*sensu* Niedźwiedź, 1992), or even higher because the warming accelerated in the 1980s (Żmudzka, 2011), which corresponds well to the fact that near-subsurface temperatures within the rock-glacier debris tend to be slightly lower than air temperatures there (Uxa & Mida, 2016, 2017). At the same time, it suggests that the higher permafrost limit as compared to Dobiński (1997, 2004, 2005) is reasonable.

Besides, Paper IV also estimated that the lower boundary of discontinuous permafrost at the Pleistocene–Holocene transition, that is, when the rock glaciers presumably originated there (Kotarba, 2007; Zasadni *et al.*, 2020), was around *ca.* 1400 m asl based on the lowest fronts of relict rock glaciers, and the associated MAAT decline was at least −5.4 °C, which is well in line with the temperature depression of *ca.* −7 to −6 °C based on glacier mass-balance modelling (Makos *et al.*, 2013). Similarly, Zasadni *et al.* (2020) also hypothesized that Younger Dryas rock glaciers should occur at elevations of 1320–1520 m asl if the MAAT depression of −5 to −4 °C would be assumed. However, they dated numerically only small rock glaciers at elevations of *ca.* 1800–2000 m asl, which formed 11.9–10.4 ka, that is, mostly in the early Holocene (Zasadni *et al.*, 2020) when climate was already warmer (Tóth *et al.*, 2012), and thus yielded the lower boundary of discontinuous permafrost of *ca.* 1800 m asl and the MAAT reduction as little as −1.6 °C, or −5.3 °C if enhanced annual air temperature amplitude was considered (Zasadni *et al.*, 2020). Moreover, they assumed tentatively that rock glaciers situated at lower elevations have emerged prior to the Younger Dryas because they further argued that permafrost disappeared much earlier at elevations of *ca.* <1600 m asl based on the presence of a so-called massive rock-glacier front found at the foot of a rock-avalanche fan at 1620 m asl (Zasadni *et al.*, 2020) dated at 15.6±0.7 ka (Engel *et al.*, 2015; Pánek *et al.*,

2016). Nonetheless, the latter landform has previously been considered to be solely a rockfall accumulation (Engel *et al.*, 2015; Pánek *et al.*, 2016) and is also not included in the rock-glacier inventory compiled by Paper IV and as such it is probably of no significance for past permafrost distribution. Also, the MAAT reduction is estimated at up to *ca.* −10 to −9 °C at the time of its origin (Makos, 2015), which would imply that permafrost extended much lower, and certainly below *ca.* 1500 m asl as indicated by cryogenic cave carbonates (Žák *et al.*, 2012). Last but not least, it should be noted that there are rock glaciers descending to *ca.* 1400 m asl in the Western Tatra Mts., which have indeed been attributed to the Younger Dryas (Engel *et al.*, 2017), suggesting that the past lower boundary of discontinuous permafrost and the associated MAAT decline provided by Paper IV is plausible.

Obviously, the relict and intact rock glaciers and thus also the past and present discontinuous permafrost limits occur on average *ca.* 400–600 and 100–250 m lower than in the Alps and the Southern Carpathians, respectively, which is attributed to increasing continentality to the east as well as to latitudinal temperature decrease (*sensu* Dobiński, 2005; Onaca *et al.*, 2017). However, it must be stressed that the deduced permafrost limits should be understood as tentative because rock glaciers can provide only a first-order evaluation of potential permafrost distribution, which generally tends to overestimate the permafrost extent at places without debris cover. Ground temperature measurements supplemented by geophysical soundings are thus needed to determine the controls on permafrost existence there in order to enhance the estimates of its past and present distribution in the mountains as well as to assess its response to the current climate warming.

Ground temperature measurements should be as long as possible, as illustrated by Paper VII, which examined one of the longest observations (2006–2016) of thermal regime and modelled active-layer thickness using the Stefan and Kudryavtsev models in the Antarctic Peninsula region as well as throughout the Antarctica, but the decadal time series proved to be still too short to capture statistically significant trends. Notwithstanding that, it detected active-layer thinning that is analogous to other locations around the Antarctic Peninsula and can be mainly attributed to declining summer temperatures and shortening of the thawing seasons, which started there around 2000 (Turner *et al.*, 2016; Oliva *et al.*, 2017), and as such it highly contrasts with what is happening in most permafrost regions in the Northern Hemisphere where air and ground temperatures as well as active-layer thickness have been steadily increasing over the past few decades (Harris *et al.*, 2009; Romanovsky *et al.*, 2010; Luo *et al.*, 2016; Biskaborn *et al.*, 2019). The Stefan and Kudryavtsev models reproduced the active-layer thickness with lower errors than in most previous studies and it was their very first successful application in Antarctica after they had been incorrectly utilized by Wilhelm *et al.* (2015) and Wilhelm & Bockheim (2016) who modelled unrealistically thick active layers on Amsler Island, western Antarctic Peninsula region, that exceeded their actual thickness by up to hundreds of percent and basically excluded the existence of near-surface permafrost there, which gave the false impression of extreme warming and as such seriously misrepresented the climate state in the region as demonstrated by Paper VI. Both Paper VI and Paper VII also highlighted some important issues of active-layer and permafrost modelling, including phase changes and latent heat effects or model parameterizations and corrections, which is useful as the models become increasingly available not only for permafrost scientists, but also for non-specialists working in permafrost environments.

Clearly, Paper I, Paper II, Paper IV, and Paper V showed that patterned ground and rock glaciers are highly sensitive to variations in climate and environmental conditions and that these can be preserved and subsequently deduced even from the Last Glacial to early Holocene features, which has important implications for present-day permafrost regions, but especially it indicates their high potential for reconstructions of past permafrost environments that should definitely be further exploited in future investigations. These should be particularly attempted to better constrain former temperature conditions associated with the patterned ground as well as the rock glaciers and to thoroughly determine their absolute chronology using numerical dating methods. So far, their age has mostly been estimated using the knowledge about the regional glaciations and/or palaeo-climates, while numerical dating was virtually lacking because it is tricky due to their complex formation history potentially spanning multiple time periods and possible reorganiza-

tion long after they have formed. Fortunately, first numerical dates have recently started to emerge at least for rock glaciers in the Western and High Tatra Mts. (Engel *et al.*, 2017; Zasadni *et al.*, 2020), but those for patterned ground in the High Sudetes Mts. will hopefully appear soon as well (Engel *et al.*, in revision). Correlations with local mountain glaciations as well as permafrost dynamics in the surrounding lowlands are also highly desirable to better comprehend the Late Quaternary landscape evolution of these regions as mountain and lowland permafrost behaviour probably highly differed both spatially and temporally, but it has not yet been addressed as most chronological data on past permafrost events in Central European areas situated north of the Alps are still available almost exclusively only from lowland locations (Isarin, 1997; Huijzer & Vandenberghe, 1998; Czudek, 2005; Marks *et al.*, 2016). Besides, the monitoring of air and near-subsurface temperatures and/or active-layer thickness, which has already been established on James Ross Island (Paper VII) and in the High Tatra Mts. (Uxa & Mida, 2016, 2017), should definitely continue in order to extend the time series so that they allow for a more thorough trend analysis that tells more about the active-layer and permafrost dynamics in these regions and their drivers, which is critical for assessing the regional contrasts of climate-change impacts on these important components of the cryosphere. Also, other locations should be included in the analysis to enhance its robustness. Lastly, complex numerical models should be employed there as they can capture the transient evolution of subsurface temperatures, including their sub-annual variability, and are thus capable to better represent the active-layer and permafrost behaviour. The latter is urgently needed also because numerical models have almost never been used in these regions.

Conclusively, the thesis contributed to a better understanding of the past and present dynamics of the examined regions, which documents that permafrost and active-layer phenomena are valuable measures of Late Quaternary environmental changes if observed in detail (Paper I, Paper II, Paper IV, Paper V, and Paper VII) and/or interpreted carefully (cf. Paper III and Paper VI). Besides, newly introduced approaches, methods, and perspectives as well as established monitoring networks enhance the breadth of details that can be retrieved from both past and present permafrost and active-layer phenomena, and thus the thesis outcomes also have notable methodological and genetic implications as well as relevance to concepts of permafrost landscape evolution. Yet, they should be viewed rather as partial but important steps that pave the way for follow-up investigations.

6 References

Amatulli, G., Domisch, S., Tuanmu, M.-N., Parmentier, B., Ranipeta, A., Malczyk, J., Jetz, W. (2018). *A suite of global, cross-scale topographic variables for environmental and biodiversity modeling, links to files in GeoTIFF format*. PANGAEA. https://doi.org/10.1594/PANGAEA.867115

Ambrožová, K., Láska, K. (2016). Změny teploty vzduchu na ostrově Jamese Rosse v kontextu Antarktického poloostrova [The Air Temperature Change on James Ross Island in the Context of the Antarctic Peninsula]. In Nováček, A. (Ed). *Sborník příspěvků z Výroční konference České geografické společnosti*. České Budějovice, Czech Republic, 20–25.

Azócar, G.F., Brenning, A. (2010). Hydrological and geomorphological significance of rock glaciers in the Dry Andes, Chile (27°–33°S). *Permafrost and Periglacial Processes*, 21(1), 42–53. https://doi.org/10.1002/ppp.669

Baeten, N.J., Forwick, M., Vogt, C., Vorren, T.O. (2010). Late Weichselian and Holocene sedimentary environments and glacial activity in Billefjorden, Svalbard. In Howe, J.A., Austin, W.E.N., Forwick, M., Paetzel, M. (Eds). *Fjord Systems and Archives*. Geological Society, Special Publications, 344, London, UK, 207–223.

Ballantyne, C.K. (1996). Formation of miniature sorted patterns by shallow ground freezing: A field experiment. *Permafrost and Periglacial Processes*, 7(4), 409–424. https://doi.org/10.1002/(SICI)1099-1530(199610)7:4<409::AID-PPP230>3.0.CO;2-3

Ballantyne, C.K. (2013). Patterned ground. In Elias, S.A., Mock, C.J. (Eds). *Encyclopedia of Quaternary Science*, 2nd Edition. Elsevier, Amsterdam, Netherlands, 452–463. https://doi.org/10.1016/B978-0-444-53643-3.00098-4

Ballantyne, C.K. (2018). *Periglacial Geomorphology*. John Wiley & Sons, Hoboken, USA.

Ballantyne, C.K., Matthews, J.A. (1982). The Development of Sorted Circles on Recently Deglaciated Terrain, Jotunheimen, Norway. *Arctic and Alpine Research*, 14(4), 341–354. https://doi.org/10.2307/1550796

Ballantyne, C.K., Harris, C. (1994). *The Periglaciation of Great Britain*. Cambridge University Press, Cambridge, UK.

Barsch, D. (1996). *Rockglaciers: Indicators for the present and former geoecology in high mountain environments*. Springer, Berlin, Germany.

Berthling, I. (2011). Beyond confusion: Rock glaciers as cryo-conditioned landforms. *Geomorphology*, 131(3–4), 98–106. https://doi.org/10.1016/j.geomorph.2011.05.002

Biskaborn, B.K., Smith, S.L., Noetzli, J., Matthes, H., Vieira, G., Streletskiy, D.A., Schoeneich, P., Romanovsky, V.E., Lewkowicz, A.G., Abramov, A., Allard, M., Boike, J., Cable, W.L., Christiansen, H.H., Delaloye, R., Diekmann, B., Drozdov, D., Etzelmüller, B., Grosse, G., Guglielmin, M., Ingeman-Nielsen, T., Isaksen, K., Ishikawa, M., Johansson, M., Johannsson, H., Joo, A., Kaverin, D., Kholodov, A., Konstantinov, P., Kröger, T., Lambiel, C., Lanckman, J.-P., Luo, D., Malkova, G., Meiklejohn, I., Moskalenko, N., Oliva, M., Phillips, M., Ramos, M., Sannel, A.B.K., Sergeev, D., Seybold, C., Skryabin, P., Vasiliev, A., Wu, Q., Yoshikawa, K., Zheleznyak, M., Lantuit, H. (2019). Permafrost is warming at a global scale. *Nature Communications*, 10(1), 264. https://doi.org/10.1038/s41467-018-08240-4

Bockheim, J., Vieira, G., Ramos, M., López-Martínez, J., Serrano, E., Guglielmin, M., Wilhelm, K., Nieuwendam, A. (2013). Climate warming and permafrost dynamics in the Antarctic Peninsula region. *Global and Planetary Change*, 100(January 2013), 215–223. https://doi.org/10.1016/j.gloplacha.2012.10.018

Bonnaventure, P.P., Lamoureux, S.F. (2013). The active layer: A conceptual review of monitoring, modelling techniques and changes in a warming climate. *Progress in Physical Geography: Earth and Environment*, 37(3), 352–376. https://doi.org/10.1177/0309133313478314

Borzotta, E., Trombotto, D. (2004). Correlation between frozen ground thickness measured in Antarctica and permafrost thickness estimated on the basis of the heat flow obtained from magnetotelluric soundings. *Cold Regions Science and Technology*, 40(1–2), 81–96. https://doi.org/10.1016/j.coldregions.2004.06.002

Brenning, A. (2005). Geomorphological, hydrological and climatic significance of rock glaciers in the Andes of Central Chile (33–35°S). *Permafrost and Periglacial Processes*, 16(3), 231–240. https://doi.org/10.1002/ppp.528

Brown, R.J.E. (1960). The Distribution of Permafrost and Its Relation to Air Temperature in Canada and the U.S.S.R. *Arctic*, 13(3), 163–177. https://doi.org/10.14430/arctic3697

Brown, R.J.E., Péwé, T.L. (1973). Distribution of Permafrost in North America and Its Relationship to the Environment: A Review. In Péwé, T.L., Mackay, J.R. (Eds). *Proceedings of the 2th International Conference on Permafrost: North American Contribution*, Yakutsk, USSR, 71–100.

Brown, J., Ferrians Jr, O.J., Heginbottom, J.A., Melnikov, E.S. (1997). *Circum-Arctic Map of Permafrost and Ground-Ice Conditions*. US Geological Survey, Reston, USA.

Burn, C.R. (1998). The Active Layer: Two Contrasting Definitions. *Permafrost and Periglacial Processes*, 9(4), 411–416. https://doi.org/10.1002/(SICI)1099-1530(199810/12)9:4%3C411::AID-PPP292%3E3.0.CO;2-6

Burn, C.R. (2013). Permafrost. In Elias, S.A., Mock, C.J. (Eds). *Encyclopedia of Quaternary Science*, 2nd Edition. Elsevier, Amsterdam, Netherlands, 464–471. https://doi.org/10.1016/B978-0-444-53643-3.00099-6

Chadburn, S.E., Burke, E.J., Cox, P.M., Friedlingstein, P., Hugelius, G., Westermann, S. (2017). An observation-based coinstraint on permafrost loss as a function of global warming. *Nature Climate Change*, 7(5), 340–344. https://doi.org/10.1038/nclimate3262

Chlupáč, I., Brzobohatý, R., Kovanda, J., Stráník, Z. (2011). *Geologická minulost České republiky*, 2nd Edition [Geological History of the Czech Republic]. Academia, Praha, Czech Republic.

Chmal, H., Traczyk, A. (1993). Plejstoceńskie lodowce gruzowe w Karkonoszach [Pleistocene Rock Glaciers in the Karkonosze Mts.]. *Czasopismo Geograficzne*, 64(3–4), 253–263.

Clark, P.U., Dyke, A.S., Shakun, J.D., Carlson, A.E., Clark, J., Wohlfarth, B., Mitrovica, J.X., Hostetler, S.W., McCabe, A.M. (2009). The Last Glacial Maximum. *Science*, 325(5941), 710–714. https://doi.org/10.1126/science.1172873

Colucci, R.R., Boccali, C., Žebre, M., Guglielmin, M. (2016). Rock glaciers, protalus ramparts and pronival ramparts in the south-eastern Alps. *Geomorphology*, 269(15 September 2016), 112–121. https://doi.org/10.1016/j.geomorph.2016.06.039

Corcho Alvarado, J.A., Leuenberger, M., Kipfer, R., Paces, T., Purtschert, R. (2011). Reconstruction of past climate conditions over central Europe from groundwater data. *Quaternary Science Reviews*, 30(23–24), 3423–3429. https://doi.org/10.1016/j.quascirev.2011.09.003

Czudek, T. (1986). Pleistocénní permafrost na území Československa [Pleistocene Permafrost in Czechoslovakia]. *Geografický časopis*, 38(2–3), 245–252.

Czudek, T. (2005). *Vývoj reliéfu krajiny České republiky v kvartéru* [Quaternary Development of Landscape Relief of the Czech Republic]. Moravské zemské muzeum, Brno, Czech Republic.

Dallmann, W.K., Piepjohn, K., Blomeier, D. (2004). *Geological Map of Billefjorden, Central Spitsbergen, Svalbard, with Geological Excursion Guide 1 : 50,000*. Norsk Polarinstitutt, Oslo, Norway.

Davies, B.J., Carrivick, J.L., Glasser, N.F., Hambrey, M.J., Smellie, J.L. (2012). Variable glacier response to atmospheric warming, northern Antarctic Peninsula, 1988–2009. *The Cryosphere*, 6, 1031–1048. https://doi.org/10.5194/tc-6-1031-2012

Delaloye, R., Lambiel, C. (2005). Evidence of winter ascending air circulation throughout talus slopes and rock glaciers situated in the lower belt of alpine discontinuous permafrost (Swiss Alps). *Norsk Geografisk Tidsskrift – Norwegian Journal of Geography*, 59(2), 194–203. https://doi.org/10.1080/00291950510020673

Delaloye, R., Reynard, E., Lambiel, C., Marescot, L., Monnet, R. (2003). Thermal anomaly in a cold scree slope (Creux du Van, Switzerland). In Phillips, M., Springman, S.M., Arenson, L.U. (Eds). *Proceedings of the 8th International Conference on Permafrost*. Zurich, Switzerland, 175–180.

de Pablo, M.A., Ramos, M., Molina, A., Prieto, M. (2018). Thaw depth spatial and temporal variability at the Limnopolar Lake CALM-S site, Byers Peninsula, Livingston Island, Antarctica. *Science of The Total Environment*, 615(15 February 2018), 814–827. https://doi.org/10.1016/j.scitotenv.2017.09.284

Dobiński, W. (1997). Distribution of mountain permafrost in the High Tatras based on freezing and thawing indices. *Biuletyn Peryglacjalny*, 36, 29–37.

Dobiński, W. (2004). Wieloletnia zmarzlina w Tatrach: Geneza, cechy, ewolucja [Permafrost in the Tatra Mts.: Genesis, features, evolution]. *Przegląd Geograficzny*, 76(3), 327–343.

Dobiński, W. (2005). Permafrost of the Carpathian and Balkan Mountains, eastern and southeastern Europe. *Permafrost and Periglacial Processes*, 16(4), 395–398. https://doi.org/10.1002/ppp.524

Dobiński, W. (2011): Permafrost. *Earth-Science Reviews*, 108(3–4), 158–169. https://doi.org/10.1016/j.earscirev.2011.06.007

Dobiński, W., Gądek, B., Żogała, B. (1996). Wyniki geoelektrycznych badań osadów czwartorzędowych w piętrze alpejskim Tatr Wysokich [Results of Geoelectrical Surveys of Quaternary Deposits in the Alpine Belt of the High Tatra Mts.]. *Przegląd Geologiczny*, 44(3), 259–261.

Dobiński, W., Żogała, B., Wzietek, K., Litwin, L. (2008). Results of geophysical surveys on Kasprowy Wierch, the Tatra Mountains, Poland. In Hauck, C., Kneisel, C. (Eds). *Applied Geophysics in Periglacial Environments*. Cambridge University Press, Cambridge, UK, 126–136. https://doi.org/10.1017/CBO9780511535628.009

Draebing, D. (2016). Application of refraction seismics in alpine permafrost studies: A review. *Earth-Science Reviews*, 155(April 2016), 136–152. https://doi.org/10.1016/j.earscirev.2016.02.006

Ehlers, J., Gibbard, P.L., Hughes, P.D. (Eds) (2011). *Quaternary Glaciations – Extent and Chronology: A Closer Look*. Elsevier, Amsterdam, Netherlands.

Engel, Z. (1997). Současný stav poznatků o pleistocenním zalednění české části Krkonoš [The Current State of Knowledge of Quaternary Glaciation in the Czech Part of the Krkonoše (Giant) Mountains]. *Geografie*, 102(4), 288–302.

Engel, Z., Nývlt, D., Láska, K. (2012). Ice thickness, areal and volumetric changes of Davies Dome and Whisky Glacier (James Ross Island, Antarctic Peninsula) in 1979–2006. *Journal of Glaciology*, 58(211), 904–914. https://doi.org/10.3189/2012JoG11J156

Engel, Z., Braucher, R., Traczyk, A., Laetitia, L., ASTER Team (2014). ^{10}Be exposure age chronology of the last glaciation in the Krkonoše Mountains, Central Europe. *Geomorphology*, 206(1 February 2014), 107–121. https://doi.org/10.1016/j.geomorph.2013.10.003

Engel, Z. Mentlík, P., Braucher, R., Minár, J., Léanni, L., ASTER Team (2015). Geomorphological evidence and ^{10}Be exposure ages for the Last Glacial Maximum and deglaciation of the Velká and Malá Studená dolina valleys in the High Tatra Mountains, central Europe. *Quaternary Science Reviews*, 124(15 September 2015), 106–123. https://doi.org/10.1016/j.quascirev.2015.07.015

Engel, Z. Mentlík, P., Braucher, R., Křížek, M., Pluháčková, M., ASTER Team (2017). ^{10}Be exposure age chronology of the last glaciation of the Roháčská Valley in the Western Tatra Mountains, central Europe. *Geomorphology*, 293, Part A(September 2017), 130–142. https://doi.org/10.1016/j.geomorph.2017.05.012

Engel, Z., Láska, K., Nývlt, D., Stachoň, Z. (2018). Surface mass balance of small glaciers on James Ross Island, North-Eastern Antarctic Peninsula, during 2009–2015. *Journal of Glaciology*, 64(245), 349–361. https://doi.org/10.1017/jog.2018.17

Engel, Z., Křížek, M., Braucher, R., Uxa, T., Krause, D., ASTER Team (in revision). ^{10}Be exposure age for sorted polygons in the Sudetes Mountains. *Permafrost and Periglacial Processes*.

Etzelmüller, B., Schuler, T.V., Isaksen, K., Christiansen, H.H., Farbrot, H., Benestad, R. (2011). Modeling the temperature evolution of Svalbard permafrost during the 20th and 21st century. *The Cryosphere*, 5, 67–79. https://doi.org/10.5194/tc-5-67-2011

Ewertowski, M.W., Tomczyk, A.M. (2015). Quantification of the ice-cored moraines' short-term dynamics in the high-Arctic glaciers Ebbabreen and Ragnarbreen, Petuniabukta, Svalbard. *Geomorphology*, 234(1 April 2015), 211–227. https://doi.org/10.1016/j.geomorph.2015.01.023

Feuillet, T., Mercier, D. (2012). Post-Little Ice Age patterned ground development on two Pyrenean proglacial areas: from deglaciation to periglaciation. *Geografiska Annaler: Series A, Physical Geography*, 94(3), 363–376. https://doi.org/10.1111/j.1468-0459.2012.00459.x

Feuillet, T., Mercier, D., Decaulne, A., Cossart, E. (2012). Classification of sorted patterned ground areas based on their environmental characteristics (Skagafjörður, Northern Iceland). *Geomorphology*, 139–140(15 February 2012), 577–587. https://doi.org/10.1016/j.geomorph.2011.12.022

French, H.M. (2017). *The Periglacial Environment*, 4th Edition. John Wiley & Sons, Hoboken, USA.

Fukuda, M., Shimokawa, K., Takahashi, N., Sone, T. (1992). Permafrost in Seymour Island and James Ross Island, Antarctic Peninsula Region. *Geographical Review of Japan, Series A*, 65(2), 124–131. https://doi.org/10.4157/grj1984a.65.2_124

Gądek, B. (2014). Climatic sensitivity of the non-glaciated mountains cryosphere (Tatra Mts., Poland and Slovakia). *Global and Planetary Change*, 121(October 2014), 1–8. https://doi.org/10.1016/j.gloplacha.2014.07.001

Gądek, B., Grabiec, M. (2008). Glacial ice and permafrost distribution in the Medena kotlina (Slovak Tatras): Mapped with application of GPR and GST measurements. *Studia Geomorphologica Carpatho-Balcanica*, 42, 5–22.

Gądek, B., Kędzia, S. (2008). Winter ground surface temperature regimes in the zone of sporadic discontinuous permafrost, Tatra Mountains (Poland and Slovakia). *Permafrost and Periglacial Processes*, 19(3), 315–321. https://doi.org/10.1002/ppp.623

Gibas, J., Rachlewicz, G., Szczuciński, W. (2005). Application of DC resistivity soundings and geomorphological surveys in studies of modern Arctic glacier marginal zones, Petuniabukta, Spitsbergen. *Polish Polar Research*, 26(4), 239–258.

Gleason, K.J., Krantz, W.B., Caine, N., George, J.H., Gunn, R.D. (1986). Geometrical Aspects of Sorted Patterned Ground in Recurrently Frozen Soil. *Science*, 232(4747), 216–220. https://doi.org/10.1126/science.232.4747.216

Goldthwait, R.P. (1976). Frost Sorted Patterned Ground: A Review. *Quaternary Research*, 6(1), 27–35. https://doi.org/10.1016/0033-5894(76)90038-7

Grab, S. (2002). Characteristics and palaeoenvironmental significance of relict sorted patterned ground, Drakensberg plateau, southern Africa. *Quaternary Science Reviews*, 21(14–15), 1729–1744. https://doi.org/10.1016/S0277-3791(01)00149-4

Grab, S. (2005). Aspect of the geomorphology, genesis and environmental significance of earth hummock (thúfur, pounus): miniature cryogenic mounds. *Progress in Physical Geography: Earth and Environment*, 29(2), 139–155. https://doi.org/10.1191/0309133305pp440ra

Gruber, S. (2012). Derivation and analysis of a high-resolution estimate of global permafrost zonation. *The Cryosphere*, 6, 221–233. https://doi.org/10.5194/tc-6-221-2012

Gruber, S., Haeberli, W. (2009). Mountain Permafrost. In Margesin, R. (Ed). *Permafrost soils*. Springer, Berlin, Germany, 33–44. https://doi.org/10.1007/978-3-540-69371-0_3

Gude, M., Dietrich, S., Mäusbacher, R., Hauck, C., Molenda, R., Ruzicka, V., Zacharda, M. (2003). Probable occurrence of sporadic permafrost in non-alpine scree slopes in central Europe. In Phillips, M., Springman, S.M., Arenson, L.U. (Eds). *Proceedings of the 8th International Conference on Permafrost*. Zurich, Switzerland, 331–336.

Hagen, J.O., Liestøl, O., Roland, E., Jørgensen, T. (1993). *Glacier atlas of Svalbard and Jan Mayen*. Norsk Polarinstitutt, Oslo, Norway.

Hallet, B. (1998). Measurements of soil motion in sorted circles, western Spitsbergen. In Lewkowicz, A.G., Allard, M. (Eds). *Proceedings of the 7th International Conference on Permafrost*. Yellowknife, Canada, 415–420.

Hallet, B., Prestrud, S. (1986). Dynamics of Periglacial Sorted Circles in Western Spitsbergen. *Quaternary Research*, 26(1), 81–99. https://doi.org/10.1016/0033-5894(86)90085-2

Harčarik, J. (2002). Microclimatic relationships of the arctic-alpine tundra. *Opera Corcontica*, 39, 45–68.

Harris, C. (1982). The distribution and altitudinal zonation of periglacial landforms, Okstindan, Norway. *Zeitschrift für Geomorphologie*, 26(3), 283–304.

Harris, C., Arenson, L.U., Christiansen, H.H., Etzelmüller, B., Frauenfelder, R., Gruber, S., Haeberli, W., Hauck, C., Hölzle, M., Humlum, O., Isaksen, K., Kääb, A., Kern-Lütschg, M.A., Lehning, M., Matsuoka, N., Murton, J.B., Nötzli, J., Phillips, M., Ross, N., Seppälä, M., Springman, S.M., Vonder Mühll, D. (2009). Permafrost and climate in Europe: Monitoring and modelling thermal, geomorphological and geotechnical responses. *Earth-Science Reviews*, 92(3–4), 117–171. https://doi.org/10.1016/j.earscirev.2008.12.002

Hauck, C., Vonder Mühll, D. (2003). Inversion and Interpretation of Two-dimensional Geoelectrical Measurements for Detecting Permafrost in Mountainous Regions. *Permafrost and Periglacial Processes*, 14(4), 305–318. https://doi.org/10.1002/ppp.462

Haugland, J.E. (2006). Short-term Periglacial Processes, Vegetation Succession, and Soil Development within Sorted Patterned Ground: Jotunheimen, Norway. *Arctic, Antarctic, and Alpine Research*, 38(1), 82–89. https://doi.org/10.1657/1523-0430(2006)038[0082:SPPVSA]2.0.CO;2

Hejcman, M., Dvořák, I.J., Kociánová, M., Pavlů, V., Nežerková, P., Vítek, O., Rauch, O., Jeník, J. (2006). Snow Depth and Vegetation Pattern in a Late-melting Snowbed Analyzed by GPS and GIS in the Giant Mountains, Czech Republic. *Arctic, Antarctic, and Alpine Research*, 38(1), 90–98. https://doi.org/10.1657/1523-0430(2006)038[0090:SDAVPI]2.0.CO;2

Heyman, B.M., Heyman, J., Fickert, T., Harbor, J.M. (2013). Paleo-climate of the central European uplands during the last glacial maximum based on glacier mass-balance modeling. *Quaternary Research*, 79(1), 49–54. https://doi.org/10.1016/j.yqres.2012.09.005

Hjort, J., Luoto, M. (2006). Modelling patterned ground distribution in Finnish Lapland: an integration of topographical, ground and remote sensing information. *Geografiska Annaler: Series A, Physical Geography*, 88(1), 19–29. https://doi.org/10.1111/j.0435-3676.2006.00280.x

Hjort, J., Karjalainen, O., Aalto, J., Westermann, S., Romanovsky, V.E., Nelson, F.E., Etzelmüller, B., Luoto, M. (2018). Degrading permafrost puts Arctic infrastructure at risk by mid-century. *Nature Communications*, 9(1), 5147. https://doi.org/10.1038/s41467-018-07557-4

Holness, S.D. (2003). Sorted circles in the maritime Subantarctic, Marion Island. *Earth Surface Processes and Landforms*, 28(4), 337–347. https://doi.org/10.1002/esp.430

Hrbáček, F., Láska, K., Engel, Z. (2016). Effect of Snow Cover on the Active-Layer Thermal Regime – A Case Study from James Ross Island, Antarctic Peninsula. *Permafrost and Periglacial Processes*, 27(3), 307–315. https://doi.org/10.1002/ppp.1871

Hrbáček, F., Kňažková, M., Nývlt, D., Láska, K., Mueller, C.W., Ondruch, J. (2017). Active layer monitoring at CALM-S site near J.G.Mendel Station, James Ross Island, eastern Antarctic Peninsula. *Science of The Total Environment*, 601–602(1 December 2017), 987–997. https://doi.org/10.1016/j.scitotenv.2017.05.266

Hrbáček, F., Nývlt, D., Láska, K., Kňažková, M., Kampová, B., Engel, Z., Oliva, M., Mueller, C.W. (2019a). Permafrost and active layer research on James Ross Island: An overview. *Czech Polar Reports*, 9(1), 20–36. https://doi.org/10.5817/CPR2019-1-3

Hrbáček, F., Vieira, G., Oliva, M., Balks, M., Guglielmin, M., de Pablo, M.A., Molina, A., Ramos, M., Goyanes, G., Meiklejohn, I., Abramov, A., Demidov, N., Fedorov-Davydov, D., Lupachev, A., Rivkina, E., Láska, K., Kňažková, M., Nývlt, D., Raffi, R., Strelin, J., Sone, T., Fukui, K., Dolgikh, A., Zazovskaya, E., Mergelov, N., Osokin, N., Miamin, V. (2019b). Active layer monitoring in Antarctica: an overview of results from 2006 to 2015. *Polar Geography*. https://doi.org/10.1080/1088937X.2017.1420105

Hughes, P.D., Gibbard, P.L., Woodward, J.C. (2003). Relict rock glaciers as indicators of Mediterranean palaeoclimate during the Last Glacial Maximum (Late Würmian) in northwest Greece. *Journal of Quaternary Science*, 18(5), 431–440. https://doi.org/10.1002/jqs.764

Huijzer, B., Vandenberghe, J. (1998). Climatic reconstruction of the Weichselian Pleniglacial in northwestern and central Europe. *Journal of Quaternary Science*, 13(5), 391–417. https://doi.org/10.1002/(SICI)1099-1417(1998090)13:5<391::AID-JQS397>3.0.CO;2-6

Humlum, O., Instanes, A., Sollid, J.L. (2003). Permafrost in Svalbard: a review of research history, climatic background and engineering challenges. *Polar Research*, 22(2), 191–215. https://doi.org/10.3402/polar.v22i2.6455

Isaksson, E., Kohler, J., Pohjola, V., Moore, J., Igarashi, M., Karlöf, L., Martma, T., Meijer, H., Motoyama, H., Vaikmäe, R., van de Wal, R.S.W. (2005). Two ice-core δ^{18}O records from Svalbard illustrating climate and sea-ice variability over the last 400 years. *The Holocene*, 15(4), 501–509. https://doi.org/10.1191/0959683605hl820rp

Isarin, R.F.B. (1997). Permafrost Distribution and Temperatures in Europe During the Younger Dryas. *Permafrost and Periglacial Processes*, 8(3), 313–333. https://doi.org/10.1002/(SICI)1099-1530(199709)8:3<313::AID-PPP255>3.0.CO;2-E

Janásková, B. (2006). Ukládání a odbourávání sněhu ve vrcholové oblasti východních Krkonoš [Accumulation and ablation of snow cover in the summit parts of the Giant Mountains]. *Opera Corcontica*, 43, 57–80.

Jones, D.B., Harrison, S., Anderson, K., Whalley, W.B. (2019). Rock glaciers and mountain hydrology: A review. *Earth-Science Reviews*, 193(June 2019), 66–90. https://doi.org/10.1016/j.earscirev.2019.04.001

Juliussen, H., Christiansen, H.H., Strand, G.S., Iversen, S., Midttømme, K., Rønning, J.S. (2010). NORPERM, the Norwegian Permafrost Database – a TSP NORWAY IPY legacy. *Earth System Science Data*, 2, 235–246. https://doi.org/10.5194/essd-2-235-2010

Jurewicz, E. (2007). Multistage evolution of the granitoid core in Tatra Mountains. In Kozłowski, A., Wiszniewska, J. (Eds). *Granitoids in Poland*. Warsaw University, Warszawa, Poland, 307–317.

Kääb, A. (2013). Rock glaciers and protalus forms. In Elias, S.A., Mock, C.J. (Eds). *Encyclopedia of Quaternary Science*, 2nd Edition. Elsevier, Amsterdam, Netherlands, 535–541. https://doi.org/10.1016/B978-0-444-53643-3.00104-7

Kääb, A., Girod, L., Berthling, I. (2014). Surface kinematics of periglacial sorted circles using structure-from-motion technology. *The Cryosphere*, 8, 1041–1056. https://doi.org/10.5194/tc-8-1041-2014

Kędzia, S. (2015). Zarys historii badań przemarzania gruntu i wieloletniej zmarzliny w polskiej części Tatr [An outline of the history of ground freezing and permafrost research in the Polish Tatra Mountains]. *Przegląd Geograficzny*, 87(1), 53–69. http://dx.doi.org/10.7163/PrzG.2015.1.3

Kellerer-Pirklbauer, A. (2008). *Aspects of glacial, paraglacial and periglacial processes and landforms of the Tauern Range, Austria*. Unpublished doctoral thesis, University of Graz, Austria.

Kellerer-Pirklbauer, A., Wagner, T., Winkler, G. (2016). Inventarisierung von blockgletscherverdächtigen Formen und deren hydrologischen Einzugsgebieten in den steirischen Niederen Tauern mit Hilfe von hochaufgelösten Geländemodellen [Inventorying rock glacier-suspected landforms and their hydrological catchments in the Styrian part of the Niedere Tauern range using high-resolution digital elevation models]. *Joannea – Geologie und Palaontologie*, 12, 53–62.

King, L. (1986). Zonation and Ecology of High Mountain Permafrost in Scandinavia. *Geografiska Annaler: Series A, Physical Geography*, 68(3), 131–139. https://doi.org/10.1080/04353676.1986.11880166

Kłapyta, P., Zasadni, J. (2017/2018). Research History on the Tatra Mountains Glaciations. *Studia Geomorphologica Carpatho-Balcanica*, 51/52, 43–85.

Kling, J. (1997). Observations on sorted circle development, Abisko, Northern Sweden. *Permafrost and Periglacial Processes*, 8(4), 447–453. https://doi.org/10.1002/(SICI)1099-1530(199710/12)8:4<447::AID-PPP266>3.0.CO;2-H

Kling, J. (1998). The difference between sorted circle and polygon morphology and their distribution in two alpine areas, northern Sweden. *Zeitschrift für Geomorphologie, N.F.*, 42(4), 439–452.

Kneisel, C., Hauck, C. (2008). Electrical methods. In Hauck, C., Kneisel, C. (Eds). *Applied Geophysics in Periglacial Environments*. Cambridge University Press, Cambridge, UK, 3–27. https://doi.org/10.1017/CBO9780511535628.002

Kneisel, C., Hauck, C., Vonder Mühll, D. (2000). Permafrost below the Timberline Confirmed and Characterized by Geoelectrical Resistivity Measurements, Bever Valley, Eastern Swiss Alps. *Permafrost and Periglacial Processes*, 11(4), 295–304. https://doi.org/10.1002/1099-1530(200012)11:4<295::AID-PPP353>3.0.CO;2-L

Kňažková, M., Hrbáček, F., Nývlt, D., Kavan, J. (2020). Effect of hyaloclastite breccia boulders on meso-scale periglacial-aeolian landsystem in semi-arid Antarctic environment, James Ross Island, Antarctic Peninsula. *Cuadernos de Investigacion Geografica*. https://doi.org/10.18172/cig.3800

Kociánová, M. (2002). Otázka projevů chladných období postglaciálu v Krkonošské tundře [Problem of cold periods of climate during postglacial time in tundra area of the Giant Mts.]. *Opera Corcontica*, 39, 143–151.

Kotarba, A. (2007). Lodowce gruzowe i wały niwalne – efekt późnoglacjalnej ewolucji rzeźby Tatr [Rock Glaciers and protalus ramparts – an effect of the Lateglacial evolution of the Tatra Mountains]. *Przegląd Geograficzny*, 79(2), 199–213.

Králík, F., Sekyra, J. (1969). Geomorfologický přehled Krkonoš [Geomorphological Overview of the Krkonoše Mts.]. In Fanta, J. (Ed). *Příroda Krkonošského národního parku*. Státní zemědělské nakladatelství, Praha, Czech Republic, 59–87.

Krzemień, K., Kłapyta, P. (2017/2018). Current state of knowledge and turning points in geomorphologic studies on the present-day evolution of the Tatra Mountains. *Studia Geomorphologica Carpatho-Balcanica*, 51/52, 107–137.

Křížek, M. (2007). Periglacial landforms above the alpine timberline in the High Sudetes. In Goudie, A.S., Kalvoda, J. (Eds). *Geomorphological Variations*. P3K, Praha, Czech Republic, 313–337.

Křížek, M. (2016). Periglacial landforms of the Hrubý Jeseník Mountains. In Pánek, T., Hradecký, J. (Eds). *Landscapes and Landforms of the Czech Republic*. Springer, Cham, Switzerland, 277–289. https://doi.org/10.1007/978-3-319-27537-6_22

Křížek, M., Treml, V., Engel, Z. (2010). Czy najwyższe partie Sudetów powyżej górnej granicy lasu są domeną peryglacjalną? [Are the highest parts of the Sudetes above the timberline a periglacial domain?]. *Czasopismo Geograficzne*, 81(1–2), 75–102.

Křížek, M., Vočadlová, K., Engel, Z. (2012). Cirque overdeepening and their relationship to morphometry. *Geomorphology*, 139–140(15 February 2012), 495–505. https://doi.org/10.1016/j.geomorph.2011.11.014

Kudryavtsev, V.A., Garagulya, L.S., Kondratyeva, K.A., Melamed, V.G. (1977). *Fundamentals of Frost Forecasting in Geological Engineering Investigations. Draft Translation 606*. U.S. Army Cold Regions Research and Engineering Laboratory, Hanover, USA.

Kurylyk, B.L., Hayashi, M. (2016). Improved Stefan Equation Correction Factors to Accommodate Sensible Heat Storage during Soil Freezing or Thawing. *Permafrost and Periglacial Processes*, 27(2), 189–203. https://doi.org/10.1002/ppp.1865

Lafrenière, M.J., Lamoureux, S.F. (2019). Effects of changing permafrost conditions on hydrological processes and fluvial fluxes. *Earth-Science Reviews*, 191(April 2019), 212–223. https://doi.org/10.1016/j.earscirev.2019.02.018

Landvik, J.Y., Bondevik, S., Elverhøi, A., Fjeldskaar, W., Mangerud, J., Salvigsen, O., Siegert, M.J., Svendsen, J.-I., Vorren, T.O. (1998). The last glacial maximum of Svalbard and the Barents Sea area: ice sheet extent and configuration. *Quaternary Science Reviews*, 17(1–3), 43–75. https://doi.org/10.1016/S0277-3791(97)00066-8

Láska, K., Witoszová, D., Prošek, P. (2010). Climate conditions of the permafrost active layer development in Petuniabukta, Billefjorden, Spitsbergen. In Mertes, J.R., Christiansen, H.H., Etzelmüller, B. (Eds). *Thermal State of Frozen Ground in a Changing Climate During the IPY*. Longyearbyen, Svalbard, p. 128.

Láska, K., Witoszová, D., Prošek, P. (2012). Weather patterns of the coastal zone of Petuniabukta, central Spitsbergen in the period 2008–2010. *Polish Polar Research*, 33(4), 297–318.

Liestøl, O. (1976). Pingos, springs, and permafrost in Spitsbergen. *Norsk Polarinstitutt Årbok*, 1975, 7–29.

Lindgren, A., Hugelius, G., Kuhry, P., Christensen, T.R., Vandenberghe, J. (2016). GIS-based Maps and Area Estimates of Northern Hemisphere Permafrost Extent during the Last Glacial Maximum. *Permafrost and Periglacial Processes*, 27(1), 6–16. https://doi.org/10.1002/ppp.1851

Long, A.J., Strzelecki, M.C., Lloyd, J.M., Bryant, C.L. (2012). Dating High Arctic Holocene relative sea level changes using juvenile articulated marine shells in raised beaches. *Quaternary Science Reviews*, 48(10 August 2012), 61–66. https://doi.org/10.1016/j.quascirev.2012.06.009

Luo, D., Wu, Q., Jin, H., Marchenko, S.S., Lü, L., Gao, S. (2016). Recent changes in the active layer thickness across the northern hemisphere. *Environmental Earth Sciences*, 75(7), 555. https://doi.org/10.1007/s12665-015-5229-2

Makos, M. (2015). Deglaciation of the High Tatra Mountains. *Cuadernos de Investigación Geográfica*, 41(2), 317–335. https://doi.org/10.18172/cig.2697

Makos, M., Nitychoruk, J., Zreda, M. (2013). The Younger Dryas climatic conditions in the Za Mnichem Valley (Polish High Tatra Mountains) based on exposure-age dating and glacier-climate modelling. *Boreas*, 42(3), 745–761. https://doi.org/10.1111/j.1502-3885.2012.00298.x

Małecki, J. (2016). Accelerating retreat and high-elevation thinning of glaciers in central Spitsbergen. *The Cryosphere*, 10, 1317–1329. https://doi.org/10.5194/tc-10-1317-2016

Mangerud, J., Bolstad, M., Elgersma, A., Helliksen, D., Landvik, J.Y., Lønne, I., Lycke, A.K., Salvigsen, O., Sandahl, T., Svendsen, J.I. (1992). The Last Glacial Maximum on Spitsbergen, Svalbard. *Quaternary Research*, 38(1), 1–31. https://doi.org/10.1016/0033-5894(92)90027-G

Marks, L., Gałązka, D., Woronko, B. (2016). Climate, environment and stratigraphy of the last Pleistocene glacial stage in Poland. *Quaternary International*, 420(28 October 2016), 259–271. https://doi.org/10.1016/j.quaint.2015.07.047

Marvánek, O. (2010). Sorted patterned ground on the James Ross Island and its morphological diversity. *Acta Geographica Silesiana*, 7, 49–53.

Matsuoka, N. (2011). Climate and material controls on periglacial soil processes: Toward improving periglacial climate indicators. *Quaternary Research*, 75(2), 356–365. https://doi.org/10.1016/j.yqres.2010.12.014

Matsuoka, N., Abe, M., Ijiri, M. (2003). Differential frost heave and sorted patterned ground: Field measurements and a laboratory experiment. *Geomorphology*, 52(1–2), 73–85. https://doi.org/10.1016/S0169-555X(02)00249-0

Migała, K., Urban, G., Tomczyński, K. (2016). Long-term air temperature variation in the Karkonosze mountains according to atmospheric circulation. *Theoretical and Applied Climatology*, 125, 337–351. https://doi.org/10.1007/s00704-015-1468-0

Millar, C.I.,Westfall, R.D., Delany, D.L. (2013). Thermal and hydrologic attributes of rock glaciers and periglacial talus landforms: Sierra Nevada, California, USA. *Quaternary International*, 310(15 October 2013), 169–180. https://doi.org/10.1016/j.quaint.2012.07.019

Mlčoch, B., Nývlt, D., Mixa, P. (Eds) (2019). *Geological map of James Ross Island – Northern part 1: 25,000*. Czech Geological Survey, Praha, Czech Republic.

Morard, S., Delaloye, R., Dorthe, J. (2008). Seasonal thermal regime of a mid-latitude ventilated debris accumulation. In Kane, D.L., Hinkel, K.M. (Eds). *Proceedings of the 9th International Conference on Permafrost*. Fairbanks, USA, 1233–1238.

Morard, S., Delaloye, R., Lambiel, C. (2010). Pluriannual thermal behavior of low elevation cold talus slopes in western Switzerland. *Geographica Helvetica*, 65(2), 124–134. https://doi.org/10.5194/gh-65-124-2010

Mościcki, J.W., Kędzia, S. (2001). Investigations of mountain permafrost in the Kozia Dolinka valley, Tatra Mountains, Poland. *Norsk Geografisk Tidsskrift – Norwegian Journal of Geography*, 55(4), 235–240. https://doi.org/10.1080/00291950152746586

Nemčok, J., Bezák, V., Biely, A., Gorek, A., Gross, P., Halouzka, R., Janák, M., Kahan, Š., Kotański, Z., Lefeld, J., Mello, J., Reichwalder, P., Rackowski, W., Roniewicz, P., Ryka, W., Wieczorek, J., Zelman, J. (1994). *Geologická mapa Tatier 1 : 50 000* [Geological map of the Tatra Mts. 1 : 50 000]. State Geological Institute of Dionýz Štúr, Bratislava, Slovakia.

Niedźwiedź, T. (1992). Climate of the Tatra Mountains. *Mountain Research and Development*, 12(2), 131–146. https://doi.org/10.2307/3673787

Niessen, A., Van Horssen, P., Koster, E.A. (1992). Altitudinal zonation of selected geomorphological phenomena in an alpine periglacial area (Abisko, Northern Sweden). *Geografiska Annaler: Series A, Physical Geography*, 74(2–3), 183–196. https://doi.org/10.1080/04353676.1992.11880361

Nordli, Ø., Przybylak, R., Ogilvie, A.E.J., Isaksen, K. (2014). Long-term temperature trends and variability on Spitsbergen: the extended Svalbard Airport temperature series, 1898–2012. *Polar Research*, 33(1), 21348. https://doi.org/10.3402/polar.v33.21349

Nývlt, D., Braucher, R., Engel, Z., Mlčoch, B., ASTER Team (2014). Timing of the Northern Prince Gustav Ice Stream retreat and the deglaciation of northern James Ross Island, Antarctic Peninsula during the last glacial–interglacial transition. *Quaternary Research*, 82(2), 441–449. https://doi.org/10.1016/j.yqres.2014.05.003

Nývlt, D., Nývltová Fišáková, M., Barták, M., Stachoň, Z., Pavel, V., Mlčoch, B., Láska, K. (2016). Death age, seasonality, taphonomy and colonization of seal carcasses from Ulu Peninsula, James Ross Island, Antarctic Peninsula. *Antarctic Science*, 28(1), 3–16. https://doi.org/10.1017/S095410201500036X

Ó Cofaigh, C., Davies, B.J., Livingstone, S.J., Smith, J.A., Johnson, J.S., Hocking, E.P., Hodgson, D.A., Anderson, J.B., Bentley, M.J., Canals, M., Domack, E., Dowdeswell, J.A., Evans, J., Glasser, N.F., Hillenbrand, C.-D., Larter, R.D., Roberts, S.J., Simms, A.R. (2014). Reconstruction of ice-sheet changes in the Antarctic Peninsula since the Last Glacial Maximum. *Quaternary Science Reviews*, 100(15 September 2014), 87–110. https://doi.org/10.1016/j.quascirev.2014.06.023

Obu, J., Westermann, S., Bartsch, A., Berdnikov, N., Christiansen, H.H., Dashtseren, A., Delaloye, R., Elberling, B., Etzelmüller, B., Kholodov, A., Khomutov, A., Kääb, A., Leibman, M.O., Lewkowicz, A.G., Panda, S.K., Romanovsky, V., Way, R.G., Westergaard-Nielsen, A., Wu, T., Yamkhin, J., Zou, D. (2019a). Northern Hemisphere permafrost map based on TTOP modelling for 2000–2016 at 1 km^2 scale. *Earth-Science Reviews*, 193(June 2019), 299–316. https://doi.org/10.1016/j.earscirev.2019.04.023

Obu, J., Westermann, S., Kääb, A., Bartsch, A. (2019b). *Ground Temperature Map, 2000–2016, Andes, New Zealand and East African Plateau Permafrost*. University of Oslo, PANGAEA. https://doi.org/10.1594/PANGAEA.905512

Obu, J., Westermann, S., Kääb, A., Bartsch, A. (2019c). *Ground Temperature Map, 2000–2017, Antarctic*. University of Oslo, PANGAEA. https://doi.org/10.1594/PANGAEA.902576

Oliva, M., Navarro, F., Hrbáček, F., Hernández, A., Nývlt, D., Pereira, P., Ruiz-Fernández, J., Trigo, R. (2017). Recent regional climate cooling on the Antarctic Peninsula and associated impacts on the cryosphere. *Science of The Total Environment*, 580(15 February 2017), 210–223. https://doi.org/10.1016/j.scitotenv.2016.12.030

Onaca, A., Ardelean, F., Urdea, P., Magori, B. (2017). Southern Carpathian rock glaciers: Inventory, distribution and environmental controlling factors. *Geomorphology*, 293, Part B(15 September 2017), 391–404. https://doi.org/10.1016/j.geomorph.2016.03.032

Pánek, T., Engel, Z., Mentlík, P., Braucher, R., Břežný, M., Škarpich, V., Zondervan, A. (2016). Cosmogenic age constraints on post-LGM catastrophic rock slope failures in the Tatra Mountains (Western Carpathians). *Catena*, 138(March 2016), 52–67. https://doi.org/10.1016/j.catena.2015.11.005

Parkhomenko, E.I. (1967). *Electrical Properties of Rocks*. Plenum Press, New York, USA.

Peterson, R.A., Krantz, W.B. (2008). Differential frost heave model for patterned ground formation: Corroboration with observations along a North American arctic transect. *Journal of Geophysical Research: Biogeosciences*, 113, G03S04. https://doi.org/10.1029/2007JG000559

Péwé, T.L. (1983). Alpine Permafrost in the Contiguous United States: A Review. *Arctic and Alpine Research*, 15(2), 145–156.

Ping, C.L., Jastrow, J.D., Jorgenson, M.T., Michaelson, G.J., Shur, Y.L. (2015). Permafrost soils and carbon cycling. *Soil*, 1, 147–171. https://doi.org/10.5194/soil-1-147-2015

Pińskwar, I., Choryński, A., Graczyk, D., Kundzewicz, Z.W. (2019). Observed changes in precipitation totals in Poland. *Geografie*, 124(3), 237–264.

Plesník, P. (1971). *Horná hranica lesa vo Vysokých a Belanských Tatrách* [Upper Timberline in the High and Belianske Tatra Mts.]. Vydavateľstvo slovenskej akadémie vied, Bratislava, Slovakia.

Popescu, R., Vespremeanu-Stroe, A., Onaca, A., Vasile, M., Cruceru, N., Pop, O. (2017). Low-altitude permafrost research in an overcooled talus slope–rock glacier system in the Romanian Carpathians (Detunata Goală, Apuseni Mountains). *Geomorphology*, 295(15 October 2017), 840–854. https://doi.org/10.1016/j.geomorph.2017.07.029

Prach, K., Klimešová, J., Košnar, J., Redčenko, O., Hais, M. (2012). Variability of contemporary vegetation around Petuniabukta, central Spitsbergen. *Polish Polar Research*, 33(4), 383–394.

Pribullová, A., Chmelík, M., Pecho, J. (2013). Air Temperature Variability in the High Tatra Mountains. In Kozák, J., Ostapowicz, K., Bytnerowicz, A., Wyżga, B. (Eds). *The Carpathians: Integrating Nature and Society Towards Sustainability*. Springer, Berlin, Germany, 111–130. https://doi.org/10.1007/978-3-642-12725-0_9

Rachlewicz, G., Styszyńska, A. (2007). Porównanie przebiegu temperatury powietrza w Petuniabukta i Svalbard-Lufthavn (Isfjord, Spitsbergen) w latach 2001–2003 [Comparison of the course of air temperature in Petuniabukta and Svalbard-Lufthavn (Isfjord, Spitsbergen) in the years 2001–2003]. *Problemy Klimatologii Polarnej*, 17, 121–134.

Rachlewicz, G., Szczuciński, W., Ewertowski, M. (2007). Post-"Little Ice Age" retreat rates of glaciers around Billefjorden in central Spitsbergen, Svalbard. *Polish Polar Research*, 28(3), 159–186.

Rachlewicz, G., Szczuciński, W. (2008). Changes in thermal structure of permafrost active layer in a dry polar climate, Petuniabukta, Svalbard. *Polish Polar Research*, 29(3), 261–278.

Rączkowska, Z. (2007). *Współczesna rzeźba peryglacjalna wysokich gór Europy* [Present-day periglacial relief in high mountains of Europe]. Polish Academy of Sciences, Warszawa, Poland.

Ramos, M., Vieira, G., de Pablo, M.A., Molina, A., Abramov, A., Goyanes, G. (2017). Recent shallowing of the thaw depth at Crater Lake, Deception Island, Antarctica (2006–2014). *Catena*, 149, Part 2(February 2017), 519–528. https://doi.org/10.1016/j.catena.2016.07.019

Ray, R.J., Krantz, W.B., Caine, T.N., Gunn, R.D. (1983). A Model for Sorted Patterned-Ground Regularity. *Journal of Glaciology*, 29(102), 317–337. https://doi.org/10.3189/S0022143000008376

Riseborough, D., Shiklomanov, N., Etzelmüller, B., Gruber, S., Marchenko, S. (2008). Recent Advances in Permafrost Modelling. *Permafrost and Periglacial Processes*, 19(2), 137–156. https://doi.org/10.1002/ppp.615

Romanovsky, V.E., Smith, S.L., Christiansen, H.H. (2010). Permafrost Thermal State in the Polar Northern Hemisphere during the International Polar Year 2007–2009: a Synthesis. *Permafrost and Periglacial Processes*, 21(2), 106–116. https://doi.org/10.1002/ppp.689

Ruiz-Fernández, J., Oliva, M., Nývlt, D., Cannone, N., García-Hernández, C., Guglielmin, M., Hrbáček, F., Roman, M., Fernández, S., López-Martínez, J., Antoniades, D. (2019). Patterns of spatio-temporal paraglacial response in the Antarctic Peninsula region and associated ecological implications. *Earth-Science Reviews*, 192(May 2019), 379–402. https://doi.org/10.1016/j.earscirev.2019.03.014

Schrott, L., Sass, O. (2008). Application of field geophysics in geomorphology: Advances and limitations exemplified by case studies. *Geomorphology*, 93(1–2), 55–73. https://doi.org/10.1016/j.geomorph.2006.12.024

Schuur, E.A.G., McGuire, A.D., Schädel, C., Grosse, G., Harden, J.W., Hayes, D.J., Hugelius G., Koven, C.D., Kuhry, P., Lawrence, D.M., Natali, S.M., Olefeldt, D., Romanovsky, V.E., Schaefer, K., Turetsky, M.R., Treat C.C., Vonk, J.E. (2015). Climate change and the permafrost carbon feedback. *Nature*, 520, 171–179. https://doi.org/10.1038/nature14338

Sekyra, J., Sekyra, Z. (1995). Recent Cryogenic processes. In Soukupová, L., Kociánová, M., Jeník, J., Sekyra, J. (Eds). *Arctic-alpine tundra in the Krkonoše, the Sudetes, Opera Corcontica*, 32, 31–37.

Sekyra, J., Kociánová, M., Štursová, H., Kalenská, J., Dvořák, I., Svoboda, M. (2002). Frost phenomena in relationship to mountain pine. *Opera Corcontica*, 39, 69–114.

Smith, M.W., Riseborough, D.W. (2002). Climate and the Limits of Permafrost: A Zonal Analysis. *Permafrost and Periglacial Processes*, 13(1), 1–15. https://doi.org/10.1002/ppp.410

Svendsen, J.I., Mangerud, J. (1997). Holocene glacial and climatic variations on Spitsbergen, Svalbard. *The Holocene*, 7(1), 45–57. https://doi.org/10.1177/095968369700700105

Stan, D., Stan-Kłeczek I., Kania M. (2017). Geophysical approach to the study of a periglacial blockfield in a mountain area (Ztracené kameny, Eastern Sudetes, Czech Republic). *Geomorphology*, 293, Part B(15 September 2017), 380–390. https://doi.org/10.1016/j.geomorph.2016.12.004

Stefan, J. (1891). Über die Theorie der Eisbildung, insbesondere über die Eisbildung im Polarmeere. *Annalen der Physik*, 278(2), 269–286. https://doi.org/10.1002/andp.18912780206

Stiegler, C., Rode, M., Sass, O., Otto, J.-C. (2014). An Undercooled Scree Slope Detected by Geophysical Investigations in Sporadic Permafrost below 1000 M ASL, Central Austria. *Permafrost and Periglacial Processes*, 25(3), 194–207. https://doi.org/10.1002/ppp.1813

Strzelecki, M.C., Long, A.J., Lloyd, J.M. (2017). Post-Little Ice Age Development of a High Arctic Paraglacial Beach Complex. *Permafrost and Periglacial Processes*, 28(1), 4–17. https://doi.org/10.1002/ppp.1879

Šafanda, J., Rajver, D. (2001). Signature of the last ice age in the present subsurface temperatures in the Czech Republic and Slovenia. *Global and Planetary Change*, 29(3–4), 241–257. https://doi.org/10.1016/S0921-8181(01)00093-5

Šebesta, J., Treml, V. (1976). Glacigenní a nivační modelace údolí a údolních uzávěrů Krkonoš [Glacigenic and nivation modelling of valleys and valley heads of the Krkonoše Mts.]. *Opera Corcontica*, 13, 7–44.

Švajda, J., Solár, J., Janiga, M., Buliak, M. (2011). Dwarf Pine (*Pinus mugo*) and Selected Abiotic Habitat Conditions in the Western Tatra Mountains. *Mountain Research and Development*, 31(3), 220–228. https://doi.org/10.1659/MRD-JOURNAL-D-09-00032.1

Telford, W.M., Geldart, L.P., Sheriff, R.E. (1990). *Applied Geophysics*. Cambridge University Press, Cambridge, UK.

Tóth, M., Magyari, E.K., Brooks, S.J., Braun, M., Buczkó, K., Bálint, M., Heiri, O. (2012). A chironomid-based reconstruction of late glacial summer temperatures in the southern Carpathians (Romania). *Quaternary Research*, 77(1), 122–131. https://doi.org/10.1016/j.yqres.2011.09.005

Traczyk, A. (2004). Late Pleistocene evolution of periglacial and glacial relief in the Karkonosze Mountains: new hypotheses and research perspectives. *AUC Geographica*, 39(1), 59–72.

Traczyk, A., Migoń, P. (2000). Cold-climate landform patterns in the Sudetes. Effects of lithology, relief and glacial history. *AUC Geographica*, 35, Supplementum, 185–210.

Treml, V., Migoń, P. (2015). Controlling factors limiting timberline position and shifts in the Sudetes: A review. *Geographia Polonica*, 88(2), 55–70. https://doi.org/10.7163/GPol.0015

Turner, J., Lu, H., White, I., King, J.C., Phillips, T., Scott Hosking, J., Bracegirdle, T.J., Marshall, G.J., Mulvaney, R., Deb, P. (2016). Absence of 21st century warming on Antarctic Peninsula consistent with natural variability. *Nature*, 535(7612), 411–415. https://doi.org/10.1038/nature18645

Uxa, T., Mida, P. (2016). First results from thermal investigations of rock glaciers in the Slovak High Tatra Mountains, Western Carpathians. In Günther, F., Morgenstern, A. (Eds). *Proceedings of the 11th International Conference on Permafrost*. Potsdam, Germany, 1060–1061.

Uxa, T., Mida, P. (2017). Ground surface thermal regime of rock glaciers in the High Tatra Mts., Slovakia. *Geophysical Research Abstracts*, 19, EGU2017–1740.

Vandenberghe, J. (2001). Permafrost During the Pleistocene in North West and Central Europe. In Paepe, R., Melnikov, V.P., Van Overloop, E., Gorokhov, V.D. (Eds). *Permafrost Response on Economic Development, Environmental Security and Natural Resources*. Springer, Dordrecht, Netherlands, 185–194.

Vandenberghe, J., French, H.M., Gorbunov, A., Marchenko, S., Velichko, A.A., Jin, H., Cui, Z., Zhang, T., Wan, X. (2014). The Last Permafrost Maximum (LPM) map of the Northern Hemisphere: permafrost extent and mean annual air temperatures, 25–17 ka BP. *Boreas*, 43(3), 652–666. https://doi.org/10.1111/bor.12070

van Everdingen, R.O. (2005). *Multi-Language Glossary of Permafrost and Related Ground-Ice Terms*. Arctic Institute of North America, University of Calgary, Calgary, Canada.

Van Vliet-Lanoë, B. (1991). Differential frost heave, load casting and convection: Converging mechanisms; a discussion of the origin of cryoturbations. *Permafrost and Periglacial Processes*, 2(2), 123–139. https://doi.org/10.1002/ppp.3430020207

Vieira, G., Bockheim, J., Guglielmin, M., Balks, M., Abramov, A.A., Boelhouwers, J., Cannone, N., Ganzert, L., Gilichinsky, D.A., Goryachkin, S., López-Martínez, J., Meiklejohn, I., Raffi, R., Ramos, M., Schaefer, C., Serrano, E., Simas, F., Sletten, R., Wagner, D. (2010). Thermal State of Permafrost and Active-layer Monitoring in the Antarctic: Advances During the International Polar Year 2007–2009. *Permafrost and Periglacial Processes*, 21(2), 182–197. https://doi.org/10.1002/ppp.685

Warburton, J. (2013). Patterned Ground and Polygons. In Shroder, J., Giardino, R., Harbor, J. (Eds). *Treatise on Geomorphology, Vol. 8, Glacial and Periglacial Geomorphology*. Elsevier, Amsterdam, Netherlands, 298–312. https://doi.org/10.1016/B978-0-12-374739-6.00213-X

Washburn, A.L. (1956). Classification of patterned ground and review of suggested origins. *Geological Society of America Bulletin*, 67(7), 823–866. https://doi.org/10.1130/0016-7606(1956)67[823:COPGAR]2.0.CO;2

Washburn, A.L. (1979). *Geocryology: A Survey of Periglacial Processes and Environments*. Edward Arnold, London, UK.

Washburn, A.L. (1980). Permafrost features as evidence of climatic change. *Earth-Science Reviews*, 15(4), 327–402. https://doi.org/10.1016/0012-8252(80)90114-2

Wicky, J., Hauck, C. (2017). Numerical modelling of convective heat transport by air flow in permafrost talus slopes. *The Cryosphere*, 11, 1311–1325. https://doi.org/10.5194/tc-11-1311-2017

Wilhelm, K.R., Bockheim, J.G., Kung, S. (2015). Active Layer Thickness Prediction on the Western Antarctic Peninsula. *Permafrost and Periglacial Processes*, 26(2), 188–199. https://doi.org/10.1002/ppp.1845

Wilhelm, K., Bockheim, J. (2016). Influence of soil properties on active layer thermal propagation along the western Antarctic Peninsula. *Earth Surface Processes and Landforms*, 41(11), 1550–1563. https://doi.org/10.1002/esp.3926

Wilhelm, K., Bockheim, J. (2017). Reply to Uxa (2016) Discussion on Active Layer Thickness Prediction on the Western Antarctic Peninsula by Wilhelm *et al*. (2015). *Permafrost and Periglacial Processes*, 28(2), 499-–503. https://doi.org/10.1002/ppp.1923

Winkler, S., Matthews, J.A., Mourne, R.W., Wilson, P. (2016). Schmidt-hammer exposure ages from periglacial patterned ground (sorted circles) in Jotunheimen, Norway, and their interpretative problems. *Geografiska Annaler: Series A, Physical Geography*, 98(3), 265–285. https://doi.org/10.1111/geoa.12134

Winkler, S., Matthews, J.A., Haselberger, S., Hill, J.L., Mourne, R.W., Owen, G., Wilson, P. (2020). Schmidt-hammer exposure-age dating (SHD) of sorted stripes on Juvflye, Jotunheimen (central South Norway): Morphodynamic and palaeoclimatic implications. *Geomorphology*, 353(15 March 2020), 107014. https://doi.org/10.1016/j.geomorph.2019.107014

Zacharda, M., Gude, M., Růžička, V. (2007). Thermal Regime of Three Low Elevation Scree Slopes in Central Europe. *Permafrost and Periglacial Processes*, 18(3), 301–308. https://doi.org/10.1002/ppp.598

Zasadni, J., Kłapyta, P. (2009). An attempt to assess the modern and the Little Ice Age climatic snowline altitude in the Tatra Mountains. *Landform Analysis*, 10, 124–133.

Zasadni, J., Kłapyta, P. (2014). The Tatra Mountains during the Last Glacial Maximum. *Journal of Maps*, 10(3), 440–456. https://doi.org/10.1080/17445647.2014.885854

Zasadni, J. Kłapyta, P., Broś, E., Ivy-Ochs, S., Świąder, A., Christl, M., Balážovičová, L. (2020). Latest Pleistocene glacier advances and post-Younger Dryas rock glacier stabilization in the Mt. Kriváň group, High Tatra Mountains, Slovakia. *Geomorphology*, 358(1 June 2020), 107093. https://doi.org/10.1016/j.geomorph.2020.107093

Zhang, T., Barry, R.G., Knowles, K., Heginbottom, J.A., Brown, J. (2008). Statistics and characteristics of permafrost and ground-ice distribution in the Northern Hemisphere. *Polar Geography*, 31(1–2), 47–68. https://doi.org/10.1080/10889370802175895

Zuber, A., Weise, S.M., Motyka, J., Osenbrück, K., Różański, K. (2004). Age and flow pattern of groundwater in a Jurassic limestone aquifer and related Tertiary sands derived from combined isotope, noble gas and chemical data. *Journal of Hydrology*, 286(1–4), 87–112. https://doi.org/10.1016/j.jhydrol.2003.09.004

Żmudzka, E. (2011). Contemporary Climate Changes in the High Mountain Part of the Tatras. *Miscellanea Geographica – Regional Studies on Development*, 15(1), 93–102. https://doi.org/10.2478/v10288-012-0005-6

Žák, K., Richter, D.K., Filippi, M., Živor, R., Deininger, M., Mangini, A., Scholz, D. (2012). Coarsely crystalline cryogenic cave carbonate – a new archive to estimate the Last Glacial minimum permafrost depth in Central Europe. *Climate of the Past*, 8, 1821–1837. https://doi.org/10.5194/cp-8-1821-2012

7 Supplements

7.1 Paper I

Křížek, M., Krause, D., **Uxa, T.**, Engel, Z., Treml, T., Traczyk, A. (2019). Patterned ground above the alpine timberline in the High Sudetes, Central Europe. *Journal of Maps*, 15(2), 563–569. https://doi.org/10.1080/17445647.2019.1636890

Journal Citation Reports 2018: IF=1.836, Q3(32/50) in Geography Physical.

Citations as of 9 June 2020: Web of Science=1, Scopus=1, Google Scholar=1, ResearchGate=1.

JOURNAL OF MAPS
2019, VOL. 15, NO. 2, 563–569
https://doi.org/10.1080/17445647.2019.1636890

Taylor & Francis
Taylor & Francis Group

Science

OPEN ACCESS Check for updates

Patterned ground above the alpine timberline in the High Sudetes, Central Europe

Marek Křížek [a], David Krause [a,b], Tomáš Uxa [a,c], Zbyněk Engel [a], Václav Treml [a] and Andrzej Traczyk [d]

[a]Department of Physical Geography and Geoecology, Faculty of Science, Charles University, Praha, Czech Republic; [b]The Krkonoše Mountains National Park Administration, Vrchlabí, Czech Republic; [c]Department of Geothermics, Institute of Geophysics, Academy of Sciences of the Czech Republic, Praha, Czech Republic; [d]Department of Geomorphology, Faculty of Earth Sciences and Environmental Management, University of Wrocław, Wrocław, Poland

ABSTRACT

Patterned ground in mountainous areas has a high palaeogeographic significance as it is associated with cold environments and frequently with permafrost conditions. Most patterned ground (i.e. sorted polygons, sorted nets, sorted stripes) in the High Sudetes is overgrown by vegetation and is relict. However, wind-blown summit areas with low snow cover allow for the activity of sorted circles, earth and peat hummocks, and some non-sorted stripes. The extent of patterned ground above the alpine timberline in the High Sudetes presented here is based on detailed field geomorphologic mapping. Patterned ground occurs on summit planation surfaces and surrounding gently sloping terrain, and covers 5.23 km^2. Sorted polygons are the highest-elevated patterned-ground type. The spatial distribution of patterned ground is shown in the map, which could be helpful for future research of the Quaternary geomorphologic evolution of the mountain landscape and for nature protection planning in the High Sudetes.

ARTICLE HISTORY
Received 10 January 2019
Accepted 24 June 2019

KEYWORDS
Patterned ground; sorted polygons; earth hummocks; High Sudetes; Central Europe

1. Introduction

The term patterned ground refers to a wide group of periglacial landforms showing more or less regular surface geometric patterning in the form of circles, polygons, irregular nets or stripes (e.g. Ballantyne, 2018; French, 2017; Warburton, 2013; Washburn, 1979). Depending on the presence or absence of particle sorting, patterned ground is genetically divided into sorted and non-sorted varieties (Washburn, 1956). Sorted patterned ground consists of fine-grained cells bordered by mostly vertically-oriented coarser clasts. Sorted polygons or nets occur on flat or gently sloping ground (3–6°), but tend to elongate downslope due to solifluction, and on steeper slopes (more than 4–11°) they evolve into sorted stripes or steps (Goldthwait, 1976). Small-scale sorted patterns usually form within the seasonally frozen ground (Haugland, 2004; Matthews, Shakesby, Berrisford, & McEwen, 1998), but large sorted polygons and nets are considered to be associated with the permafrost environment (French, 2017). Non-sorted patterned ground is defined by microrelief and/or vegetation cover (Ballantyne, 2018; French, 2017; Washburn, 1979). Semi-circular, dome-shaped (hummocky) non-sorted patterned ground arising on flat surfaces or gentle slopes is commonly named as earth or peat hummocks (e.g. Grab, 2005; Treml, Křížek, & Engel, 2010; Van Vliet-Lanoë & Seppälä, 2002). Likewise, earth hummocks turn to non-sorted stripes as a result of solifluction on steeper slopes (Washburn, 1979). These stripes are sometimes termed hummock stripes or relief stripes (Ballantyne, 2018). Non-sorted patterned ground also frequently forms within the permafrost active layer, but analogously to small-scale sorted patterned ground, they may form in the seasonally frozen ground as well (Ballantyne, 1996; French, 2017).

Different patterned-ground types require distinct climate conditions, and this is reflected in their spatial and altitudinal distribution (Harris, 1982; Jahn, 1979; Niessen, Van Horssen, & Koster, 1992; Washburn, 1970) and morphology (Křížek & Uxa, 2013; Uxa, Mida, & Křížek, 2017), but they could be modified by lithology, grain size distribution, depth of groundwater table, or slope angle etc. Thus, the relict patterned ground can be used to reconstruct permafrost and climate history of the region, especially in summit areas of mountains, where other palaeoclimate indicators do not occur. Different morphology of patterned-ground types can be used as a distinguishing factor for their classification. Thus, the field mapping of different types of patterned ground is an important issue regarding both validation

CONTACT David Krause david.krause@natur.cuni.cz
Supplemental data for this article can be accessed at https://doi.org/10.1080/17445647.2019.1636890. The shapefiles of patterned-ground polygons could be provided on request by the authors.

data for an automatic classification of these periglacial phenomena (Hjort & Luoto, 2006) and palaeoenvironmental reconstruction models.

The main aim of the paper is to present the first cross-border overview map of patterned ground above the alpine timberline in the whole High Sudetes, Central Europe, based on field geomorphological mapping.

2. Study area and patterned ground in the High Sudetes

The High Sudetes, along the border of the Czech Republic and Poland, consist of three isolated mountain ranges (Main map; Front page): the Krkonoše Mts. (the Giant Mts. or the Karkonosze Mts. or Riesengebirge) on the west and the Králický Sněžník Mts. (the Masyw Śnieżnika Mts. or Glatzer Schneegebirge) and the Hrubý Jeseník Mts. (the Wysoki Jesionik Mts. or Altvatergebirge) on the east. Their highest peaks are Mt. Sněžka (1603 m asl) in the Krkonoše Mts., Mt. Praděd (1491 m asl) in the Hrubý Jeseník Mts. and Mt. Králický Sněžník (1424 m asl). The High Sudetes are Variscan fault-block ranges with deep valleys, steep slopes affecting current debris flow (Gába, 1992; Křížek, Krause, & Raschová, 2018; Pilous, 1973) and avalanche (Kociánová, Kořízek, Spusta, & Brzeziński, 2013; Krause & Křížek, 2018) activity, and summit plateaus at elevations of 1300–1555 m asl, which rise above the alpine timberline (Treml & Migoń, 2015). The western part of the High Sudetes is mainly built of metamorphic (gneiss, mica schist, phyllite, and quartzite) and plutonic rocks (granite), while the eastern part of the High Sudetes is dominated by metamorphic rocks (gneiss, mica schist, phyllite, quartzite, and calc-silicate hornfel) (Chlupáč, Brzobohatý, Kovanda, & Stráník, 2011). The summit planation surfaces, as a result of long-term denudation and remnant of peneplain, probably started to form around 75 Ma (Danišík et al., 2010) and differentially uplifted in the Neogene and Quaternary. The total Cenozoic uplift is estimated at up to 1200 m (Kopecký, 1986).

The High Sudetes were 120 km (for the Krkonoše Mts.) to 180 km (for the Hrubý Jeseník Mts. and Králický Sněžník Mts.) south of the Scandinavian ice sheet during the last Pleistocene glaciation, and thus most of their area was affected by periglacial conditions (Czudek, 2005). The summit planation surfaces were very important for the formation of glacial and periglacial landforms in the Quaternary. Snow was largely blown from the summit planation surfaces and deposited in the leeward parts of valleys where about 15 (i.e. some cirque locations are still under debate) mostly cirque glaciers and up to 5 km long valley glaciers developed in the last glacial period (MIS 2) (Engel, Braucher, Traczyk, & Laetitia, 2014; Králík & Sekyra, 1969; Křížek, Vočadlová, & Engel, 2012). The equilibrium line altitude occurred at 1060 m asl on the western part of the High Sudetes (Křížek et al., 2012), while it was at 1170 m asl on the eastern part of the High Sudetes (Křížek, 2016). On the other hand, thin snow cover on the wind-exposed summit plateaus enabled deeper ground freezing and more intensive freeze–thaw cycles, frost weathering and sorting (Křížek & Uxa, 2013; Sekyra, 1960), which led to the origin and development of sorted polygons, nets and stripes (Klementowski, 1998; Křížek, 2016; Kunský & Záruba, 1950; Prosová, 1952; Traczyk, 1996; Treml et al., 2010) during the last glacial period (Sekyra et al., 2002; Sekyra & Sekyra, 1995; Traczyk & Migoń, 2000) in the permafrost conditions (Czudek, 2005). These above-mentioned large-scale sorted polygons, nets and stripes have not been active during the Holocene (Treml et al., 2010) and most of them are currently partly or fully overgrown by graminoids. The secondary sorting centres of sorted polygons and nets, as an evidence of their possible reactivation, were observed only at the top of Mt. Luční hora, but the reactivation did not lead to any significant changes in the overall structure of sorted polygons and the secondary sorting centres are an order of magnitude smaller than the respective sorted polygons, and thus it was of marginal importance (Křížek & Uxa, 2013). However, current climatic conditions in the summit deflation areas with low snow cover allow the activity of sorted circles, earth hummocks, peat hummocks, and some non-sorted stripes (Kociánová, Štursová, Váňa, & Jankovská, 2005; Křížek, 2016; Křížek, Treml, & Engel, 2010; Prosová, 1958; Sekyra & Sekyra, 1995; Treml et al., 2010). The current mean annual air temperature in the highest parts of the High Sudetes is from 0 to +2°C (Mt. Sněžka 1881–2010: +0.5°C; Migała, Urban, & Tomczyński, 2016; Mt. Praděd 1960–1990: +1.7°C; Coufal, Míková, & Langová, 1992) and mean annual precipitation increases with altitude about 1500 mm (Jeník & Sekyra, 1995), but there is no credible evidence of near-surface permafrost occurrence in the patterned-ground areas in the High Sudetes (Křížek, 2016; Uxa et al., 2019). The study area is situated in above the alpine timberline defined by Treml and Migoń (2015), and its area is 45.78 km^2 (the Krkonoše Mts. 38.73 km^2, the Králický Sněžník Mts. 0.78 km^2, the Hrubý Jeseník Mts. 6.27 km^2). The average elevation of the alpine timberline is located at ca 1250 m asl in the Krkonoše Mts., but in the Hrubý Jeseník Mts. and the Králický Sněžník Mts. it is above 1300 m asl because of their greater continentality (Treml & Migoń, 2015). This alpine timberline ecotone naturally lacked dwarf pine (*Pinus mugo*), which is a native species in the Krkonoše Mts. and a non-native species in the Hrubý Jeseník Mts. (Rybníček & Rybníčková, 2004). However, dwarf pine was planted near the alpine timberline in the second half of the nineteenth century, and today covers large areas above it and has gradually covered part of patterned-ground areas (Treml & Křížek, 2006).

3. Methods

3.1. Data collection

The extent of patterned ground is based on detailed field geomorphological mapping of the forest-free area above the alpine timberline in the whole High Sudetes. Each patterned-ground area was delineated by hand-held GPS device (horizontal accuracy of ±3 m) and classified into one of the following patterned-ground categories: (1) sorted polygons, (2) sorted nets, (3) sorted circles, (4) sorted stripes, (5) earth hummocks, (6) peat hummocks, and (7) non-sorted stripes (Figure 1). Trenching was used in selected localities to check the inner structure of the patterned ground and to distinguish between the sorted and non-sorted patterns. Additionally, aerial photos from 2006, 2009–2010, 2014–2015, 2017 (GEODIS and TopGis) and orthorectified aerial photographs from the year 2016 (the Czech State Administration of Land Surveying and Cadastre) supported the field

Figure 1. Examples of patterned ground in the High Sudetes. 1 – sorted polygons at Mt. Břidličná, the Hrubý Jeseník Mts.; 2 – sorted nets at the Modré sedlo Saddle, the Krkonoše Mts.; 3 – sorted circle at the Modré sedlo Saddle, the Krkonoše Mts.; 4 – sorted stripes on southern slope of Mt. Luční hora, the Krkonoše Mts.; 5 – profile through the earth hummock at Mt. Praděd, the Hrubý Jeseník Mts.; 6 – peat hummocks on the Bílá louka Meadow, the Krkonoše Mts.; 7 – non-sorted stripes on the Bílá louka Meadow, the Krkonoše Mts.

mapping and helped refine the patterned-ground boundaries. The default digital elevation model (DEM) of 1 × 1 m grid and 0.1–0.2 m vertical resolution was derived from the light detection and ranging (LiDAR) point clouds provided by the Czech State Administration of Land Surveying and Cadastre and the Polish Head Office for Geodesy and Cartography. The LiDAR-based DEM was used to derive the raster images such as hillshade, aspect and slope, which also helped to delineate the boundaries of patterned-ground areas in detail.

Morphometric parameters of each patterned-ground type were computed from the above-mentioned DEM. The basic statistics of elevation, slope angle and aspect were based on all raster cells intersecting the areas of each patterned-ground type in the three studied parts of the High Sudetes.

3.2. Map creation

The mapping results are presented in five separate maps on three pages of A1 landscape format. Each of these maps covers one separated area above the alpine timberline in the High Sudetes: the western and eastern part of the Krkonoše Mts., the Králický Sněžník Mts., and the southern and northern part of the Hrubý Jeseník Mts. The scale of all these maps is 1:14,000 and the projected coordinate system is S-JTSK – Krovak East-North (EPSG 5514). The background maps contain the DEM-derived hillshade image (standard illumination azimuth 315°, altitude 45°) and contour lines with an interval of 50 vertical metres. The names and elevations of main mountain peaks are printed. Basic topographic map colour scheme was used in the background maps (*sensu* Kraak & Ormeling, 2013). The patterned-ground areas, as the main content of the maps, are visualized in colour hatch according to each of the seven patterned-ground categories to be easily readable and distinguishable: the sorted patterns in the black hatch and the non-sorted patterns in the brown hatch. Moreover, each patterned-ground category has a unique colour to support the map legibility: (1) light yellow for sorted polygons, (2) light blue for sorted nets, (3) pink for sorted circles, (4) light green for sorted stripes, (5) light salmon for earth hummocks, (6) light beige for peat hummocks, and (7) light ocher for non-sorted stripes.

4. Mapping results and conclusions

Patterned ground of the High Sudetes comprises sorted (i.e. sorted polygons, sorted nets, sorted stripes, sorted circles) and non-sorted (earth hummocks, peat hummocks and non-sorted stripes) variety (Figure 1). The total area of patterned ground is 5.23 km^2, which represents ca 11.4% of the area above the alpine timberline in the High Sudetes. The largest areas cover sorted nets and sorted stripes, ca 2.96 km^2 (57% of the total patterned-ground area) and ca 1.86 km^2 (36% of the total patterned-ground area), respectively (Table 1). On the contrary, sorted circles cover less than 450 m^2 (0.009% of the total patterned-ground area).

Sorted circles (0.7–1.4 m in diameter) occur exclusively on flat to gently sloping surfaces (Figure 2) at the Modré sedlo Saddle (1510 m asl) and Mt. Luční hora (1555 m asl) in the Krkonoše Mts. Their initial forms (about 0.2 m in diameter) also emerge occasionally at a very limited spot at the wind-exposed top of Mt. Keprník (1423 m asl) in the Hrubý Jeseník Mts., but these small-scale sorted circles are usually trampled and damaged by tourists.

Sorted polygons (length: 1.6–10.5 m; width: 1.4–6.0 m; height: 0–0.45 m) developed mostly on gentle slopes (2–4°, Figure 2) and they are the highest-elevated patterned-ground type in the High Sudetes. More than 90% of these landforms occur in the Krkonoše Mts. (Main map; page 1, 2) between 1483 and 1551 m asl (Figure 3). In the Králický Sněžník Mts. and the Hrubý Jeseník Mts. (Main map; page 3), they occur at lower altitudes (from 1355 to 1419 m asl) because of the lower altitude of these mountain ranges in general.

Most sorted nets (length: 1.0–6.1 m; width: 0.8–4.8 m; height: 0.1–0.7 m) occur on flat surfaces to gentle slopes (1–3°, Figure 2) at altitudes from 1382 to 1462 m asl, which show no substantial variations across the High Sudetes (Figure 3). Sorted polygons and nets

Table 1. Patterned-ground types in the High Sudetes and their extents.

Patterned-ground category	High Sudetes		Krkonoše Mts.		Králický Sněžník Mts.		Hrubý Jeseník Mts.	
	Area (km^2)	Percentage	Area (km^2)	Percentage of total patterned-ground area in the High Sudetes	Area (km^2)	Percentage of total patterned-ground area in the High Sudetes	Area (km^2)	Percentage of total patterned-ground area in the High Sudetes
Sorted polygons	0.12816	2.45	0.11583	90.38	0.00033	0.26	0.01200	9.36
Sorted nets	1.86198	35.57	1.29805	69.71	0.06443	3.46	0.49950	26.83
Sorted circles	0.00045	0.00009	0.00045	100	–	–	–	–
Sorted stripes	2.96081	56.56	2.01750	68.14	0.02568	0.87	0.91763	30.99
Earth hummocks	0.01670	0.32	–	–	–	–	0.01670	100
Peat hummocks	0.07093	1.35	0.07093	100	–	–	–	–
Non-sorted stripes	0.19608	3.75	0.00865	4.41	–	–	0.18743	95.59

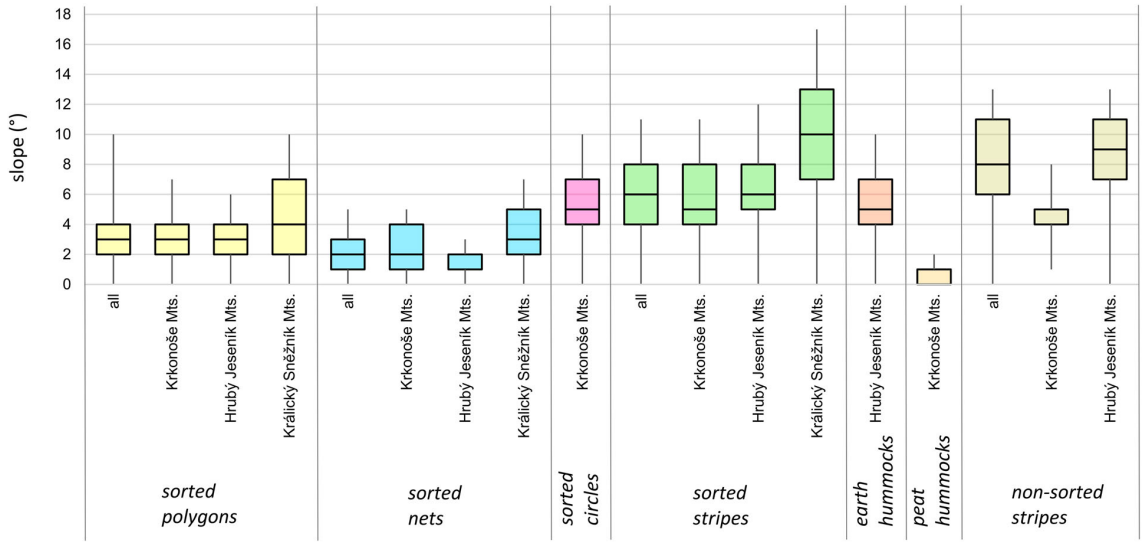

Figure 2. Boxplots showing differences in slope angle between different types of patterned ground among locations of the High Sudetes. The boxes show median values (thick horizontal line) and the first and third quartiles (bottom and top of boxes, respectively). Whiskers represent the minimum and maximum values, excluding outliers (values lying 1.5 interquartile ranges below and above the first and third quartiles, respectively).

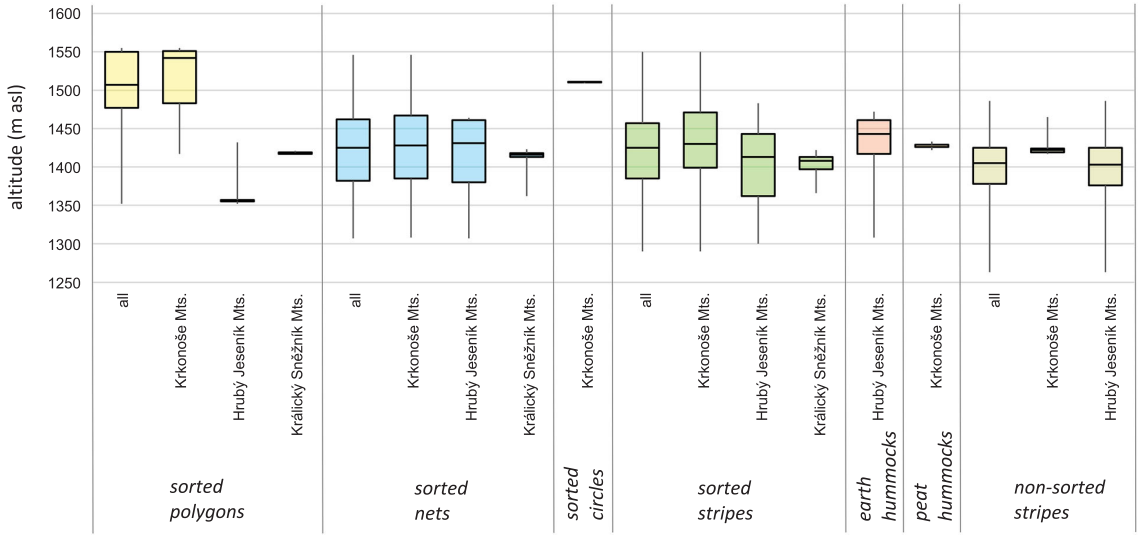

Figure 3. Boxplots showing differences in altitude between different types of patterned ground among locations of the High Sudetes. The boxes show median values (thick horizontal line) and the first and third quartiles (bottom and top of boxes, respectively). Whiskers represent minimum and maximum values, excluding outliers (values lying 1.5 interquartile ranges below and above the first and third quartiles, respectively).

elongate due to solifluction when slope angle increases, and change to sorted stripes on slopes with prevailing the angle from 4° to 8°. Sorted stripes (length: from a few metres to several tens of metres; width: 1.5–3.0 m; height: 0.1–0.2 m) are located at similar altitudes as sorted nets (1385–1457 m asl, Figure 3).

Non-sorted patterned ground occupies only 5.4% of the total patterned-ground area in the High Sudetes. While peat hummocks occur only in the Krkonoše Mts. (Main map; page 2), earth hummocks are developed exclusively in the Hrubý Jeseník Mts. (Main map; page 3). Peat hummocks (0.7–2.5 m in diameter) occur on flat surfaces (0–2°) between 1422 and 1433 m asl. Earth hummocks (length: 0.65–3.90 m; width: 0.55–2.30 m; height: 0.19–0.65 m) are mostly situated between 1417 and 1461 m asl on gentle slopes (4–7°), while on steeper slopes (6–11°) they are transformed by solifluction into non-sorted stripes (length: from a few metres to several tens of metres; width: 0.45–1.50 m; height: 0.15–0.40 m), which occur between 1376 and 1425 m asl (Figures 2 and 3).

From the viewpoint of altitudinal zonation, the sorted polygons are located at the summit parts, with more severe microclimate (*sensu* Washburn, 1979),

followed by sorted nets at lower altitudes. Since these patterned-ground types are relict, they prove the existence of mountain periglacial zonation (*sensu* Harris, 1982; Niessen et al., 1992) in the High Sudetes during the last glacial period when these sorted polygons and nets were formed (Sekyra et al., 2002; Sekyra & Sekyra, 1995; Traczyk & Migoń, 2000). In addition, sorted polygons and nets prove the presence of permafrost at the time of their formation.

This paper presents the first map of the spatial distribution of patterned ground above the alpine timberline in the whole High Sudetes. Our uniform geomorphological mapping was carried out in all sub-regions of the High Sudetes (i.e. the Krkonoše Mts., the Králický Sněžník Mts. and the Hrubý Jeseník Mts.) in both the Czech Republic and Poland (Main map). The importance of the map is for palaeogeographical and palaeoenvironmental studies as well as for future environmental planning and nature protection management (e.g. protected area zoning, hiking trail managing, designing of footpaths, removing of non-indigenous vegetation overgrowing active patterned ground, etc.). The map can also serve as a validation dataset for automatic distribution modelling of patterned ground in mountain areas using statistical models and/or machine learning techniques.

Software

Mapping of patterned ground and the DEM analyses were carried out in ArcMap 10.3 (ESRI, 2014). The R language (R Development Core Team, 2008) in the interface of RStudio 1.1.453 (RStudio Team, 2016) was used for the statistical analyses. The final layout of the map set was produced in ArcGIS Pro (ESRI, 2017).

Acknowledgements

We appreciate the administrations of the Krkonoše Mountains National Park, the Karkonosze National Park and the Jeseníky Protected Landscape Area for permissions to conduct research in strictly protected areas.

Disclosure statement

No potential conflict of interest was reported by the authors.

Funding

This work was supported by the Czech Science Foundation [grant number 17-21612S].

ORCID

Marek Křížek http://orcid.org/0000-0001-5791-571X
David Krause http://orcid.org/0000-0001-5224-8954
Tomáš Uxa http://orcid.org/0000-0001-9911-6529
Zbyněk Engel http://orcid.org/0000-0002-5209-7823
Václav Treml http://orcid.org/0000-0001-5067-3308
Andrzej Traczyk http://orcid.org/0000-0002-1641-2021

References

Ballantyne, C. K. (1996). Formation of miniature sorted patterns by shallow ground freezing: A field experiment. *Permafrost and Periglacial Processes*, *7*(4), 409–424.

Ballantyne, C. K. (2018). *Periglacial geomorphology*. Chichester: John Wiley & Sons.

Chlupáč, I., Brzobohatý, R., Kovanda, J., & Stráník, Z. (2011). *Geologická minulost České republiky* [Geological history of the Czech Republic]. Prague: Academia.

Coufal, L., Míková, T., & Langová, P. (1992). *Meteorologická data na území ČR za období 1961-90* [Meteorological data from the territory of the Czech Republic of the 1961-1990 period]. Prague: Czech Hydrometeorological Institute.

Czudek, T. (2005). *Vývoj reliéfu krajiny České republiky v kvartéru* [Quaternary landscape development of the Czech Republic]. Brno: Moravian Museum.

Danišík, M., Migoń, P., Kuhlemann, J., Evans, N. J., Dunkl, I., & Frisch, W. (2010). Thermochronological constraints on the long-term erosional history of the Karkonosze Mts., Central Europe. *Geomorphology*, *117*(1–2), 78–89. doi:10.1016/j.geomorph.2009.11.010

Engel, Z., Braucher, R., Traczyk, A., Laetitia, L., & ASTER Team. (2014). ^{10}Be exposure age chronology of the last glaciation in the Krkonoše Mountains, Central Europe. *Geomorphology*, *206*, 107–121. doi:10.1016/j.geomorph.2013.10.003

French, H. M. (2017). *The periglacial environment* (4th ed.). Hoboken: John Wiley & Sons.

Gába, Z. (1992). Mury pod Keprníkem v červenci 1991 [Debris flows under the Keprník Mt. in July 1991]. *Severní Morava*, *64*, 43–49.

Goldthwait, R. P. (1976). Frost sorted patterned ground: A review. *Quaternary Research*, *6*, 27–35. doi:10.1016/0033-5894(76)90038-7

Grab, S. (2005). Aspects of the geomorphology, genesis and environmental significance of earth hummocks (thúfur, pounus): miniature cryogenic mounds. *Progress in Physical Geography*, *29*(2), 139–155. doi:10.1191/0309133305pp440ra

Harris, C. (1982). The distribution and altitudinal zonation of periglacial landforms, Okstindan, Norway. *Zeitschrift Für Geomorphologie*, *26*(3), 283–304.

Haugland, J. E. (2004). Formation of patterned ground and fine-scale soil development within two late Holocene glacial chronosequences: Jotunheimen, Norway. *Geomorphology*, *61*, 287–301. doi:10.1016/j.geomorph.2004.01.004

Hjort, J., & Luoto, M. (2006). Modelling patterned ground distribution in Finnish Lapland: An integration of topographical, ground and remote sensing information. *Geografiska Annaler: Series A, Physical Geography*, *88*(1), 19–29. doi:10.1111/j.0435-3676.2006.00280.x

Jahn, A. (1979). The Varanger Peninsula (Norway) and the problem of the fossilisation of periglacial phenomena in Europe. *Geografiska Annaler: Series A, Physical Geography*, *61*(1–2), 1–10.

Jeník, J., & Sekyra, J. (1995). Exodynamic and climatic factors. *In Arctic-Alpine Tundra in the Krkonoše, the Sudetes. Opera Corcontica*, *32*, 1–18.

Klementowski, J. (1998). Nowe stanowisko gruntów strukturalnych na Śnieżniku [New occurrence of patterned ground on the Králický Sněžník Mt]. *Czasopismo Geograficzne*, *69*, 73–85.

Kociánová, M., Kořízek, V., Spusta, V., & Brzeziński, A. (2013). *Laviny v Krkonoších: Příroda, katastr, historie, prevence, záchrana* [Avalanches in the Krkonoše Mts.:

nature, cadastre, history, prevention, rescue]. Vrchlabí: Správa Krkonošského národního parku.

Kociánová, M., Štursová, H., Váňa, J., & Jankovská, V. (2005). Kryogenní kopečky – pounus – ve Skandinávii a v Krkonoších [Cryogennic hummocks – pounus – in Scandinavia and in the Giant Mountains]. *Opera Corcontica*, *42*, 31–55.

Kopecký, A. (1986). Neotektonika Hrubého Jeseníku a východní části Orlických hor [Neotectonics of the Hrubý Jeseník Mts. and the eastern part of the Orlické hory Mts.]. *Časopis Slezského Muzea – Vědy přírodní (A)*, *35*(2), 117–141.

Kraak, M. J., & Ormeling, F. J. (2013). *Cartography: Visualization of spatial data*. London: Routledge.

Krause, D., & Křížek, M. (2018). Dating of recent avalanche events in the Eastern High Sudetes, Czech Republic. *Quaternary International*, *470*, 166–175. doi:10.1016/j.quaint.2017.09.001

Králík, F., & Sekyra, J. (1969). Geomorfologický přehled Krkonoš [Geomorphological overview of the Krkonoše Mts.]. In J. Fanta (Ed.), *Příroda Krkonošského národního parku* [Nature of the Krkonoše National Park] (pp. 59–87). Prague: SZN.

Křížek, M. (2016). Periglacial landforms of the Hrubý Jeseník Mountains. In T. Pánek & J. Hradecký (Eds.), *Landscapes and landforms of the Czech Republic* (pp. 277–289). Cham: Springer. doi:10.1007/978-3-319-27537-6_22

Křížek, M., Krause, D., & Raschová, T. (2018). Debris flows in the Hrubý Jeseník Mountains, Bohemian Massif, Czech Republic. *Journal of Maps*, *14*(2), 428–434. doi:10.1080/17445647.2018.1486241

Křížek, M., Treml, V., & Engel, Z. (2010). Czy najwyższe partie Sudetów powyżej górnej granicy lasu są domeną peryglacjalną? [Are the highest parts of the Sudetes above timberline the periglacial domain?]. *Czasopismo Geograficzne*, *81*, 75–102.

Křížek, M., & Uxa, T. (2013). Morphology, sorting and microclimates of relict sorted polygons, Krkonoše Mountains, Czech Republic. *Permafrost and Periglacial Processes*, *24*(4), 313–321. doi:10.1002/ppp.1789

Křížek, M., Vočadlová, K., & Engel, Z. (2012). Cirque overdeepening and their relationship to morphometry. *Geomorphology*, *139–140*, 495–505. doi:10.1016/j.geomorph.2011.11.014

Kunský, J., & Záruba, Q. (1950). Periglaciální strukturní půdy v Krkonoších [Periglacial patterned ground in the Krkonoše Mts.]. *Sborník ČSSZ*, *65*(1/2), 10–14.

Matthews, J. A., Shakesby, R. A., Berrisford, M. S., & McEwen, L. J. (1998). Periglacial patterned ground on the Styggedalsbreen Glacier Foreland, Jotunheimen, southern Norway: Micro-topographic, Paraglacial and Geoecological Controls. *Permafrost and Periglacial Processes*, *9*, 147–166. doi:10.1002/(SICI)1099-1530(199804/06)9:2<147::AID-PPP278>3.0.CO;2-9

Migała, K., Urban, G., & Tomczyński, K. (2016). Long-term air temperature variation in the Karkonosze mountains according to atmospheric circulation. *Theoretical and Applied Climatology*, *125*, 337–351. doi:10.1007/s00704-015-1468-0

Niessen, A., Van Horssen, P., & Koster, E. A. (1992). Altitudinal zonation of selected geomorphological phenomena in an alpine periglacial area (Abisko, Northern Sweden). *Geografiska Annaler: Series A, Physical Geography*, *74*(2–3), 183–196.

Pilous, V. (1973). Strukturní mury v Krkonoších – I._část [Debris flows in the Giant Mountains – 1st part]. *Opera Corcontica*, *10*, 15–69.

Prosová, M. (1952). Předběžná zpráva o polygonálních půdách ve Vysokém Jeseníku [Preliminary results on sorted polygons in the Hrubý Jeseník Mts.]. *Přírodovědecký sborník Ostravského kraje*, *13*(1–2), 262–270.

Prosová, M. (1958). *Kvartér Hrubého Jeseníku (vrcholová část hlavního hřbetu)* [The Hrubý Jeseník Mts. during Quaternary (summit parts of the main ridge)] (Doctoral thesis). Faculty of Science, Charles University, Prague.

Rybníček, K., & Rybníčková, E. (2004). Pollen analyses of sediments from the summit of the Praděd range in the Hrubý Jeseník Mts. (Eastern Sudetes). *Preslia*, *76*(4), 331–347.

Sekyra, J. (1960). *Působení mrazu na půdu – Kryopedologie se zvláštním zřetelem k ČSR* [Effects of frost on soil: Cryopedology with special emphasis on Czechoslovakia]. Prague: Nakladatelství ČSAV.

Sekyra, J., Kociánová, M., Štursová, H., Kalenská, J., Dvořák, I., & Svoboda, M. (2002). Frost phenomena in relationship to mountain pine. *Opera Corcontica*, *39*, 69–114.

Sekyra, J., & Sekyra, Z. (1995). Recent cryogenic processes. In Arctic-alpine tundra in the Krkonoše, the Sudetes. *Opera Corcontica*, *32*, 31–37.

Traczyk, A. (1996). Formy i osady peryglacjalne w Masywie Śnieżnika Kłodzkiego [Periglacial landforms in the Králický Sněžník Mts.]. *Acta Universitatis Wratislaviensis*, *1808*, 111–119.

Traczyk, A., & Migoń, P. (2000). Cold-climate landform patterns in the Sudetes. Effects of lithology, relief and glacial history. *Acta Universitatis Carolinae*, *35*(Supplementum), 185–210.

Treml, V., & Křížek, M. (2006). Effects of dwarf pine (*Pinus mugo*) on patterned ground in the Czech part of the High Sudetes. *Opera Corcontica*, *43*, 45–56.

Treml, V., Křížek, M., & Engel, Z. (2010). Classification of patterned ground based on morphometry and site characteristics: A case study from the High Sudetes, Central Europe. *Permafrost and Periglacial Processes*, *21*(1), 67–77. doi:10.1002/ppp.671

Treml, V., & Migoń, P. (2015). Controlling factors limiting timberline position and shifts in the Sudetes: A review. *Geographia Polonica*, *88*(2), 55–70. doi:10.7163/GPol.0015

Uxa, T., Křížek, M., Krause, D., Hartvich, F., Tábořík, P., & Kasprzak, M. (2019). Comment on "Geophysical approach to the study of a periglacial blockfield in a mountain area (Ztracené kameny, eastern Sudetes, Czech Republic)" by Stan et al. (2017). *Geomorphology*, *328*, 231–237. doi:10.1016/j.geomorph.2018.10.010

Uxa, T., Mida, P., & Křížek, M. (2017). Effect of climate on morphology and development of sorted circles and polygons. *Permafrost and Periglacial Processes*, *28*(4), 663–674. doi:10.1002/ppp.1949

Van Vliet-Lanoë, B., & Seppälä, M. (2002). Stratigraphy, age and formation of peaty earth hummocks (pounus), Finnish Lapland. *The Holocene*, *12*(2), 187–199. doi:10.1191/0959683602hl534rp

Warburton, J. (2013). Patterned ground and polygons. In J. F. Schroder (Ed.), *Treatise on Geomorphology* (pp. 298–312). Elsevier. doi:10.1016/B978-0-12-374739-6.00213-X

Washburn, A. L. (1956). Classification of patterned ground and review of suggested origins. *Geological Society of America Bulletin*, *67*(7), 823–866.

Washburn, A. L. (1970). An approach to a genetic classification of patterned ground. *Acta Geographica Lodziensia*, *24*, 437–446.

Washburn, A. L. (1979). *Geocryology: A survey of periglacial processes and environments*. London: E. Arnold.

Patterned ground above the alpine timberline in the High Sudetes, Central Europe

Marek Křížek[a], David Krause[a,b], Tomáš Uxa[a,c], Zbyněk Engel[a], Václav Treml[a] and Andrzej Traczyk[d]

a) Department of Physical Geography and Geoecology, Faculty of Science, Charles University, Praha, Czech Republic
b) The Krkonoše Mountains National Park Administration, Vrchlabí, Czech Republic
c) Department of Geothermics, Institute of Geophysics, Academy of Sciences of the Czech Republic, Praha, Czech Republic
d) Department of Geomorphology, Faculty of Earth Sciences and Environmental Management, University of Wrocław, Wrocław, Poland

Abstract

Patterned ground in mountainous areas has a high paleogeographic significance as it is associated with cold environments and frequently with permafrost conditions. Most patterned ground (i.e. sorted polygons, sorted nets, sorted stripes) in the High Sudetes is overgrown by vegetation and is relict. However, wind-blown summit areas with low snow cover allow for the activity of sorted circles, earth and peat hummocks, and some non-sorted stripes. The extent of patterned ground above the alpine timberline in the High Sudetes presented here is based on detailed field geomorphologic mapping. Patterned ground occurs on summit planation surfaces and surrounding gently sloping terrain, and covers 5.23 km^2. Sorted polygons are the highest-elevated patterned-ground type. The spatial distribution of patterned ground is shown in the map, which could be helpful for future research of the Quaternary geomorphologic evolution of the mountain landscape and for nature protection planning in the High Sudetes.

Study Area

The High Sudetes, along the border of the Czech Republic and Poland, consist of three isolated mountain ranges: (A,B) the Krkonoše Mts. (the Giant Mts. or the Karkonosze Mts. or Riesengebirge) on the west and the Králický Sněžník Mts. (the Masyw Śnieżnika Mts. or Glatzer Schneegebirge) and the Hrubý Jeseník Mts. (the Wysoki Jesioník Mts. or Altvatergebirge) on the east. Their highest peaks are Mt. Sněžka (1603 m asl), in the Krkonoše Mts., Mt. Praděd (1491 m asl) in the Hrubý Jeseník Mts. and Mt. Králický Sněžník (1424 m asl).
The study area is situated above alpine timberline defined by Treml & Migoń (2015), and its the total area of which is 45.78 km^2 (the Krkonoše Mts. 38.73 km^2, the Králický Sněžník Mts. 0.78 km^2, the Hrubý Jeseník Mts. 6.27 km^2). The alpine timberline is located at ca 1250 m asl in the Krkonoše Mts., but in the Hrubý Jeseník Mts. and the Králický Sněžník, Mts. is above 1300 m asl because of their greater continentality (Treml, & Migoń, 2015).

Examples of patterned ground

Patterned ground is a wide group of periglacial landforms, showing more or less regular surface geometric patterning in the form of circles, polygons, irregular nets or stripes (e.g. Ballantyne, 2018; French, 2017; Warburton, 2013; Washburn, 1979). Depending on the presence or absence of particle sorting, patterned ground is genetically divided into sorted and non-sorted varieties (Washburn, 1956). Sorted patterned ground consists of fine-grained centres (cells on flat or gently sloping ground, or ridges on steeper slopes) bordered by mostly vertically-oriented coarser clasts. Small-scale sorted patterns usually form within seasonally frozen ground (Haugland, 2004), but large sorted polygons and nets are considered to be associated with the permafrost environment (French, 2017). Non-sorted patterned ground is defined by microrelief and/or vegetation cover (Ballantyne, 2018; French, 2017; Washburn, 1979).

Sorted polygons

Sorted polygons on the third highest-elevated cryoplanation terrace (1540 m asl) of Mt. Luční hora (1555 m asl) in the Krkonoše Mts. are characterised by their regular polygonal morphology with straight stony borders, slightly depressed relative to the centres.

Sorted nets

Sorted nets with irregular cells at the Modré sedlo Saddle (1510 m asl) in the Krkonoše Mts.

Sorted circles

Active sorted circles sized from 70 to 140 cm occur on wind-swept site at the Modré sedlo Saddle (1510 m asl) in the Krkonoše Mts.

Sorted stripes

Sorted stripes on southern slope of Mt. Luční hora (1555 m asl), which consist of up-domed fine-grained bands overgrown by vegetation between narrower coarse stripes elongated downslope.

Earth hummocks

Earth hummocks on wind-swept site at the top of Mt. Kepník (1423 m asl) in the Hrubý Jeseník Mts. They have small horizontal dimensions and a relatively high up-domed centres (mean height ca 40 cm).

Peat hummocks

Peat hummocks on the Bílá louka Meadow (1427 m asl) in the Krkonoše Mts. undergo shape changes connected with the segregated ice core expansion.

Non-sorted stripes

Non-sorted stripes at Mt. Kepník (1423 m asl) in the Hrubý Jeseník Mts. consist of up-domed centre, which is elongated downslope.

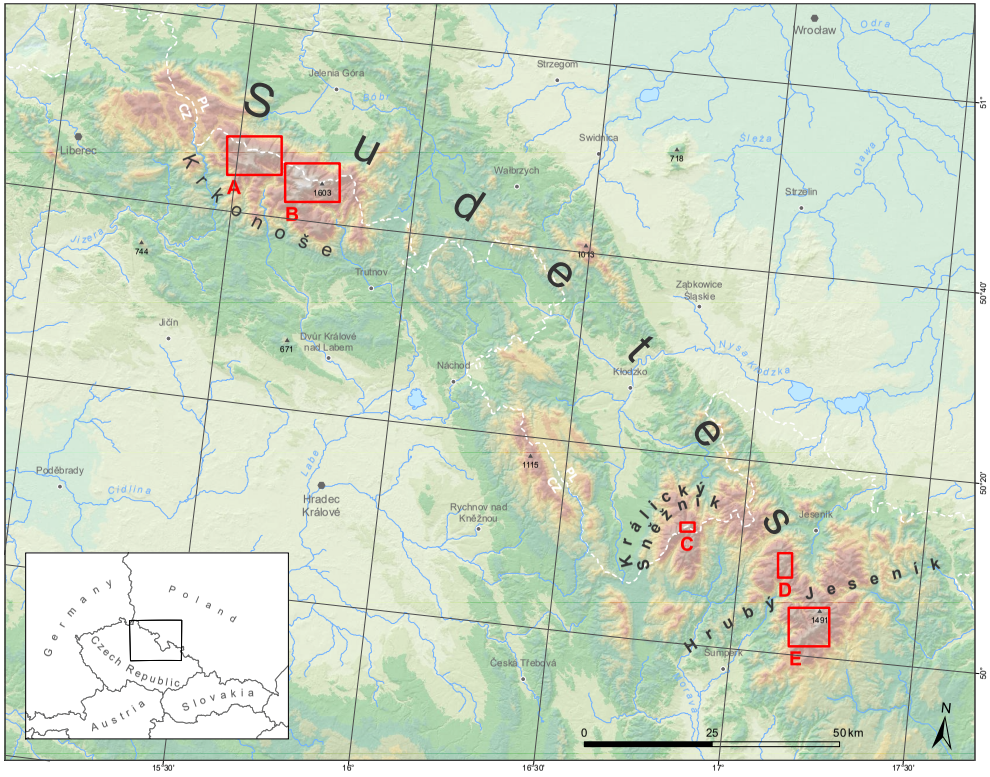

List of map set contents

References

Ballantyne, C. K. (2018). Periglacial geomorphology. Chichester: John Wiley & Sons.

French, H. M. (2017). The periglacial environment (Fourth edition). Hoboken: John Wiley & Sons.

Haugland, J. E. (2004). Formation of patterned ground and fine-scale soil development within two late Holocene glacial chronosequences: Jotunheimen, Norway. Geomorphology, 61, 287–301.

Treml, V., & Migoń, P. (2015). Controlling factors limiting timberline position and shifts in the Sudetes: A review. Geographia Polonica, 88(2), 55–70.

Warburton, J. (2013). Patterned Ground and Polygons. In J. F. Schroder (Ed.), Treatise on Geomorphology (pp. 298–312). Elsevier.

Washburn, A. L. (1956). Classification of patterned ground and review of suggested origins. Geological Society of America Bulletin, 67(7), 823–866.

Washburn, A. L. (1979). Geocryology: a survey of periglacial processes and environments. London: E. Arnold.

Acknowledgements

We appreciate the administrations of the Krkonoše Mountains National Park, the Karkonosze National Park and the Jeseníky Protected Landscape Area for permissions to conduct research in strictly protected areas.

The study was supported by the Czech Science Foundation, project no. 17-21612S.

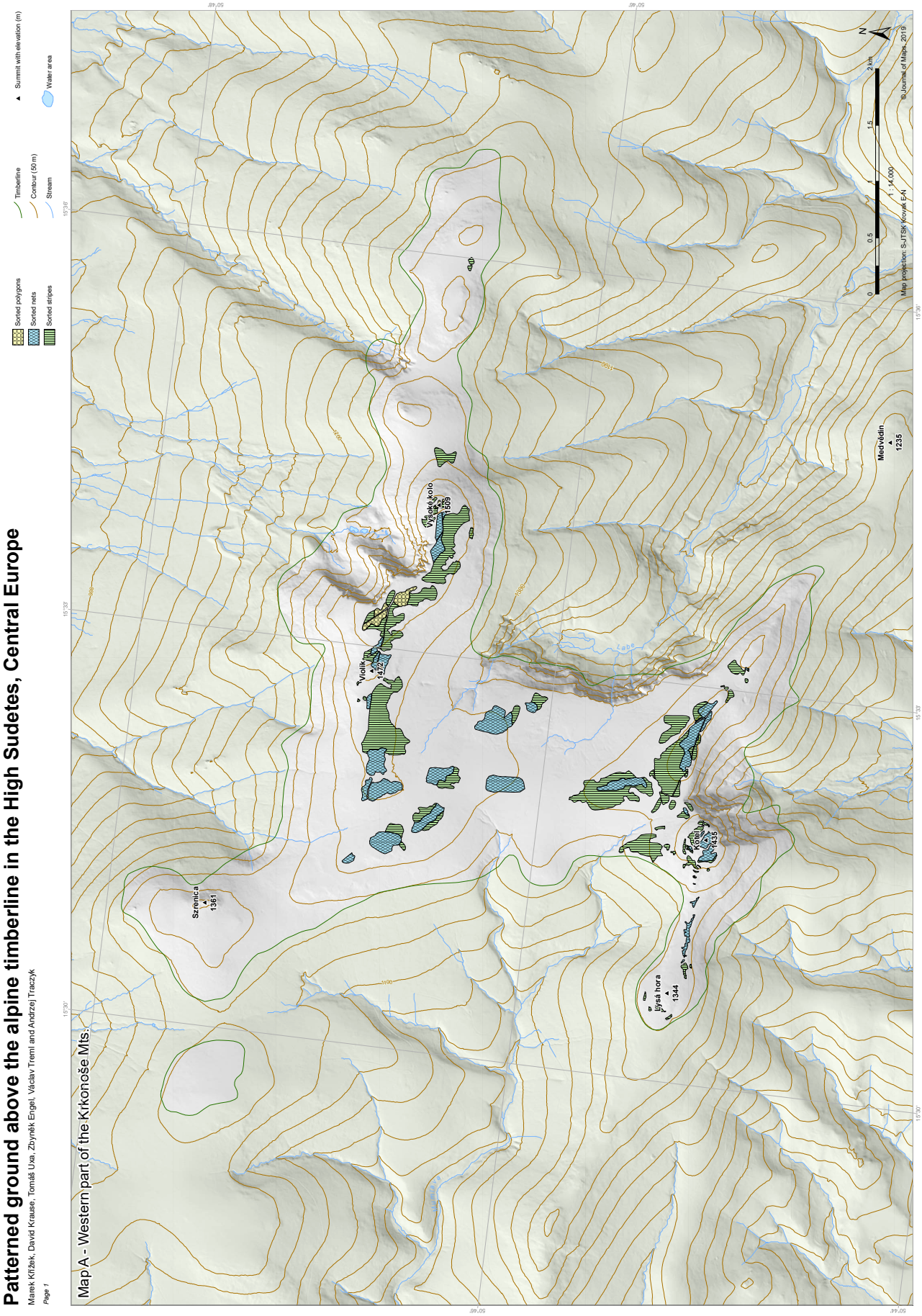
Patterned ground above the alpine timberline in the High Sudetes, Central Europe
Marek Křížek, David Krause, Tomáš Uxa, Zbyněk Engel, Václav Treml and Andrzej Traczyk
Page 1
Map A - Western part of the Krkonoše Mts.
Sorted polygons
Sorted nets
Sorted stripes
Timberline
Contour (50 m)
Stream
Summit with elevation (m)
Water area
Vysoké kolo
1509
Vrchlabská jáma
1435
Vysoká hora
1344
Medvědín
1235
Map projection: S-JTSK Krovak E-N
1 : 14,000
© Journal of Maps, 2019

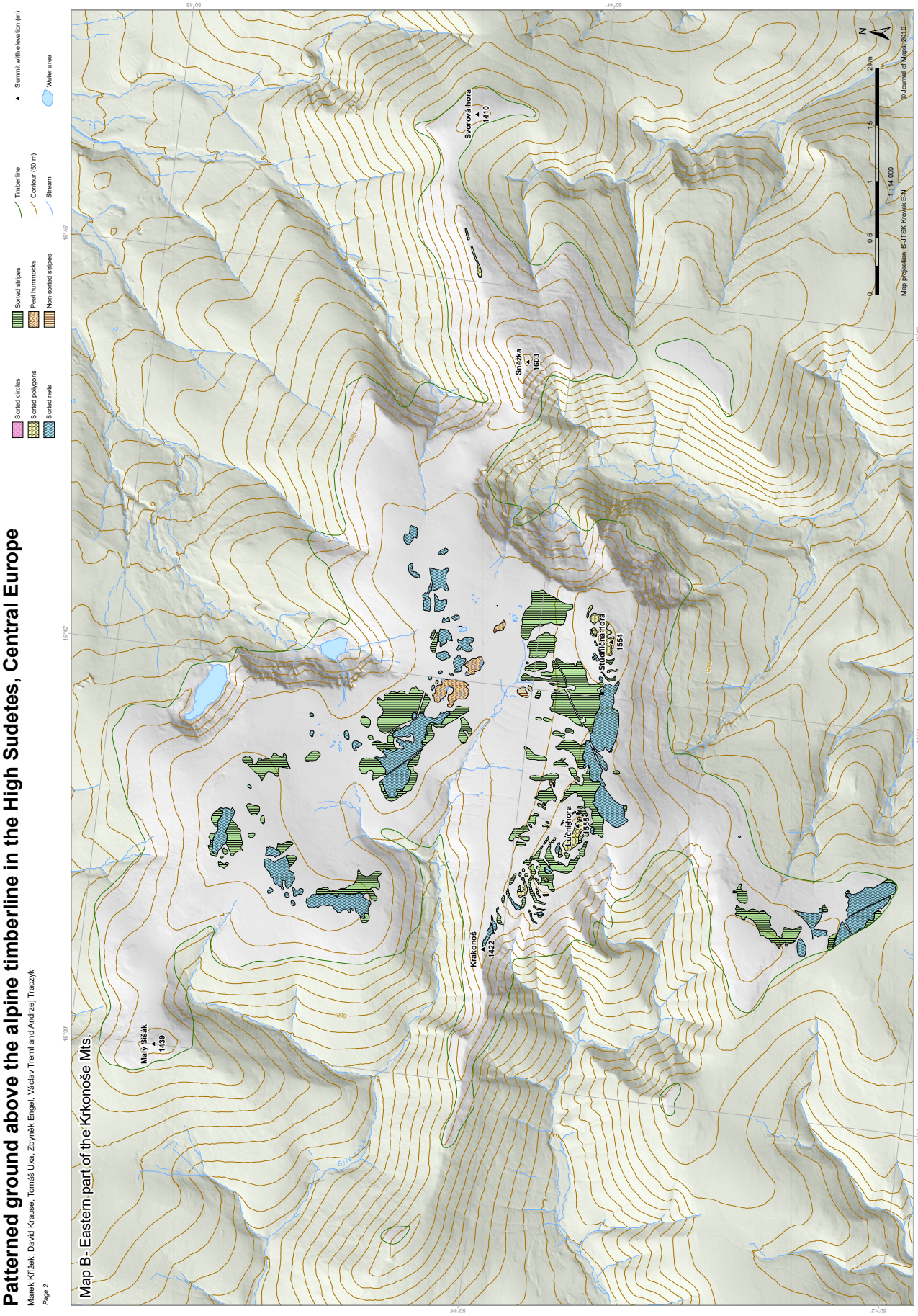
Patterned ground above the alpine timberline in the High Sudetes, Central Europe
Marek Křížek, David Kraus, Tomáš Uxa, Zbyněk Engel, Václav Treml and Andrzej Traczyk
Page 2
Map B - Eastern part of the Krkonoše Mts.
Sorted circles
Sorted polygons
Sorted nets
Sorted stripes
Peat hummocks
Non-sorted stripes
Timberline
Contour (50 m)
Stream
Summit with elevation (m)
Water area
Malý Šišák
1439
Krakonoš
1422
Studniční hora
1554
Sněžka
1603
Svorová hora
1410
N
0
0.5
1
1.5
2 km
1 : 14 000
Map projection: S-JTSK Krovak E-N
© Journal of Maps 2019

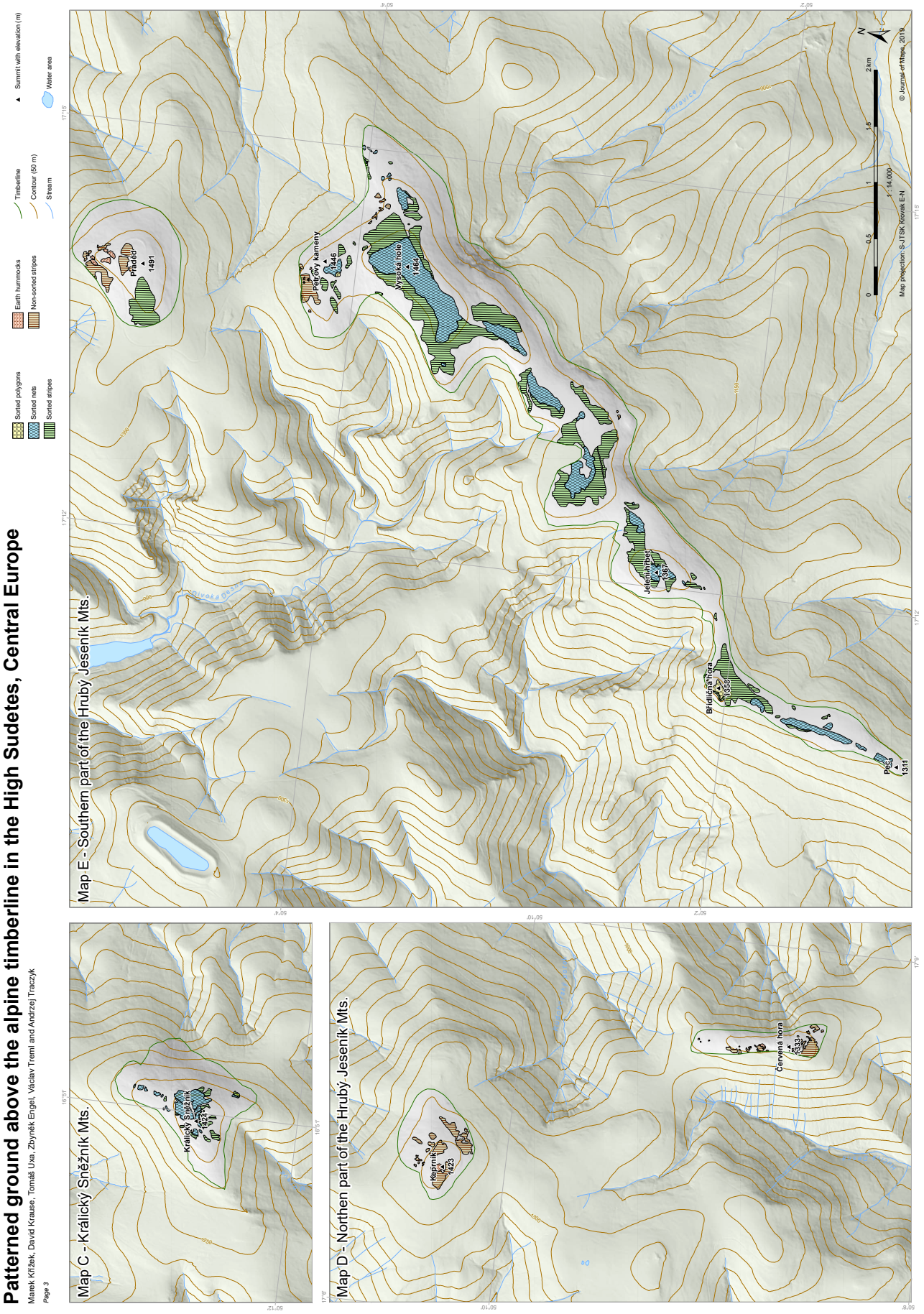
Patterned ground above the alpine timberline in the High Sudetes, Central Europe
Marek Křížek, David Krause, Tomáš Uxa, Zbyněk Engel, Václav Treml and Andrzej Traczyk
Page 3
Sorted polygons
Sorted nets
Sorted stripes
Earth hummocks
Non-sorted stripes
Timberline
Contour (50 m)
Stream
Summit with elevation (m)
Water area
Map C - Králický Sněžník Mts.
Map D - Northen part of the Hrubý Jeseník Mts.
Map E - Southern part of the Hrubý Jeseník Mts.
Králický Sněžník
1424
Nejvrchnější
1423
Červená hora
1333
Praděd
1491
Petrovy kameny
1446
Vysoká hole
1464
Jelení hřbet
1437
Břidličná hora
1369
Pec
1311
Map projection: S-JTSK Krovak E-N
1 : 14 000
0
0,5
1
1,5
2 km
© Journal of Maps, 2019

7.2 Paper II

Křížek, M., **Uxa, T.** (2013). Morphology, Sorting and Microclimates of Relict Sorted Polygons, Krkonoše Mountains, Czech Republic. *Permafrost and Periglacial Processes*, 24(4), 313–321. https://doi.org/10.1002/ppp.1789

Journal Citation Reports 2012: IF=3.049, Q1(10/45) in Geography Physical, Q1(4/47) in Geology.

Citations as of 9 June 2020: Web of Science=4, Scopus=5, Google Scholar=7, ResearchGate=9.

PERMAFROST AND PERIGLACIAL PROCESSES
Permafrost and Periglac. Process. **24**: 313–321 (2013)
Published online 11 October 2013 in Wiley Online Library
(wileyonlinelibrary.com) DOI: 10.1002/ppp.1789

Morphology, Sorting and Microclimates of Relict Sorted Polygons, Krkonoše Mountains, Czech Republic

Marek Křížek and Tomáš Uxa*

Department of Physical Geography and Geoecology, Faculty of Science, Charles University in Prague, Prague, Czech Republic

ABSTRACT

The influence of past microclimates on the morphology and distribution of clasts is considered for relict large-scale sorted polygons in the Krkonoše Mountains (Czech Republic). Sixty-two sorted polygons with an average length of 194 cm and an average height of 21.5 cm were measured at four sites on Mt Luční hora, at elevations of 1455 to 1555 m asl. The polygons consist of tabular clasts with a mean length of 11 cm at the borders and 5 cm in the interiors. Smaller polygons are better sorted because of the shorter distances for the clasts to reach their borders. Polygons with greater relative height are better sorted due to more intensive slope processes associated with differential frost heaving. Better sorted and more domed polygons at higher altitudes suggest more severe and longer-lasting microclimates suitable for the development of sorted polygons. The altitudinal gradient in polygon morphology and sorting suggests the dominant role of microclimate in the periglacial environment of the summit area of the Krkonoše Mountains during the Last Glacial/Holocene period. Polygon development probably involves positive feedback between morphology and frost susceptibility, driven by microclimate. The proposed method for evaluating frost sorting allows for rapid non-invasive assessment of sorting using modern methods including high-resolution remote sensing (especially terrestrial photogrammetry). Copyright © 2013 John Wiley & Sons, Ltd.

KEY WORDS: sorted polygons; frost sorting; morphometry; Krkonoše Mountains; central Europe

INTRODUCTION

The development of periglacial patterned ground is related to freeze-thaw cycles, the frequency and/or intensity of which is determined by regional climatic factors and site-specific factors that influence the local microclimate, such as relief, lithology, snow cover, drainage and vegetation (Washburn, 1979; Harris, 1982; Ballantyne, 2007). Prevailing wind flow is also important as it produces uneven spatial distribution of snow cover, which generates different thermal and moisture regimes (Seppälä, 2004), and therefore influences the spatial distribution and morphology of patterned ground (e.g. Luoto and Hjort, 2004, 2006; Hjort and Luoto, 2006; Grab *et al*., 2009; Treml *et al*., 2010; Feuillet *et al*., 2012). Thus, patterned ground provides a geoindicator (André, 2009) that is sensitive to climate and environmental changes (e.g. Ballantyne and Matthews, 1982, 1983; Haugland, 2004, 2006).

* Correspondence to: M. Křížek, Department of Physical Geography and Geoecology, Faculty of Science, Charles University in Prague, Prague, Czech Republic. E-mail: marek.krizek@natur.cuni.cz

The occurrence, activity or morphology of sorted patterned ground in relation to environmental conditions has been studied more frequently than the arrangement of clasts (e.g. Ballantyne and Matthews, 1982, 1983; Van Vliet-Lanoë, 1991; Kling, 1998; Matthews *et al*., 1998; Holness, 2003; Haugland, 2004, 2006; Luoto and Hjort, 2004, 2006; Hjort and Luoto, 2006; Treml *et al*., 2010; Feuillet, 2011; Feuillet *et al*., 2012; Feuillet and Mercier, 2012). For sorted circles (Harris, 1990; Grab, 1997, 2002; Kling, 1997; Holness, 2003), sorted polygons (Ballantyne and Matthews, 1983; Grab, 1997), sorted nets (Dąbski, 2005), sorted stripes (Nelson, 1982) or circle-stripe transitional forms (Sumner, 2004), most researchers have described the orientation or size distribution of clasts, but neglected the variability in clast arrangement relative to environmental conditions (Ballantyne and Matthews, 1983) or patterned-ground morphology (Kling, 1997), although the clast arrangement (as a manifestation of frost sorting) is closely related to the origin of sorted patterned ground. Clast arrangement in large-scale sorted polygons is unknown.

The aims of this paper are: (1) to determine the relations between relict large-scale sorted polygon morphology and clast distribution in the Krkonoše Mountains; (2) to determine

Received 4 October 2012
Revised 27 August 2013
Accepted 16 September 2013

the extent to which the morphology and clast distribution of the polygons were influenced by past microclimates; and (3) to present palaeoenvironmental evidence from the periglacial environment of the summit area of the Krkonoše Mountains during the Last Glacial/Holocene period.

STUDY AREA

The Krkonoše Mountains, on the border of the Czech Republic and Poland (Figure 1), are a Hercynian mountain range with planation surfaces at elevations of 1300–1555 m asl (Kunský, 1948) built by crystalline rocks (Chaloupský *et al*., 1989). The study area is located on Mt Luční hora (1555 m asl; 50°43'40"N; 15°40'57"E), close to the highest peak of the Krkonoše Mountains, Mt Sněžka (1602 m asl).

The current mean annual air temperature in the highest parts of the Krkonoše Mountains ranges from 0 to 2 °C (Mt Sněžka 1961–2000: 0.1 °C; Głowicki, 1997) and mean annual precipitation is up to 1500 mm (Jeník and Sekyra, 1995). Sorted patterned ground in the Krkonoše Mountains, including the studied sorted polygons on Mt Luční hora (Figure 2), is considered to be mostly inactive (Sekyra, 1960; Křížek *et al*., 2010). Only the sorted circles at the top of Mt Luční hora and in the Modré sedlo Saddle are active (Sekyra and Sekyra, 1995; Křížek, 2007). The sorted polygons in the Krkonoše Mountains were most likely formed during the Last Glacial period (Sekyra and Sekyra, 1995; Traczyk and Migoń, 2000; Sekyra *et al*., 2002) in the presence of permafrost (Jahn, 1977; Czudek, 2005). The study area is above the Holocene alpine timberline (Treml *et al*., 2008).

The sorted polygons studied on Mt Luční hora are 1455 to 1555 m asl, on slopes of up to 2° (Figure 1). They occur on westerly oriented cryoplanation terraces (Figure 1) on homogeneous quartzite bedrock covered by coarse sand to gravel regolith (Treml *et al*., 2010) of low frost susceptibility (*sensu* Beskow, 1935). These sites were influenced by strong westerly winds in the Last Glacial period and the Holocene (Jeník and Sekyra, 1995), as indicated by glacial cirques and snowfields leeward of the summit plateaus (Migoń, 1999). Even today these sites experience severe climatic conditions (Sekyra *et al*., 2002). Higher altitudes of Mt Luční hora are exposed to strong westerly winds which cause thinner snow cover and earlier snow melting and promote deeper ground freezing and intensive freeze-thaw cycles (Harčarik, 2002; Sekyra *et al*., 2002; Table 1). Thus, the distribution and morphology of periglacial landforms in the Krkonoše Mountains during the Last Glacial period and the Holocene were controlled by similar factors as today (Křížek *et al*., 2010), which allows us to consider altitude as a proxy measure of past microclimate.

MATERIAL AND METHODS

Morphometric Characteristics

Sixty-two randomly selected sorted polygons in the summit area (LH A – sites LH A1, LH A2, LH A3) and on the northwestern slope of Mt Luční hora (LH B; Figure 1) were studied.

The sorted polygons were characterised by length (L), width (W) and height (H) (Figure 3). The length of a sorted polygon refers to the greatest horizontal dimension. The width corresponds to the direction perpendicular to the length axis and

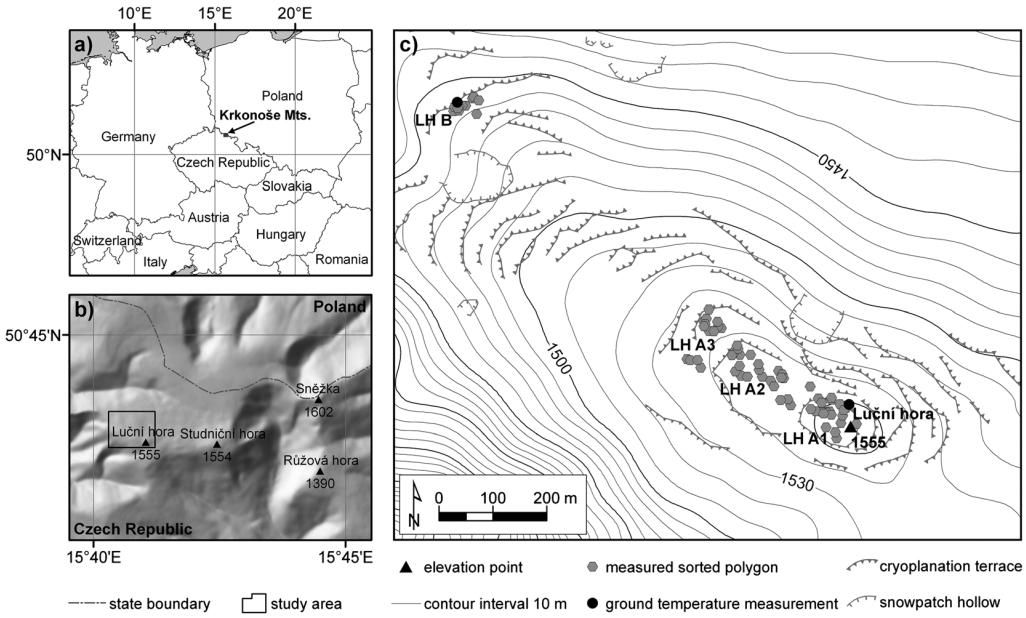

Figure 1 Location of (a) the Krkonoše Mountains; (b) the study area; and (c) the study sites (LH A1, LH A2, LH A3, LH B) with spatial distribution of relict sorted polygons and ground temperature measurements.

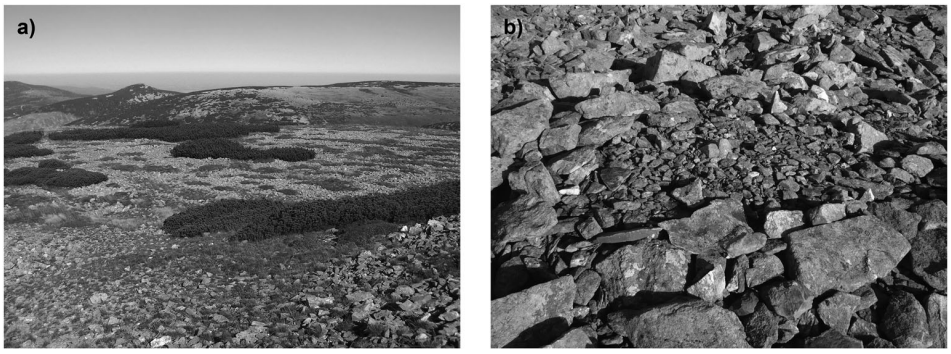

Figure 2 (a) Sorted polygons on a cryoplanation terrace of Mt Luční hora; (b) detailed view of a sorted polygon at the top of Mt Luční hora.

Table 1 Maximum snow-cover thickness and ground thermal regime at 15-cm depth within sorted polygons on the top (LH A), and at the lowest (LH B) site, of Mt Luční hora in the winter of 2010–11.

Site characteristics	LH A	LH B
Altitude (m asl)	1555	1455
Maximum snow cover thickness (cm)	21	47
Days with minimum temperature <0 °C	182	154
0 °C-crossing cycles	21	15
Minimum temperature (°C)	-8.9	-7.4
Freezing degree-days (*sensu* Kade *et al*., 2006)	497.3	332.6

crosses the centre of the polygon. The height of a sorted polygon corresponds to the difference between the lowest point on the border and the up-domed centre of the landform. The elongation index (L/W) represents the ratio of the length to the width of a sorted polygon. The relative height (H/W) (Treml *et al*., 2010) is the ratio of the height to the width of a sorted polygon.

Size and Shape of the Clasts

The size of ten randomly chosen clasts greater than 10 mm in the a-axis (the longest axis; Hubbard and Glasser, 2005) was measured at the centre of the sorted polygon (C), on the borders (B), and at one-third (1/3) and two-thirds (2/3) of the distance from the border to the centre along the length and width axes (Figure 3). In total, 7740 clasts from 62 sorted polygons were analysed.

The mean clast size ($\bar{a}$) of a sorted polygon was determined as the arithmetic mean of the lengths of the clasts located on the borders and at the one-third and two-third positions. The centres were excluded from the calculation because some sorted polygons were partly overgrown with vegetation.

In 12 of the studied sorted polygons, the dimensions of all three orthogonal axes of clasts were measured (a – the longest, b – the middle, c – the shortest; Hubbard and Glasser, 2005). These values were used to describe the clast shape, which was subsequently analysed using the TRI-PLOT spreadsheet

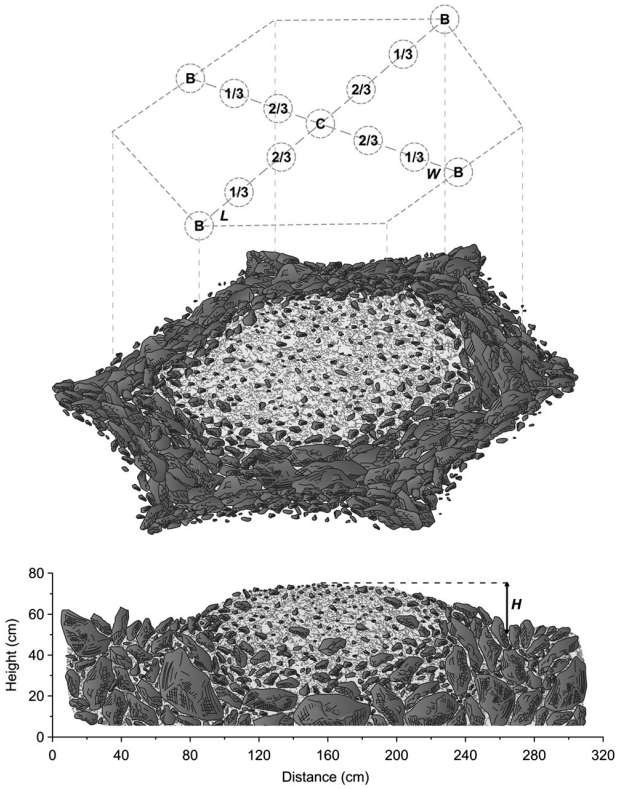

Figure 3 Measured characteristics of a sorted polygon: L = length; W = width; H = height; B = measured a-axis of ten randomly chosen clasts on the border of a polygon; 1/3 = measured a-axis of ten randomly chosen clasts at one-third of the distance from the border to the centre; 2/3 = measured a-axis of ten randomly chosen clasts at two-thirds of the distance from the border to the centre; C = measured a-axis of ten randomly chosen clasts at the centre of the polygon.

(Graham and Midgley, 2000) and classified according to Sneed and Folk (1958).

Sorting Degree

All evaluated sorted polygons had to have similar-sized clasts at the corresponding (border or one-third or two-third)

positions on the length and width axes, respectively, to preclude errors in the sorting indices due to processes unrelated to frost sorting.

The sorting index (SI) represents the degree of clast segregation according to size. The index value is proportional to the size difference between the clasts from the border and those from the interiors. The SI for single parts of the sorted polygons is defined as the ratio of the mean clast size on the border ($\bar{a}_B$) and at the one-third ($\bar{a}_{1/3}$) or two-third ($\bar{a}_{2/3}$) positions (i.e. for one-third ($SI_{1/3} = \bar{a}_B/\bar{a}_{1/3}$) and for two-thirds ($SI_{2/3} = \bar{a}_B/\bar{a}_{2/3}$)).

A total sorting index (TSI) was formulated to characterise the total sorting of a sorted polygon:

$$TSI = \frac{\overline{a}_B}{\overline{a}} / \frac{\overline{a}_{1/3}}{\overline{a}} / \frac{\overline{a}_{2/3}}{\overline{a}} = \frac{\overline{a}_B \cdot \overline{a}}{\overline{a}_{1/3} \cdot \overline{a}_{2/3}}.$$

The SI is more appropriate for relict sorted polygons than comparisons of the percentage weight of single grain size fractions (e.g. Ballantyne and Matthews, 1983; Grab, 1997) because its calculation excludes fine-grained fractions modified by Holocene pedogenesis (e.g. Haugland, 2004, 2006) and wind action (e.g. Grab, 1997; Matthews *et al*., 1998; Sekyra *et al*., 2002) after patterned-ground activity had ceased.

Statistical Analysis

The parameters above were tested for normality using the Shapiro-Wilk test (Shapiro and Wilk, 1965), and a log transformation was applied to the parameters H, H/W, ā, $SI_{1/3}$, $SI_{2/3}$ and TSI in order to meet the criterion of normality (Meloun *et al*., 2005). Relationships between the parameters were analysed by the Pearson correlation coefficient and a t-test. Differences between the climatically most exposed and least exposed sites were assessed by one-way ANOVA and F-tests. Confidence levels for the t-tests and F-tests were $p = 0.05$. Statistical operations were performed using the software STATISTICA (StatSoft, Inc., 2009).

RESULTS

Polygon Size and Morphology

The polygons are on average 194 cm long, 21.5 cm high and slightly elongated (mean elongation index = 1.33). Their distribution can be grouped by altitude (which reflects climatic severity) into sorted polygons at the top of Mt Luční hora (LH A – sites LH A1, LH A2, LH A3), with greater microclimatic severity, and those on the lowest cryoplanation terrace (LH B), with less severe microclimates (Table 1).

Mean polygon width is significantly smaller atop Mt Luční hora, whereas relative height and the elongation index have significantly larger values than for polygons at lower elevation (Table 2). Larger sorted polygons are higher and formed from larger clasts (Table 3). Larger sorted

Table 2 Comparison of the morphometric characteristics of sorted polygons at the top of Mt Luční hora (LH A: N = 49) and on the lowest cryoplanation terrace (LH B: N = 13).

Morphometric characteristic	LH A				LH B				Statistical significance of ANOVA
	Mean (cm)	SD (cm)	Min (cm)	Max (cm)	Mean (cm)	SD (cm)	Min (cm)	Max (cm)	
Length	188	51	110	290	215	66	120	320	F (1; 60) = 1.998; $p = 0.1627$
Width	143	47	70	265	180	59	100	260	**F (1; 60) = 4.644; $p = 0.0352$**
Elongation index	1.36	0.21	1.08	2.00	1.22	0.16	1.04	1.67	**F (1; 60) = 7.395; $p = 0.0085$**
Height	21.8	9.5	11	55	20.1	10.7	6	37	F (1; 60) = 1.912; $p = 0.1719$
Relative height	0.16	0.05	0.08	0.34	0.11	0.04	0.05	0.18	**F (1; 60) = 14.898; $p = 0.0003$**
Mean clast size	7.4[a]	2.2[a]	5.0[a]	14.6[a]	7.5[b]	1.7[b]	5.1[b]	10.1[b]	F (1; 55) = 0.1000; $p = 0.7530$

Marked differences (bold) are significant at $p < 0.05$ as determined by the F-test.
[a]N = 46 (number of sorted polygons with at least 20 clast measurements from the two-third position).
[b]N = 11 (number of sorted polygons with at least 20 clast measurements from the two-third position).

Table 3 Correlations between selected morphometric characteristics and sorting indices of the polygons.

Variable	Length	Width	Height	Relative height	Mean clast size	$SI_{1/3}$	$SI_{2/3}$	TSI
Length	1.00	**0.91**	**0.62**	-0.14	**0.66**[a]	**-0.48**	**-0.35**[a]	**-0.63**[a]
Width	**0.91**	1.00	**0.60**	-0.25	**0.58**[a]	**-0.54**	**-0.41**[a]	**-0.66**[a]
Height	**0.62**	**0.60**	1.00	**0.62**	**0.59**[a]	-0.04	0.15[a]	-0.15[a]
Relative height	-0.14	-0.25	**0.62**	1.00	0.15[a]	**0.48**	**0.54**[a]	**0.43**[a]
Mean clast size	**0.66**[a]	**0.58**[a]	**0.59**[a]	0.15[a]	1.00	**-0.36**[a]	**-0.33**[a]	**-0.56**[a]
$SI_{1/3}$	**-0.48**	**-0.54**	-0.04	**0.48**	**-0.36**[a]	1.00	**0.84**[a]	**0.82**[a]
$SI_{2/3}$	**-0.35**[a]	**-0.41**[a]	0.15[a]	**0.54**[a]	**-0.33**[a]	**0.84**[a]	1.00	**0.85**[a]
TSI	**-0.63**[a]	**-0.66**[a]	-0.15[a]	**0.43**[a]	**-0.56**[a]	**0.82**[a]	**0.85**[a]	1.00

Marked correlations (bold) are significant at $p < 0.05$ as determined by the t-test (N = 62).
[a]N = 57 (number of sorted polygons with at least 20 clast measurements from the two-third position). See text for abbreviations.

polygons tend to be vegetated by grass, moss or heather, while smaller polygons have little or no grass cover. The size difference between the two groups of sorted polygons (with and without vegetation cover) is statistically significant (ANOVA, L = 263 cm vs 175 cm: F (1; 60) = 45.468; $p < 0.0001$; W = 221 cm vs 131 cm: F (1; 60) = 51.523; $p < 0.0001$).

Clast Shape and Size

Tabular clasts dominate the sorted polygons (Figure 4). Polygon borders consist of coarse clasts (mean a-axis length = 11 cm), with several clasts 25 to 30 cm long, whereas the inner parts of the polygons (positions one-third, two-thirds and C) consist of smaller clasts (mean length = 5 cm). The greatest differences in clast size are commonly between clasts on the border and at the one-third position (Figure 5). The smallest differences in clast size are between the two-third position and the polygon centre (Figure 5). In the inner parts, 67 per cent of the polygons display secondary sorting and 94 per cent of such polygons are located at the top of Mt Luční hora.

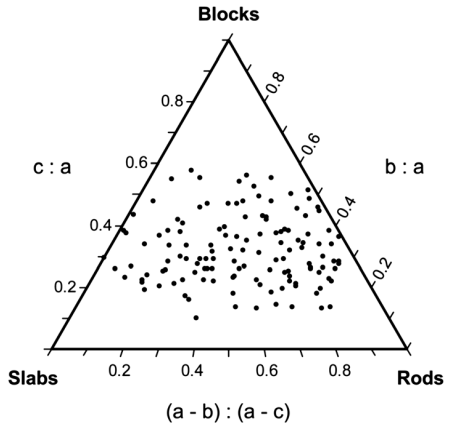

Figure 4 Clast shapes (*sensu* Sneed and Folk, 1958) in sorted polygons at the top of Mt Luční hora.

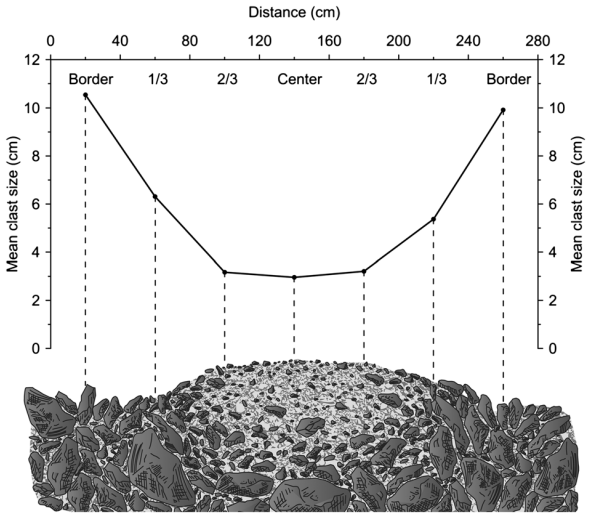

Figure 5 Mean clast size along the length axis of sorted polygon at the top of Mt Luční hora.

Sorting

The sorting indices correlate negatively with pattern dimensions and mean clast size, and positively with relative height (Table 3). Relationships between sorting and height are not statistically significant (Table 3).

Since a strong relationship exists between sorting and most morphometric characteristics (Table 3), only sorted polygons of similar dimensions were used to analyse the influence of microclimate on sorting. The contribution of relative height to the variance of sorting was not removed because up-doming is dominantly a function of microclimatic severity (e.g. Holness, 2003; Treml *et al*., 2010), and is probably the main driving mechanism of frost sorting (Kling, 1997; Matsuoka *et al*., 2003). The sorted polygons at the top of Mt Luční hora (LH A) were chosen as a reference because of their smaller size variability (Table 2). For comparison, sorted polygons with widths in range of mean W at LH A ± standard deviation of W at LH A (143 ± 47; Table 2) were selected. Thirty polygons in the

summit area (LH A) and seven at the site LH B met this criterion and did not display a significant difference in width (ANOVA, F (1;35) = 0.0085; $p = 0.9272$).

The sorting indices of similar-sized polygons are significantly higher at the top of Mt Luční hora (LH A) than at site LH B (Figure 6). Thus, the polygons located at higher altitudes are better sorted than the sorted polygons at lower altitudes ($SI_{1/3}$: r = 0.56; $SI_{2/3}$: r = 0.49; TSI: r = 0.53; significant at $p < 0.05$). Increased sorting with increased altitude is also observed within the summit sites LH A1, LH A2, LH A3. However, this dependence is not significant at a confidence level of $p = 0.05$ ($SI_{1/3}$: r = 0.27; $SI_{2/3}$: r = 0.23; TSI: r = 0.14) because of the limited number of sorted polygons from individual sites.

The relative height of similar-sized polygons is greater at the summit area (ANOVA, F (1; 35) = 9.2460; $p = 0.0044$) and has a strong relationship with sorting (Figure 7).

DISCUSSION

Relationship between Sorted Polygon Morphology and Clast Distribution

Smaller polygons are better sorted than larger ones because of the shorter distances for the clasts to move to the polygon borders. Thus, smaller polygons do not need as high frequency and/or intensity of processes to move clasts (e.g. Goldthwait, 1976; Washburn, 1979; Grab, 2002) and achieve the same sorting as larger polygons. This hypothesis is supported by experimental results (Matsuoka *et al.*, 2003) and field evidence (Ballantyne and Matthews, 1983), which revealed a positive correlation between the sorting of miniature polygons and an increasing number of freeze-thaw cycles or time since deglaciation.

Faster sorting of smaller polygons is likely accelerated by positive feedback. Since frost sorting affects all grain size fractions (Ballantyne and Matthews, 1983), sorting increases frost susceptibility in polygon centres, which in turn leads to more intensive ice segregation and cryogenic processes and therefore to further sorting – a self-sustaining or self-perpetuating process (Ballantyne, 1996, 2007). These effects lead to mass displacement and frost disturbances, likely restricting vegetation succession (e.g. Haugland and Beatty, 2005; Haugland, 2006) over the smaller polygons at Mt Luční hora, while the larger ones show a denser vegetation cover.

The relationship between polygon size and sorting is in agreement with the observations of Jeong (2006), which showed a positive correlation between sorted circle diameters and ^{14}C ages and suggested size-dependent circulatory movements (e.g. Ray *et al.*, 1983; Hallet and Prestrud, 1986) during circle formation and the lateral sorting of

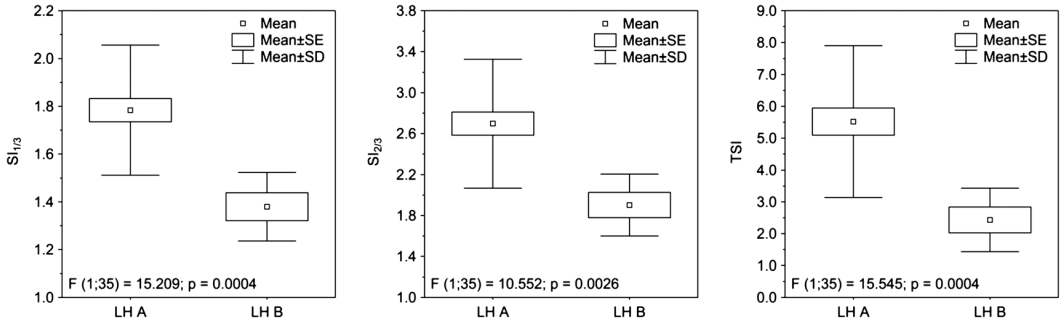

Figure 6 Differences in sorting indices ($SI_{1/3}$, $SI_{2/3}$, TSI) of sorted polygons between the top of Mt Luční hora (LH A) and the lowest site (LH B). Only similar-sized polygons were compared. See text for abbreviations.

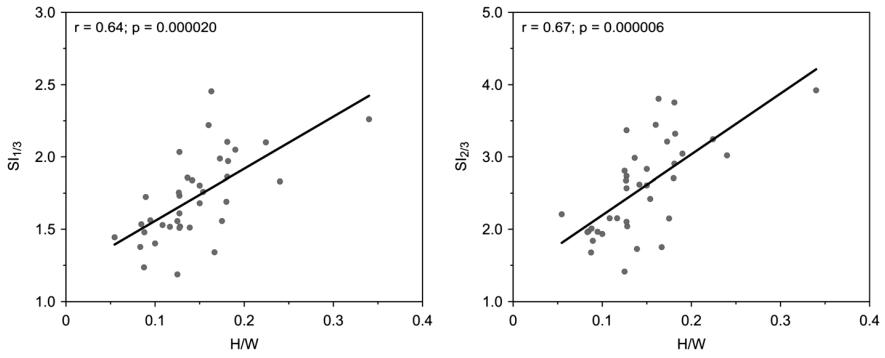

Figure 7 Relationship between relative height (H/W) and sorting indices ($SI_{1/3}$ and $SI_{2/3}$) of similar-sized sorted polygons. See text for abbreviations.

clasts. Therefore, they may also have played a role in the formation of sorted polygons on Mt Luční hora.

The better sorting of polygons with greater relative height (Figure 7) is associated with the steeply inclined surfaces of these polygons, where more intensive slope processes, such as frost creep and needle-ice creep (Ballantyne, 1996; Matsuoka *et al*., 2003), take place. The magnitude of clast movement is directly proportional to the slope of the sorted polygon surface (Kling, 1997; Matsuoka *et al*., 2003). In addition, increasing frost susceptibility due to better sorting is likely enhancing frost heaving of polygon centres (e.g. Van Vliet-Lanoë, 1991; Matsuoka *et al*., 2003; Ballantyne, 2007) and promoting accelerated sorting.

Influence of Microclimate on Sorted Polygon Morphology and Clast Distribution

Larger sorted polygons tend to occur in more severe microclimates (Washburn, 1979). However, microclimate is modified by complex interactions of site-specific factors, therefore considerable heterogeneity exists in the relationship of polygon size and altitude (cf. Grab, 1997; Kling, 1996, 1998; Holness, 2003; Rączkowska, 2003; Marvánek, 2010a, 2010b; Treml *et al*., 2010; Feuillet *et al*., 2012).

In the study area, polygons at the lowest site (LH B) are significantly wider than those from the top of Mt Luční hora (LH A; Table 2) despite higher temperatures and thicker snow cover at lower altitudes (Table 1). Since homogeneous bedrock likely produces similar mean clast size throughout the study area (Table 2), the larger sizes of these sorted polygons could be attributed either to the higher moisture content or higher groundwater table at the time of polygon formation (e.g. Nicholson, 1976; Kling, 1996, 1998). This is also consistent with the lower relative height of polygons at site LH B, which is typical for poorly drained sites (Van Vliet-Lanoë, 1991). Higher moisture contents and a higher groundwater table in the lower part of the study area (LH B) are indicated by nearby springs and thicker snow cover (Table 1) that supply water to the regolith. Nevertheless, the summit sites most likely have sufficient moisture for effective freeze-thaw action (e.g. Matsuoka and Murton, 2008), especially during spring thaw (Lukešová *et al*., 2010).

The increasing relative height of similar-sized polygons with increasing altitude is attributed to both lower moisture content (e.g. Van Vliet-Lanoë, 1991) and more severe microclimates (e.g. Holness, 2003; Treml *et al*., 2010) on the top of Mt Luční hora. Thinner snow cover due to more intense wind action and lower air temperatures cause considerable ground temperature oscillations and deeper freezing at higher altitudes of the study area (Table 1). Thus, more frequent and intense cryogenic processes operate at these sites (Harčarik, 2002; Sekyra *et al*., 2002). As wind directions were approximately the same in the Last Glacial period and the Holocene as at present (Jeník and Sekyra, 1995), more domed and better sorted polygons in the summit area (Figure 6) likely record greater microclimatic severity, which enhanced differential frost heaving and frost sorting (e.g. Washburn, 1979; Ballantyne and Matthews, 1983; Traczyk, 1995). The altitudinal gradient in polygon morphology and sorting is consistent with climate-topography patterns in the summit area of the Krkonoše Mountains (Jeník, 1961), suggesting the dominant role of microclimate in polygon formation during the Last Glacial period.

Although the polygons in the study area are of the same age (Sekyra and Sekyra, 1995; Traczyk and Migoń, 2000; Sekyra *et al*., 2002), the better sorting and greater relative height of those from higher altitudes may have been influenced by a longer period of activity or less intensive pattern degradation. Higher altitudes typically exhibit more severe microclimates and delayed vegetation succession, which could weaken cryogenic processes (e.g. Haugland and Beatty, 2005; Haugland, 2006). This could explain the formation of the secondary sorting centres (*sensu* Warburton, 1990), which are developed almost exclusively within the summit sorted polygons and are most likely related to the reactivation of frost sorting during the colder periods of the Holocene (Kociánová, 2002). However, since the secondary sorting centres are an order of magnitude smaller than the respective sorted polygons, we believe that the reactivation did not lead to any significant changes in the overall structure of sorted polygons and therefore was of marginal importance. Pattern degradational processes, such as rillwash erosion or colluviation, were also of marginal importance, owing to the flat or convex topography of the study sites and permanent forest-free area (Treml *et al*., 2008, 2010).

CONCLUSION

The following conclusions are drawn from the study of relict large-scale sorted polygons in the Krkonoše Mountains:

1. Larger sorted polygons are formed by larger clasts and tend to occur in poorly drained sites at lower altitudes.
2. Smaller polygons and polygons with greater relative height are better sorted.
3. More up-domed and better sorted polygons are located at the summit area of Mt Luční hora.
4. The up-doming of fine centres of sorted polygons and the displacement of clasts towards the borders of sorted polygons are a result of positive feedback between polygon morphology and frost susceptibility, driven by microclimate.
5. Differences in the morphology and distribution of clasts in sorted polygons, preserved since the Last Glacial period, indicate the high palaeoenvironmental potential of the relict large-scale sorted polygons located on flat or convex parts of the terrain.
6. The proposed method for evaluating frost sorting (based on clast size measurements) allows for rapid non-invasive assessment of sorting using modern methods, including high-resolution remote sensing (especially terrestrial photogrammetry) and modifications of the sampling strategy and repetitive measurements within individual sorted patterned-ground features. This method is designed for general use in periglacial landscapes.

ACKNOWLEDGEMENTS

The study was supported by the Grant Agency of the Academy of Sciences of the Czech Republic, project no. KJB301110804, and the Grant Agency of Charles University, project no. 674512. We appreciate the Krkonoše National Park Administration for providing permission to conduct research in a strictly protected area. We would like to thank Petra Nyplová for field assistance and Professor Olav Slaymaker for reviewing the paper and his valuable suggestions. We also thank two anonymous reviewers for their useful comments. We give special thanks to the Editor, Julian B. Murton, for his constructive suggestions and helpful comments and for improving the English.

REFERENCES

André MF. 2009. From climatic to global change geomorphology: contemporary shifts in periglacial geomorphology. In *Periglacial and Paraglacial Processes and Environments*, Knight J, Harrison S (eds). The Geological Society: London; 5–28.

Ballantyne CK. 1996. Formation of a miniature sorted patterns by shallow ground freezing: A field experiment. *Permafrost and Periglacial Processes* **7**: 409–424. DOI: 10.1002/(SICI)1099-1530(199610)7:4<409::AID-PPP230>3.0.CO;2-3

Ballantyne CK. 2007. Patterned ground. In *Encyclopedia of Quaternary Science*, Elias SA (ed). Elsevier: New York; 2182–2191.

Ballantyne CK, Matthews JA. 1982. The development of sorted circles on recently deglaciated terrain, Jotunheimen, Norway. *Arctic and Alpine Research* **14**: 341–354.

Ballantyne CK, Matthews JA. 1983. Desiccation Cracking and Sorted Polygon Development, Jotunheimen, Norway. *Arctic and Alpine Research* **15**: 339–349.

Beskow G. 1935. *Tjälbildningen och tjällyftningen med särskild hänsyn till vägar och järnvägar* (Soil freezing and frost heaving with special application to roads and railroads) (in Swedish). Sveriges Geologiska Undersökning: Stockholm; 242pp.

Chaloupský J, Červenka J, Jetel J, Králík F, Líbalová J, Píchová E, Pokorný J, Pošmourný K, Sekyra J, Shrbený O, Šamanský K, Šrámek J, Václ J. 1989. *Geologie Krkonoš a Jizerských hor* (Geology of the Krkonoše and Jizerské hory Mts) (in Czech). Academia: Praha; 288pp.

Czudek T. 2005. *Vývoj reliéfu krajiny České republiky v kvartéru* (Quaternary development of landscape relief of the Czech Republic) (in Czech). Moravské zemské muzeum: Brno; 238pp.

Dąbski M. 2005. Small-scale Sorted Nets on Glacial Till, Fláajökull (Southeast Iceland) and Elisbreen (Northwest Spitsbergen). *Permafrost and Periglacial Processes* **16**: 305–310. DOI: 10.1002/ppp.527

Feuillet T. 2011. Statistical Analyses of Active Patterned Ground Occurrence in the Taillon Massif (Pyrénées, France/Spain). *Permafrost and Periglacial Processes* **22**: 228–238. DOI: 10.1002/ppp.726

Feuillet T, Mercier D. 2012. Post-Little Ice Age patterned ground development on two Pyrenean proglacial areas: from deglaciation to periglaciation. *Geografiska Annaler* **94A**: 363–376. DOI: 10.1111/j.1468-0459.2012.00459.x

Feuillet T, Mercier D, Decaulne A, Cossart E. 2012. Classification of sorted patterned ground areas based on their environmental characteristics (Skagafjörður, Northern Iceland). *Geomorphology* **139–140**: 577–587. DOI: 10.1016/j.geomorph.2011.12.022

Głowicki B. 1997. Wieloletnia seria pomiarow temperatury powietrza na Śnieżce (Long-term series of air temperature measurements on Mt. Sněžka) (in Polish). In *Geoekologiczne problemy Karkonoszy I*, Sarosiek J, Štursa J (eds). Wydawnictwo Acarus: Poznań; 117–123.

Goldthwait RP. 1976. Frost sorted patterned ground: A review. *Quaternary Research* **6**: 27–35. DOI: 10.1016/0033-5894(76)90038-7

Grab S. 2002. Characteristics and palaeoenvironmental significance of relict sorted patterned ground, Drakensberg plateau, southern Africa. *Quaternary Science Reviews* **21**: 1729–1744. DOI: 10.1016/S0277-3791(01)00149-4

Grab SW. 1997. Annually re-forming miniature sorted patterned ground in the High Drakensberg, southern Africa. *Earth Surface Processes and Landforms* **22**: 733–745. DOI: 10.1002/(SICI)1096-9837(199708)22:8<733::AID-ESP764>3.0.CO;2-L

Grab SW, Mulder NA, Mills SC. 2009. Spatial associations between longest-lasting winter snow cover and cold region landforms in the high Drakensberg, southern Africa. *Geografiska Annaler* **91A**: 83–97. DOI: 10.1111/j.1468-0459.2009.00356.x

Graham DJ, Midgley NG. 2000. Graphical representation of particle shape using triangular diagrams: An Excel spreadsheet method. *Earth Surface Processes and Landforms* **25**: 1473–1477. DOI: 10.1002/1096-9837(200012)25:13<1473::AID-ESP158>3.0.CO;2-C

Hallet B, Prestrud S. 1986. Dynamics of periglacial sorted circles in Western Spitsbergen. *Quaternary Research* **26**: 81–99. DOI: 10.1016/0033-5894(86)90085-2

Harčarik J. 2002. Microclimatic relationships of the arctic-alpine tundra. *Opera Corcontica* **39**: 45–68.

Harris C. 1982. The distribution and altitudinal zonation of periglacial landforms, Okstindan, Norway. *Zeitschrift für Geomorphologie, N.F.* **26**: 283–304.

Harris C. 1990. Micromorphology and microfabrics of sorted circles, Front Range, Colorado, USA. In *Proceedings of the 5th Canadian Permafrost Conference*, Burgess MM, Harry DG, Sego DC (eds). Collection Nordicana 54, National Research Council of Canada: Ottawa; 89–94.

Haugland JE. 2004. Formation of patterned ground and fine-scale soil development within two late Holocene glacial chronosequences: Jotunheimen, Norway. *Geomorphology* **61**: 287–301. DOI: 10.1016/j.geomorph.2004.01.004

Haugland JE. 2006. Short-term Periglacial Processes, Vegetation Succession, and Soil Development within Sorted Patterned Ground: Jotunheimen, Norway. *Arctic, Antarctic, and Alpine Research* **38**: 82–89. DOI: 10.1657/1523-0430(2006)038[0082:SPPVSA]2.0.CO;2

Haugland JE, Beatty SW. 2005. Vegetation establishment, succession, and microsite frost disturbance on glacier forelands within patterned ground chronosequences. *Journal of Biogeography* **32**: 145–153. DOI: 10.1111/j.1365-2699.2004.01175.x

Hjort J, Luoto M. 2006. Modelling patterned ground distribution in Finnish Lapland: an integration of topographical, ground and remote sensing information. *Geografiska Annaler* **88A**: 19–29. DOI: 10.1111/j.0435-3676.2006.00280.x

Holness SD. 2003. Sorted circles in the maritime Subantarctic, Marion Island. *Earth Surface Processes and Landforms* **28**: 337–347. DOI: 10.1002/esp.430

Hubbard B, Glasser N. 2005. *Field Techniques in Glaciology and Glacial Geomorphology*. University of Wales: Aberystwyth; 400pp.

Jahn A. 1977. The permafrost active layer in the Sudety Mountains during the last glaciation. *Quaestiones Geographicae* **4**: 29–42.

Jeník J. 1961. *Alpinská vegetace Krkonoš, Hrubého Jeseníku a Králického sněžníku. Teorie anemo-orografických systémů* (Alpine vegetation of the High Sudetes.

The theory of anemo-orographic systems) (in Czech). Academia: Praha; 407pp.

Jeník J, Sekyra J. 1995. Exodynamic and climatic factors. In Arctic-alpine tundra in the Krkonoše, the Sudetes, Soukupová L, Kociánová M, Jeník J, Sekyra J (eds). *Opera Corcontica* **32**: 13–18.

Jeong GJ. 2006. Radiocarbon ages of sorted circles on King George Island, South Shetland Islands, West Antarctica. *Antarctic Science* **18**: 265–270. DOI: 10.1017/S0954102006000307

Kade A, Romanovsky VE, Walker DA. 2006: The N-factor of nonsorted circles along a climate gradient in arctic Alaska. *Permafrost and Periglacial Processes* **17**: 279–289. DOI: 10.1002/ppp.563

Kling J. 1996. Relict sorted patterned ground in Rostu, northernmost Sweden. *Geografiska Annaler* **78A**: 61–72.

Kling J. 1997. Observations on sorted circle development, Abisko, Northern Sweden. *Permafrost and Periglacial Processes* **8**: 447–453. DOI: 10.1002/(SICI)1099-1530(199710/12)8:4<447::AID-PPP266>3.0.CO;2-H

Kling J. 1998. The difference between sorted circle and polygon morphology and their distribution in two alpine areas, northern Sweden. *Zeitschrift für Geomorphologie, N.F.* **42**: 439–452.

Kociánová M. 2002. Otázka projevů chladných období postglaciálu v krkonošské tundře (Problem of cold periods of climate during postglacial time in tundra area of the Giant Mts.) (in Czech). *Opera Corcontica* **39**: 143–151.

Křížek M. 2007. Periglacial landforms above the alpine timberline in the High Sudetes. In *Geomorphological Variations*, Goudie AS, Kalvoda J (eds). P3K: Praha; 313–337.

Křížek M, Treml V, Engel Z. 2010. Czy najwyższe partie Sudetów powyżej górnej granicy lasu są domeną peryglacjalną? (Are the highest parts of the Sudetes above the upper timber line a periglacial domain?) (in Polish). *Czasopismo Geograficzne* **81**: 75–102.

Kunský J. 1948. Geomorfologický náčrt Krkonoš (The geomorphological map of the Krkonoše Mts.) (in Czech). In *Příroda v Krkonoších*, Černý W, Gregor A, Klika J. (eds). Česká grafická unie: Praha; 54–89.

Lukešová A, Kociánová M, Váňa J, Štursová H, Elster J, Harčarik J, Halda J, Kocourková J, Jankovská V. 2010. Vyvařované půdy tundry Krkonoš a Abisko Mts – předběžná srovnávací studie (Mud boils of the Giant Mts. and Abisko Mts. tundra – preliminary comparative study) (in Czech). *Opera Corcontica* **47**: 55–82.

Luoto M, Hjort J. 2004. Generalized linear modelling in periglacial studies: terrain parameters and patterned ground. *Permafrost and Periglacial Processes* **15**: 327–338. DOI: 10.1002/ppp.482

Luoto M, Hjort J. 2006. Scale matters - A multi-resolution study of the determinants of patterned ground activity in subarctic Finland. *Geomorphology* **80**: 282–294. DOI: 10.1016/j.geomorph.2006.03.001

Marvánek O. 2010a. Periglacial Features in the Krumgampen Valley, Ötztal Alps, Austria. *Moravian Geographical Reports* **18**: 46–55.

Marvánek O. 2010b. Sorted patterned ground on the James Ross Island and its morphological diversity. *Acta Geographica Silesiana* **7**: 49–53.

Matsuoka N, Murton J. 2008. Frost Weathering: Recent Advances and Future Directions. *Permafrost and Periglacial Processes* **19**: 195–210. DOI: 10.1002/ppp.620

Matsuoka N, Abe M, Ijiri M. 2003. Differential frost heave and sorted patterned ground: Field measurements and a laboratory experiment. *Geomorphology* **52**: 73–85. DOI: 10.1016/S0169-555X(02)00249-0

Matthews JA, Shakesby RA, Berrisford MS, McEwen LJ. 1998. Periglacial Patterned Ground on the Styggedalsbreen Glacier Foreland, Jotunheimen, Southern Norway: Micro-Topographic, Paraglacial and Geoecological Controls. *Permafrost and Periglacial Processes* **9**: 147–166. DOI: 10.1002/(SICI)1099-1530(199804/06)9:2<147::AID-PPP278>3.0.CO;2-9

Meloun M, Militký J, Hill M. 2005. *Počítačová analýza vícerozměrných dat v příkladech* (Computer analysis of multivariate data in examples) (in Czech). Academia: Praha; 449pp.

Migoń P. 1999. The role of preglacial relief in the development of mountain glaciation in the Sudetes, with the special references to the Karkonosze Mountains. *Zeitschrift für Geomorphologie N.F., Supplement-Band* **113**: 33–44.

Nelson F. 1982. Sorted-stripe macrofabrics. *Geografiska Annaler* **64A**: 25–33.

Nicholson FH. 1976. Patterned Ground Formation and Description as Suggested by Low Arctic and Subarctic Examples. *Arctic and Alpine Research* **8**: 329–342.

Rączkowska Z. 2003. Periglacial landforms of Northern Sweden Mt. with the Tarfala valley as example. *Studia Geomorphologia Carpatho-Balcanica* **37**: 45–57.

Ray RJ, Krantz WB, Caine TN, Gunn RD. 1983. A model for sorted patterned-ground regularity. *Journal of Glaciology* **29**: 317–337.

Sekyra J. 1960. *Působení mrazu na půdu: kryopedologie se zvláštním zřetelem k ČSR* (Effects of frost on soil: cryopedology with special emphasis on Czechoslovakia) (in Czech). Nakladatelství ČSAV: Praha; 164pp.

Sekyra J, Sekyra Z. 1995. Recent cryogenic processes. In Arctic-alpine tundra in the Krkonoše, the Sudetes, Soukupová L, Kociánová M, Jeník J, Sekyra J (eds). *Opera Corcontica* **32**: 31–37.

Sekyra J, Kociánová M, Štursová H, Dvořák IJ, Svoboda M. 2002. Frost phenomena in relationship to mountain pine. *Opera Corcontica* **39**: 69–114.

Seppälä M. 2004. *Wind as a Geomorphic Agent in Cold Climates*. Cambridge University Press: New York; 358pp.

Shapiro SS, Wilk MB. 1965. An analysis of variance test for normality (complete samples). *Biometrica* **52**: 591–611.

Sneed ED, Folk RL. 1958. Pebbles in the lower Colorado river, Texas. A study in particle morphogenesis. *Journal of Geology* **66**: 114–150.

StatSoft, Inc. 2009. STATISTICA (data analysis software system), version 9. www.statsoft.com.

Sumner P. 2004. Relict Sorted Patterned Ground in Lesotho. *Permafrost and Periglacial Processes* **15**: 89–93. DOI: 10.1002/ppp.459

Traczyk A. 1995. Morfologia peryglacjalna Śnieżki i Czarnego Grzbietu w Karkonoszach. (Periglacial morphology of Mt. Śnieżka and Czarny Grzbiet ridge in the Karkonosze Mts.) (in Polish). *Czasopismo Geograficzne* **66**: 157–173.

Traczyk A, Migoń P. 2000. Cold-climate landform patterns in the Sudetes. Effects of lithology, relief and glacial history. *AUC Geographica* **35**: 185–210.

Treml V, Jankovská V, Petr L. 2008. Holocene dynamics of the alpine timberline in the High Sudetes. *Biologica* **63**: 73–80. DOI: 10.2478/s11756-008-0021-3

Treml V, Křížek M, Engel Z. 2010. Classification of Patterned Ground Based on Morphometry and Site Characteristics: A Case Study from the High Sudetes, Central Europe. *Permafrost and Periglacial Processes* **21**: 66–77. DOI: 10.1002/ppp.671

Van Vliet-Lanoë B. 1991. Differential frost heave, load casting and convection: Converging mechanisms; a discussion of the origin of cryoturbations. *Permafrost and Periglacial Processes* **2**: 123–139. DOI: 10.1002/ppp.3430020207

Warburton J. 1990. Secondary Sorting of Sorted Patterned ground. *Permafrost and Periglacial Processes* **1**: 313–318. DOI: 10.1002/ppp.3430010312

Washburn AL. 1979. *Geocryology – A Survey of Periglacial Processes and Environments*. Edward Arnold: London; 406pp.

7.3 Paper III

Uxa, T., Křížek, M., Krause, D., Hartvich, F., Tábořík, P., Kasprzak, M. (2019). Comment on 'Geophysical approach to the study of a periglacial blockfield in a mountain area (Ztracené kameny, Eastern Sudetes, Czech Republic)' by Stan *et al.* (2017). *Geomorphology*, 328(1 March 2019), 231–237. https://doi.org/10.1016/j.geomorph.2018.10.010

Journal Citation Reports 2018: IF=3.681, Q2(14/50) in Physical Geography, Q1(35/196) in Geosciences Multidisciplinary.

Citations as of 9 June 2020: Web of Science=2, Scopus=1, Google Scholar=3, ResearchGate=2.

Geomorphology 328 (2019) 231–237

Contents lists available at ScienceDirect

Geomorphology

journal homepage: www.elsevier.com/locate/geomorph

Comment on 'Geophysical approach to the study of a periglacial blockfield in a mountain area (Ztracené kameny, Eastern Sudetes, Czech Republic)' by Stan et al. (2017)

Tomáš Uxa [a,b,*], Marek Křížek [a], David Krause [a], Filip Hartvich [a,c], Petr Tábořík [d,c], Marek Kasprzak [e]

[a] Department of Physical Geography and Geoecology, Faculty of Science, Charles University, Albertov 6, 128 43 Prague 2, Czech Republic
[b] Institute of Geophysics, Czech Academy of Sciences, Boční II 1401, 141 31 Prague, 4, Czech Republic
[c] Institute of Rock Structure and Mechanics, Czech Academy of Sciences, V Holešovičkách 41, 182 09 Prague, 8, Czech Republic
[d] Institute of Hydrogeology, Engineering Geology and Applied Geophysics, Faculty of Science, Charles University, Albertov 6, 128 43 Prague 2, Czech Republic
[e] Department of Geomorphology, Institute of Geography and Regional Development, University of Wrocław, pl. Uniwersytecki 1, 50-137 Wrocław, Poland

ARTICLE INFO

Article history:
Received 3 July 2018
Received in revised form 10 October 2018
Accepted 10 October 2018
Available online 13 October 2018

Keywords:
Blockfield
Permafrost
Electrical resistivity tomography
Seismic refraction tomography
Eastern High Sudetes
Central Europe

ABSTRACT

Stan et al. (2017) investigated the internal structure of two periglacial blockfields on the Ztracené kameny site, Eastern High Sudetes, Czech Republic, using electrical resistivity tomography and seismic refraction tomography and interpreted two high-resistivity and high-velocity zones as remnants of the Pleistocene permafrost. However, we believe that in reality no permafrost occurs on the site, and we provide alternate, non-permafrost interpretations of the geophysical measurements by Stan et al. (2017) that are well consistent with other evidences such as climate and topographic attributes of the blockfields, permafrost-disqualifying ground thermal regimes, and common characteristics of mid-latitude, low-altitude permafrost locations from elsewhere. We also rectify some misconceptions about the study site that are stated by Stan et al. (2017).

1. Introduction

Openwork debris of blockfields, talus slopes, or rock glaciers permits the air to flow through the pore spaces and to develop a seasonally reversing, gravity-driven internal air circulation. This convective heat transfer induces inhomogeneous temperature distribution across the scree slopes; with up to several degrees Celsius cooler air in their lower parts. The latter places frequently show notable negative thermal anomalies, which are essential for potential maintenance of subzero mean annual ground temperature (MAGT) even if mean annual air temperature (MAAT) is well above zero (e.g., Delaloye and Lambiel 2005; Wicky and Hauck 2017). The difference between MAGT and MAAT is mostly a few degrees Celsius below zero (e.g., Delaloye et al. 2003; Gorbunov et al. 2004), but it can achieve −5 °C or less (e.g., Zacharda et al. 2007; Morard et al. 2010; Popescu et al. 2017). Consequently, scree slopes are capable to host perennial ice patches in surprisingly low altitudes and otherwise permafrost-free environments (Table 1). Such locations are therefore of high interest for permafrost researchers as well as for biologists because these azonal permafrost spots are abundantly colonized by boreo-alpine flora and fauna species characteristic of much higher altitudes or latitudes, which can even be relics from glacial periods (e.g., Gude et al. 2003; Stiegler et al. 2014). However, controls on permafrost occurrence in such specific places and anomalous regional environmental conditions as well as their state under a changing climate are still little understood as these locations are very scarce (Table 1). Each new report is therefore of high scientific importance and worthy of attention and should be properly documented as it can alter our understanding of azonal permafrost occurrence. Such a report is also the recently published study of Stan et al. (2017) aimed at a shallow geophysical survey of the internal structure of two periglacial blockfields on the Ztracené kameny (1250 m asl), Eastern High Sudetes, Czech Republic, utilizing electrical resistivity tomography (ERT) and seismic refraction tomography (SRT; commonly called 'shallow seismic refraction'), in which the authors interpreted two isolated high-resistivity and high-velocity zones as permafrost patches that were, moreover, thought to be of Pleistocene age. We have serious doubts about the validity of the purely geophysically suggested contemporary permafrost occurrence on the Ztracené kameny by Stan et al. (2017) because we consider their interpretation of the ERT and SRT measurements to be oversimplifying and unilaterally favouring the

* Corresponding author at: Department of Physical Geography and Geoecology, Faculty of Science, Charles University, Albertov 6, 128 43 Prague 2, Czech Republic.
E-mail address: tomas.uxa@natur.cuni.cz (T. Uxa).

https://doi.org/10.1016/j.geomorph.2018.10.010
0169-555X/

Table 1
Characteristics of the geophysically prospected mid-latitude, low-altitude permafrost sites in Europe.

Country	Switzerland	France	Germany	Germany	Switzerland	Germany	Austria	Czech Republic	Czech Republic	Romania
Location	Creux-du-Van Jura Mts.	La Glacière Vosges Mts.	Präg Schwarzwald Mts.	Zastler Schwarzwald Mts.	Val Bever Swiss Alps	Odertal Harz Mts.	Toteisboden Schladminger Tauern Range	Kamená hůra Central Bohemian Highlands	Klíč Central Bohemian Highlands	Detunata Goală Apuseni Mts.
Landform	Talus slope	Scree slope	Scree slope	Scree slope	Scree slope	Talus slope -moraine	Talus slope	Talus slope	Talus slope	Talus slope-rock glacier
Longitude	6°44′ E	6°58′ E	7°58′ E	8°00′ E	9°51′ E	10°33′ E	13°42′ E	14°21′ E	14°34′ E	23°12′ E
Latitude	46°56′ N	48°06′ N	47°47′ N	47°55′ N	46°33′ N	51°44′ N	47°21′ N	50°42′ N	50°47′ N	46°17′ N
Altitude (m)	1170–1300	680	720	590	1790–1900	600	990–1040	300–360	520–600	1020–1110
Vertical range (m)	130	–	–	–	110	–	50	60	80	90
Aspect	N	–	–	–	N	W	N	N	SW	W
MAAT (°C)	5.4	–	–	–	1	6.2	4.7	8	7.1	8.4
MAGT in the lower part (°C)	0.7 to 3.3	–	–	–	−0.9	1.6	−0.8	−0.9	0.4	1.0–2.6
Temperature offset (°C)	−4.7 to −2.1	–	–	–	−1.9[a]	−4.6	−5.5[a]	−8.9	−6.7	−7.4 to −5.8
Resistivity (kΩ·m)	5–37	<100	<100	<100	>20 to 60–140	–	30–50 to 200	–	>360	20–65
P-wave velocity ($m \cdot s^{-1}$)	–	<2000	<2000	<2000	1700–4300	2500–3500	>1500	<1000	2000–3000	–
Scree thickness (m)	20	–	10?	10?	>11–23	>15	>6–25	10–15	15–20	>10–25
Active-layer thickness (m)	2–3	1–5	–	–	1–3	–	1–5	–	2–5	4–9
Permafrost thickness (m)	15–20	ca. 5	<10	<10	10–20	–	5–20	–	<2	6–16
Lower limit of discontinuous permafrost (m)	2200–2400	–	–	–	2400	–	2400	–	–	–
Lithology	Limestone	–	–	–	–	–	Granite-gneiss	Olivine basalt	Phonolite	Basaltic andesite
Vegetation	Organic soil and patches of dwarf red spruce in the lower part	Sparse vegetation	Sparse vegetation	Sparse vegetation	Small larch trees	–	Mosses and cryophilic plants with isolated spots of dwarf birch	Dense cover of non-vascular plants in the lower part	Lichens and mosses in the lower part	Mosses and dwarf trees in the lower part
Source	Delaloye et al. (2003) Morard et al. (2008)	Hauck and Kneisel (2008)	Hauck and Kneisel (2008)	Hauck and Kneisel (2008)	Kneisel et al. (2000) Kneisel (2010)	Gude et al. (2003) Růžička et al. (2015)	Stiegler et al. (2014)	Gude et al. (2003) Zacharda et al. (2005) Růžička et al. (2015)	Gude et al. (2003) Zacharda et al. (2005) Růžička et al. (2015)	Popescu et al. (2017)

[a] Temperature offset calculation based on the long-term MAAT.

presence of permafrost although the local conditions are highly disadvantageous for its existence.

In this comment, we propose an alternate explanation of these ambiguous geophysical data sets and provide other considerations, which lead us to believe that no buried perennial ground ice actually exists there.

2. Geophysical outputs and their reinterpretation

Shallow geophysical techniques, such as ERT and SRT, have been widely employed in mid-latitude, low-altitude permafrost detection (e.g., Kneisel et al. 2000; Delaloye et al. 2003; Gude et al. 2003; Hauck and Kneisel 2008; Stiegler et al. 2014; Popescu et al. 2017) because ice and ice-rich sediments show high electrical resistivities (ca. 10^3–10^6 Ω·m) and high P-wave velocities (ca. 1500–5300 m.s^{-1} and mostly ca. 2000–4000 m·s^{-1}), which commonly contrast well with those of the surrounding materials (Kneisel and Hauck 2008; Schrott and Hoffmann 2008; Schrott and Sass 2008; Draebing 2016). Both methods are therefore extremely useful for localizing and quantifying ground-ice bodies, especially when combined; but in no case have they been applied to mid-latitude, low-altitude permafrost exploration independently of other, mostly temperature-based methods (air and ground temperature monitoring, mapping of the bottom temperature of snow cover, spring-water temperature measurements, infrared imaging; e.g., Kneisel et al. 2000; Delaloye et al. 2003; Gude et al. 2003; Stiegler et al. 2014; Popescu et al. 2017) because influences that can make their interpretation difficult are numerous (Draebing 2016). The characteristic values of electrical resistivity and P-wave velocity usually considered for ice-bearing materials in mid-latitude, low-altitude locations are rather low and range between ca. 5–50 kΩ·m and <100 kΩ·m (e.g., Kneisel et al. 2000; Delaloye et al. 2003; Stiegler et al. 2014; Popescu et al. 2017) and 2000–3500 m·s^{-1} respectively (e.g., Kneisel et al. 2000; Gude et al. 2003) because permafrost at most of these places is assumed to be warm, with temperatures close to 0 °C and low ice contents or high unfrozen water contents (Kneisel et al. 2000). The resistivities around 100 kΩ·m and higher are commonly assigned to large ice-coated boulders with air-filled voids (e.g., Kneisel et al. 2000; Stiegler et al. 2014) rather than to massive ice bodies that are typical for high-alpine environments (Hauck and Vonder Mühll 2003). Furthermore, P-wave velocities of 2500–3500 m·s^{-1} can indicate the occurrence of ice as well as the presence of bedrock (Gude et al. 2003).

Stan et al. (2017) identified an isolated zone of high resistivities well over 100 kΩ·m (up to ca. 200 kΩ·m) at an average depth of ca. 6 m (depth range of ca. 4–8 m) on their ERT profile E1, located in the lower part of the 'eastern' blockfield, which spatially coincides with the zone of high P-wave velocities of up to 3000 m·s^{-1} on the SRT profile E3, perpendicularly intersecting the profile E1 (see Fig. 7 in Stan et al. 2017, p. 384). Similarly, an isolated zone of high resistivities over 80 kΩ·m at an average depth of ca. 5.5 m (depth range of ca. 2–7 m) was recorded on their ERT profile W6, located in the lower part of the 'western' blockfield, which corresponds with the zone of high P-wave velocities of up to 2000 m·s^{-1} on the SRT profile W3, transversally crossing the profile W6 (see Fig. 11 in Stan et al. 2017, p. 387). Both these high-resistivity and high-velocity zones were interpreted by Stan et al. (2017) as the remnants of probably Pleistocene permafrost.

Generally, some of the electrical resistivity values measured by Stan et al. (2017) on the Ztracené kameny may suggest the presence of permafrost as they largely overlap the entire interval of resistivities that are characteristic of ice and ice-rich sediments (see above). On the contrary, the maximum resistivities mostly attain or even exceed the highest values documented from mid-latitude, low-altitude permafrost sites (cf. Kneisel et al. 2000; Delaloye et al. 2003; Gude et al. 2003; Stiegler et al. 2014; Popescu et al. 2017), rather resembling the massive ice (sensu Hauck and Vonder Mühll 2003). However, the resistivities of up to ca. 200 kΩ·m recorded within the 'eastern' blockfield are probably too large to be produced by ground ice alone in this permafrost-hostile environment (see Section 3), and thus a certain share of ice-free voids would likely be needed to generate such extreme values (sensu Kneisel et al. 2000; Stiegler et al. 2014). Nonetheless, the P-wave velocities of up to 3000 m·s^{-1} measured in the same place unambiguously exclude a larger presence of air as it itself achieves values as low as 300–330 m.s^{-1} and the typical values for air-filled layers commonly show the left-skewed range of ca. 350–1500 m·s^{-1} (Draebing 2016), which, in fact, includes almost the entire velocity span of ca. 250–1200 m·s^{-1} observed by Stan et al. (2017) in these substrates. Likewise, the maximum resistivities over 80 kΩ.m measured within the 'western' blockfield would presumably also need the presence of air-filled voids to attain such high values, but the P-wave velocities of this lenticular structure are up to 2000 m·s^{-1}, which almost certainly excludes the presence of air and ice (cf. Kneisel et al. 2000; Gude et al. 2003; Schrott and Hoffmann 2008; Draebing 2016). Because the existence of large amounts of perennial ice is highly improbable in this altitude (ca. 1100–1250 m asl) and the presence of air-ice mixture can be declined as well (sensu Kneisel et al. 2000; Stiegler et al. 2014), the high-resistivity and high-velocity zones can hardly be interpreted as permafrost lenses. Notably, Stan et al. (2017) also measured comparably high electrical resistivities in other parts of their ERT profiles E1 and W6 as well as P1 (see Figs. 6, 7, and 11 in Stan et al. 2017, pp. 384 and 387), which locally have even larger spatial extents than the two 'permafrost' patches; but surprisingly, these zones attracted substantially less attention of Stan et al. (2017), and if so, they were mostly interpreted as loosely packed blockfield with air-filled voids.

Our alternate explanation for such widespread occurrence of the extreme resistivities on the Ztracené kameny is that both blockfields are composed of a mixture of Palaeozoic metamorphic rocks, with a dominance of quartzites. High quartz content of rocks (see the right photograph on Fig. 3 and Fig. 1 in Stan et al. 2017, p. 381) is certainly able to produce very high electrical resistivities because quartzites show a huge range of values between 10 and 10^9 Ω·m (Kneisel and Hauck 2008) and pure quartz even well above 10^{10} Ω·m (e.g., Parkhomenko 1967; Telford et al. 1990). Consequently, the high-resistivity zones can be associated with the occurrences of solid quartzite bedrock, larger quartzite boulders, quartz veins traversing the blockfields, or locally increased quartz content. The ERT profile E1 (see Fig. 7 in Stan et al. 2017, p. 384) transversally intersects the assumed quartzite insertions or veins (Stan et al. 2017), running roughly in the NE-SW direction (Fig. 1), the most compact sections of which probably achieve the highest resistivities over ca. 70 kΩ·m, while their disrupted parts exhibit somewhat lower values of ca. >20 kΩ·m. This layer is superposed by packed blocks with voids filled by organics and other fine materials (Stan et al. 2017, p. 385) as well as by air, which reach an average depth of ca. 4 m and are characterized by resistivities and P-wave velocities less than ca. 20 kΩ·m and ca. 1200 m·s^{-1} respectively. The high-resistivity zone (>80 kΩ·m) on the ERT profile W6 (see Fig. 11 in Stan et al. 2017, p. 387) could be attributed to the presence of a large isolated boulder with high quartz content, which is set inside the less resistive environment composed of smaller blocks with void-filling organics and fine materials, which also have the resistivities lower than ca. 20 kΩ·m and P-wave velocities ca. 1200 m·s^{-1} as in the 'eastern' blockfield. The comparably high resistivities in the ca. 3 m thick uppermost layer, located in the entire above-lying part of profile W6, are likely caused by a block cover with air-filled voids. The high resistivity (ca. >20 kΩ·m) in the SW section of ERT profile P1 (see Fig. 6 in Stan et al. 2017, p. 384) is related to shallow or exposed bedrock around and on the top rock formation of the Ztracené kameny as actually stated by Stan et al. (2017) as well.

The blockfields probably tend to increase their thickness downslope because the ERT profiles E4, E5, W7, W8, and W9 (see Figs. 8, 12, and 13 in Stan et al. 2017, pp. 385, 387, and 388), situated in the lower-lying densely forested areas, show the uppermost layer of ca. 10–15 m with resistivity <20 kΩ·m, which is probably composed of highly weathered quartzite blocks and voids completely filled with fine material. This layer likely corresponds to the second layer identified in the

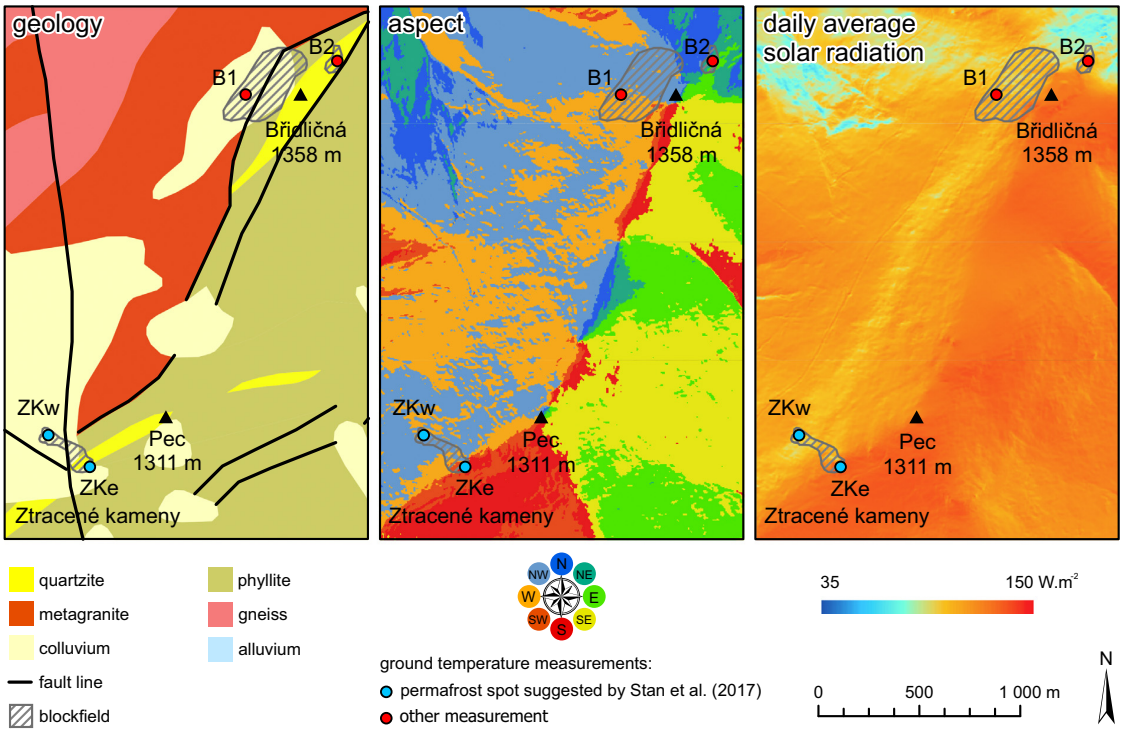

Fig. 1. Geology, aspect, and solar radiation in the study area. ZKw – permafrost spot suggested by Stan et al. (2017) on the 'western' blockfield on the Ztracené kameny; ZKe – permafrost spot suggested by Stan et al. (2017) on the 'eastern' blockfield on the Ztracené kameny; B1 – ground temperature measurement site on the Mt. Břidličná blockfield 1; B2 – ground temperature measurement site on the Mt. Břidličná blockfield 2.

unvegetated parts of the blockfields as both have very similar resistivities. The latter, however, extends to smaller depth as most ERT and SRT profiles in the forest-free parts of the blockfields suggest the bedrock occurrence at ca. 8–12 m (see Figs. 6, 7, 9, 10, and 11 in Stan et al. 2017, pp. 384, 386, and 387).

3. A brief insight into permafrost history and present-day environmental setting

Undoubtedly, permafrost existed in the Eastern High Sudetes and their lower-elevated surroundings during the last glacial period based on the presence of permafrost-related landforms, such as cryoplanation terraces, blockfields and block streams, or large-scale sorted patterned ground (e.g., Křížek 2016), and according to the subsurface ground temperature history (Šafanda and Rajver 2001). It surely occupied this region particularly during the Last Glacial Maximum (26.5–19 ka BP) or the Last Permafrost Maximum (25–17 ka BP) respectively (Vandenberghe et al. 2014; Lindgren et al. 2016) when its modelled maximum thickness was up to 220–245 m in the summit area (Czudek 1986). Permafrost began to decay at the Pleistocene-Holocene transition when the ground surface temperature rose above 0 °C (Šafanda and Rajver 2001), and it is believed to completely disappear until the middle Holocene (Czudek 1986, 1997). This probably coincides with the period of somewhat higher regional MAAT than at present as suggested by numerous evidence (e.g., Šafanda and Rajver 2001; Rybníček and Rybníčková 2004; Dudová et al. 2013). However, Stan et al. (2017) still argued that the blockfields on the Ztracené kameny have favourable topoclimatic conditions for the permafrost preservation because they (i) have concave topography around the high-resistivity zones, (ii) are colder, (iii) have long-lasting insulating snow cover, (iv) are shaded, (v) lie on the edge of a forest, and (vi) have limited thermal insulation (Stan et al. 2017, pp. 387–388). Except for the last point, which is nonsensical by nature because it in itself excludes the persistence of perennial ice under the positive MAAT and also largely contradicts point (iii), we address the remaining statements thoroughly in the next paragraph.

Stan et al. (2017, p. 381) stated that the MAAT in the 'summit areas' of the Eastern High Sudetes is as low as 1.1 °C. However, the MAAT at Mt. Praděd (1491 m asl; the highest peak of the mountain range) and at Mt. Šerák (1328 m asl), located ca. 8.5 km and ca. 19.7 km from the Ztracené kameny respectively in 1985–1996 and 2004–2017 was 1.3 °C and 3.4 °C respectively (Jeseníky Protected Landscape Area authority; National Oceanic and Atmospheric Administration Climate Data Online). The MAAT in the study area (1100–1250 m asl) is therefore likely to be 2.9–4.9 °C if the standard air temperature lapse rate of 0.0065 $K \cdot m^{-1}$ is considered. This could facilitate potential permafrost maintenance if temperature offset is sufficient. Nonetheless, the mean ground temperature recorded directly at the suggested permafrost spots (Fig. 1) in the 'western' and 'eastern' blockfield between 25 May 2017 and 18 May 2018 at a depth of ca. 0.40 m and ca. 0.55 m below ground surface respectively was as high as 5.3 °C and 4.8 °C respectively, which was ca. 0.8 °C and ca. 0.9 °C above the mean air temperature estimated based on data from the Mt. Šerák station respectively (Fig. 2). Likewise, the ground temperatures had reached their absolute minima of −7.1 °C and −7.5 °C respectively before the snow cover established at the turn of November–December and, except of some cooling events caused by rapid drops of air temperature, they remained mostly above −2 °C throughout the winter (Fig. 2). This evidence alone almost totally excludes the presence of permafrost on the Ztracené kameny. Moreover, the MAGTs measured at mid-latitude, low-altitude permafrost sites were substantially lower, and importantly, none of these locations showed a positive temperature offset (Table 1). In fact, most mid-latitude, low-altitude permafrost occurrences have been reported particularly from north-, east-, or west-facing debris-covered sites (Table 1), which are colder than south-facing slopes because of limited sunshine duration (Kneisel et al. 2000; Gorbunov et al. 2004). Furthermore, these permafrost-prone debris accumulations commonly have

Fig. 2. Mean daily ground temperatures measured at the 'western' (ZKw) and 'eastern' (ZKe) permafrost spot suggested by Stan et al. (2017) within the blockfields on the Ztracené kameny and mean daily air temperature (AT) estimated for their average altitude based on data from the Mt. Šerák station and the standard air temperature lapse rate of 0.0065 $K \cdot m^{-1}$.

Fig. 3. The 'eastern' blockfield on the Ztracené kameny on 16 February 2017 when snow cover culminated (upper) and the same site on 30 October 2010 without snow (lower). On the left photograph, note the boulders sticking out of the relatively thin snow cover, with only the smallest blocks covered completely.

the elevation extent of higher tens or even hundreds of meters and are at least 10–15 m thick (Table 1), which allows air circulation to fully develop and also isolates the ice body from warmer ambient air temperatures because of the enhanced temperature offset (sensu Gorbunov et al. 2004). Thicker screes also accumulate larger amounts of ice in winter, which are then able to persist throughout the summer (Delaloye et al. 2003). Importantly, the blockfields surveyed by Stan et al. (2017) are titled based on their relative position to the top rock formation, but in reality, the 'western' and 'eastern' blockfields face to the northwest (298°) and south (193°) respectively (Fig. 1; see also Figs. 3 and 4 in Stan et al. 2017, pp. 382 and 383). This causes a high solar radiation input particularly to the south-oriented blockfield, which is, moreover, only partly shaded by trees (Fig. 1; cf. Stan et al. 2017, p. 387). Symptomatic of rather warm and dry conditions within both blockfields is also the absence of a denser vegetation cover consisting of mosses and cryophilic plants, which are frequently found in most mid-latitude, low-altitude permafrost sites (e.g., Delaloye et al. 2003; Gude et al. 2003; Zacharda et al. 2007; Stiegler et al. 2014; Popescu et al. 2017). Instead, the blockfields host scattered dwarf shrubs or trees spreading from the neighbouring forest, the dead organics of which fills the interior voids together with other fine materials (see Stan et al. 2017, p. 385), and thus prevents the air circulation. Furthermore, the 100–200 cm maximum thickness of up to six months lasting snow cover stated by Stan et al. (2017, p. 381) can well occur particularly on the leeward sides of the summit plateaus (Jeník 1961). However, the Ztracené kameny site is situated a little lower, below the alpine timberline, implying that somewhat thinner snowpack is to be expected there. Indeed, the snow is usually not thick enough to cover the blockfields continuously (Fig. 3) throughout the winter and mostly completely disappears in March–April, and then the ground temperature rises sharply (Fig. 2). Therefore, the blockfields are insulated over a limited part of the year, and even during this period the insulation is debatable because air can penetrate easily around the boulders protruding from the snow. Moreover, it is unclear whether this amount of snow can accumulate sufficient volumes of ice that could survive to the following winter (sensu Delaloye et al. 2003). Finally, both blockfields have rather low elevation extent of ca. 65 m (lower, uninterrupted part of the 'western' blockfield) and ca. 20 m respectively, are relatively shallow with bedrock depth in forest-free parts commonly up to ca. 8–12 m (as can be seen on most ERT and SRT profiles; see Figs. 6, 7, 9, 10, and 11 in Stan et al. 2017, pp. 384, 386, and 387), and have relatively straight slopes with no distinct concave areas around the suggested permafrost spots (Fig. 4) described by Stan et al. (2017, p. 387). This likely considerably reduces the potential for internal air circulation and formation of cold reservoirs in lower parts of the blockfields (sensu Delaloye et al. 2003; Delaloye and Lambiel 2005; Morard et al. 2008, 2010; Popescu et al. 2017). Consequently, in summary, the environmental setting of the Ztracené kameny is probably unable to host permafrost under the present-day climate conditions. This statement is also supported by the ground thermal regimes in the lower parts of two blockfields of the same geology, located on the northwestern and northeastern slopes of Mt. Břidličná (1358 m asl) ca. 2 km north of the Ztracené kameny (Fig. 1), which showed permafrost-disfavouring MAGT of 4.1 °C and 5.0 °C respectively in 2014 (Křížek, unpublished data from temperature dataloggers) when Stan et al. (2017) performed their geophysical survey. If we consider that the blockfields at Mt. Břidličná are potentially more suitable for permafrost occurrence because they have lower estimated MAAT (2.5–3.6 °C), receive equal or less solar radiation (daily average of 111 and 110 $W \cdot m^{-2}$ for Mt. Břidličná vs. 107 and 141 $W \cdot m^{-2}$ for the 'western' and 'eastern' blockfields on the Ztracené kameny; Fig. 1), and are larger and thicker than those on the Ztracené kameny as well, then the permafrost suggestions of Stan et al. (2017) seem even more dubious.

The above implies that permafrost could not exist on the Ztracené kameny in the middle Holocene as well (cf. Czudek 1986, 1997) when MAAT was up to 3 °C higher than at present (Rybníček and Rybníčková 2004; Czudek 2005; Dudová et al. 2013) and also when the precipitation totals were higher, and thus larger amounts of water could enter the blockfields and supply additional heat for potential ice melting. Moreover, the blockfields probably had more extensive vegetation and soil cover, which filled the interior voids, and thus further

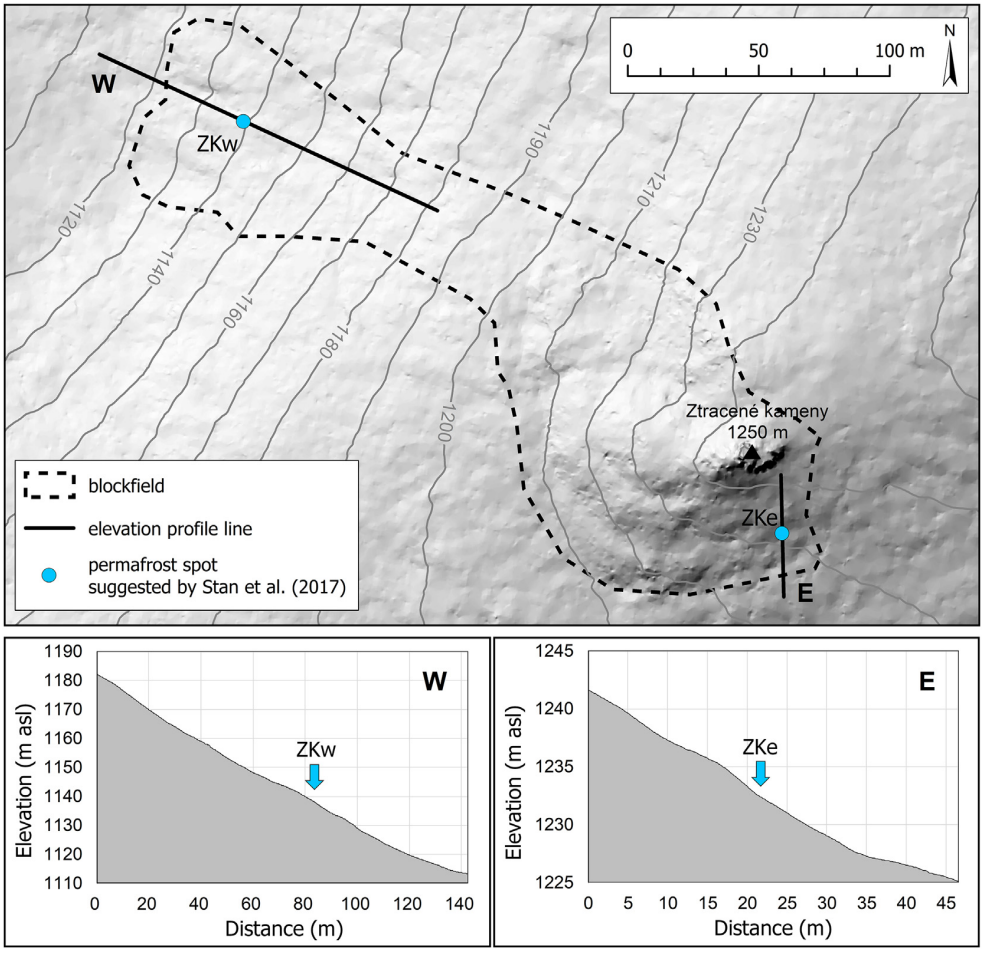

Fig. 4. Longitudinal elevation profiles across the 'western' (W) and 'eastern' (E) blockfields on the Ztracené kameny based on the 1 m DEM (State Administration of Land Surveying and Cadastre, 2017) with highlighted positions of the permafrost spots (ZKw and ZKe) suggested by Stan et al. (2017). Note that both spots are located on straight slopes.

reduced the potential for permafrost preservation. Consequently, even if present, the alleged ground-ice patches could hardly be termed as the remnants of Pleistocene permafrost as stated by Stan et al. (2017) because it thawed in the meantime (i.e., in the middle Holocene). Such shallow and tiny permafrost bodies are impacted by year-to-year air temperature variations, and thus they must exist under more-or-less equilibrium with contemporary climate otherwise they disappear. True relict permafrost reflects a colder past climate and is usually situated tens to hundreds of meters beneath the ground surface (e.g., Szewczyk and Nawrocki 2011) where it persists until the positive temperatures propagate into its depth level.

4. Conclusions

The contemporary permafrost existence in the two blockfields on the Ztracené kameny unilaterally proposed by Stan et al. (2017) is of doubtful validity as it relies on ambiguous geophysical data sets alone, poorly supported by other evidence. Maximum resistivity and P-wave velocity values should be attributed to the presence of high-resistivity quartzites and loose debris with air-filled voids, which produce geophysical images mimicking the permafrost conditions. The latter, non-permafrost hypothesis is also favoured by numerous evidence, such as the disadvantageous climate and topographic attributes of the blockfields, permafrost-disqualifying ground thermal regimes on the Ztracené kameny and in nearby blockfields, and common characteristics of mid-latitude, low-altitude permafrost locations from elsewhere, which all suggest it is highly improbable that the blockfields on the Ztracené kameny contain permafrost under the present climate.

Finally, we emphasize that geophysics delivers only indirect information with an artificial visualisation of the approximate subsurface distribution of physical parameters, which includes the ambiguity of the computed model and of the interpretation. Geophysical surveying therefore requires other non-geophysical inputs and a good knowledge of local conditions to support the hypothesized explanation as can be ultimately exemplified in most earlier mid-latitude, low-altitude permafrost investigations (e.g., Kneisel et al. 2000; Delaloye et al. 2003; Gude et al. 2003; Stiegler et al. 2014; Popescu et al. 2017). If no such information is available, then the reliable interpretation is almost impossible (Schrott and Sass 2008).

Declarations of interest

None.

Acknowledgements

We would like to thank two anonymous reviewers for their constructive comments, and the Editor-in-Chief, Richard A. Marston, for

final editing of the paper. This work was supported by the Czech Science Foundation (grant number 17-21612S) and the Center for Geosphere Dynamics (grant number UNCE/SCI/006).

Appendix A. Supplementary data

Supplementary data associated with this article can be found in the online version at doi:https://doi.org/10.1016/j.geomorph.2018.10.010. These data include the Google map of the most important areas described in this article.

References

Czudek, T., 1986. Pleistocénní permafrost na území Československa. Geografický časopis 38, 245–252.

Czudek, T., 1997. Reliéf Moravy a Slezska v kvartéru. Sursum, Tišnov.

Czudek, T., 2005. Vývoj reliéfu krajiny České republiky v kvartéru. Moravské zemské muzeum, Brno.

Delaloye, R., Lambiel, C., 2005. Evidence of winter ascending air circulation throughout talus slopes and rock glaciers situated in the lower belt of alpine discontinuous permafrost (Swiss Alps). Nor. Geol. Tidsskr. 59, 194–203. https://doi.org/10.1080/00291950510020673.

Delaloye, R., Reynard, E., Lambiel, C., Marescot, L., Monnet, R., 2003. Thermal anomaly in a cold scree slope (Creux du Van, Switzerland). In: Phillips, M., Springman, S.M., Arenson, L.U. (Eds.), Proceedings of the 8th International Conference on Permafrost. Zurich, Switzerland, pp. 175–180.

Draebing, D., 2016. Application of refraction seismics in alpine permafrost studies: A review. Earth Sci. Rev. 155, 136–152. https://doi.org/10.1016/j.earscirev.2016.02.006.

Dudová, L., Hájková, P., Buchtová, H., Opravilová, V., 2013. Formation, succession and landscape history of Central-European summit raised bogs: A multiproxy study from the Hrubý Jeseník Mountains. The Holocene 23, 230–242. https://doi.org/10.1177/0959683612455540.

Gorbunov, A.P., Marchenko, S.S., Seversky, E.V., 2004. The Thermal Environment of Blocky Materials in the Mountains of Central Asia. Permafr. Periglac. Process. 15, 95–98. https://doi.org/10.1002/ppp.478.

Gude, M., Dietrich, S., Mäusbacher, R., Hauck, C., Molenda, R., Ruzicka, V., Zacharda, M., 2003. Probable occurrence of sporadic permafrost in non-alpine scree slopes in central Europe. In: Phillips, M., Springman, S.M., Arenson, L.U. (Eds.), Proceedings of the 8th International Conference on Permafrost. Zurich, Switzerland, pp. 331–336.

Hauck, C., Kneisel, C., 2008. Quantifying the ice content in low-altitude scree slopes using geophysical methods. In: Hauck, C., Kneisel, C. (Eds.), Applied Geophysics in Periglacial Environments. Cambridge University Press, Cambridge, pp. 153–164.

Hauck, C., Vonder Mühll, D., 2003. Inversion and Interpretation of Two-dimensional Geoelectrical Measurements for Detecting Permafrost in Mountainous Regions. Permafr. Periglac. Process. 14, 305–318. https://doi.org/10.1002/ppp.462.

Jeník, J., 1961. Alpinská vegetace Krkonoš, Králického Sněžníku a Hrubého Jeseníku. Nakladatelství ČSAV, Praha.

Kneisel, C., 2010. The nature and dynamics of frozen ground in alpine and subarctic periglacial environments. The Holocene 20, 423–445. https://doi.org/10.1177/0959683609353432.

Kneisel, C., Hauck, C., 2008. Electrical methods. In: Hauck, C., Kneisel, C. (Eds.), Applied Geophysics in Periglacial Environments. Cambridge University Press, Cambridge, pp. 3–27.

Kneisel, C., Hauck, C., Vonder Mühll, D., 2000. Permafrost below the Timberline Confirmed and Characterized by Geoelectrical Resistivity Measurements, Bever Valley, Eastern Swiss Alps. Permafr. Periglac. Process. 11, 295–304. https://doi.org/10.1002/1099-1530(200012)11:4<295::AID-PPP353>3.0.CO;2-L.

Křížek, M., 2016. Periglacial landforms of the Hrubý Jeseník Mountains. In: Pánek, T., Hradecký, J. (Eds.), Landscapes and Landforms of the Czech Republic. Springer, Cham, pp. 277–289.

Lindgren, A., Hugelius, G., Kuhry, P., Christensen, T.R., Vandenberghe, J., 2016. GIS-based Maps and Area Estimates of Northern Hemisphere Permafrost Extent during the Last Glacial Maximum. Permafr. Periglac. Process. 27, 6–16. https://doi.org/10.1002/ppp.1851.

Morard, S., Delaloye, R., Dorthe, J., 2008. Seasonal thermal regime of a mid-latitude ventilated debris accumulation. In: Kane, D.L., Hinkel, K.M. (Eds.), Proceedings of the 9th International Conference on Permafrost. Fairbanks, Alaska, pp. 1233–1238.

Morard, S., Delaloye, R., Lambiel, C., 2010. Pluriannual thermal behavior of low elevation cold talus slopes in western Switzerland. Geogr. Helv. 65, 124–134. https://doi.org/10.5194/gh-65-124-2010.

Parkhomenko, E.I., 1967. Electrical Properties of Rocks. Plenum Press, New York.

Popescu, R., Vespremeanu-Stroe, A., Onaca, A., Vasile, M., Cruceru, N., Pop, O., 2017. Low-altitude permafrost research in an overcooled talus slope-rock glacier system in the Romanian Carpathians (Detunata Goală, Apuseni Mountains). Geomorphology 295, 840–854. https://doi.org/10.1016/j.geomorph.2017.07.029.

Růžička, V., Zacharda, M., Šmilauer, P., Kučera, T., 2015. Can paleorefugia of cold-adapted species in talus slopes resist global warming? Boreal Environ. Res. 20, 403–412.

Rybníček, K., Rybníčková, E., 2004. Pollen analyses of sediments from the summit of the Praděd range in the Hrubý Jeseník Mts (Eastern Sudetes). Preslia 76, 331–347.

Šafanda, J., Rajver, D., 2001. Signature of the last ice age in the present subsurface temperatures in the Czech Republic and Slovenia. Glob. Planet. Chang. 29, 241–257. https://doi.org/10.1016/S0921-8181(01)00093-5.

Schrott, L., Hoffmann, T., 2008. Refraction seismics. In: Hauck, C., Kneisel, C. (Eds.), Applied Geophysics in Periglacial Environments. Cambridge University Press, Cambridge, pp. 57–80.

Schrott, L., Sass, O., 2008. Application of field geophysics in geomorphology: advances and limitations exemplified by case studies. Geomorphology 93, 55–73. https://doi.org/10.1016/j.geomorph.2006.12.024.

Stan, D., Stan-Kłeczek, I., Kania, M., 2017. Geophysical approach to the study of a periglacial blockfield in a mountain area (Ztracené kameny, Eastern Sudetes, Czech Republic). Geomorphology 293, 380–390. https://doi.org/10.1016/j.geomorph.2016.12.004.

Stiegler, C., Rode, M., Sass, O., Otto, J.C., 2014. An Undercooled Scree Slope Detected by Geophysical Investigations in Sporadic Permafrost below 1000 M ASL, Central Austria. Permafr. Periglac. Process. 25, 194–207. https://doi.org/10.1002/ppp.1813.

Szewczyk, J., Nawrocki, J., 2011. Deep-seated relict permafrost in northeastern Poland. Boreas 40, 385–388. https://doi.org/10.1111/j.1502-3885.2011.00218.x.

Telford, W.M., Geldart, L.P., Sheriff, R.E., 1990. Applied Geophysics. Cambridge University Press, Cambridge.

Vandenberghe, J., French, H.M., Gorbunov, A., Marchenko, S., Velichko, A.A., Jin, H., Cui, Z., Zhang, T., Wan, X., 2014. The Last Permafrost Maximum (LPM) map of the Northern Hemisphere: permafrost extent and mean annual air temperatures, 25–17 ka BP. Boreas 43, 652–666. https://doi.org/10.1111/bor.12070.

Wicky, J., Hauck, C., 2017. Numerical modelling of convective heat transport by air flow in permafrost talus slopes. The Cryosphere 11, 1311–1325. https://doi.org/10.5194/tc-11-1311-2017.

Zacharda, M., Gude, M., Kraus, S., Hauck, C., Molenda, R., Růžička, V., 2005. The Relict Mite *Rhagidia gelida* (Acari, Rhagidiidae) as a Biological Cryoindicator of Periglacial Microclimate in European Highland Screes. Arct. Antarct. Alp. Res. 37, 402–408. https://doi.org/10.1657/1523-0430(2005)037[0402:TRMRGA]2.0.CO;2.

Zacharda, M., Gude, M., Růžička, V., 2007. Thermal Regime of Three Low Elevation Scree Slopes in Central Europe. Permafr. Periglac. Process. 18, 301–308. https://doi.org/10.1002/ppp.598.

7.4 Paper IV

Uxa, T., Mida, P. (2017). Rock Glaciers in the Western and High Tatra Mountains, Western Carpathians. *Journal of Maps*, 13(2), 844–857. https://doi.org/10.1080/17445647.2017.1378136

Journal Citation Reports 2016: IF= 2.174, Q3(33/49) in Geography Physical.

Citations as of 9 June 2020: Web of Science=5, Scopus=4, Google Scholar=7, ResearchGate=5.

JOURNAL OF MAPS, 2017
VOL. 13, NO. 2, 844–857
https://doi.org/10.1080/17445647.2017.1378136

Taylor & Francis
Taylor & Francis Group

Science

OPEN ACCESS Check for updates

Rock glaciers in the Western and High Tatra Mountains, Western Carpathians

Tomáš Uxa [a,b] and Peter Mida [a]

[a]Department of Physical Geography and Geoecology, Faculty of Science, Charles University, Praha, Czech Republic; [b]Department of Geothermics, Institute of Geophysics, Academy of Sciences of the Czech Republic, Praha, Czech Republic

ABSTRACT

A detailed map of rock glaciers at a scale of 1 : 40 000 is produced for the Western and High Tatra Mts., Western Carpathians, based on remotely sensed mapping. We inventoried a total of 383 rock glaciers, covering a total area of 13.84 km^2. Most rock glaciers (85 %) are considered relict (without permafrost). These landforms have an average lower limit of 1684 m asl and occupy a total area of 12.50 km^2. In contrast, intact rock glaciers (containing permafrost) cover a total area of 1.34 km^2 and their average lower limit is located at 1986 m asl, which is 56 m above the previously suggested lower limit of discontinuous permafrost. The inventory adds new information about rock-glacier occurrence in the European high-mountain areas and improves the understanding of present and past environmental conditions in the region.

ARTICLE HISTORY
Received 31 October 2016
Revised 5 September 2017
Accepted 7 September 2017

KEYWORDS
Rock glaciers; inventory; Western and High Tatra Mts.; Carpathians; Slovakia; Poland

1. Introduction

Rock glaciers are tongue- or lobate-shaped landforms resulting from downslope creeping of ice-rich debris in mountain permafrost conditions (e.g. Barsch, 1996; Berthling, 2011; Kääb, 2013). Most rock glaciers exhibit characteristic surface morphology consisting of steep frontal and lateral slopes (for active rock glaciers mostly steeper than the angle of repose) enclosing rugged upper surface with frequent longitudinal and transversal ridges and furrows emerging due to the compression of debris-ice mixture associated with the rock-glacier flow, closely resembling lava streams (Kääb, 2013). Because of high portion of non-ice component, rock glaciers are usually able to retain much of their morphology long after the permafrost body has completely thawed (Hughes, Gibbard, & Woodward, 2003), meaning they can be identified even in a relict state and under vegetation cover if high-resolution remotely sensed imagery or digital elevation models are available (e.g. Colucci, Boccali, Žebre, & Guglielmin, 2016; Kellerer-Pirklbauer, Wagner, & Winkler, 2016).

Active and inactive rock glaciers represent important component of mountain cryosphere because they contain significant volumes of ground ice and act as long-term stores of water, even in arid or semi-arid regions (e.g. Azócar & Brenning, 2010; Brenning, 2005; Burger, Degenhardt, & Giardino, 1999; Millar, Westfall, & Delany, 2013). Analogously, relict rock glaciers indicate the existence of large amounts of ground ice in the past (e.g. Barsch, 1996; Kääb, 2013) and because of a high storage capacity they noticeably affect current hydrology of mountain watersheds as well (e.g. Wagner, Pauritsch, & Winkler, 2016; Winkler et al., 2016). Furthermore, rock glaciers are highly sensitive indicators of both present and past climate and permafrost evolution (e.g. Barsch, 1996; Frauenfelder & Kääb, 2000; Haeberli et al., 2006), which can be mapped rapidly and at low cost to build-up extensive databases of permafrost evidence over large spatial scales. Consequently, there is a worldwide interest to compile rock-glacier inventories for a number of both purely scientific and practical reasons. In Europe, these investigations have been realized in larger scale particularly in the Alps (e.g. Baroni, Carton, & Seppi, 2004; Colucci et al., 2016; Kellerer-Pirklbauer, Lieb, & Kleinferchner, 2012; Krainer & Ribis, 2012; Nyenhuis, Hoelzle, & Dikau, 2005; Scotti, Brardinoni, Alberti, Frattini, & Crosta, 2013; Seppi et al., 2012), the Pyrenees (e.g. Chueca, 1992; Serrano, Agudo, & Martinez de Pisón, 1999), the Scandinavian Mts. (e.g. Lilleøren & Etzelmüller, 2011; Sollid & Sørbel, 1992) and the Southern Carpathians (e.g. Onaca, Ardelean, Urdea, & Magori, 2017; Urdea, 1992).

Unlike the above regions, rock-glacier mapping in the Western and High Tatra Mts., Western Carpathians (Slovakia and Poland), has been much less intensive. Rock glaciers in the study area were first noted by Partsch (1923) who reported their occurrence in the High Tatra Mts. Later on, Klimaszewski (1948, 1988) and Jahn (1958) described rock glaciers in the Polish territory of the region and called them 'debris

CONTACT Tomáš Uxa tomas.uxa@natur.cuni.cz Department of Physical Geography and Geoecology, Faculty of Science, Charles University, Albertov 6, 128 43 Praha 2, Czech Republic; Department of Geothermics, Institute of Geophysics, Academy of Sciences of the Czech Republic, Boční II 1401, 141 31 Praha 4, Czech Republic

glaciers' and 'patch rock glaciers', respectively. In the Slovak territory, many rock glaciers were described by Lukniš (1973) throughout the entire area of the High Tatra Mts., but they were referred to as 'firn moraines'. A year later, Nemčok and Mahr (1974) published the most extensive rock-glacier inventory to date, in which they reported 13 and 18 sites with rock-glacier occurrence in the Slovak territory of the Western and High Tatra Mts., respectively, but a number of landforms have remained unmapped. After more than a 10-year hiatus, many rock-glacier studies have emerged since the turn of the eighties and nineties (Baumgart-Kotarba & Kotarba, 2001; Dzierżek, Lindner, & Nitychoruk, 1987; Dzierżek & Nitychoruk, 1986; Kaszowski, Krzemień, & Libelt, 1988; Kociuba, 1996; Kotarba, 1986, 1988, 1991–1992, 1992; Kotarba, Kaszowski, & Krzemień, 1987; Libelt, 1988), but exclusively from the Polish side of the mountains. This imbalance began to equalize from 2004 when Kędzia, Kotarba, and Mościcki (2004) published their case study of a single rock glacier located near the Veľké Hincovo pleso Lake in the Slovak High Tatra Mts. and since then, a large amount of work related to rock glaciers has been carried out in both Slovak (Kłapyta, 2009, 2010, 2011, 2012, 2013a, 2013b; Pánek et al., 2015; Pánek et al., 2016; Zasadni & Kłapyta, 2014) and Polish territory (Kłapyta, 2008, 2013b, 2015; Kłapyta & Kołaczek, 2009; Kotarba, 2007, 2013; Makos, Rinterknecht, Braucher, Żarnowski, & Aster Team, 2016; Zasadni & Kłapyta, 2016) of the mountain ranges. In a surprising contrast, no rock glaciers have been reported in the regional overview of periglacial landforms occurring in the Western and High Tatra Mts. compiled by Rączkowska (2007). Most rock glaciers in the region are thought to be relict landforms (Kędzia, 2014) of the Late Glacial or the early Holocene age (e.g. Kaszowski et al., 1988; Kłapyta, 2011, 2013a; Kotarba, 1988, 2007).

Despite a considerable effort resulting in the above extensive list of literature, there still remain large areas both in the Western and High Tatra Mts., where rock glaciers have not been mapped yet. Furthermore, many previous investigations are only descriptive, incomplete and do not enable to determine the rock-glacier occurrence precisely or to extract their morphological attributes. Finally, none of the above rock-glacier studies have focused on the entire area of the Western and High Tatra Mts. Accordingly, the aim of our study is to complete the information on rock-glacier occurrence based on remotely sensed mapping, validated by field and literature data, and to introduce the first detailed map of rock glaciers covering the entire area of the Western and High Tatra Mts.

2. Study area

The Western and High Tatra Mts. are *c.* 42 km and *c.* 26 km, respectively, long mountain ranges, located in the northernmost part of the Carpathian arc and stretching longitudinally along the Slovak-Polish border (Figure 1). They reach their maximum elevations of 2248 m asl and 2655 m asl at the top of Bystrá Peak and Gerlachovský štít Peak, respectively. Geology of the mountain ranges is dominated by Carboniferous-Permian granitic rocks, enriched with Palaeozoic metamorphic rocks, such as gneisses, migmatites or amplibolites in the Western Tatra Mts. On northern sides of the mountain ranges, the crystalline core is overlaid by thrust sheets of Mesozoic sedimentary rocks, particularly limestones and dolomites. The foothills have an extensive cover of Cretaceous-Palaeogene flysch rocks, such as claystones, siltstones, sandstones, conglomerates and breccias (Jurewicz, 2007; Nemčok et al., 1994; Figure 2).

Extensive glaciers recurrently evolved during the cold phases of the Pleistocene (Figure 3), which resulted in typical alpine-type topography with numerous cirques, U-shaped valleys and distinct moraine ridges in both mountain ranges (e.g. Křížek & Mida, 2013; Makos, Nitychoruk, & Zreda, 2013a, 2013b; Zasadni & Kłapyta, 2014), but all pronouncedly more developed in the High Tatra Mts. Currently, the mountains host no glaciers, but perennial snowfields and firn-ice patches can be found in suitable locations (Gądek, 2014). In the period 1981–2010, the mean annual air temperature (MAAT) at the top of Lomnický štít Peak, at 2635 m asl, was –3.4 °C and mean annual precipitation amounted 1653 mm (Slovak Hydrometerological Institute). The present-day climatic snowline has been calculated at *c.* 2500–2600 m asl and *c.* 2700–2800 m asl on northern and southern slopes, respectively (Zasadni & Kłapyta, 2009), and the lower limit of discontinuous permafrost has been estimated at 1930 ± 150–200 m asl based on the analysis of air thawing and freezing indices and complementary geophysical soundings and measurements of bottom temperature of snow (Dobiński, 1997a, 2004, 2005).

3. Methods

3.1. Areal extent and coordinate system

The map focuses on the Western and High Tatra Mts. in a scale of 1 : 40 000 and covers the area of 838.34 km^2 between *c.* 49°06′–49°17′ N and *c.* 19°39′–20°15′ E (Figure 1). The map is projected in the coordinate system WGS 1984 UTM Zone 34N. Accordingly, some layers, originally acquired in the coordinate system S-JTSK (based on Bessel ellipsoid), had to be transformed into the map projection. Considering the medium map scale, we converted the data using the transformation tools implemented in ESRI ArcMap 10.3. We employed the most accurate transformation algorithm (*c.* 1 m error) according to our own testing of the conversion accuracy between the above two coordinate systems (Křížek, Uxa, & Mida, 2016).

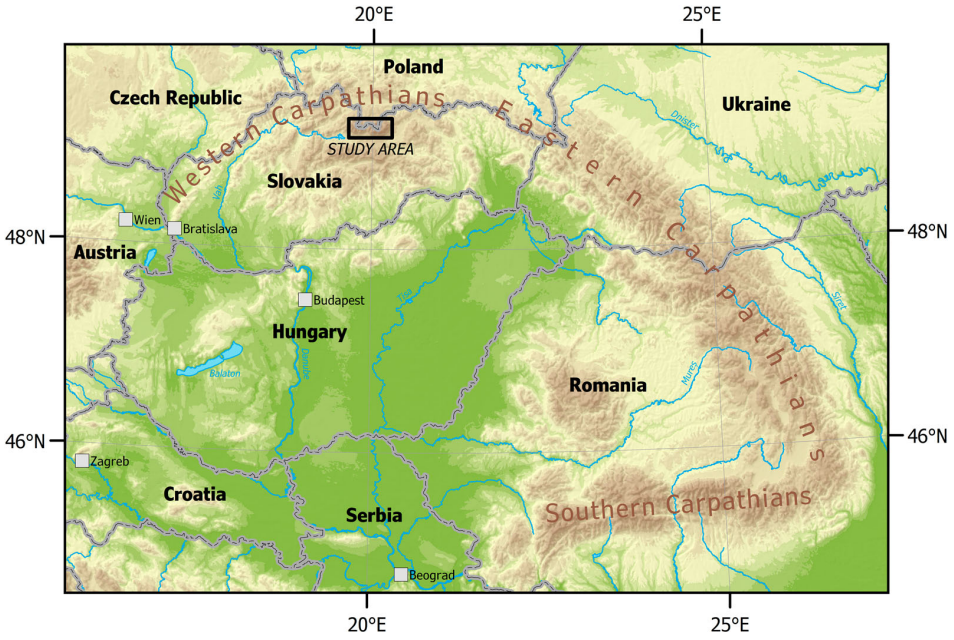

Figure 1. Location map of the Western and High Tatra Mts. within Carpathians. Topography is based on 1 × 1 km resolution digital elevation model (DEM) derived from GTOPO30 and provided by the European Environment Agency (www.eea.europa.eu).
Note: The same data source was utilized to compile the inset map in the Main Map.

3.2. Topography and additional map content

3.2.1. Digital elevation model

We used the existing digital elevation model (DEM) with a horizontal resolution of 10 m produced by stereo photogrammetry from aerial images (Tatra National Park, 2009) as a primary topographic base for the Main Map and as a supplementary source of information for mapping of rock glaciers, delineation of their contributing areas and extraction of elevation attributes. The model represents the most detailed and most widely utilized DEM covering the entire study area to date. Nonetheless, it contains elevation errors and other defects, such as straight break lines, which are mostly located in lower elevated areas unoccupied by rock glaciers, particularly along the alpine treeline and adjacent forest belt located on southern slopes (c.f. Zasadni & Kłapyta, 2014). Therefore, the model was adjusted prior to final map compilation so that the defective parts and their immediate surroundings (accounting for *c.* 11 % of the DEM area) were replaced by a supportive co-registrated 10 m DEM constructed from contour data with equidistance of 10 m provided by the Geodetic and Cartographic Institute Bratislava (GCIB). Both models were merged together and filtered by averaging within a moving window of 5 × 5 cells to ensure smooth transition at the contact of the models. Subsequently, shaded relief and contours with equidistance of 50 m were generated based on this updated and smoothed DEM and thereafter used in the final map.

3.2.2. Other topographic features

Beside the above DEM-based elements, we also added a set of elevation points into the map to provide complementary elevation information. In addition, other topographic features, such as watercourses, lakes, roads, railways, cable cars, built-up areas and state boundary, were integrated into the map for better orientation.

The elevation points and cable cars were obtained by digitizing the national topographic map series in a scale of 1 : 25 000 and 1 : 50 000 accessible on geoportals of the GCIB (geoportal.sk) and the Head Office of Geodesy and Cartography (HOGC; geoportal.gov.pl). In the Slovak territory of the study region, watercourses and lakes were taken from the database SVM 50, which is based on the Basemap of Slovak Republic in a scale of 1 : 50 000. In the Polish territory, these topographic features were acquired by manual digitization of the topographic map accessible at the geoportal of HOGC. Roads, railways and built-up areas for the entire area were extracted from the freely available OpenStreetMap database (download.geofabrik.de).

The topographic layers were checked for quality and particularly their mutual consistency and, if necessary, they were manually adjusted, for example, watercourse directions were slightly changed to appropriately fit the contour lines.

3.2.3. Additional map content

We included a schematic geological map (Figure 2) based on Nemčok et al. (1994) and Bezák et al.

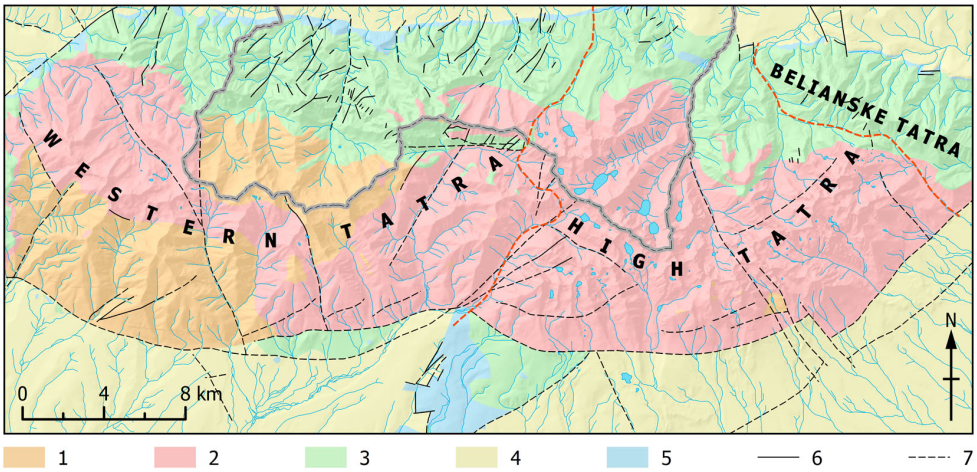

Figure 2. Schematic geological map of the Tatra Mts. based on Nemčok et al. (1994) and Bezák et al. (2013). Legend: 1 – gneiss rocks, migmatite, amphibolite (Palaeozoic); 2 – granitic rocks (Carboniferous-Permian); 3 – limestone, dolomite, sandstone, shale, quartzite (Mesozoic); 4 – claystone, siltstone, sandstone, conglomerate, breccia (Cretaceous-Palaeogene); 5 – sandstone, limestone, conglomerate, breccia (Palaeogene); 6 – fault (proved); 7 – fault (assumed). Red dashed lines indicate geographic subdivision of the Tatra Mts.

(2013) as a background layer in the Main Map in order to infer bedrock lithology of rock glaciers, with division into five geological units: Palaeozoic gneiss rocks, migmatite and amphibolite; Carboniferous-Permian granitic rocks; Mesozoic limestone, dolomite, sandstone, shale and quartzite; Cretaceous-Palaeogene claystone, siltstone, sandstone, conglomerate and breccia; and Palaeogene sandstone, limestone, conglomerate and breccia. Furthermore, the above layer was complemented with both proved and assumed faults based on the same data sources.

We also added the Last Glacial Maximum glacier extent in the Tatra Mts. (Figure 3) after Zasadni and Kłapyta (2014) to provide information about the relationship between rock glaciers and former glaciation limit.

Finally, as rock glaciers are widely accepted indicators of the lower limit of discontinuous mountain permafrost (Barsch, 1996), we show the level of 1930 m asl in the Main Map, which corresponds to the average minimum elevation of discontinuous permafrost occurrence in the Tatra Mts. suggested by Dobiński (1997a, 2004, 2005).

3.3. Rock glaciers

3.3.1. Rock-glacier mapping

We mapped rock glaciers (Figure 4) throughout the entire area of the Western and High Tatra Mts. using aerial photographs from years 2010–2015 with a resolution of 0.1, 0.25, 0.5 and 1 m accessible on geoportals of the GCIB and HOGC and on Google Earth. Rock glaciers were identified and double-checked by both authors based on their typical surface morphological features visible on aerial imagery (Figure 5), such as steep frontal and lateral slopes and longitudinal and/

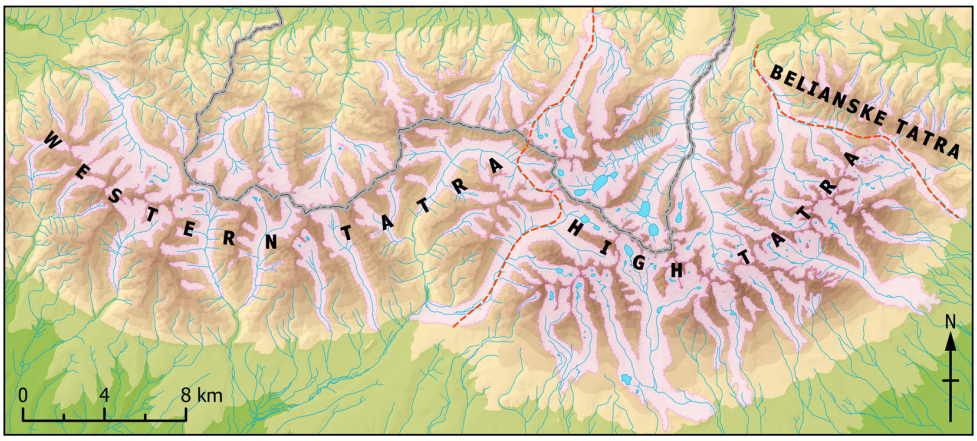

Figure 3. Last Glacial Maximum glacier extent (purple polygons) in the Tatra Mts. after Zasadni and Kłapyta (2014). Red dashed lines indicate geographic subdivision of the Tatra Mts. (color online).

Figure 4. (A) Intact talus rock glacier near the Pusté pleso Lake in the Veľká Studená Valley, High Tatra Mts.; (B) relict talus rock glacier in the Kobylia Valley, Western Tatra Mts.; (C) fronts of intact and relict debris rock glaciers in the Slavkovská Valley, High Tatra Mts.; (D) densely vegetated relict talus rock glacier in the Furkotská Valley, High Tatra Mts.; note the person in the foreground for scale.

Note: White dashed lines delineate rock-glacier fronts.

or transverse ridges and furrows. In areas with closed or semi-closed vegetation cover, we followed vegetation patterns associated with the rock-glacier surface morphology as well (Barsch, 1996). The mapping was also supported by field inspections in 2014, 2015 and 2016, during which *c.* 22 % of the mapped landforms, mostly located in the High Tatra Mts., were visited and their occurrence and delineation was verified. The survey was supported by previous literature reports and maps as well (Dzierżek & Nitychoruk, 1986; Kłapyta, 2008, 2009, 2010, 2011, 2012, 2013a, 2013b, 2015; Kłapyta & Kołaczek, 2009; Kotarba, 1988, 1991–1992, 2007; Nemčok & Mahr, 1974; Zasadni & Kłapyta, 2016) that enable to extract precise information about the location of rock glaciers. However, we did not take over the literature information completely in all cases because the above mappings have emerged over several decades and had inconsistent data sources and mapping methodologies. Consequently, there is occasionally no consensus among researchers regarding the landform identification or classification. An excellent example of this inconsistency is the debris accumulation located near the Zadni Staw Polski Lake in the Pięciu Stawów Polskich Valley in the Polish High Tatra Mts., which was classified as a rock glacier (Dzierżek et al., 1987), a moraine ridge (Makos et al., 2013a) as well as a rock avalanche (Zasadni & Kłapyta, 2016). Therefore, we carefully considered the integration of each individual previously mapped landform into the database mainly based on its appearance on aerial imagery in order to ensure the consistency of the inventory in terms of landform identification, classification and delineation throughout the whole region.

Each rock glacier was manually delineated along the foot of its frontal and lateral slopes towards the rooting zone (Figure 5) based on aerial photographs (c.f. Baroni et al., 2004; Colucci et al., 2016; Kellerer-Pirklbauer et al., 2012; Krainer & Ribis, 2012; Nyenhuis et al., 2005; Onaca et al., 2017; Scotti et al., 2013). In the lower part, the interface between the rock glacier and its surroundings was in most cases clearly discernible. On the contrary, a distinction between the rock-glacier rooting zone and the above-lying contributing area was often much more difficult to differentiate (c.f. Colucci et al., 2016; Krainer & Ribis, 2012). In such cases, the boundary was identified by both visual inspection of aerial images and searching for a sudden change in the DEM-derived slope inclination. Places with gradient exceeding the angle of repose of *c.* 35° (Barsch, 1996) were implicitly considered as parts of the contributing area, probably corresponding to debris-free rock slopes or rock walls (*sensu* Gądek, Grabiec, Kędzia, & Rączkowska, 2016). The layers of slope inclination

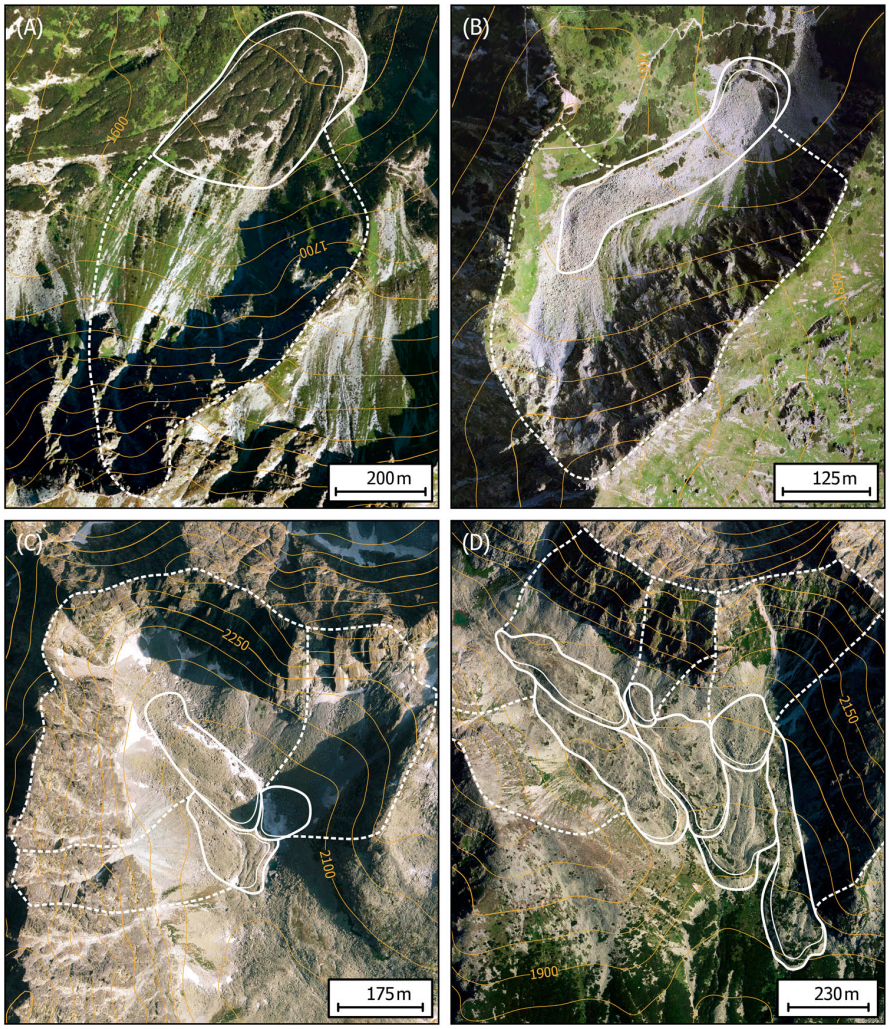

Figure 5. Aerial photographs showing the delineation of rock glaciers and their fronts (white solid lines) as well as contributing areas (white dashed lines); note well-defined ridge-and-furrow topography on some of the rock glaciers. (A) Relict debris rock glacier in the Spálená Valley, Western Tatra Mts.; (B) relict debris rock glacier in the Świstówka Roztocka Valley, High Tatra Mts.; (C) intact talus and debris rock glaciers forming a multipart rock glacier in the Batizovská Valley, High Tatra Mts.; (D) intact and relict talus and debris rock glaciers forming a multipart rock glacier in the Slavkovská Valley, High Tatra Mts. All the figures have a northern orientation.

Note: Parts of other rock glaciers and their contributing areas extending into the images are not highlighted.

and shaded relief were also employed to refine the delineation of some large rock-glacier outlines. In cases where more rock-glacier bodies merge to form so-called multipart rock glacier (Barsch, 1996), we delineated each of these distinguishable parts individually (c.f. Falaschi, Castro, Masiokas, Tadono, & Ahumada, 2014; Kellerer-Pirklbauer et al., 2012).

3.3.2. Rock-glacier classification

After completion of the rock-glacier mapping, we classified rock glaciers according to the main source of material, permafrost presence and activity, and bedrock lithology.

Two rock-glacier categories, talus rock glaciers and debris rock glaciers (Barsch, 1996; Figure 4), were adopted to differentiate the landforms based on the main source of material. As talus rock glaciers are regarded those landforms, which are unambiguously related to talus slopes situated above, delivering frost-shattered rock fragments for rock-glacier formation, and do not significantly extend down to the bottom of the valley. By contrast, debris rock glaciers are usually more extensive debris deposits, mostly covering valley floors, which evolve particularly from moraine-derived materials. We also include the most distinct landforms referred to as protalus (pronival) ramparts into the first category for two main reasons. Firstly, these landforms are usually very difficult to differentiate from talus rock glaciers not only from aerial imagery, but also in the field (e.g. Hedding, 2016; Hedding & Sumner, 2013). Secondly, these geomorphic features are largely genetically related to talus rock glaciers and

many researchers describe them as embryonic stage of rock glaciers, that is, a kind of developmental continuum, closely resembling them in morphology, internal structure, ice content and morphodynamics (e.g. Barsch, 1996; Haeberli, 1985; Scapozza, 2015).

Intact and relict classes were set to differentiate the rock glaciers according to the presence of permafrost and activity (Barsch, 1996). Intact rock glaciers (including both active and inactive landforms) host permafrost inside and may (active rock glaciers) or may not (inactive rock glaciers) move due to permafrost creep. In contrast, permafrost has completely thawed within relict rock glaciers. Borehole drilling, ground temperature measurements, geophysical soundings and/or monitoring of rock-glacier movements are particularly helpful to distinguish between the intact and relict rock glaciers (e.g. Haeberli et al., 2006). Some of the above methods have been employed in the High Tatra Mts., suggesting probable permafrost presence in several rock glaciers (Kędzia, 2014), but the data are available for a limited number of landforms (Dobiński, 1997b; Gądek & Kędzia, 2008, 2009; Kędzia et al., 2004; Uxa & Mida, 2016, 2017). Consequently, the classification is largely based on morphological attributes discernible on aerial imagery that are widely accepted to be indicative of ground ice presence or absence and were adopted in many recent rock-glacier inventories as well (e.g. Colucci et al., 2016; Falaschi et al., 2014; Onaca et al., 2017; Scotti et al., 2013). Intact rock glaciers are characterized by steep frontal and lateral slopes, which often exceed the angle of repose of *c.* 35°, exhibit well-defined ridge-and-furrow topography, and completely lack or have sparse vegetation cover. In contrast, relict rock glaciers are typical of subdued topography with gentler slopes caused by permafrost degradation, and usually have extensive vegetation cover.

The bedrock lithology of individual rock glaciers was inferred from the schematic geological map (see section 3.2.3; Figure 2) based on rock-glacier outlines. In total, three geological units were identified for the mapped rock glaciers: Palaeozoic gneiss rocks, migmatite and amphibolite; Carboniferous-Permian granitic rocks; and Mesozoic limestone, dolomite, sandstone, shale and quartzite.

3.3.3. Rock-glacier contributing areas

Contributing area of each rock glacier, that is, the zone where source material for its formation is collected (Figure 5), was computed using the Hydrology tools (e.g. Bolch & Gorbunov, 2014) implemented in ESRI ArcMap 10.3 based on the void-filled DEM (see section 3.2.1.). Because this debris-contributing area (*sensu* Janke & Frauenfelder, 2008) may not be identical to the hydrological catchment of a rock glacier (particularly in the case of debris rock glaciers), only those parts of the respective rock glaciers, which presumably received material directly from the source zone (i.e. not secondarily through the rock-glacier flow), were used as the lower modelling limit. Several lines of evidence, such as the orientation of ridges and furrows and the connection between the outer edge of a rock glacier and neighbouring slope, were considered to determine these rock-glacier parts. The delineated contributing areas are essentially based on calculations confined to locations outside the rock glaciers, and therefore no problems that could be expected on rugged rock-glacier topography, such as flow divergence or presence of sinks with undefined flow direction, have been encountered. The contributing areas of lower-lying rock glaciers forming parts of multipart rock glaciers were set to include both the area of all the above-lying and genetically related rock glaciers and their contributing areas.

4. Mapping results and interpretation

The inventory contains a total of 383 rock glaciers occupying the area of 13.84 km^2, which are supplied by rock material from 51.81 km^2 of contributing areas (Table 1). Hence, the total rock-glacier-affected area in both mountain ranges constitutes 65.65 km^2, which comprises *c.* 16 % of the area above 1375 m asl (~lower limit of rock-glacier occurrence). The average rock-glacier density above this limit is 0.93 landforms per km^2 and the average specific rock-glacier area accounts for 3.34 ha per km^2. Less rock glaciers, 183 (*c.* 48 %), occur in the Western Tatra Mts. than in the High Tatra Mts. where 200 rock glaciers (*c.* 52 %) are located. However, this does not translate into the difference in the total rock-glacier area, which is by 0.45 km^2 larger in the Western Tatra Mts. On the other hand, the total contributing area is by 2.60 km^2 more extensive in the High Tatra Mts. (Table 1).

Talus rock glaciers predominate in both mountain ranges, with *c.* 63 % and *c.* 74 % in the Western Tatra and High Tatra Mts., respectively, but their total area represents only *c.* 25 % and *c.* 42 % of all the rock glaciers. Accordingly, debris rock glaciers are substantially larger in size, which is on average around four to five times the average size of talus rock glaciers (Table 1). Debris rock glaciers also have substantially larger contributing areas (Table 1), which are capable to supply these voluminous landforms with a sufficient amount of material necessary for their development. Most rock glaciers are considered as relict; only seven landforms were classified as intact in the Western Tatra Mts. (*c.* 4 %) and other forty nine in the High Tatra Mts. (*c.* 25 %), representing *c.* 15 % of the total number of rock glaciers in the entire study region and covering the total area of 1.34 km^2 (Table 1). Relict landforms extend down to 1375 m asl and 1414 m asl in the Western and High Tatra Mts., respectively, with the average front elevation of 1644 ± 119 m asl and 1731

Table 1. General distribution and areal characteristics of rock glaciers and their contributing areas in the Western and High Tatra Mts.

		Rock-glacier area (ha)				Contributing area (ha)			
Rock glaciers	Number	Mean	Min	Max	Sum	Mean	Min	Max	Sum
Western Tatra Mts.									
Talus	115	1.56	0.09	6.13	179.09	6.23	0.37	32.24	716.03
Debris	68	7.87	1.11	49.85	535.15	25.65	0.96	139.84	1744.42
Intact	7	2.18	0.33	5.29	15.24	14.77	0.92	32.55	103.40
Relict	176	3.97	0.09	49.85	698.99	13.39	0.37	139.84	2357.05
Total	183	3.90	0.09	49.85	714.23	13.45	0.37	139.84	2460.45
High Tatra Mts.									
Talus	147	1.90	0.15	8.76	279.15	8.17	0.78	49.59	1201.04
Debris	53	7.36	1.76	44.42	390.34	28.67	2.46	105.34	1519.43
Intact	49	2.42	0.18	14.63	118.54	11.69	0.78	44.30	572.92
Relict	151	3.65	0.15	44.42	550.96	14.22	1.09	105.34	2147.54
Total	200	3.35	0.15	44.42	669.50	13.60	0.78	105.34	2720.46

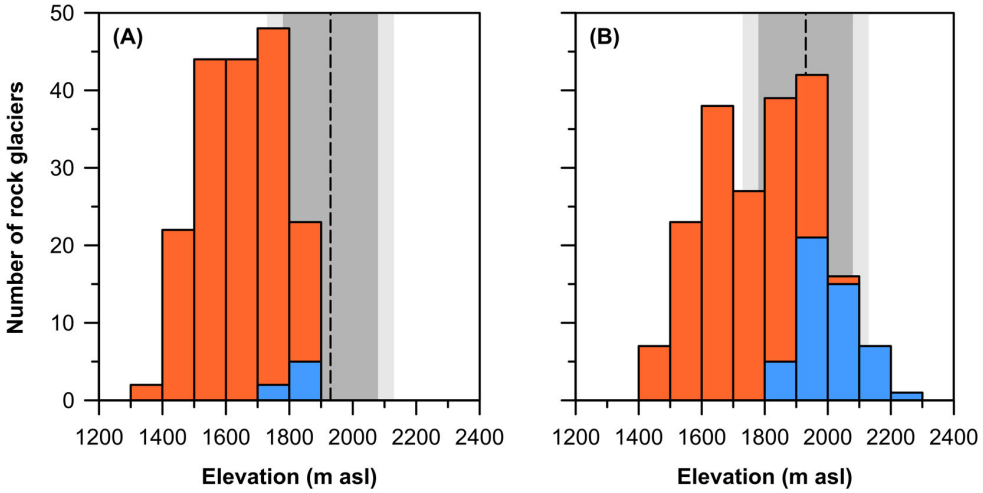

Figure 6. Minimum elevation of rock-glacier fronts in the (A) Western and (B) High Tatra Mts. Orange bars represent relict rock glaciers; intact rock glaciers are shown in blue. Black dashed line and contiguous grey areas indicate the lower limit of discontinuous permafrost occurrence of 1930 ± 150–200 m asl proposed by Dobiński (1997a, 2004, 2005).

± 143 m asl, respectively (Figure 6). Lower limit of intact rock glaciers occurs at 1761 m asl and 1831 m asl in the Western and High Tatra Mts., respectively, and their front elevation averages 1812 ± 30 m asl and 2011 ± 92 m asl, respectively. The discrepancy of nearly 200 m between the mountain ranges between the mountain ranges in the latter parameter results from wider elevation range where intact rock glaciers occur in the High Tatra Mts., and also from the limited number of intact landforms in the Western Tatra Mts. Consistently with the distribution patterns observed elsewhere (see Barsch, 1996), both relict and intact rock glaciers have their lower limits located higher in southern aspects than in northerly exposed places. In the Western Tatra Mts., the average front elevation of relict and intact rock glaciers facing the NW–NE directions is at 1599 ± 107 m asl and 1823 ± 37 m asl, respectively, while landforms oriented to the SW–SE are at 1723 ± 103 m asl and 1819 ± 18 m asl, respectively. In the High Tatra Mts., the respective elevations are 1692 ± 159 m asl and 1943 ± 63 m asl for the NW–NE sectors and 1768 ± 116 m asl and 2018 ± 88 m asl for the SW–SE. Intact rock glaciers are mostly of talus type, with *c.* 86 % and *c.* 78 % in the Western and High Tatra Mts., respectively, and have on average around one and a half to two times smaller size than relict landforms (Table 1).

Rock glaciers occur in three different geological units (Table 2), which represent 100 % and *c.* 97 % of the area above 1375 m asl in the Western and High Tatra Mts., respectively. The total numbers and areas of rock glaciers built by different substrates well correlate with the areal proportion of these materials in the study region. Granitic rocks predominate here (Figure 2), and therefore *c.* 65 % and 96 % of rock glaciers, covering the total area of 4.84 km^2 and 6.46 km^2, are formed within these substrates in the Western and High Tatra Mts., respectively (Table 2). More diverse geology of the Western Tatra Mts. promotes *c.* 27 % of rock glaciers (2.00 km^2) consisting of Palaeozoic metamorphic rocks (particularly gneisses and migmatites) and *c.* 8 % of the landforms (0.31 km^2) developed within Mesozoic

Table 2. Areal extent of geological units above 1375 m asl (~lower limit of rock-glacier occurrence) and rock-glacier presence in the Western and High Tatra Mts.

		Rock glaciers				
Geological unit	Area (km^2)	Number	Total area (ha)	Mean area (ha)	Mean specific area (ha/km^2)	Density (n/km^2)
Western Tatra Mts.						
Gneiss rocks, migmatite, amphibolite	69.59	50	199.75	4.00	2.87	0.72
Granitic rocks	102.48	119	483.82	4.07	4.72	1.16
Limestone, dolomite, sandstone, shale, quartzite	38.34	14	30.66	2.19	0.80	0.37
High Tatra Mts.						
Gneiss rocks, migmatite, amphibolite	1.06	2	6.83	3.42	6.44	1.89
Granitic rocks	175.08	192	645.53	3.36	3.69	1.10
Limestone, dolomite, sandstone, shale, quartzite	21.04	6	17.14	2.86	0.81	0.29

Note: Only the geological units hosting rock glaciers are listed.

limestones, dolomites, sandstones, shales and quartzites. On the contrary, only 1 % and 3 % of rock glaciers (0.07 km^2 and 0.17 km^2) in the High Tatra Mts. are formed by these materials (Table 2). In total, the non-granitic rock glaciers cover the area of 2.31 km^2 and 0.24 km^2 in the Western and High Tatra Mts., respectively.

Rock glaciers consisting of Mesozoic limestones, dolomites, sandstones, shales and quartzites have the smallest average size and also show the lowest rock-glacier density as well as the lowest specific rock-glacier area in both mountain ranges (Table 2), which suggests that these materials are less favourable for rock-glacier formation in the study region. In contrast, rock glaciers built by granitic rocks and Palaeozoic metamorphic rocks are substantially larger and occur more frequently within the hosting geological units (Table 2). Their average sizes are almost identical in the individual mountain ranges, but in total the latter landforms are slightly larger, which is associated with both comparatively greater abundance of Palaeozoic metamorphic rocks in the Western Tatra Mts. and more extensive rock glaciers occurring there. On the other hand, the average rock-glacier density in the entire study region is distinctly the highest for granitic rocks, 1.12 landforms per km^2, as is the average specific rock-glacier area, which in these substrates equals 4.07 ha per km^2.

Intact rock glaciers can be utilized to approximate the contemporary lower limit of discontinuous permafrost on a regional scale, and relict rock glaciers can indicate the variations in discontinuous permafrost extent in the past (e.g. Barsch, 1996; Haeberli et al., 2006). The average front elevation of intact rock glaciers calculated collectively for both mountain ranges is at 1986 ± 109 m asl, which on average represents the area of 60.45 km^2 above this level in the entire study region. The average value of 1986 m asl is 56 m above the previously proposed average discontinuous permafrost boundary of 1930 m asl (Dobiński, 1997a, 2004, 2005). Undoubtedly, the difference is principally affected by distinct methodologies. The former investigations (Dobiński, 1997a, 2004, 2005) assessed the permafrost occurrence in principle via the elevation of zero isotherm of air temperature, while the present study builds on the visual inspection of rock-glacier activity based on aerial imagery. Active rock glaciers typically exist in areas where MAAT is −2 °C or less (Barsch, 1996). However, internal ice core may persist inside inactive rock glaciers even under positive MAAT because coarse blocky materials of rock glaciers tend to be substantially colder than outside air (e.g. Gorbunov, Marchenko, & Seversky, 2004; Harris & Pedersen, 1998). Because inactive rock glaciers dominate the intact category in the Western and High Tatra Mts. and the cooling effect has been extensively observed here as well (Uxa & Mida, 2016, 2017), the average elevation of the intact rock-glacier front and the zero isotherm of air temperature should likely be reversed. This issue may be attributed to climate warming because the earlier estimates of permafrost distribution (Dobiński, 1997a, 2004, 2005) were mostly based on air temperature series two to three decades older (from 1985–1989 or 1985–1994) than our aerial images. The air temperature at Kasprowy Wierch (1991 m asl), located almost exactly in the middle of the study region, has been increasing on average by 0.02 °C per year (Żmudzka, 2011) during 1966–2006 and has continued to rise at least until 2010 (Gądek & Leszkiewicz, 2012). Such a warming rate would elevate the zero isotherm level by 73–109 m in 20–30 years, assuming the average temperature lapse rate of 0.0055 °C per m that is based on 1951–1970 data from the eight highest elevated stations in the Western and High Tatra Mts. (Niedzwiedz, 1992). In that case, the zero isotherm of air temperature would be at 2003–2039 m asl, which much better fits the presumed relation between air temperature and distribution of mostly inactive rock glaciers. In addition, the contemporary zero isotherm level may lie even higher because the warming apparently accelerated in the eighties of the last century (see e.g. Gądek & Leszkiewicz, 2012; Żmudzka, 2011).

Because the lowest fronts of relict rock glaciers descend to around 1400 m asl (Figure 6), the lower boundary of discontinuous permafrost in the Western and High Tatra Mts. in the Late Glacial or the early Holocene probably occurred around this level, provided that the rock glaciers could fully develop under the given climate conditions. In that case, discontinuous

Table 3. Overview of front elevations of intact and relict rock glaciers in the European Alps and the Carpathians.

			Intact		Relict			
Region	Longitude	Latitude	Number	Front elevation	Number	Front elevation	Intact–Relict	Source
Graian Alps, Italy	6°52′	45°50′	–	2484[a]	–	–	–	Guglielmin and Smiraglia (1998)
Prealps, Vaud, Switzerland	7°08′	46°24′	0	–	25	1761 ± 165	–	Schoeneich (1998)
Maritime Alps, Italy	7°11′	44°14′	–	2179[a]	–	–	–	Guglielmin and Smiraglia (1998)
Entremont, Valais, Switzerland	7°12′	45°56′	166	2626 ± 132	155	2400 ± 168	226	Delaloye and Morand (1998)
Cottian Alps, Italy	7°15′	44°40′	–	2458[a]	–	–	–	Guglielmin and Smiraglia (1998)
Printse Valley, Valais, Switzerland	7°19′	46°06′	40	2715 ± 165	31	2342 ± 166	373	Reynard, Lambiel, and Wenker (1998)
Turtmanntal, Valais, Switzerland	7°42′	46°12′	62	2621 ± 119	21	2496 ± 145	125	Nyenhuis et al. (2005)
Bernese Alps, western Switzerland	7°47′	46°28′	41	2515 ± 136	41	2183 ± 330	332	Imhof (1998)
Pennine Alps, Italy	7°52′	45°56′	–	2457[a]	–	–	–	Guglielmin and Smiraglia (1998)
Fletschhorn area, Valais, Switzerland	7°58′	46°11′	51	2617 ± 177	25	2508 ± 203	109	Frauenfelder (1998)
Lepontine Alps, Italy	8°08′	46°24′	–	2168[a]	–	–	–	Guglielmin and Smiraglia (1998)
Upper Engadin, Switzerland	9°49′	46°28′	144	2637 ± 135	26	2370 ± 205	267	Hoelzle (1998)
Central Italian Alps, Italy	9°52′	46°10′	639	2590[b] ± 129[c]	875	2205[b] ± 149[c]	385	Scotti et al. (2013)
Rhaetian Alps, Italy	10°00′	46°48′	–	2319[a]	–	–	–	Guglielmin and Smiraglia (1998)
Adamello-Presanella Massif, Italian Alps, Italy	10°37′	46°07′	88	2485 ± 186	128	2058 ± 149	427	Baroni et al. (2004)
Tyrolean Alps, Austria	10°53′	47°01′	1432	2573	1713	2279	294	Krainer and Ribis (2012)
Atesine Alps, Italy	10°56′	46°36′	–	2438[a]	–	–	–	Guglielmin and Smiraglia (1998)
Eastern Italian Alps, Italy	11°12′	46°05′	173	2632 ± 205	532	2169 ± 211	463	Seppi et al. (2012)
Dolomites, Italy	11°51′	46°26′	–	2236[a]	–	–	–	Guglielmin and Smiraglia (1998)
Carnic Alps, Italy	12°53′	46°36′	–	1744[a]	–	–	–	Guglielmin and Smiraglia (1998)
Eastern European Alps, Austria	14°19′	47°20′	347	2515 ± 106[c]	1300	2102 ± 171[c]	413	Kellerer-Pirklbauer et al. (2012)
Southeastern Alps, Italy	14°28′	46°09′	4	1827[b]	49	1778[b]±69[c]	49	Colucci et al. (2016)
Western and High Tatra Mts., Slovakia and Poland	19°57′	49°12′	56	1986 ± 109	327	1684 ± 137	302	This study
Southern Carpathians, Romania	23°42′	45°25′	48	2088 ± 49[c]	258	1930 ± 99[c]	158	Onaca et al. (2017)

Note: Averages and standard deviations are reported if not defined otherwise.
[a]Unweighted average of mean front elevations of active and inactive rock glaciers.
[b]Median subtracted from boxplot diagram.
[c]Half of the interquartile range subtracted from boxplot diagram.

permafrost would occupy the area of *c.* 393 km^2 in the entire study region, that is, around six and a half times more than the estimated contemporary discontinuous permafrost extent, and the MAAT at 1400 m asl could be −2 °C or less if we accept this value to be valid for active rock glaciers to develop (Barsch, 1996). The contemporary MAAT at this elevation is estimated to be +3.4 °C based on the 1981–2010 temperature record from Lomnický štít Peak and the present average lapse rate of 0.0055 °C per m. Consequently, the temperature at the time of the rock-glacier formation was probably at least 5.4 °C lower than at present.

The spread between the average front elevation of intact and relict rock glaciers in the Western and High Tatra Mts. is well within the ranges observed in most surrounding regions, but local rock glaciers occur on average about 400–600 m lower than in the European Alps (Table 3). The decline in the front elevation is similar to that reported from some of the easternmost sub-regions of the European Alps and the Southern Carpathians (Table 3), which has been attributed to less precipitation towards the east (e.g. Onaca et al., 2017), causing thinner snow cover during winter, and thus lower ground temperatures (*sensu* Gruber & Haeberli, 2009). About 100 m lower average front elevation of the intact rock glaciers in the Western and High Tatra Mts. than in the Southern Carpathians is most likely due to latitudinal temperature decrease, and is close to the previously reported difference in the contemporary lower limit of discontinuous permafrost of 70 m between these two Carpathian regions (Dobiński, 2005).

5. Conclusions

The map includes a total of 383 rock glaciers, making it the most comprehensive rock-glacier inventory for the entire area of the Western and High Tatra Mts. to date. Relict rock glaciers account for 85 % of the database

and cover the total area of 12.50 km^2. These landforms have their lowest limit around 1400 m asl, and thus the lower boundary of discontinuous permafrost zone in the Late Glacial or the early Holocene probably lied at this level, and covered the total area of around *c.* 393 km^2. Intact rock glaciers constitute 15 % of the inventory and cover the total area of 1.34 km^2. Their average front elevation of 1986 ± 109 m asl delineates the contemporary lower limit of discontinuous permafrost zone on a regional scale that occupies the total area of 60.45 km^2.

The rock-glacier inventory adds to the current state of knowledge about the occurrence of these permafrost landforms in less investigated high-mountain regions located east of the European Alps. However, it must be emphasized that the inferred permafrost limits and extents should be understood as rather tentative in nature. Rock glaciers can provide a first-order evaluation of potential permafrost distribution, which generally tends to overestimate the permafrost extent at places without debris cover. Consequently, the present work is rather a starting point towards more thorough analyses of rock-glacier distribution and morphology and modelling of discontinuous permafrost distribution, which will substantially improve the understanding of present and past environmental conditions in the Western and High Tatra Mts.

Software

The mapping, digitizing, analyses of DEM and map compilation were all carried out using ESRI ArcMap 10.3. Final merger of vector and raster map elements was done in Adobe Acrobat Pro DC.

Data availability

The shapefiles of rock-glacier outlines and contributing areas are available on request by the authors. Data users are requested to inform the data owners about the planned activities and invite them to contribute to any work that would lead to a co-authorship.

Acknowledgements

We would like to sincerely thank Marek Křížek for selfless financial support with payment of an article publishing charge. We also thank Bieke Cattoor, Daniel Falaschi and especially Andreas Kellerer-Pirklbauer for their thorough reviews that helped us to substantially improve both the article and the map. The Associate Editor, Jan-Christoph Otto, and the Editor-in-Chief, Mike J. Smith, are thanked for their editorial assistance.

Disclosure statement

No potential conflict of interest was reported by the authors.

Funding

This work was supported by the Charles University [grant numbers GAUK 1312214; SVV 260438].

ORCID

Tomáš Uxa http://orcid.org/0000-0001-9911-6529
Peter Mida http://orcid.org/0000-0001-8847-9615

References

Azócar, G. F., & Brenning, A. (2010). Hydrological and geomorphological significance of rock glaciers in the Dry Andes, Chile (27°–33°S). *Permafrost and Periglacial Processes*, *21*, 42–53. doi:10.1002/ppp.669

Baroni, C., Carton, A., & Seppi, R. (2004). Distribution and behaviour of rock glaciers in the Adamello-Presanella Massif (Italian Alps). *Permafrost and Periglacial Processes*, *15*, 243–259. doi:10.1002/ppp.497

Barsch, D. (1996). *Rockglaciers: Indicators for the present and former geoecology in high mountain environments*. Berlin: Springer.

Baumgart-Kotarba, M., & Kotarba, A. (2001). Deglaciation in the Sucha Woda and Pańszczyca Valleys in the Polish High Tatras. *Studia Geomorphologica Carpatho-Balcanica*, *35*, 7–38.

Berthling, I. (2011). Beyond confusion: Rock glaciers as cryo-conditioned landforms. *Geomorphology*, *131*, 98–106. doi:10.1016/j.geomorph.2011.05.002

Bezák, V., Maglay, J., Polák, M., Kohút, M., Gross, P., Piotrowska, K., … Raczkowski, W. (2013). *Geologicko-náučná mapa Tatier 1 : 50 000* [Geological-educational map of the Tatra Mts. 1 : 50 000]. Bratislava: State Geological Institute of Dionýz Štúr. Retrieved from http://mapserver.geology.sk/vtatry

Bolch, T., & Gorbunov, A. P. (2014). Characteristics and origin of rock glaciers in northern Tien Shan (Kazakhstan/Kyrgyzstan). *Permafrost and Periglacial Processes*, *25*, 320–332. doi:10.1002/ppp.1825

Brenning, A. (2005). Geomorphological, hydrological and climatic significance of rock glaciers in the Andes of central Chile (33–35°S). *Permafrost and Periglacial Processes*, *16*, 231–240. doi:10.1002/ppp.528

Burger, K. C., Degenhardt, J. J., & Giardino, J. R. (1999). Engineering geomorphology of rock glaciers. *Geomorphology*, *31*, 93–132. doi:10.1016/S0169-555X(99)00074-4

Chueca, J. (1992). A statistical analysis of the spatial distribution of rock glaciers, Spanish Central Pyrenees. *Permafrost and Periglacial Processes*, *3*, 261–265. doi:10.1002/ppp.3430030316

Colucci, R. R., Boccali, C., Žebre, M., & Guglielmin, M. (2016). Rock glaciers, protalus ramparts and pronival ramparts in the south-eastern Alps. *Geomorphology*, *269*, 112–121. doi:10.1016/j.geomorph.2016.06.039

Delaloye, R., & Morand, S. (1998). *Rock glaciers, Entremont, Valais, Switzerland* [International Permafrost Association, Data and Information Working Group, comp. Circumpolar Active-Layer Permafrost System (CAPS), version 1.0]. Retrieved from http://nsidc.org/data/docs/fgdc/ggd290_rockglac_switzer/index.html

Dobiński, W. (1997a). Distribution of mountain permafrost in the High Tatras based on freezing and thawing indices. *Biuletyn Peryglacjalny*, *36*, 29–37.

Dobiński, W. (1997b). *Warunki występowania zmarzliny w alpejskim piętrze Tatr Wysokich* [The conditions of permafrost occurrence in the alpine belt of the High Tatra Mts.]. (Unpublished PhD thesis). Uniwersytet Śląski, Sosnowiec.

Dobiński, W. (2004). Wieloletnia zmarzlina w Tatrach: Geneza, cechy, ewolucja [Permafrost in the Tatra Mts.: Genesis, features, evolution]. *Przegląd Geograficzny*, *76*, 327–343.

Dobiński, W. (2005). Permafrost of the Carpathian and Balkan Mountains, eastern and southeastern Europe. *Permafrost and Periglacial Processes*, *16*, 395–398. doi:10.1002/ppp.524

Dzierżek, J., Lindner, L., & Nitychoruk, J. (1987). Rzeźba i osady czwartorzędowe Doliny Pięciu Stawow Polskich (Wysokie Tatry) [Relief and Quaternary sediments in the Pięć Stawów Polskich Valley (Wysokie Tatry Range)]. *Przegląd Geologiczny*, *35*, 8–15.

Dzierżek, J., & Nitychoruk, J. (1986). Types of fossil rock glaciers in the Polish High Tatra Mts. *Bulletin of the Polish Academy of Sciences. Earth Sciences*, *34*, 409–418.

Falaschi, D., Castro, M., Masiokas, M., Tadono, T., & Ahumada, A. L. (2014). Rock glacier inventory of the Valles Calchaquíes region (~ 25°S), Salta, Argentina, derived from ALOS data. *Permafrost and Periglacial Processes*, *25*, 69–75. doi:10.1002/ppp.1801

Frauenfelder, R. (1998). *Rock glaciers, Fletschhorn area, Valais, Switzerland* [International Permafrost Association, Data and Information Working Group, comp. Circumpolar Active-Layer Permafrost System (CAPS), version 1.0]. Retrieved from http://nsidc.org/data/docs/fgdc/ggd287_rockglac_switzer/index.html

Frauenfelder, R., & Kääb, A. (2000). Towards a palaeoclimatic model of rock-glacier formation in the Swiss Alps. *Annals of Glaciology*, *31*, 281–286. doi:10.3189/172756400781820264

Gądek, B. (2014). Climatic sensitivity of the non-glaciated mountains cryosphere (Tatra Mts., Poland and Slovakia). *Global and Planetary Change*, *121*, 1–8. doi:10.1016/j.gloplacha.2014.07.001

Gądek, B., Grabiec, M., Kędzia, S., & Rączkowska, Z. (2016). Reflection of climate changes in the structure and morphodynamics of talus slopes (the Tatra Mountains, Poland). *Geomorphology*, *263*, 39–49. doi:10.1016/j.geomorph.2016.03.024

Gądek, B., & Kędzia, S. (2008). Winter ground surface temperature regimes in the zone of sporadic discontinuous permafrost, Tatra Mountains (Poland and Slovakia). *Permafrost and Periglacial Processes*, *19*, 315–321. doi:10.1002/ppp.623

Gądek, B., & Kędzia, S. (2009). Problemy detekcji wieloletniej zmarzliny na podstawie temperatury u spągu zimowej pokrywy śnieżnej na przykładzie Tatr [The problem of permafrost detection based on bottom temperature snow cover – The Tatra Mts. case]. *Przegląd Geograficzny*, *81*, 75–91. doi:10.7163/PrzG.2009.4.3

Gądek, B., & Leszkiewicz, J. (2012). Impact of climate warming on the ground surface temperature in the sporadic permafrost zone of the Tatra mountains, Poland and Slovakia. *Cold Regions Science and Technology*, *79–80*, 75–83. doi:10.1016/j.coldregions.2012.03.006

Gorbunov, A. P., Marchenko, S. S., & Seversky, E. V. (2004). The thermal environment of blocky materials in the mountains of Central Asia. *Permafrost and Periglacial Processes*, *15*, 95–98. doi:10.1002/ppp.478

Gruber, S., & Haeberli, W. (2009). Mountain permafrost. In R. Margesin (Ed.), *Permafrost soils* (pp. 33–44). Berlin: Springer.

Guglielmin, M., & Smiraglia, C. (1998). The rock glacier inventory of the Italian Alps. In A. G. Lewkowicz & M. Allard (Eds.), *Proceedings of the Seventh International Conference on Permafrost* (pp. 375–382). Ottawa: National Research Council of Canada.

Haeberli, W. (1985). Creep of mountain permafrost: Internal structure and flow of alpine rock glaciers. *Mitteilungen der Versuchsanstalt für Wasserbau, Hydrologie und Glaziologie*, *77*, 1–142.

Haeberli, W., Hallet, B., Arenson, L., Elconin, R., Humlum, O., Kääb, A., … Vonder Mühll, D. (2006). Permafrost creep and rock glacier dynamics. *Permafrost and Periglacial Processes*, *17*, 189–214. doi:10.1002/ppp.561

Harris, S. A., & Pedersen, D. E. (1998). Thermal regimes beneath coarse blocky materials. *Permafrost and Periglacial Processes*, *9*, 107–120. doi:10.1002/(SICI)1099-1530(199804/06)9:2<107::AID-PPP277>3.0.CO;2-G

Hedding, D. W. (2016). Pronival ramparts: Origin and development of terminology. *Erdkunde*, *70*, 141–151. doi:10.3112/erdkunde.2016.02.03

Hedding, D. W., & Sumner, P. (2013). Diagnostic criteria for pronival ramparts: Site, morphological and sedimentological characteristics. *Geografiska Annaler: Series A, Physical Geography*, *95*, 315–322. doi:10.1111/geoa.12021

Hoelzle, M. (1998). *Rock glaciers, Upper Engadin, Switzerland* [International Permafrost Association, Data and Information Working Group, comp. Circumpolar Active-Layer Permafrost System (CAPS), version 1.0]. Retrieved from http://nsidc.org/data/docs/fgdc/ggd288_rockglac_switzer/

Hughes, P. D., Gibbard, P. L., & Woodward, J. C. (2003). Relict rock glaciers as indicators of Mediterranean palaeoclimate during the Last Glacial Maximum (Late Würmian) in northwest Greece. *Journal of Quaternary Science*, *18*, 431–440. doi:10.1002/jqs.764

Imhof, M. (1998). *Rock glaciers, Bernese Alps, Western Switzerland* [International Permafrost Association, Data and Information Working Group, comp. Circumpolar Active-Layer Permafrost System (CAPS), version 1.0]. Retrieved from https://nsidc.org/data/docs/fgdc/ggd286_rockglac_switzer/index.html

Jahn, A. (1958). Mikrorelief peryglacjalny Tatr i Babiej Góry [Periglacial microrelief of the Tatras and Babia Góra Massif]. *Biuletyn Peryglacjalny*, *6*, 57–80.

Janke, J., & Frauenfelder, R. (2008). The relationship between rock glacier and contributing area parameters in the Front Range of Colorado. *Journal of Quaternary Science*, *23*, 153–163. doi:10.1002/jqs.1133

Jurewicz, E. (2007). Multistage evolution of the granitoid core in Tatra Mountains. In A. Kozłowski & J. Wiszniewska (Eds.), *Granitoids in Poland* (pp. 307–317). Warszawa: Warsaw University.

Kaszowski, L., Krzemień, K., & Libelt, P. (1988). Postglacjalne modelowanie cyrków lodowcowych w Tatrach Zachodnich [Postglacial modelling of the glacial cirques in the Western Tatras]. *Prace Geograficzne*, *71*, 121–141.

Kääb, A. (2013). Rock glaciers and protalus forms. In S. A. Elias & C. J. Mock (Eds.), *Encyclopedia of Quaternary science* (2nd ed., pp. 535–541). Amsterdam: Elsevier.

Kellerer-Pirklbauer, A., Lieb, G. K., & Kleinferchner, H. (2012). A new rock glacier inventory of the eastern European Alps. *Austrian Journal of Earth Sciences*, *105*, 78–93.

Kellerer-Pirklbauer, A., Wagner, T., & Winkler, G. (2016). Inventarisierung von blockgletscherverdächtigen Formen

und deren hydrologischen Einzugsgebieten in den steirischen Niederen Tauern mit Hilfe von hochaufgelösten Geländemodellen [Inventorying rock glacier-suspected landforms and their hydrological catchments in the Styrian part of the Niedere Tauern range using high-resolution digital elevation models]. *Joannea – Geologie und Palaontologie*, *12*, 53–62.

Kędzia, S. (2014). Are there any active rock glaciers in the Tatra Mountains? *Studia Geomorphologica Carpatho-Balcanica*, *48*, 5–16. doi:10.1515/sgcb-2015-0001

Kędzia, S., Kotarba, A., & Mościcki, J. (2004). Lodowiec gruzowy nad Wielkim Hińczowym Stawem w Tatrach Słowackich – wyniki wstępnych badań termicznych [Rock glacier above the Wielki Hińczowy Staw in the Slovak Tatra Mts. – Preliminary results of thermal investigations]. In A. Styczyńska & A. A. Marsz (Eds.), *XXX Międzynarodowe sympozjum polarne* (pp. 167–177). Gdynia: Akademia Morska.

Klimaszewski, M. (1948). *Polskie Karpaty Zachodnie w okresie dyluwialnym* [Polish Western Carpathians during the diluvium]. Wrocław: Wrocławskie towarzystwo naukowe.

Klimaszewski, M. (1988). *Rzeźba Tatr Polskich* [Relief of the Polish Tatra Mountains]. Warszawa: Państwowe Wydawnictwa Naukowe.

Kłapyta, P. (2008). Reliktowe wały lodowo-morenowe w zachodniej Cyrku Pyszniańskiego, Tatry Zachodnie [Relic ice-cored lateral moraines in the western part of the Pyszniański Cirque, the Western Tatra Mts.]. *Prace Geograficzne*, *120*, 65–77.

Kłapyta, P. (2009). Glacial and periglacial relief on the southern slopes of the Western Tatra Mts. (Slovakia) – The results of the first detailed geomorphological mapping of the Žiarska, Jamnicka, Račkova and Bystra Valleys. *Landform Analysis*, *10*, 50–57.

Kłapyta, P. (2010). Przebieg deglacjacji Doliny Bystrej (Tatry Zachodnie, Słowacja) podczas ostatniego zlodowacenia w świetle analiz geomorfologicznych oraz datowania względnego form metodą młotka Schmidta [Deglaciation of the Bystra Valley (Western Tatra Mts., Slovakia) during the last glaciation in the light of geomorphological analyses and relative age dating by Schmidt hammer]. In Z. Krzan (Ed.), *Nauka a zarządzanie obszarem Tatr i ich otoczeniem, Tom I – Nauki o Ziemi* (pp. 63–68). Zakopane: Tatrzański Park Narodowy.

Kłapyta, P. (2011). Relative surface dating of rock glacier systems in the Žiarska Valley, the Western Tatra Mountains, Slovakia. *Studia Geomorphologica Carpatho-Balcanica*, *45*, 89–106.

Kłapyta, P. (2012). *Ewolucja rzeźby wysokogórskiej Tatr Zachodnich w późnym glacjale i holocenie* [Late glacial and Holocene evolution of alpine relief of the Western Tatra Mts.]. (Unpublished PhD thesis). Uniwersytet Jagielloński, Kraków.

Kłapyta, P. (2013a). Application of Schmidt hammer relative age dating to Late Pleistocene moraines and rock glaciers in the Western Tatra Mountains, Slovakia. *Catena*, *111*, 104–121. doi:10.1016/j.catena.2013.07.004

Kłapyta, P. (2013b). Ewolucja rzeźby wysokogórskiej Tatr Zachodnich w późnym glacjale [Late glacial evolution of the Western Tatras' alpine relief]. In R. K. Borówka, A. Cedro, & I. Kavetskyy (Eds.), *Współczesne problemy badań geograficznych* (pp. 73–82). Szczecin: University of Szczecin.

Kłapyta, P. (2015). Deglacjacja północnego i południowego skłonu Tatr Zachodnich w trakcie ostatniego zlodowacenia w świetle dotychczasowych badań geomorfologicznych [Deglaciation of northern and southern slope of the Tatra Mountains during the last glaciation, in the light of geomorphological studies]. In A. Chrobak & A. Kotarba (Eds.), *NAUKA TATROM, Tom I – Nauki o Ziemi* (pp. 67–78). Zakopane: Tatrzański Park Narodowy.

Kłapyta, P., & Kołaczek, P. (2009). The last millenium slope processes and anthropogenic activity recorded in the sediments from the Pyszniańska Glade, Western Tatra Mountains (Poland). *Studia Geomorphologica Carpatho-Balcanica*, *43*, 145–163.

Kociuba, W. (1996). Textural features of some debrises patches in the High Tatra. In J. Repelewska-Pękalowa & K. Pękala (Eds.), *Wyprawy Geograficzne na Spitsbergen* (pp. 163–172). Lublin: Maria Curie-Skłodowska University.

Kotarba, A. (1986). Lodowce gruzowe w Tatrach [Rock glaciers in the Tatra Mountains]. *Wszechświat*, *87*, 97–99.

Kotarba, A. (1988). Fossil rock glaciers in the Polish Tatra Mountains: Origin and age. In M. Pecsi & S. Starkel (Eds.), *Palaeography of Carpathian regions* (pp. 161–169). Budapest: Hungarian Academy of Sciences.

Kotarba, A. (1991–1992). Reliktowe lodowce gruzowe jako element deglacjacji Tatr Wysokich [Relict rock glaciers as an element of the deglaciation of the High Tatra Mountains]. *Studia Geomorphologica Carpatho-Balcanica*, *25–26*, 133–149.

Kotarba, A. (1992). Natural environment and landform dynamics of the Tatra Mountains. *Mountain Research and Development*, *12*, 105–129. doi:10.2307/3673786

Kotarba, A. (2007). Lodowce gruzowe i wały niwalne – efekt późnoglacjalnej ewolucji rzeźby Tatr [Rock glaciers and protalus ramparts – An effect of the Lateglacial evolution of the Tatra Mountains]. *Przegląd Geograficzny*, *79*, 199–213.

Kotarba, A. (2013). Rzeźba systemu dolinnego Suchej Wody i Pańszczycy [Relief of valley systems of the Suchej Wody and Pańszczyca Valleys]. In Z. Rączkowska & A. Kotarba (Eds.), *Dolina Suchej Wody w Tatrach. Środowisko i jego współczesne przemiany* (pp. 15–33). Warszawa: Polish Academy of Sciences.

Kotarba, A., Kaszowski, L., & Krzemień, K. (1987). High-mountain denudational system of the Polish Tatra Mountains. *Prace Geograficzne, Special Issue*, *3*, 69–95.

Krainer, K., & Ribis, M. (2012). A rock glacier inventory of the Tyrolean Alps (Austria). *Austrian Journal of Earth Sciences*, *105*, 42–47.

Křížek, M., & Mida, P. (2013). The influence of aspect and altitude on the size, shape and spatial distribution of glacial cirques in the High Tatras (Slovakia, Poland). *Geomorphology*, *198*, 57–68. doi:10.1016/j.geomorph.2013.05.012

Křížek, M., Uxa, T., & Mida, P. (2016). *Praktikum morfometrických analýz reliéfu* [Practicum of morphometric analyses of relief]. Praha: Karolinum.

Libelt, P. (1988). Warunki i przebieg sedymentacji osadów postglacjalnych w cyrkach lodowcowych Tatr Zachodnich na przykładzie Kotła Staroroboclańskiego [Conditions and course of sedimentation of postglacial deposits by taking as example the Staroroboclański Cirque, Western Tatra Mts.]. *Studia Geomorphologica Carpatho-Balcanica*, *22*, 63–82.

Lilleøren, K. S., & Etzelmüller, B. (2011). A regional inventory of rock glaciers and ice-cored moraines in Norway. *Geografiska Annaler: Series A, Physical Geography*, *93*, 175–191. doi:10.1111/j.1468-0459.2011.00430.x

Lukniš, M. (1973). *Reliéf Vysokých Tatier a ich predpolia* [Relief of the High Tatra Mountains and their foreland]. Bratislava: Vydavateľstvo Slovenskej akadémie vied.

Makos, M., Nitychoruk, J., & Zreda, M. (2013a). Deglaciation chronology and paleoclimate of the Pięciu Stawów Polskich/Roztoki Valley, High Tatra Mountains, Western Carpathians, since the Last Glacial Maximum, inferred from ^{36}Cl exposure dating and glacier–climate modelling. *Quaternary International*, *293*, 63–78. doi:10.1016/j.quaint.2012.01.016

Makos, M., Nitychoruk, J., & Zreda, M. (2013b). The Younger Dryas climatic conditions in the Za Mnichem Valley (Polish High Tatra Mountains) based on exposure-age dating and glacier-climate modelling. *Boreas*, *42*, 745–761. doi:10.1111/j.1502-3885.2012.00298.x

Makos, M., Rinterknecht, V., Braucher, R., Żarnowski, M., & Aster Team. (2016). Glacial chronology and palaeoclimate in the Bystra catchment, Western Tatra Mountains (Poland) during the Late Pleistocene. *Quaternary Science Reviews*, *134*, 74–91. doi:10.1016/j.quascirev.2016.01.004

Millar, C. I., Westfall, R. D., & Delany, D. L. (2013). Thermal and hydrologic attributes of rock glaciers and periglacial talus landforms: Sierra Nevada, California, USA. *Quaternary International*, *310*, 169–180. doi:10.1016/j.quaint.2012.07.019

Nemčok, A., & Mahr, T. (1974). Kamenné ľadovce v Tatrách [Fossil rock glaciers in Tatras]. *Geografický časopis*, *26*, 359–373.

Nemčok, J., Bezák, V., Biely, A., Gorek, A., Gross, P., Halouzka, R., … Zelman, J. (1994). *Geologická mapa Tatier 1 : 50 000* [Geological map of the Tatra Mts. 1 : 50 000]. Bratislava: State Geological Institute of Dionýz Štúr.

Niedzwiedz, T. (1992). Climate of the Tatra Mountains. *Mountain Research and Development*, *12*, 131–146. doi:10.2307/3673787

Nyenhuis, M., Hoelzle, M., & Dikau, R. (2005). Rock glacier mapping and permafrost distribution modelling in the Turtmanntal, Valais, Switzerland. *Zeitschrift für Geomorphologie*, *49*, 275–292.

Onaca, A., Ardelean, F., Urdea, P., & Magori, B. (2017). Southern Carpathian rock glaciers: Inventory, distribution and environmental controlling factors. *Geomorphology*, *293*, Part B, 391–404. doi:10.1016/j.geomorph.2016.03.032

Partsch, J. (1923). *Die Hohe Tatra zur Eiszeit* [The High Tatra Mountains in the Ice Age]. Leipzig: F. Hirt & Sohn.

Pánek, T., Engel, Z., Mentlík, P., Braucher, R., Břežný, M., Škarpich, V., & Zondervan, A. (2016). Cosmogenic age constraints on post-LGM catastrophic rock slope failures in the Tatra Mountains (Western Carpathians). *Catena*, *138*, 52–67. doi:10.1016/j.catena.2015.11.005

Pánek, T., Mentlík, P., Ditchburn, B., Zondervan, A., Norton, K., & Hradecký, J. (2015). Are sackungen diagnostic features of (de)glaciated mountains? *Geomorphology*, *248*, 396–410. doi:10.1016/j.geomorph.2015.07.022

Rączkowska, Z. (2007). *Współczesna rzeźba peryglacjalna wysokich gór Europy* [Present-day periglacial relief in high mountains of Europe]. Warszawa: Polish Academy of Sciences.

Reynard, E., Lambiel, C., & Wenker, L. (1998). *Rock glaciers, Printse Valley, Valais, Switzerland.* [International Permafrost Association, Data and Information Working Group, comp. Circumpolar Active-Layer Permafrost System (CAPS), version 1.0]. Retrieved from http://nsidc.org/data/docs/fgdc/ggd291_rockglac_switzer/

Scapozza, C. (2015). Investigation on protalus ramparts in the Swiss Alps. *Geographica Helvetica*, *70*, 135–139. doi:10.5194/gh-70-135-2015

Schoeneich, P. (1998). *Rock glaciers of the Prealps, Vaud, Switzerland* [International Permafrost Association, Data and Information Working Group, comp. Circumpolar Active-Layer Permafrost System (CAPS), version 1.0]. Retrieved from http://nsidc.org/data/docs/fgdc/ggd292_rockglac_switzer/index.html

Scotti, R., Brardinoni, F., Alberti, S., Frattini, P., & Crosta, G. B. (2013). A regional inventory of rock glaciers and protalus ramparts in the central Italian Alps. *Geomorphology*, *186*, 136–149. doi:10.1016/j.geomorph.2012.12.028

Seppi, R., Carton, A., Zumiani, M., Dall'Amico, M., Zampedri, G., & Rigon, R. (2012). Inventory, distribution and topographic features of rock glaciers in the southern region of the Eastern Italian Alps (Trentino). *Geografia Fisica e Dinamica Quaternaria*, *35*, 185–197. doi:10.4461/GFDQ.2012.35.17

Serrano, E., Agudo, C., & Martinez de Pisón, E. (1999). Rock glaciers in the Pyrenees. *Permafrost and Periglacial Processes*, *10*, 101–106. doi:10.1002/(SICI)1099-1530(199901/03)10:1<101::AID-PPP308>3.0.CO;2-U

Sollid, J. L., & Sørbel, L. (1992). Rock glaciers in Svalbard and Norway. *Permafrost and Periglacial Processes*, *3*, 215–220. doi:10.1002/ppp.3430030307

Urdea, P. (1992). Rock glaciers and periglacial phenomena in the Southern Carpathians. *Permafrost and Periglacial Processes*, *3*, 267–273. doi:10.1002/ppp.3430030317

Uxa, T., & Mida, P. (2016). First results from thermal investigations of rock glaciers in the Slovak High Tatra Mountains, Western Carpathians. In F. Günther & A. Morgenstern (Eds.), *XI. International Conference on Permafrost – Book of abstracts* (pp. 1060–1061). Potsdam: Bibliothek Wissenschaftspark Albert Einstein.

Uxa, T., & Mida, P. (2017). Ground surface thermal regime of rock glaciers in the High Tatra Mts., Slovakia. *Geophysical Research Abstracts*, *19*, EGU2017–1740.

Wagner, T., Pauritsch, M., & Winkler, G. (2016). Impact of relict rock glaciers on spring and stream flow of alpine watersheds: Examples of the Niedere Tauern range, Eastern Alps (Austria). *Austrian Journal of Earth Sciences*, *109*, 84–98. doi:10.17738/ajes.2016.0006

Winkler, G., Wagner, T., Pauritsch, M., Birk, S., Kellerer-Pirklbauer, A., Benischke, R., … Hergarten, S. (2016). Identification and assessment of groundwater flow and storage components of the relict Schöneben rock glacier, Niedere Tauern range, Eastern Alps (Austria). *Hydrogeology Journal*, *24*, 937–953. doi:10.1007/s10040-015-1348-9

Zasadni, J., & Kłapyta, P. (2009). An attempt to assess the modern and the Little Ice Age climatic snowline altitude in the Tatra Mountains. *Landform Analysis*, *10*, 124–133.

Zasadni, J., & Kłapyta, P. (2014). The Tatra Mountains during the Last Glacial Maximum. *Journal of Maps*, *10*, 440–456. doi:10.1080/17445647.2014.885854

Zasadni, J., & Kłapyta, P. (2016). From valley to marginal glaciation in alpine-type relief: Lateglacial glacier advances in the Pięć Stawów Polskich/Roztoka Valley, High Tatra Mountains, Poland. *Geomorphology*, *253*, 406–424. doi:10.1016/j.geomorph.2015.10.032

Żmudzka, E. (2011). Contemporary climate changes in the high mountain part of the Tatras. *Miscellanea Geographica – Regional Studies on Development*, *15*, 93–102. doi:10.2478/v10288-012-0005-6

ROCK GLACIERS IN THE WESTERN AND HIGH TATRA MOUNTAINS, WESTERN CARPATHIANS

Tomáš Uxa[1,2] & Peter Mida[1]

[1] Department of Physical Geography and Geoecology, Faculty of Science, Charles University, Albertov 6, 128 43 Praha 2, Czech Republic
[2] Department of Geothermics, Institute of Geophysics, Academy of Sciences of the Czech Republic, Boční II 1401, 141 31 Praha 4, Czech Republic

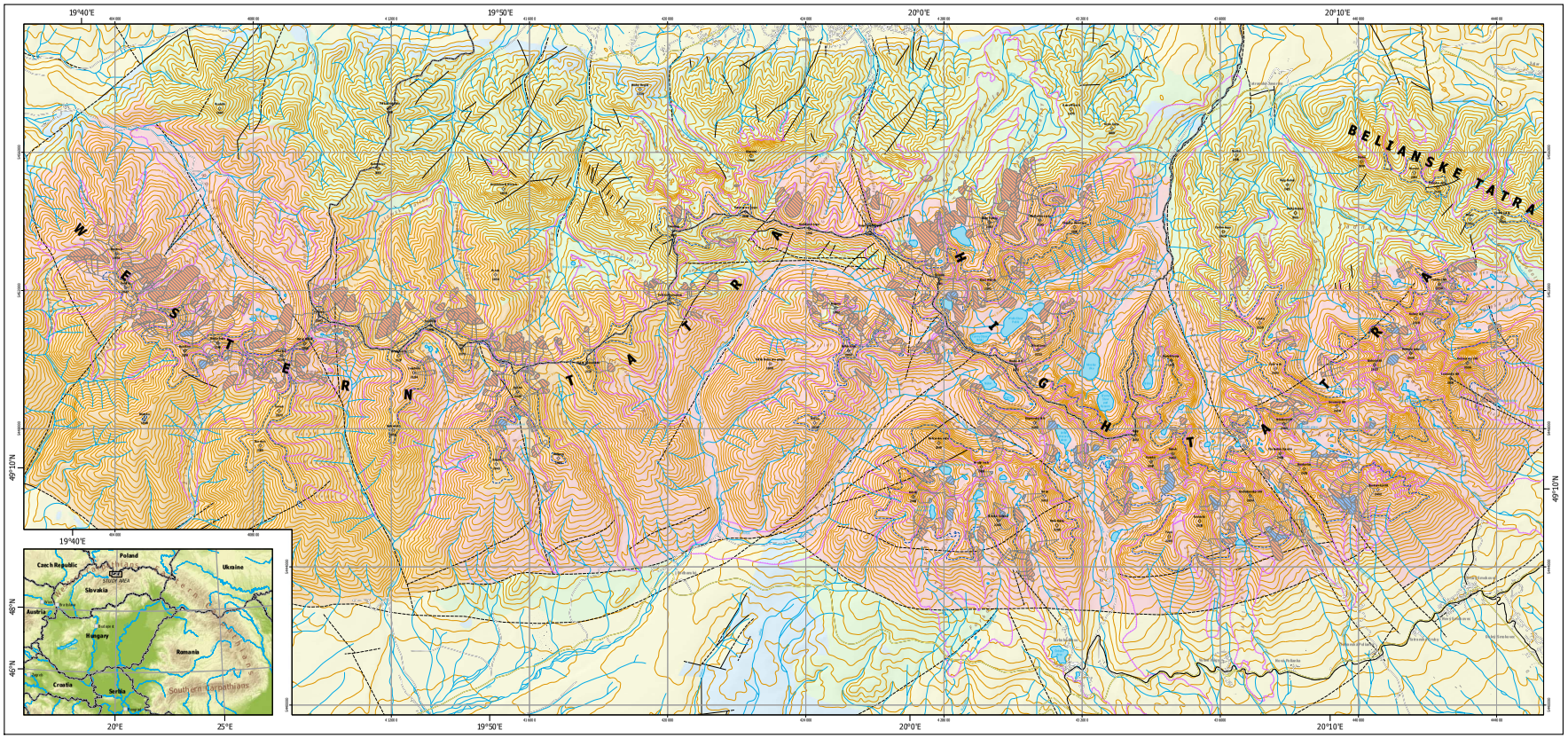

Rock glaciers
- talus rock glacier
- debris rock glacier
- intact rock glacier
- relict rock glacier
- contributing area

Geological units
- gneiss rocks, migmatite, amphibolite *(Paleozoic)*
- granitic rocks *(Carboniferous-Permian)*
- limestone, dolomite, sandstone, shale, quartzite *(Mesozoic)*
- claystone, siltstone, sandstone, conglomerate, breccia *(Cretaceous-Paleogene)*
- sandstone, limestone, conglomerate, breccia *(Paleogene)*

Structural elements
- fault (proved)
- fault (assumed)

Permafrost boundary
- lower limit of discontinuous permafrost (1930 m asl)

Glaciers
- LGM glacier extent

Elevation and hydrology
- elevation point
- contours with equidistance of 50 m
- watercourse
- lake

Antropogenic and administrative objects
- major road
- minor road
- railway
- cable car
- buildings
- state boundary

0 1 2 4 6 8 km

1 : 40 000
If printed in A0

Coordinate system: WGS 1984 UTM Zone 34N

N W E S

Mapping details: Rock glaciers were mapped in 2014 and 2015 based on aerial photographs from years 2010–2015 with a resolution of 0.1, 0.25, 0.5 and 1 m accesible on geoportals of the Geodetic and Cartographic Institute Bratislava (GCIB) and the Head Office of Geodesy and Cartography (HOGC) and on Google Earth. Digital elevation model (DEM) with a horizontal resolution of 10 m (Tatra National Park, 2009) was utilized as a supplementary source of information for mapping of rock glaciers and delineation of their contributing areas.

Other features: Geological units and structural elements are based on the geological maps of the Tatra Mountains (Nemčok et al., 1994; Bezák et al., 2013). Lower discontinuous permafrost limit is taken from Dobiński (1997). LGM glacier extent is from Zasadni & Kłapyta (2014). Contours were derived from DEM. The elevation points, watercourses, lakes and cable cars were obtained by digitizing topographic maps in a scale of 1 : 25 000 and 1 : 50 000 accessible on geoportals of the GCIB and the HOGC. In the Slovak part of the study region, watercourses and lakes were taken from the database SVM 50. Buildings, roads and railways for the entire area were extracted from the freely available OpenStreetMap database.

Software: The mapping, digitizing, analyses of digital elevation model and map compilation were all carried out using ESRI ArcMap 10.3. Final merger of vector and raster map elements was done in Adobe Acrobat Pro DC.

Citation: Uxa, T., & Mida, P. (2017). Rock Glaciers in the Western and High Tatra Mountains, Western Carpathians. *Journal of Maps*, XX, XX–XX.

7.5 Paper V

Uxa, T., Mida, P., Křížek, M. (2017). Effect of Climate on Morphology and Development of Sorted Circles and Polygons. *Permafrost and Periglacial Processes*, 28(4), 663–674. https://doi.org/10.1002/ppp.1949

Journal Citation Reports 2016: Impact factor 2.815, Q2(16/49) in Geography Physical, Q1(6/47) in Geology.

Citations as of 9 June 2020: Web of Science=3, Scopus=2, Google Scholar=3, ResearchGate=5.

PERMAFROST AND PERIGLACIAL PROCESSES
Permafrost and Periglac. Process. **28**: 663–674 (2017)
Published online 31 May 2017 in Wiley Online Library
(wileyonlinelibrary.com) DOI: 10.1002/ppp.1949

Effect of Climate on Morphology and Development of Sorted Circles and Polygons

Tomáš Uxa,[1,2]* *Peter Mida*[1] *and Marek Křížek*[1]

[1] Department of Physical Geography and Geoecology, Faculty of Science, Charles University, Praha, Czech Republic
[2] Department of Geothermics, Institute of Geophysics, Academy of Sciences of the Czech Republic, Praha, Czech Republic

ABSTRACT

Sorted circles and polygons are widespread features of periglacial landscapes, but the controls on their development remain poorly understood, impeding their use as palaeoenvironmental indicators. We investigate the relationship of sorted circles and polygons to altitude in the northern Billefjorden area, central Svalbard. The patterns occur in two distinct elevation zones, below 200–250 m asl and above 600 m asl. The higher-elevated patterns have smaller diameters and shallower sorting depths due to a thinner active layer at higher elevations, suggesting that sorted patterns can indicate climate conditions and ground thermal state when the patterns initiated. Geology is believed to be of less importance for pattern morphology in the study area, causing only its fine-scale variations. The pattern diameter-to-sorting depth ratios have a median value of 3.57, consistent with previous studies and theoretical models of patterned-ground formation involving circulation mechanisms. Large-scale sorted patterns may develop over centennial timescales in this high-Arctic environment. They are probably not in equilibrium with present-day climate conditions and have probably formed throughout the Holocene. Copyright © 2017 John Wiley & Sons, Ltd.

KEY WORDS: patterned ground; sorted circles and polygons; morphology; active layer; Svalbard; high Arctic

INTRODUCTION

Periglacial sorted circles and polygons are common on unvegetated or sparsely vegetated surfaces composed of a mixture of unconsolidated fine and coarse materials (Warburton, 2013). They develop by repeated freezing and thawing of the ground. However, less consensus exists regarding their formation mechanism, developmental dynamics or environmental controls (Ballantyne, 2013, and citations therein).

Advances in determining the environmental factors and limits of patterned ground have been made using statistical modelling on spatially variable binary data representing patterned-ground occurrence or activity (e.g. Luoto and Hjort, 2005; Hjort and Luoto, 2006; Feuillet, 2011). However, the main shortcoming of such approaches is that they group all patterns of the same type, irrespective of their morphology. Although individual pattern types have some common features, which allow classification based on morphology and/or site characteristics (e.g. Treml *et al.*, 2010; Feuillet *et al.*, 2012; Watanabe *et al.*, 2017), high variability of shape and size results from a wide range of environmental settings in which they develop (see Goldthwait, 1976; Washburn, 1980; Grab, 2002). Such variability makes it difficult to draw specific conclusions from a purely binary-data approach. As quantitative data about sorted patterned-ground morphology from areas of permafrost and seasonally frozen ground on a wider scale are scarce (e.g. Holness, 2003; Treml *et al.*, 2010; Feuillet *et al.*, 2012), their environmental controls are still poorly understood, impeding their use as indicators of present and past environmental conditions. Hence, quantitative data about pattern distribution and morphology are needed from a wide range of environmental settings.

Most studies of patterned ground in Svalbard have provided detailed observations of sorted patterns on a local scale, particularly on coastal plains (strandflats) near polar stations, mainly in western and southern Svalbard (e.g. Jahn, 1963; Hallet and Prestrud, 1986; Van Vliet-Lanoë, 1991; Kääb *et al.*, 2014). Less work has been conducted on a wider scale, and still less on patterns at higher elevations. Studies from the interior regions of Svalbard, such as the northern Billefjorden area, are limited, with no detailed observations of sorted patterns published.

* Correspondence to: T. Uxa, Department of Physical Geography and Geoecology, Faculty of Science, Charles University, Praha, Czech Republic. E-mail: tomas.uxa@natur.cuni.cz

Received 31 May 2016
Revised 6 February 2017
Accepted 24 March 2017

Here, we describe for the first time the distribution and morphology of sorted circles and polygons in the northern Billefjorden area, central Svalbard (79° N), and we investigate their relationship to altitude. We hypothesise about their developmental rates, chronology and relation to active-layer thickness (ALT) and present-day climate conditions.

STUDY AREA

The study area is located around the Petuniabukta and Adolfbukta bays in the northernmost Billefjorden, central Svalbard, between 78°40′–78°44′ N and 16°16′–16°56′ E (Figure 1). Bedrock at patterned-ground sites consists mostly of sandstones with areas of shales, limestones, mica-schists and gneisses (Dallmann *et al.*, 2004). At lower elevations, sparse vegetation is dominated by *Dryas octopetala* and *Saxifraga oppositifolia* communities (Prach *et al.*, 2012), whereas higher elevations lack vegetation (Figure 2).

The area has some of the highest summer air temperatures (Przybylak *et al.*, 2014) and is among the driest regions in Svalbard (Hagen *et al.*, 1993). The nearest meteorological station with long-term observations is located about 50–60 km south from the study area, at Svalbard Airport (28 m asl), near Longyearbyen. Mean annual air temperature (MAAT) there during 1981–2010 was −5.1 °C and mean air temperatures of the coldest (February) and warmest (July) month were −13.5 and +6.4 °C, respectively (Nordli *et al.*, 2014). The inner-fjord climate of the northern Billefjorden, however, shows slightly higher temperature amplitudes and up to about 1 °C lower MAAT based on local short-term studies (Rachlewicz and Styszyńska, 2007; Láska *et al.*, 2012). Total annual precipitation in the area is estimated at around 200 mm (Hagen *et al.*, 1993).

Svalbard was largely covered by the Late Weichselian ice sheet during the Last Glacial Maximum (LGM) (Landvik

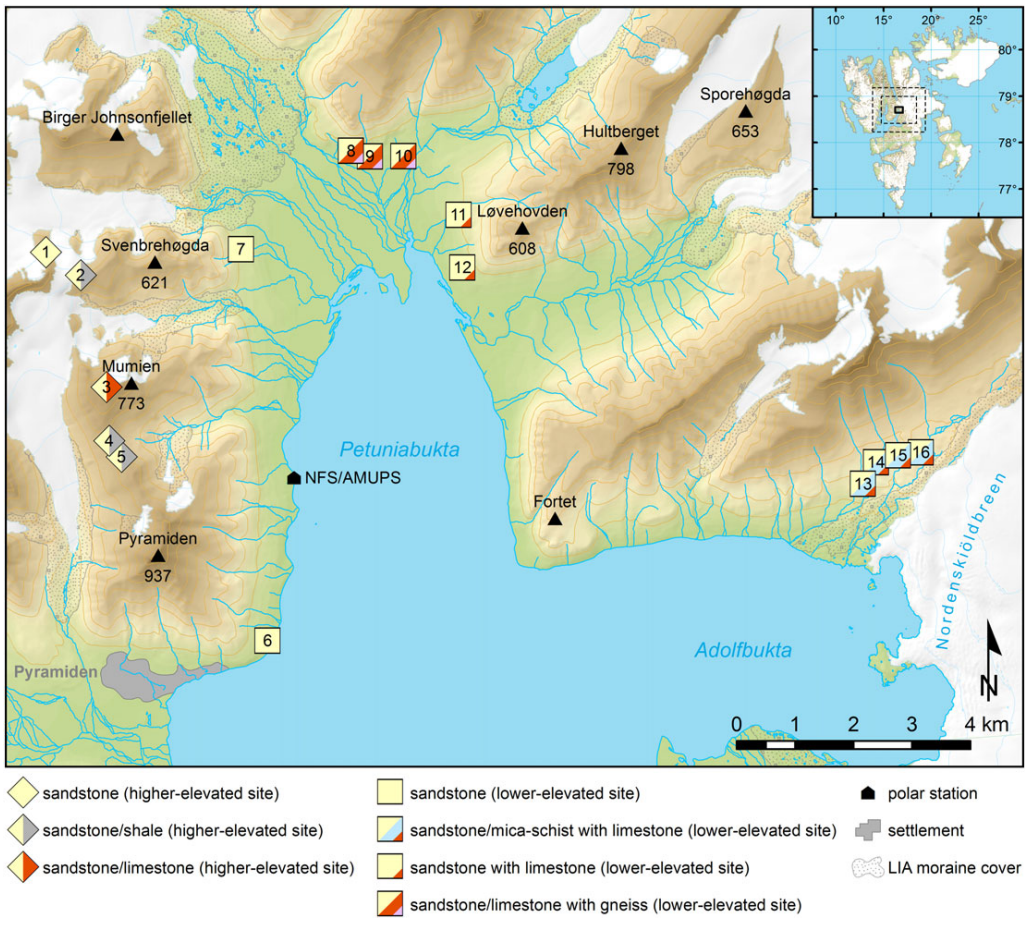

Figure 1 Location map of Petuniabukta and Adolfbukta and the investigated patterned-ground sites. Sites 6–12 are located on marine terraces; sites 13–16 occur on kame terraces. Contour interval is 100 m. NFS/AMUPS are acronyms for the Czech Nostoc Field Station and Polish Adam Mickiewicz University Polar Station, respectively. Inset map shows Svalbard archipelago. Topography: Norwegian Polar Institute®. [Colour figure can be viewed at wileyonlinelibrary.com]

Figure 2 Photographs of (a) sorted circles on a flat mountain top at 680 m asl (site 2 in Figure 1); (b) sorted polygons on a raised marine terrace at 80 m asl (site 7); (c) sorted polygons on a kame terrace at 234 m asl (site 15); and (d) sorted circles on the Little Ice Age moraine of Nordenskiöldbreen, approximately 0.5 km south of the site 13. [Colour figure can be viewed at wileyonlinelibrary.com]

et al., 1998). Deglaciation of the Billefjorden began after about 12.3 kyr BP (Mangerud *et al.*, 1992). Local glaciers had retreated close to their present extent by the end of the Pleistocene (Baeten *et al.*, 2010) and the glacierized area declined further during the early and mid-Holocene (Landvik *et al.*, 1998). Glaciers started to readvance about 3 kyr BP, attaining their maximum Holocene extent during the Little Ice Age (LIA) (Landvik *et al.*, 1998), implying that the surfaces non-glaciated during this period have been mostly ice-free throughout the Holocene. Since the LIA, air temperatures in central Svalbard have increased substantially, averaging 0.026 °C yr^{-1} (Nordli *et al.*, 2014). This has led to rapid glacier retreat (Rachlewicz *et al.*, 2007; Małecki, 2016) and paraglacial landscape transformation (e.g. Stacke *et al.*, 2013; Ewertowski and Tomczyk, 2015; Strzelecki *et al.*, 2017).

Continuous permafrost underlies the extensive non-glacierized areas (Figure 1) (Humlum *et al.*, 2003), with ALT generally reaching 0.3–1.6 m, and in diamicton occasionally up to 2.5 m (Gibas *et al.*, 2005; Rachlewicz and Szczuciński, 2008; Láska *et al.*, 2010). The ALT has increased about 0.01–0.03 m yr^{-1} since the 1990s in central Svalbard and the thickening is expected to continue along with climate warming (Etzelmüller *et al.*, 2011), but the response may be affected by complex interactions of forcing meteorological variables and their interannual variations (Christiansen and Humlum, 2008).

METHODS

Sampling Strategy, Morphometric Parameters and Grain-Size Analysis

Sorted circles and polygons (Figure 2) were investigated at sites with a continuous network of at least 10 patterns on flat or gently inclined terrain (up to 5°). In total, 290 sorted

circles and polygons were examined at 16 locations, at elevations of 28–773 m asl (Figure 1).

Length, width and height of 10 or 20 randomly selected sorted patterned-ground features were measured at each study site, depending on the number of patterns present. The length is defined as a maximum horizontal dimension of the pattern measured between the opposite centres of coarse borders, while the width is the largest dimension in a direction perpendicular to the length and intersecting it at the pattern centre. The height is a maximum vertical distance between the lowest point at the pattern border and the highest point at its updomed centre (*sensu* Křížek and Uxa, 2013).

At three sites at elevations of 31, 598 and 773 m asl (sites 6, 5 and 3 in Figure 1), the sorting depth was determined by excavations as a maximum depth where a distinct boundary between the sediments beneath the fine centre and coarse border was visible.

Grain-size analysis was carried out on eight samples collected at five study sites (sites 2, 3, 5, 6 and 7 in Figure 1) from depths of 0.05–0.15 m at pattern centres. The samples were air-dried, gently crushed and mechanically sieved through a set of sieves up to 0.125 mm, while finer fractions under 0.125 mm were examined by timed sedimentation in a suspension.

Statistical Analysis

All morphometric parameters show a log-normal distribution, and thus they were log-transformed to meet the criterion of normality according to the Shapiro–Wilk test (Shapiro and Wilk, 1965). Accordingly, their median values are reported hereafter. Relations between the morphometric parameters were examined using the Pearson correlation coefficient. Between-group differences were assessed by a one-way ANOVA and *F*-test. Cluster analysis was applied on standardised site averages to search for potential geological influences on patterned-ground morphology. All statistical testing was at a significance level of 0.05, and analyses were done using the software STATISTICA (StatSoft, Inc., 2009).

RESULTS

Altitudinal Distribution and Substrate Characteristics

One group of sorted circles and polygons (69 % of the investigated patterns) is located mainly on raised marine and kame terraces at elevations up to 200–250 m asl. A second group (31%) occurs on adjacent flat mountain tops and ridges above elevations of around 600 m asl (Figure 1). These two distinct elevation zones are separated by steep talus slopes, which are highly unfavourable for patterned-ground formation. Glacier forelands developed since the LIA are occupied only by rare small-scale and poorly developed patterns (Figure 2d) that were not specifically examined in this work.

The sorted circles and polygons at higher elevations are formed within sediments or poorly developed soils derived from *in situ* weathered sedimentary rocks, particularly sandstones associated with shales and limestones. The lower-lying patterns are mostly derived from secondary deposits of weathered materials, which are dominated by sandstones associated with limestones, mica-schists or gneisses (Figure 1). Particles smaller than 2 mm constitute 11–61 % of the samples collected at patterned-ground sites. This fraction contains 5–24 % clay (<0.002 mm) and clay–silt (<0.063 mm) represents 6–49 %. The samples are frost-susceptible (*sensu* Beskow, 1935), although at one site they contain little silt (Figure 3).

Morphology

Horizontal dimensions of the sorted circles and polygons range from several decimetres to 4.5 m, with median values of 1.8 and 1.4 m for the length and width, respectively (Figure 4). Because the patterns occur on flat or gently inclined surfaces, both characteristics are highly correlated ($r = 0.90$, $p < 0.0001$) and the length-to-width ratios show low values (median of 1.25). The median height is 0.15 m (Figure 4), but it reaches up to 0.5 m depending on the pattern size (for length $r = 0.50$, $p < 0.0001$; for width $r = 0.53$, $p < 0.0001$). The median height-to-width ratio equals 0.1 (Figure 4).

Sorting depths of the sorted circles and polygons range between 0.44 and 0.64 m. The diameters (averages of the length and width) of the respective patterns range between 1.64 and 1.77 m, resulting in pattern diameter-to-sorting depth ratios of 2.77–3.73 (median 3.57) (Figure 5).

Higher elevations generally host patterns with significantly smaller horizontal dimensions than lower elevations (Figure 6). Likewise, shallower sorting occurs at higher altitudes, although the sample size is not representative. In contrast, sorted circles and polygons with significantly larger heights and height-to-width ratios occur at higher elevations (Figure 6).

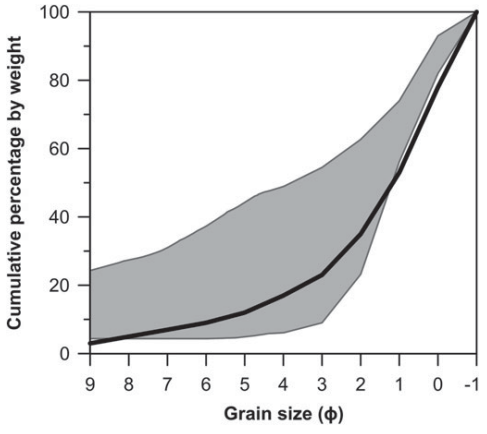

Figure 3 Grain-size envelope for eight sorted patterns in comparison with the frost-susceptibility limit of Beskow (1935) (thick black line).

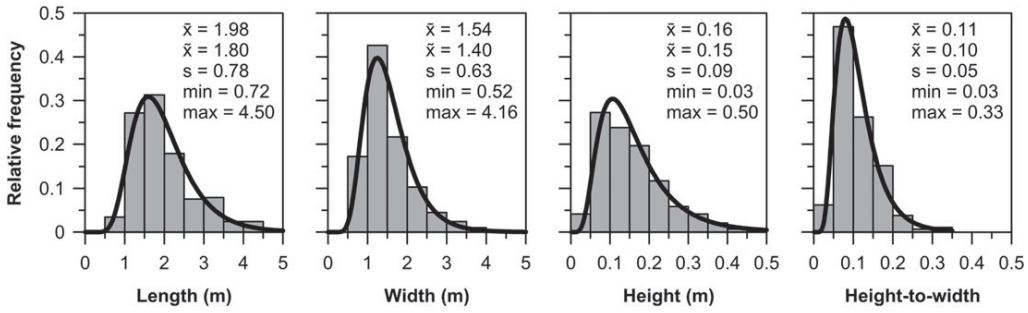

Figure 4 Histograms of the length, width, height and height-to-width ratio of sorted circles and polygons (n = 290) showing typical log-normal distributions. $\bar{x}$ – average; $\tilde{x}$ – median; s – standard deviation; min – minimum; max – maximum.

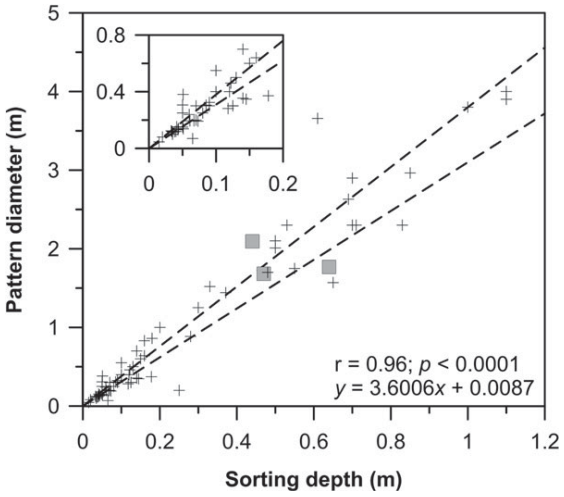

Figure 5 Scatterplot of relation between pattern diameter and sorting depth. Squares mark sorted circles and polygons investigated in the present study. Crosses are 67 previously published values for sorted circles and polygons found in Troll (1944), Furrer (1955), Henderson (1968), Freund (1971), Ellenberg (1976), Ballantyne and Matthews (1982), Ray *et al.* (1983), Gleason *et al.* (1986), Wilson and Clark (1991), Wilson (1992), Ballantyne and Harris (1994), Love (1995), Kück (1996), Grab (1997, 2002), Humlum and Christiansen (1998), Holness (2003) and collected by other personal observations on two small-scale patterns located on an LIA moraine in the Petuniabukta area. The dashed lines define theoretical limits of pattern diameter-to-sorting depth ratios (3.1–3.8), based on model predictions (e.g. Ray *et al.*, 1983; Gleason *et al.*, 1986; Hallet and Prestrud, 1986). Although the individual data points are scattered around the theoretical limits, the general strength of the relationship is remarkable. The median value of all 70 data points is 3.54.

DISCUSSION

Sorted Patterned-Ground Morphology in Relation to Altitude

We recorded a relatively narrow range of pattern diameter-to-sorting depth ratios (Figure 5) that are consistent with other field data and theoretical models of patterned-ground formation based on linear stability theory (e.g. Ray *et al.*, 1983; Gleason *et al.*, 1986; Hallet and Prestrud, 1986; Peterson and Krantz, 2008). According to these studies, patterned ground shows a fixed pattern diameter-to-sorting depth ratio (for an overview refer to Figure 5) where the pattern size is controlled by the thickness of the active layer in permafrost areas or by the freezing depth in seasonally frozen ground areas, respectively.

Because climate acts as a first-order control on ALT (Bonnaventure and Lamoureux, 2013), we assume that the active layer thins towards higher elevations because of the temperature lapse rate. Thus, a thinner active layer can explain the smaller diameters of patterns at higher elevations (Figure 6). The validity of this interpretation is further underpinned by similar relations between pattern diameter and altitude reported from other continuous (Marvánek, 2010) and discontinuous (Kling, 1998) permafrost areas and also from regions with former permafrost (e.g. Křížek and Uxa, 2013). Consistent with theoretical considerations, the opposite altitudinal trends have been observed in seasonally frozen ground areas (Holness, 2003; Feuillet *et al.*, 2012) because of increasing freezing depth towards higher elevations. All these observations suggest that the morphology of sorted patterns can indicate climate conditions, while the altitudinal trends can indicate ground thermal state (i.e. permafrost or seasonally frozen ground conditions) when the patterns initiated (*sensu* Peterson and Krantz, 2008).

Nevertheless, site-specific factors such as geology and ground material can also influence pattern size. For instance, pattern diameter tends to be positively correlated with the amount of fine material (Treml *et al.*, 2010; Feuillet *et al.*, 2012). Likewise, clast size, which has been stated to be interconnected with pattern size (Goldthwait, 1976; Feuillet *et al.*, 2012), or differences among pattern types (e.g. Kling, 1998; Treml *et al.*, 2010) could interfere in this relationship. However, no clustering into morphologically homogeneous groups corresponding to identical geological conditions was found for both the lower- and the higher-elevated pattern sites (Figure 7). This is probably due to the general abundance of sandstones that more or less predominate at most sites, while other components are less represented. Accordingly, we believe that geology causes only fine-scale variations in pattern morphology in the study area, and thus is of limited importance for the investigated patterns.

The occurrence of patterns with significantly larger height and height-to-width ratios at higher elevations

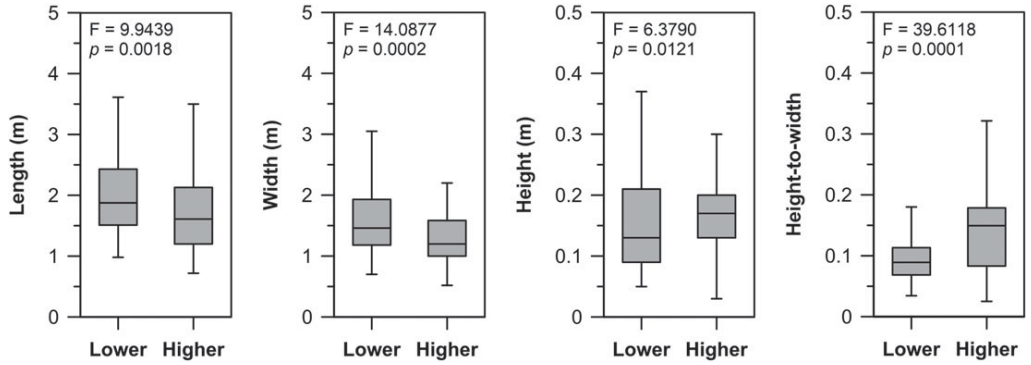

Figure 6 Boxplots showing morphological differences between the lower- and higher-elevated groups of sorted circles and polygons (n = 290). The boxes show median values (thick horizontal line) and the first and third quartiles (bottom and top of boxes, respectively). Whiskers represent minimum and maximum values, excluding outliers (values lying 1.5 interquartile ranges below and above the first and third quartiles, respectively).

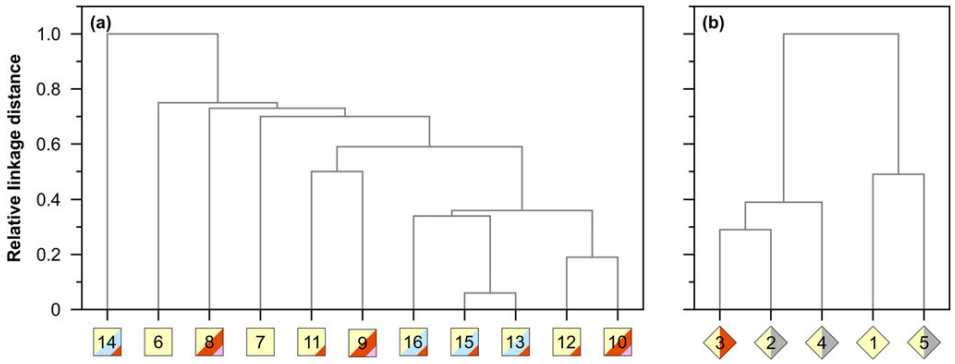

Figure 7 Cluster tree for the (a) lower- and (b) higher-elevated pattern sites based on the single-linkage method and Euclidean distances. Standardised site averages of uncorrelated morphometric parameters (length and heigth-to-width ratio) were used in the analysis. Site numbers and symbols are given in Figure 1. [Colour figure can be viewed at wileyonlinelibrary.com]

(Figure 6) is probably due to more severe climate conditions and less moisture. Well-drained sites generally host patterns with better developed microtopography than at poorly drained locations (Van Vliet-Lanoë, 1991). In Svalbard, precipitation tends to increase with altitude (Hagen *et al.*, 1993; Humlum, 2002), but local topographic effects can alter this pattern. Wind redistributes snow across the entire archipelago (Humlum, 2002), and high wind speeds clear snow from exposed mountain summits and ridges in winter (Jaedicke and Sandvik, 2002; Jaedicke and Gauer, 2005). This effect can be reasonably expected in the study area as well (*sensu* Małecki, 2015). Furthermore, a larger fraction of precipitation falls as snow at higher elevations (Hagen *et al.*, 1993; Winther *et al.*, 1998) and can be easily drifted away if neither compacted nor crusted. At lower elevations, most pattern sites are likely to be less wind-affected, and rain occurs more frequently and can quickly soak into the ground. Consequently, the amount of snow and liquid water at the higher-elevated sites is believed to be lower. Naturally, these locations may also be temporarily saturated during the early thaw season and fine centres can even show a thixotropic behaviour (Figure 8a), but as the thaw front descends, they drain progressively and desiccation cracks frequently form on pattern surfaces (Figure 8b). In contrast, lower elevations show higher moisture contents and fewer desiccation fissures. The onset of thawing is also earlier here, which enhances settling of the ground (Hallet and Prestrud, 1986; Hallet, 1998, 2013) and produces rather flat microtopography (*sensu* Van Vliet-Lanoë, 1991).

Developmental Rates

Sorted patterns commonly develop in front of retreating glaciers (Ballantyne and Matthews, 1982; Haugland, 2006) and perennial or late-lying snow patches (Kling, 1998). Because these settings often provide favourable ground material properties, moisture supply, ground thermal regime and topography for patterned-ground formation, sorted circles and polygons can rapidly emerge and develop within a few decades (Ballantyne and Matthews, 1982; Matthews *et al.*, 1998; Feuillet and Mercier, 2012). In Svalbard, the

Figure 8 Photographs of (a) sorted-polygon centre at 773 m asl in a thixotropic state (site 3 in Figure 1); and (b) desiccation cracks developed on sorted-circle surface at 598 m asl (site 5). [Colour figure can be viewed at wileyonlinelibrary.com]

LIA ended rapidly in the early 20th century (Hagen *et al.*, 1993; Svendsen and Mangerud, 1997; Isaksson *et al.*, 2005) and, since then, land-terminating glaciers in the northern Billefjorden have continuously retreated at a rate of 5–15 m yr^{-1} and exposed extensive areas (Rachlewicz *et al.*, 2007). Many of these proglacial areas are composed of ice-cored sediments with thick active layers (Gibas *et al.*, 2005) and experience highly dynamic topography changes (e.g. Ewertowski, 2014; Ewertowski and Tomczyk, 2015), potentially disturbing the patterning processes. However, stable surfaces occur here as well. These sediments also have favourable grain-size composition (e.g. Stankowska, 1989; Pleskot, 2015) with high frost-susceptibility, as it is at the investigated sites with sorted patterns (Figure 3). Furthermore, they can provide sufficient moisture for pattern formation, even at places more distant from the moisture-supplying glacier and influenced by strong katabatic winds, which accelerate desiccation of the ground. Nevertheless, despite favourable conditions and about a century to develop, patterns on the LIA moraines and glacier forelands in the northern Billefjorden are rare, small-scale and poorly developed (Figure 2d). Large-scale (>1 m in width) patterns are common in locations immediately adjacent to proglacial areas, but on pre-LIA terrains (Figure 1). Although small-scale sorted circles and polygons may occur on these surfaces as well, they are much more typical for post-LIA glacier forelands and other fresh surfaces. Similar distribution patterns are reported from other regions of Svalbard (e.g. Jahn, 1963; Cannone *et al.*, 2004; Dąbski, 2005; Szymański *et al.*, 2015).

We hypothesise from the above findings that large-scale sorted patterns in Svalbard develop on centennial timescales. This is an order of magnitude longer than previous estimates based on sorted patterns across glacial chronosequences (e.g. Ballantyne and Matthews, 1982; Haugland, 2006; Feuillet and Mercier, 2012). The latter are valid particularly for small-scale sorted patterns and mid-latitude alpine climates, characterised by well-developed seasonal and diurnal temperature variations and numerous freeze–thaw cycles. However, high-Arctic climates are dominated by a strong seasonal cycle, with weak diurnal variations and fewer freeze–thaw cycles (Fraser, 1959; French, 2007).

Measurements of ground motions in large-scale sorted patterns support the hypothesis of their development over centennial timescales. In Kvadehuksletta, western Svalbard, radially outward movements of 10–30 mm yr^{-1} were observed within the fine domains of large-scale sorted circles as a surface imprint of cell-like circulation (Hallet and Prestrud, 1986; Hallet, 1998; Kääb *et al.*, 2014). The surface travel times required to reach the centre–border interface have been estimated to be up to 100 years (Kääb *et al.*, 2014), while the entire circulation may take 300–500 years or longer, assuming decreasing velocity towards depth (Hallet, 1998; Kääb *et al.*, 2014). Thus, it may take up to 100 years for large-scale patterns to emerge in a poorly developed form and hundreds more years to achieve higher developmental stage, consistent with our observations from northern Billefjorden. On the other hand, most sorted patterns we have observed lack distinctly raised stone rings (Figure 2) typical of sorted circles in Kvadehuksletta, and therefore their dynamics may differ. In addition, the above measurements were performed on mature patterns that are among the best developed on Earth (Hallet, 2013). Since frost sorting progressively alters the grain-size distribution in pattern centres and increases their frost-susceptibility (Ballantyne and Matthews, 1983), the displacement rates within well-developed patterns are likely to be faster than those within poorly developed or initial forms, consisting of poorly sorted materials (*sensu* Křížek and Uxa, 2013). Although the non-linear formation mode is likely (e.g. Kessler *et al.*, 2001; Peterson and Krantz, 2008), it lacks a strong experimental support. However, if our hypothesis is valid, then the actual transition time from initial to well-developed patterns should be longer than the above estimates (cf. Hallet, 1998; Kääb *et al.*, 2014).

Chronology

The patterned-ground sites on marine terraces between 20 and 45 m asl may have been continuously exposed to periglacial conditions for most of the Holocene, and those on beaches up to 80 m asl since the Late Weichselian. The northern Billefjorden region was glacio-isostatically uplifted in response to local deglaciation, and associated sea level fall was up to 90 m during the Middle to Late Weichselian and the Holocene (Salvigsen, 1984; Kłysz *et al.*, 1988, 1989; Szczuciński and Rachlewicz, 2007). Dating of marine shells and sediments showed that marine terraces above 20 m asl, where all the investigated lower-elevated sorted circles and polygons occur, formed before *c.* 8.7 cal kyr BP, the terrace sequence up to 40–45 m asl dates from *c.* 10 cal kyr BP (Long *et al.*, 2012) to 12.8 kyr (van der Meij *et al.*, 2016), and terraces up to 80 m asl are attributed to the Middle Weichselian (Kłysz *et al.*, 1988, 1989). However, the highest terrace sequence was probably ice-covered during the LGM (Landvik *et al.*, 1998). The kame-terrace sites probably post-date the major advance of Nordenskiöldbreen (Figure 1), which took place after 18 kyr (Landvik *et al.*, 1998). They may also have formed after its early Holocene readvance about 8–9 kyr, referred to as the Thomsondalen Stage (Kłysz *et al.*, 1988), but this event finds no support in more recent work (e.g. Rachlewicz, 2010). There is no geomorphic evidence that the higher-elevated pattern sites were glaciated during the Late Weichselian. However, summer temperatures were probably constantly below 0 °C during this period and therefore at least a thin perennial snow cover was probably present at these sites. Since patterned-ground formation was highly improbable under these conditions, its origin is probably limited to warmer conditions allowing summer snow melting. Hence, the upper age limit of sorted patterns at most sites is probably the Pleistocene–Holocene transition.

The climate of Svalbard was up to 1–2 °C warmer than at present during much of the early and mid-Holocene (Svendsen and Mangerud, 1997), which would result in MAAT values of *c.* −5 to −3 °C in the study area. These values are almost at the upper limit proposed for development of large-scale sorted circles and polygons in permafrost regions (Goldthwait, 1976; Washburn, 1980; Grab, 2002). Thus, the most favourable conditions for patterned-ground initiation in northern Billefjorden probably occurred shortly after local deglaciation or during the Holocene glacial readvance after 3 kyr BP (Landvik *et al.*, 1998) when temperatures were lower than present. Initiation during the LIA is unlikely for such well-developed patterns because of the limited time available. Accordingly, the sorted patterns are probably several thousands of years old, consistent with morphostratigraphical considerations (Hallet and Prestrud, 1986) and rare ^{14}C data from large-scale sorted circles (Hallet *et al.*, 1988; Cannone *et al.*, 2004) in western Svalbard, which suggested an age of hundreds or thousands of years. Likewise, large-scale sorted circles and polygons in Jotunheimen, southern Norway, are thought to have formed soon after deglaciation in the early Holocene, based on relative-age and Schmidt-hammer exposure-age dating techniques (Cook-Talbot, 1991; Winkler *et al.*, 2016), although this environment is not a perfect analogue to that of high-Arctic Svalbard.

Relationship to Active-Layer Thickness

In permafrost areas, sorting depth is confined by the base of the active layer (e.g. Ray *et al.*, 1983; Hallet and Prestrud, 1986). The frost table was observed only at one excavation site near sea level (31 m asl; site 6 in Figure 1) and reached 1 m at the end of the thawing season (end of August 2014), which is 0.36 m below the sorting depth. At other two excavation sites at higher elevations (558 and 773 m asl; sites 5 and 3 in Figure 1), the frost table was not encountered up to 0.1 m below the sorting depth, even though the thaw depth still might have not been at its maximum (cf. Christiansen and Humlum, 2008; Rachlewicz and Szczuciński, 2008). The ALT varies interannually by up to tens of per cent (Shur *et al.*, 2005). In 2014, summer air temperature at Svalbard Airport (https://www.ncdc.noaa.gov) was *c.* 1 °C above average for the period 1981–2010 (Nordli *et al.*, 2014), and the positive MAAT anomaly was even more pronounced, which probably typifies the mode of the current Svalbard climate (cf. Kääb *et al.*, 2014; Przybylak *et al.*, 2014). However, the thaw depth at the lowest excavation site exceeded the sorting depth by *c.* 56 % at the time of excavation. It is reasonable to assume that the sorting depth of active sorted patterned ground in steady-state conditions is slightly shallower compared to the active layer, although evidence for this is lacking. Nevertheless, the observed difference is probably too large. Therefore, we believe that at least at lower elevations, sorted circles and polygons are not in equilibrium with present-day climate conditions, which also favours their non-recent origin. On the other hand, it raises further questions about the significance of sorted patterns located in present-day periglacial environments under a changing climate.

CONCLUSIONS

Based on the investigations of 290 sorted circles and polygons in northern Billefjorden, central Svalbard, we draw the following conclusions:

1. The sorted circles and polygons form two distinct elevation zones, which significantly differ in pattern morphology.
2. Patterns at higher elevations have smaller diameters and shallower sorting depths because ALT decreases as elevation increases, suggesting that sorted patterns indicate climate conditions and ground thermal state (i.e. permafrost or seasonally frozen ground) when the patterns initiated. In contrast, the heights and height-to-width ratios of higher-lying sorted circles and polygons

are larger. Bedrock lithology is believed to cause only fine-scale variations in pattern morphology.

3. The ratios of pattern diameter-to-sorting depth in sorted circles and polygons have a median of 3.57, consistent with previous studies (median of 3.54; Figure 5) and theoretical models of patterned-ground formation involving circulation mechanisms. This allows estimation of the sorting depth based on patterned-ground surficial morphology, which can be used to reconstruct former active layers and associated temperature conditions.
4. Sorted circles and polygons in this high-Arctic environment may develop over centennial timescales, unlike those in lower latitudes.
5. The sorted circles and polygons are probably not in equilibrium with present-day climate conditions.
6. The sorted circles and polygons have probably been forming throughout the Holocene.

ACKNOWLEDGEMENTS

We are grateful to Jan Kavan for logistical support during the field research, and Michal Břežný, Zbyněk Engel, Martin Hanáček and Daniel Nývlt for field assistance. We also thank the two anonymous reviewers for their valuable comments and suggestions on the manuscript, and especially to the Editor, Julian B. Murton, for tremendous and unselfish editorial assistance with final editing of the paper. The research was financially supported by the Charles University Grant Agency, project number 674512, and the Czech Science Foundation, project number 17-21612S. The Centre for Polar Ecology of the University of South Bohemia in České Budějovice is thanked for the opportunity to use the Czech Arctic Research Infrastructure 'Josef Svoboda Station' in Svalbard.

REFERENCES

Baeten NJ, Forwick M, Vogt C, Vorren TO. 2010. Late Weichselian and Holocene sedimentary environments and glacial activity in Billefjorden, Svalbard. In *Fjord Systems and Archives*, Howe JA, Austin WEN, Forwick M, Paetzel M (eds). Geological Society, Special Publication London, UK **344**; 207–223.

Ballantyne CK. 2013. Patterned ground. In *Encyclopedia of Quaternary Science*, Second edition, Elias SA, Mock CJ (eds). Elsevier: Amsterdam, Netherlands; 452–463.

Ballantyne CK, Harris C. 1994. *The Periglaciation of Great Britain*. Cambridge University Press: Cambridge, UK; 330.

Ballantyne CK, Matthews JA. 1982. The development of sorted circles on recently deglaciated terrain, Jotunheimen, Norway. *Arctic and Alpine Research* **14**: 341–354. https://doi.org/10.2307/1550796

Ballantyne CK, Matthews JA. 1983. Desiccation cracking and sorted polygon development, Jotunheimen, Norway. *Arctic and Alpine Research* **15**: 339–349. https://doi.org/10.2307/1550830

Beskow G. 1935. *Tjälbildningen och tjällyftningen med särskild hänsyn till vägar och järnvägar (Soil freezing and frost heaving with special application to roads and railroads)* (in Swedish). Sveriges Geologiska Undersökning: Stockholm, Sweden; 242.

Bonnaventure PP, Lamoureux SF. 2013. The active layer: a conceptual review of monitoring, modelling techniques and changes in a warming climate. *Progress in Physical Geography* **37**: 352–376. https://doi.org/10.1177/0309133313478314

Cannone N, Guglielmin M, Gerdol R. 2004. Relationships between vegetation patterns and periglacial landforms in northwestern Svalbard. *Polar Biology* **27**: 562–571. https://doi.org/10.1007/s00300-004-0622-4

Christiansen HH, Humlum O. 2008. Interannual variations in active layer thickness in Svalbard. In *Proceedings of the Ninth International Conference on Permafrost*, Kane DL, Hinkel KM (eds), **1**. Institute of Northern Engineering, University of Alaska Fairbanks: Fairbanks, USA; 257–262.

Cook-Talbot JD. 1991. Sorted circles, relative-age dating and palaeoenvironmental reconstruction in an alpine periglacial environment, eastern Jotunheimen, Norway: lichenometric and weathering-based approaches. *The Holocene* **1**: 128–141. https://doi.org/10.1177/095968369100100205

Dąbski M. 2005. Small-scale sorted nets on glacial till, Fláajökull (southeast Iceland) and Elisbreen (northwest Spitsbergen). *Permafrost and Periglacial Processes* **16**: 305–310. https://doi.org/10.1002/ppp.527

Dallmann WK, Piepjohn K, Blomeier D. 2004. Geological Map of Billefjorden, Central Spitsbergen, Svalbard, with Geological Excursion Guide. Norsk Polarinstitutt.

Ellenberg L. 1976. Rezente Periglazialerscheinungen auf Cheju Dô, Südkorea. *Geographica Helvetica* **31**: 69–74. https://doi.org/10.5194/gh-31-69-1976

Etzelmüller B, Schuler TV, Isaksen K, Christiansen HH, Farbrot H, Benestad R. 2011. Modeling the temperature evolution of Svalbard permafrost during the 20th and 21st century. *The Cryosphere* **5**: 67–79. https://doi.org/10.5194/tc-5-67-2011

Ewertowski M. 2014. Recent transformations in the high-Arctic glacier landsystem, Ragnarbreen, Svalbard. *Geografiska Annaler. Series A, Physical Geography* **96**: 265–285. https://doi.org/10.1111/geoa.12049

Ewertowski MW, Tomczyk AM. 2015. Quantification of the ice-cored moraines' short-term dynamics in the high-Arctic glaciers Ebbabreen and Ragnarbreen, Petuniabukta, Svalbard. *Geomorphology* **234**: 211–227. https://doi.org/10.1016/j.geomorph.2015.01.023

Feuillet T. 2011. Statistical analyses of active patterned ground occurrence in the Taillon massif (Pyrénées, France/Spain). *Permafrost and Periglacial Processes* **22**: 228–238. https://doi.org/10.1002/ppp.726

Feuillet T, Mercier D. 2012. Post-Little Ice Age patterned ground development on two Pyrenean proglacial areas: from deglaciation to periglaciation. *Geografiska Annaler. Series A, Physical Geography* **94**: 363–376. https://doi.org/10.1111/j.1468-0459.2012.00459.x

Feuillet T, Mercier D, Decaulne A, Cossart E. 2012. Classification of sorted patterned ground areas based on their environmental characteristics (Skagafjörður, Northern Iceland). *Geomorphology* **139–140**: 577–587. https://doi.org/10.1016/j.geomorph.2011.12.022

Fraser JK. 1959. Freeze–thaw frequencies and mechanical weathering in Canada. *Arctic* **12**: 40–53. https://doi.org/10.14430/arctic3712

French HM. 2007. *The Periglacial Environment*, Third edition. John Wiley & Sons: Chichester, UK; 458.

Freund R. 1971. Die Kleinformen der Frostmusterböden: Vergleich Arktis - Alpen - Tropisches Hochgebirge (Small-scale Patterned Ground: Comparison of Arctic - Alps - Tropical High Moutains) (in German). *Geographica Helvetica* **26**: 142–147. https://doi.org/10.5194/gh-26-142-1971

Furrer G. 1955. Die Strukturbodenformen der Alpen. *Geographica Helvetica* **10**: 193–213. https://doi.org/10.5194/gh-10-193-1955

Gibas J, Rachlewicz G, Szczuciński W. 2005. Application of DC resistivity soundings and geomorphological surveys in studies of modern Arctic glacier marginal zones, Petuniabukta, Spitsbergen. *Polish Polar Research* **26**: 239–258.

Gleason KJ, Krantz WB, Caine N, George JH, Gunn RD. 1986. Geometrical aspects of sorted patterned ground in recurrently frozen soil. *Science* **232**: 216–220. https://doi.org/10.1126/science.232.4747.216

Goldthwait RP. 1976. Frost sorted patterned ground: a review. *Quaternary Research* **6**: 27–35. https://doi.org/10.1016/0033-5894(76)90038-7

Grab S. 2002. Characteristics and palaeoenvironmental significance of relict sorted patterned ground, Drakensberg plateau, southern Africa. *Quaternary Science Reviews* **21**: 1729–1744. https://doi.org/10.1016/S0277-3791(01)00149-4

Grab SW. 1997. Annually re-forming miniature sorted patterned ground in the High Drakensberg, southern Africa. *Earth Surface Processes and Landforms* **22**: 733–745. https://doi.org/10.1002/(SICI)1096-9837(199708)22:8<733::AID-ESP764>3.0.CO;2-L

Hagen JO, Liestøl O, Roland E, Jørgensen T. 1993. Glacier atlas of Svalbard and Jan Mayen. *Norsk Polarinstitutt, Meddelelser* **112**: 141.

Hallet B. 1998. Measurements of soil motion in sorted circles, western Spitsbergen. In *Proceedings of the Seventh International Conference on Permafrost*, Lewkowicz AG, Allard M (eds), Collection Nordicana 55. National Research Council of Canada: Ottawa, Canada; 415–420.

Hallet B. 2013. Stone circles: form and soil kinematics. *Philosophical Transactions of the Royal Society A: Mathematical, Physical and Engineering Sciences* **371**: 20120357. https://doi.org/10.1098/rsta.2012.0357

Hallet B, Anderson SP, Stubbs CW, Gregory EC. 1988. Surface soil displacements in sorted circles, western Spitsbergen. In *Proceedings of the Fifth International Conference on Permafrost*, Senneset K (ed), **1**. Tapir Publishers: Trondheim, Norway; 770–775.

Hallet B, Prestrud S. 1986. Dynamics of periglacial sorted circles in western Spitsbergen. *Quaternary Research* **26**: 81–99. https://doi.org/10.1016/0033-5894(86)90085-2

Haugland JE. 2006. Short-term periglacial processes, vegetation succession, and soil development within sorted patterned ground: Jotunheimen, Norway. *Arctic, Antarctic, and Alpine Research* **38**: 82–89. https://doi.org/10.1657/1523-0430(2006)038[0082:SPPVSA]2.0.CO;2

Henderson EP. 1968. Patterned ground in southeastern Newfoundland. *Canadian Journal of Earth Sciences* **5**: 1443–1453. https://doi.org/10.1139/e68-143

Hjort J, Luoto M. 2006. Modelling patterned ground distribution in Finnish Lapland: an integration of topographical, ground and remote sensing information. *Geografiska Annaler. Series A, Physical Geography* **88**: 19–29. https://doi.org/10.1111/j.0435-3676.2006.00280.x

Holness SD. 2003. Sorted circles in the maritime Subantarctic, Marion Island. *Earth Surface Processes and Landforms* **28**: 337–347. https://doi.org/10.1002/esp.430

Humlum O. 2002. Modelling late 20th-century precipitation in Nordenskiold Land, Svalbard, by geomorphic means. *Norsk Geografisk Tidsskrift - Norwegian Journal of Geography* **56**: 96–103. https://doi.org/10.1080/002919502760056413

Humlum O, Christiansen HH. 1998. Mountain climate and periglacial phenomena in the Faeroe Islands. *Permafrost and Periglacial Processes* **9**: 189–211. https://doi.org/10.1002/(SICI)1099-1530(199807/09)9:3<189::AID-PPP287>3.0.CO;2-N

Humlum O, Instanes A, Sollid JL. 2003. Permafrost in Svalbard: a review of research history, climatic background and engineering challenges. *Polar Research* **22**: 191–215. https://doi.org/10.1111/j.1751-8369.2003.tb00107.x

Isaksson E, Kohler J, Pohjola V, Moore J, Igarashi M, Karlöf L, Martma T, Meijer H, Motoyama H, Vaikmäe R, van de Wal RSW. 2005. Two ice-core $\delta^{18}O$ records from Svalbard illustrating climate and sea-ice variability over the last 400 years. *Holocene* **15**: 501–509. https://doi.org/10.1191/0959683605hl820rp

Jaedicke C, Gauer P. 2005. The influence of drifting snow on the location of glaciers on western Spitsbergen, Svalbard. *Annals of Glaciology* **42**: 237–242. https://doi.org/10.3189/172756405781812628

Jaedicke C, Sandvik AD. 2002. High resolution snow distribution data from complex Arctic terrain: a tool for model validation. *Natural Hazards and Earth System Science* **2**: 147–155. https://doi.org/10.5194/nhess-2-147-2002

Jahn A. 1963. Origin and development of patterned ground in Spitsbergen. In *Proceedings of the First International Conference on Permafrost*, Woods KB (ed). National Academy of Sciences National Research Council, Publication 1287: Washington, DC, USA; 140–145.

Kääb A, Girod L, Berthling I. 2014. Surface kinematics of periglacial sorted circles using structure-from-motion technology. *The Cryosphere* **8**: 1041–1056. https://doi.org/10.5194/tc-8-1041-2014

Kessler MA, Murray AB, Werner BT, Hallet B. 2001. A model for sorted circles as self-organized patterns. *Journal of Geophysical Research - Solid Earth* **106**: 13287–13306. https://doi.org/10.1029/2001JB000279

Kling J. 1998. The difference between sorted circle and polygon morphology and their distribution in two alpine areas, northern Sweden. *Zeitschrift für Geomorphologie, N.F.* **42**: 439–452.

Kłysz P, Lindner L, Makowska A, Marks L, Wysokiński L. 1988. Late Quaternary glacial episodes and sea level changes in the northeastern Billefjorden region, Central Spitsbergen. *Acta Geologica Polonica* **38**: 107–123.

Kłysz P, Lindner L, Marks L, Wysokiński L. 1989. Late Pleistocene and Holocene relief remodelling in the Ebbadalen-Nordenskiöldbreen region in Olav V Land, central Spitsbergen. *Polish Polar Research* **10**: 277–301.

Křížek M, Uxa T. 2013. Morphology, sorting and microclimates of relict sorted polygons, Krkonoše Mountains, Czech Republic. *Permafrost and Periglacial Processes* **24**: 313–321. https://doi.org/10.1002/ppp.1789

Kück KM. 1996. Periglacial features in the vicinity of Tiffindell ski resort, North East Cape Drakensberg, South Africa, and their implications for the development of the resort. PhD thesis, Department of Geography, Rhodes University, Grahamstown, South Africa. Available from https://core.ac.uk/download/pdf/11985324.pdf [accessed 2 February 2013]

Landvik JY, Bondevik S, Elverhøi A, Fjeldskaar W, Mangerud J, Salvigsen O, Siegert MJ, Svendsen JI, Vorren TO. 1998. The last glacial maximum of Svalbard and the Barents Sea area: ice sheet extent and configuration. *Quaternary Science Reviews* **17**: 43–75. https://doi.org/10.1016/S0277-3791(97)00066-8

Láska K, Witoszová D, Prošek P. 2012. Weather patterns of the coastal zone of Petuniabukta, central Spitsbergen in the period 2008–2010. *Polish Polar Research* **33**: 297–318. https://doi.org/10.2478/v10183−012−0025−0

Láska K, Witoszová D, Prošek P. 2010. Climate conditions of the permafrost active layer development in Petuniabukta, Billefjorden, Spitsbergen. In *Thermal State of Frozen Ground in a Changing Climate During the IPY*, Mertes JR, Christiansen HH, Etzelmüller B (eds). The University Centre in Svalbard: Longyearbyen, Svalbard; 128.

Long AJ, Strzelecki MC, Lloyd JM, Bryant CL. 2012. Dating High Arctic Holocene relative sea level changes using juvenile articulated marine shells in raised beaches.

Quaternary Science Reviews **48**: 61–66. https://doi.org/10.1016/j.quascirev.2012.06.009

Love A. 1995. Patterned ground at Beartooth Butte and East Summit, Wyoming: geometry, analysis, and origin. In *Quaternary Geology of the Clarks Fork Region, Northwestern Wyoming and Adjacent Montana*, Carson RJ, DeSimone D, Leonard EM (eds). Keck Geology Consortium: Claremont, CA, USA; 113–116.

Luoto M, Hjort J. 2005. Evaluation of current statistical approaches for predictive geomorphological mapping. *Geomorphology* **67**: 299–315. https://doi.org/10.1016/j.geomorph.2004.10.006

Małecki J. 2015. Snow accumulation on a small high-Arctic glacier Svenbreen: variability and topographic controls. *Geografiska Annaler. Series A, Physical Geography* **97**: 809–817. https://doi.org/10.1111/geoa.12115

Małecki J. 2016. Accelerating retreat and high-elevation thinning of glaciers in central Spitsbergen. *The Cryosphere* **10**: 1317–1329. https://doi.org/10.5194/tc-10-1317-2016

Mangerud J, Bolstad M, Elgersma A, Helliksen D, Landvik JY, Lønne I, Lycke AK, Salvigsen O, Sandahl T, Svendsen JI. 1992. The last glacial maximum on Spitsbergen, Svalbard. *Quaternary Research* **38**: 1–31. https://doi.org/10.1016/0033-5894(92)90027-G

Marvánek O. 2010. Sorted patterned ground on the James Ross Island and its morphological diversity. *Acta Geographica Silesiana* **7**: 49–53.

Matthews JA, Shakesby RA, Berrisford MS, McEwen LJ. 1998. Periglacial patterned ground on the Styggedalsbreen Glacier foreland, Jotunheimen, southern Norway: micro-topographic, paraglacial and geoecological controls. *Permafrost and Periglacial Processes* **9**: 147–166. https://doi.org/10.1002/(SICI)1099-1530(199804/06)9:2<147::AID-PPP278>3.0.CO;2-9

Nordli Ø, Przybylak R, Ogilvie AEJ, Isaksen K. 2014. Long-term temperature trends and variability on Spitsbergen: the extended Svalbard Airport temperature series, 1898–2012. *Polar Research* **33**: 21348. https://doi.org/10.3402/polar.v33.21349

Peterson RA, Krantz WB. 2008. Differential frost heave model for patterned ground formation: corroboration with observations along a North American arctic transect. *Journal of Geophysical Research* **113**: G03S04. https://doi.org/10.1029/2007JG000559

Pleskot K. 2015. Sedimentological characteristics of debris flow Deposits within ice−cored moraine of Ebbabreen, central Spitsbergen. *Polish Polar Research* **36**: 125–144. https://doi.org/10.1515/popore-2015-0006

Prach K, Klimešová J, Košnar J, Redčenko O, Hais M. 2012. Variability of contemporary vegetation around Petuniabukta, central Spitsbergen. *Polish Polar Research* **33**: 383–394. https://doi.org/10.2478/v10183-012-0026-z

Przybylak R, Araźny A, Nordli Ø, Finkelnburg R, Kejna M, Budzik T, Migała K, Sikora S, Puczko D, Rymer K, Rachlewicz G. 2014. Spatial distribution of air temperature on Svalbard during 1 year with campaign measurements. *International Journal of Climatology* **34**: 3702–3719. https://doi.org/10.1002/joc.3937

Rachlewicz G. 2010. Paraglacial modifications of glacial sediments over millennial to decadal time-scales in the high Arctic (Billefjorden, central Spitsbergen, Svalbard). *Quaestiones Geographicae* **29**: 59–67. https://doi.org/10.2478/v10117-010-0023-4

Rachlewicz G, Styszyńska A. 2007. Porównanie przebiegu temperatury powietrza w Petuniabukta i Svalbard-Lufthavn (Isfjord, Spitsbergen) w latach 2001–2003 (comparison of the course of air temperature in Petuniabukta and Svalbard-Lufthavn (Isfjord, Spitsbergen) in the years 2001–2003) (in Polish). *Problemy Klimatologii Polarnej* **17**: 121–134.

Rachlewicz G, Szczuciński W. 2008. Changes in thermal structure of permafrost active layer in a dry polar climate, Petuniabukta, Svalbard. *Polish Polar Research* **29**: 261–278.

Rachlewicz G, Szczuciński W, Ewertowski M. 2007. Post-"Little Ice Age" retreat rates of glaciers around Billefjorden in central Spitsbergen, Svalbard. *Polish Polar Research* **28**: 159–186.

Ray RJ, Krantz WB, Caine TN, Gunn RD. 1983. A model for sorted patterned-ground regularity. *Journal of Glaciology* **29**: 317–337. https://doi.org/10.1017/S0022143000008376

Salvigsen O. 1984. Occurrence of pumice on raised beaches and Holocene shoreline displacement in the inner Isfjorden area, Svalbard. *Polar Research* **2**: 107–113. https://doi.org/10.1111/j.1751-8369.1984.tb00488.x

Shapiro SS, Wilk MB. 1965. An analysis of variance test for normality (complete samples). *Biometrika* **52**: 591–611. https://doi.org/10.1093/biomet/52.3-4.591

Shur Y, Hinkel KM, Nelson FE. 2005. The transient layer: implications for geocryology and climate-change science. *Permafrost and Periglacial Processes* **16**: 5–17. https://doi.org/10.1002/ppp.518

Stacke V, Mida P, Lehejček J, Tóthová G, Nývlt D. 2013. Recent landscape changes in terminoglacial area of the Nordenskiöldbreen, central Spitsbergen, Svalbard. *Czech Polar Reports* **3**: 3–6. https://doi.org/10.5817/CPR2013-1-2

Stankowska A. 1989. Glacial deposits of the northern region adjacent to Petuniabukta in the light of mineralogical and chemical studies, central Spitsbergen. *Polish Polar Research* **10**: 303–316.

Strzelecki MC, Long AJ, Lloyd JM. 2017. Post-Little Ice Age development of a high arctic paraglacial beach complex. *Permafrost and Periglacial Processes* **28**: 4–17. https://doi.org/10.1002/ppp.1879

Svendsen JI, Mangerud J. 1997. Holocene glacial and climatic variations on Spitsbergen, Svalbard. *Holocene* **7**: 45–57. https://doi.org/10.1177/095968369700700105

Szczuciński W, Rachlewicz G. 2007. Geological setting of the Petuniabukta region. *Landform Analysis* **5**: 212–215.

Szymański W, Skiba M, Wojtuń B, Drewnik M. 2015. Soil properties, micromorphology, and mineralogy of Cryosols from sorted and unsorted patterned grounds in the Hornsund area, SW Spitsbergen. *Geoderma* **253–254**: 1–11. https://doi.org/10.1016/j.geoderma.2015.03.029

Treml V, Krizek M, Engel Z. 2010. Classification of patterned ground based on morphometry and site characteristics: a case study from the high Sudetes, Central Europe. *Permafrost and Periglacial Processes* **21**: 67–77. https://doi.org/10.1002/ppp.671

Troll C. 1944. Strukturböden, Solifluktion und Frostklimate der Erde. *Geologische Rundschau* **34**: 545–694. (Also as Structure Soils, Solifluction, and Frost Climates of the Earth, U.S. Army Snow Ice and Permafrost Research Establishment, Translation 43, Wilmette, Illinois, 121 pp.).

van der Meij WM, Temme AJAM, de Kleijn CMFJJ, Reimann T, Heuvelink GBM, Zwoliński Z, Rachlewicz G, Rymer K, Sommer M. 2016. Arctic soil development on a series of marine terraces on central Spitsbergen, Svalbard: a combined geochronology, fieldwork and modelling approach. *The Soil* **2**: 221–240. https://doi.org/10.5194/soil-2-221-2016

Van Vliet-Lanoë B. 1991. Differential frost heave, load casting and convection: converging mechanisms; a discussion of the origin of cryoturbations. *Permafrost and Periglacial Processes* **2**: 123–139. https://doi.org/10.1002/ppp.3430020207

Warburton J. 2013. Patterned ground and polygons. In *Treatise on Geomorphology, Vol. 8, Glacial and Periglacial Geomorphology*, Shroder J, Giardino R, Harbor J (eds). Academic Press: San Diego, USA; 298–312.

Washburn AL. 1980. Permafrost features as evidence of climatic change. *Earth-Science*

Reviews **15**: 327–402. https://doi.org/10.1016/0012-8252(80)90114-2

Watanabe T, Matsuoka N, Christiansen HH, Cable S. 2017. Soil physical and environmental conditions controlling patterned-ground variability at a continuous permafrost site, Svalbard. *Permafrost and Periglacial Processes* **28**: 433–445. https://doi.org/10.1002/ppp.1924

Wilson P. 1992. Small-scale patterned ground, Comeragh Mountains, southeast Ireland. *Permafrost and Periglacial Processes* **3**: 63–70. https://doi.org/10.1002/ppp.3430030109

Wilson P, Clark R. 1991. Development of miniature sorted patterned ground following soil erosion in East Falkland, South Atlantic. *Earth Surface Processes and Landforms* **16**: 369–376. https://doi.org/10.1002/esp.3290160409

Winkler S, Matthews JA, Mourne RW, Wilson P. 2016. Schmidt-hammer exposure ages from periglacial patterned ground (sorted circles) in Jotunheimen, Norway, and their interpretative problems. *Geografiska Annaler. Series A, Physical Geography* **98**: 265–285. https://doi.org/10.1111/geoa.12134

Winther JG, Bruland O, Sand K, Killingtveit Å, Marechal D. 1998. Snow accumulation distribution on Spitsbergen, Svalbard, in 1997. *Polar Research* **17**: 155–164. https://doi.org/10.1111/j.1751-8369.1998.tb00269.x

7.6 Paper VI

Uxa, T. (2017). Discussion on 'Active Layer Thickness Prediction on the Western Antarctic Peninsula' by Wilhelm *et al.* (2015). *Permafrost and Periglacial Processes*, 28(2), 493–498. https://doi.org/10.1002/ppp.1888

Journal Citation Reports 2016: Impact factor 2.815, Q2(16/49) in Geography Physical, Q1(6/47) in Geology.

Citations as of 9 June 2020: Web of Science=3, Scopus=3, Google Scholar=3, ResearchGate=4.

PERMAFROST AND PERIGLACIAL PROCESSES
Permafrost and Periglac. Process. **28**: 493–498 (2017)
Published online 2 February 2016 in Wiley Online Library
(wileyonlinelibrary.com) DOI: 10.1002/ppp.1888

Short Communication
Discussion on 'Active Layer Thickness Prediction on the Western Antarctic Peninsula' by Wilhelm *et al.* (2015)

*Tomáš Uxa**

Department of Physical Geography and Geoecology, Faculty of Science, Charles University in Prague, Praha, Czech Republic

ABSTRACT

Wilhelm *et al*. (2015) employed the widely used Stefan and Kudryavtsev equations to predict the maximum active-layer thickness (ALT) on Amsler Island, Western Antarctic Peninsula. Their predictions far exceed the observations of ALT reported from other parts of the region. Here, I demonstrate that the values of ALT are significantly overestimated by the predictive equations because the authors incorrectly assumed that little or no latent heat of phase change is absorbed during thawing. Although the area is the warmest in the Antarctic Peninsula region, with a rapid increase in air temperature and permafrost temperatures close to 0 °C, the active layer is likely to be substantially thinner than values predicted by Wilhelm *et al*. (2015). Copyright © 2016 John Wiley & Sons, Ltd.

KEY WORDS: active-layer thickness; permafrost; Stefan equation; Kudryavtsev equation; thermal modelling; Antarctic Peninsula

INTRODUCTION

Wilhelm *et al*. (2015) examined the ability of the Stefan and Kudryavtsev equations and the HYDRUS thermal model to predict maximum active-layer thickness (ALT) and active-layer temperature dynamics at three sites located on Amsler Island (Palmer Archipelago), in the Western Antarctic Peninsula region. The ALT was predicted to be 4.7–8.7 m in soils and unconsolidated materials, and 11.9–18.6 m in bedrock. These values of ALT are exceedingly large compared to others reported from the region (usually up to 1–2 m in unconsolidated materials and up to 2–6 m in bedrock; Vieira *et al*., 2010; Bockheim *et al*., 2013) and were attributed to regional climate warming.

I consider this explanation to be oversimplified for the following reasons: (i) the values of ALT predicted by the Stefan and Kudryavtsev equations represent upper limits that assume negligible or no latent heat of phase change is absorbed during thawing; (ii) the ALTs were not validated against any reference ground temperature records from depths exceeding the predicted ALTs (except at the bedrock summit site); and (iii) the predicted ALTs far exceed the ALT ranges reported elsewhere in the Antarctic Peninsula region. Hence, the values of ALT predicted by Wilhelm *et al*. (2015) are thought to be of doubtful validity.

Here, I address these issues by recalculating the original values of ALT predicted by Wilhelm *et al*. (2015) using the Stefan and Kudryavtsev equations and I briefly discuss the ALT in the context of active-layer dynamics in the Antarctic Peninsula region.

ALT PREDICTIONS

The Stefan and Kudryavtsev equations are simplified analytical solutions that have been extensively used for predicting depths of thawing and freezing in unconsolidated sediments/soils (e.g. Romanovsky and Osterkamp, 1997; Klene *et al*., 2001; Heggem *et al*., 2006) and rock materials (e.g. Matsuoka, 2008). Both equations incorporate the volumetric latent heat of phase change of water Q_L (J.m^{-3}):

$$Q_L = \rho L(\omega\text{-}\omega_u) \quad (1)$$

where ρ is the dry bulk density of the ground (kg.m^{-3}), L is the latent heat of phase change of water (J.kg^{-1}), ω is the total gravimetric water content expressed as a proportion of the mass of total water to the mass of dry ground and ω_u is the unfrozen gravimetric water content (i.e. water not involved in the phase change) expressed as a proportion

*Correspondence to: T. Uxa, Department of Physical Geography and Geoecology, Faculty of Science, Charles Univeristy in Prague, Albertov 6, 128 43 Praha 2, Czech Republic. E-mail: tomas.uxa@natur.cuni.cz

Received 3 August 2015
Revised 20 October 2015
Accepted 4 November 2015

of the mass of unfrozen water to the mass of dry ground. Note that Wilhelm *et al*. (2015) incorrectly used the expression ρL for the volumetric latent heat of phase change in their Equations 1 and 2 (i.e. excluding the water content members). This would imply very high values of volumetric latent heat of phase change and thus a thin active layer.

In order to review the values of ALT predicted by Wilhelm *et al*. (2015), I recalculated the ALT using the Stefan and Kudryavtsev equations with ground temperature data and ground material properties reported in their paper (Table 1). Several scenarios of unfrozen water content (which controls the amount of latent heat of phase change) were entered into the equations in order to obtain ALT limits at the solifluction lobe and climate station sites. Only one scenario was considered for the bedrock summit site, where a total water content of zero was observed. The minimum difference between the total and unfrozen water contents was set to 0.1 % in the Stefan equation to avoid division by zero.

The ALT recalculations most closely match the original ALTs predicted by Wilhelm *et al*. (2015) when the unfrozen water contents are set close to or equal to total water contents. Under these conditions, the recalculated values of ALT average 4.6–8.9 m at the solifluction lobe and climate station sites, and 10.1–16.5 m at the bedrock summit site (Figure 1; Table 2). The relatively small difference between the original and recalculated ALTs likely results from the fact that statistical characteristics (averages and standard deviations) of ground temperature data for the whole observation period entered the calculations instead of real annual ground temperature data. Secondly, the fixed 0.1 % minimum difference between the total and unfrozen water contents (to avoid division by zero in the Stefan equation) likely results in different amounts of latent heat of phase change entering the calculations than in the original paper by Wilhelm *et al*. (2015), which may lead to significant differences in the predicted ALTs due to the exponential nature of the equation. In fact, changes in the unfrozen water content in the order of tenths of a per cent may produce decimetre- to metre-scale differences in the predicted ALTs in cases when little water is involved in the phase change.

Nevertheless, the above predictions represent upper ALT limits by assuming unrealistically high unfrozen water contents. The equations significantly overestimate ALTs in this situation (particularly the Stefan equation), because negligible or no latent heat of phase change enters the calculations. However, the Stefan equation was derived with the assumption that the latent heat of phase change in the active layer is much larger than the sensible heat. If the latent heat approaches zero, then the equation gives invalid results (Romanovsky and Osterkamp, 1997). On the other hand, the Kudryavtsev equation builds on Fourier temperature wave propagation theory and therefore, substituting the latent heat for zero, predicts the maximum depth of the 0 °C isotherm without phase change (Romanovsky and Osterkamp, 1997). Since the soils and unconsolidated

Table 1 Ground temperature data and ground material properties used as input data in the active-layer thickness predictions (averages and standard deviations).

Site	FDD_s	TDD_s	MAGST	A_s	T_z	K_t	C_t	ρ	ω
Solifluction lobe	888 ± 164	307 ± 91	−1.6 ± 0.2	14.0 ± 2.1	−0.7 ± 0.3	0.84	1.45	1700	5.7
Climate station	966 ± 140	175 ± 39	−2.2 ± 0.3	10.4 ± 3.4	−1.9 ± 0.5	1.34	1.83	1520	8.4
Bedrock summit	980 ± 110	219 ± 52	−2.1 ± 0.2	14.8 ± 1.8	−1.3 ± 0.6	3.57	0.78	4000	0.0

FDD_s = surface freezing degree-days (°C.days); TDD_s = surface thawing degree-days (°C.days); MAGST = mean annual ground surface temperature (°C); A_s = annual ground surface temperature amplitude (°C); T_z = mean annual temperature at the top of permafrost (°C); K_t = thermal conductivity of the ground in the thawed state ($W.m^{-1}.°C^{-1}$); C_t = volumetric heat capacity of the ground in the thawed state ($J.m^{-3}.°C^{-1} \times 10^6$); ρ = dry bulk density of the ground ($kg.m^{-3}$) calculated as weighted average of horizon thicknesses; ω = total gravimetric water content (%).

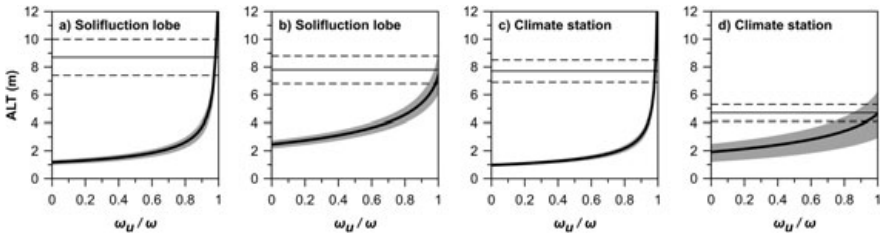

Figure 1 Active-layer thicknesses (ALTs) at the solifluction lobe (a, b) and climate station (c, d) sites as a function of the unfrozen to total water content ratios (ω_u / ω) predicted by the Stefan (a, c) and Kudryavtsev (b, d) equations. Thick black lines show the average ALTs derived on the basis of the average ground temperature data. Grey zones outline the upper and lower ALT thresholds derived on the basis of the standard deviations of ground temperature data. Black solid and dashed horizontal lines represent the original average ALTs and their standard deviations reported by Wilhelm *et al*. (2015).

Table 2 Comparison of the original (Wilhelm *et al*., 2015) and recalculated active-layer thickness (ALT) predictions (averages and standard deviations).

Site	ALTs (m)		
	Solifluction lobe	Climate station	Bedrock summit
Observed ALT by Wilhelm *et al.* (2015)	—	—	12.5–14.5
Stefan equation			
Original ALT predicted by Wilhelm *et al.* (2015)	8.7 ± 1.3	7.7 ± 0.8	11.9 ± 1.4
Recalculated ALT for $\omega_u \rightarrow \omega$	8.9 ± 1.3	8.9 ± 1.0	10.1 ± 1.2
Recalculated ALT for ω_u = 2 %	1.5 ± 0.2	1.1 ± 0.1	—
Recalculated ALT for ω_u = 0 %	1.2 ± 0.2	1.0 ± 0.1	—
Kudryavtsev equation			
Original ALT predicted by Wilhelm *et al.* (2015)	7.8 ± 1.0	4.7 ± 0.6	18.6 ± 4.9
Recalculated ALT for $\omega_u = \omega$	7.2 ± 1.5	4.6 ± 1.7	16.5 ± 4.2
Recalculated ALT for ω_u = 2 %	3.0 ± 0.3	2.2 ± 0.7	—
Recalculated ALT for ω_u = 0 %	2.5 ± 0.3	1.9 ± 0.6	—
HYDRUS-predicted ALT by Wilhelm *et al.* (2015)	6–8	4–6	8–10

Note: The minimum difference between the total and unfrozen water contents was set to 0.1 % in the Stefan equation to avoid division by zero. ω_u = unfrozen gravimetric water content; ω = total gravimetric water content.

materials at the solifluction lobe and climate station sites have a sand or silty sand texture and winter ground temperatures are well below 0 °C (Wilhelm *et al*., 2015), the unfrozen water contents are likely very low (Andersland and Ladanyi, 2004). This means that most of the water is involved in the phase change and absorbs the latent heat during thawing, which decelerates active-layer thickening. This is confirmed by Figures 3, 4 and 6 in Wilhelm *et al*. (2015), which clearly show the zero-curtain periods during freezing and thawing at the solifluction lobe and climate station sites. Accordingly, at the bedrock summit site, where the total water content was zero, no zero curtain was observed (see Figures 5 and 8 in Wilhelm *et al*., 2015). I therefore conclude that the values of ALT at the solifluction lobe and climate station sites should be substantially smaller than those predicted by Wilhelm *et al*. (2015).

Because maximum annual ground temperatures measured at the solifluction lobe and climate station sites in the shallow boreholes at 2 m depths did not fall below 0 °C during the observation period and no ice was present in the excavations (Wilhelm *et al*., 2015), the ALTs should range between 2 m and the upper ALT limits shown in the previous paragraphs (Figure 1; Table 2). There is a little change in ALTs predicted by the Stefan equation within a wide range of unfrozen water contents until a certain threshold is reached (Figure 1). The unfrozen water contents necessary to exceed the ALT of 2 m are approximately 3.7 % and 6.4 % at the solifluction lobe and climate station sites, respectively (i.e. 65 % and 76 % of the total water content, respectively). However, these unfrozen water contents are too high for sand or silty sand materials (Andersland and Ladanyi, 2004). On the other hand, the Kudryavtsev equation predicts an active layer thicker than 2 m for unfrozen water contents equal to 0 % and 0.7 % at the solifluction lobe and climate station sites, respectively (i.e. 0 % and 8 % of the total water content, respectively), which is much closer to the real situation. Since part of the water always remains unfrozen in the form of thin layers on particle surfaces (Andersland and Ladanyi, 2004), the unfrozen water contents are likely a little higher at these sites (up to 1–2 %). It should generate slightly thicker active layers, on average 2.2–3 m for unfrozen water contents of 2 % (Figure 1; Table 2). In this context, the Kudryavtsev equation seems to provide more accurate ALT predictions than the Stefan equation.

Because the Stefan and Kudryavtsev equations, in their simplest forms, assume homogeneous and temporally invariant ground material properties within the profile (e.g. Kurylyk, 2015), special attention must be paid to the careful collection of representative input data. Although the Palmer Archipelago has one of the largest precipitation rates in the Antarctic Peninsula region (Bockheim *et al*., 2013) and winter snow cover thickness can exceed 1 m (Wilhelm *et al*., 2015), the total water contents reported at the solifluction lobe and climate station sites (Table 1) are smaller than elsewhere in the region (e.g. Cannone *et al*., 2006; Michel *et al*., 2012). The reason may be that the samples used for determining ground material properties were collected only from near-surface horizons at the end of the thawing season (in April). In summer, however, water migrates downwards under a negative temperature gradient and the total water content at the bottom of the active layer and the upper part of permafrost increases, while it decreases near the ground surface (French, 2007). It is therefore possible that the total water contents reported by Wilhelm *et al*. (2015) are close to their seasonal minima. This is particularly important because the water content and its distribution within the active layer define the amount of latent heat and the rate of thawing, but also the thermal properties, as these parameters are interdependent (Shur *et al*., 2005). Additionally, the bulk density, also determining the amount of latent heat, was estimated from sand and organic matter contents using pedotransfer functions given in Minasny and Hartemink (2011). These

equations can be particularly useful in cases when input data are lacking or cannot be obtained directly, but they generally show a considerable scatter. More importantly, they were calibrated for predicting bulk densities in the tropics and their accuracy in polar soils has not yet been tested, which may further complicate ALT predictions.

ALT VALIDATION

Wilhelm *et al.* (2015) measured ground temperatures using iButton® DS1922L loggers (Maxim Integrated Inc.) with a resolution of ±0.0625 °C and an accuracy of ±0.5 °C, which have also been used elsewhere in the Antarctic Peninsula region (e.g. Ramos *et al.*, 2009; De Pablo *et al.*, 2014). Although Gubler *et al.* (2011) stated that the accuracy of these devices can be as good as ±0.125 °C, it should be emphasised that they can show a significant offset (Schoeneich, 2011), occasionally even beyond the manufacturer-specified limits (personal observations of Tomáš Uxa and Peter Mida). Hence, the loggers should be calibrated at 0 °C in an ice-water bath or using the zero curtain to obtain more accurate ground temperature data (Schoeneich, 2011). If not calibrated, the data should be treated with caution. Because Wilhelm *et al.* (2015) did not calibrate the loggers, their ground temperature data may significantly deviate from real conditions. This is important, especially with respect to ground temperatures in the deep borehole at the bedrock summit site, where minimum and maximum annual ground temperatures at a depth of 8 to 14.5 m are between −0.5 and 0.5 °C (see Figure 7 in Wilhelm *et al.*, 2015). Given the accuracy of the loggers, the active layer at this site may be much thinner than the values of 12.5 to 14.5 m reported by Wilhelm *et al.* (2015). Further, the temperature of the deep borehole should be considered carefully because it was drilled using a water-cooled system that generally causes great thermal disturbance (e.g. Ramos *et al.*, 2009) and the time required to re-establish thermal equilibrium can take up to several weeks or even months (Andersland and Ladanyi, 2004; Miller, 2004).

One of the major problems of the paper by Wilhelm *et al.* (2015) is the absence of any reference ground temperature records below 2 m depth at the solifluction lobe and climate station sites, which would allow the authors to directly validate the accuracy of the predicted ALTs. Instead, it relies on tests of accuracy carried out in previous studies (e.g. Romanovsky and Osterkamp, 1997; Klene *et al.*, 2001; Heggem *et al.*, 2006) and on the ALTs predicted by the HYDRUS thermal model. The HYDRUS-predicted ALTs were generally smaller than those obtained by the Stefan and Kudryavtsev equations, which exceeded or ranged around the upper HYDRUS-predicted ALT limits (Table 2). However, HYDRUS is unable to accurately model isothermal conditions associated with the latent heat release and absorption during freezing and thawing (the zero-curtain effect) in the soils and unconsolidated materials (see Figures 4 and 6 in Wilhelm *et al.*, 2015). This causes, on the one hand, temperature overestimation during the thawing periods and, on the other, temperature underestimation during the freezing periods. Although the authors state that the difference between the observed and HYDRUS-modelled temperatures became negligible after a few weeks of thawing or freezing, even this relatively small difference may result in modelled active layers that are substantially thicker than the real ones. Further, the comparison of the observed and HYDRUS-modelled temperatures was done for relatively shallow depths (60 and 80 cm). But temperatures at these depths are strongly controlled by the upper boundary conditions, and the model may perform much worse at greater depths. Therefore, with respect to ALT predictions, model validation against the deepest temperature sensors located at 2 m depth would be more appropriate.

Another important source of error in the HYDRUS-modelled temperature is setting the initial ground temperatures at −1 °C at all the modelling depths without model equilibration prior to the start of the modelling period. Consequently, the model deviates from the actual conditions at the beginning of the modelling period (see Figures 4 and 6 in Wilhelm *et al.*, 2015). However, much more importantly, the 3-year model run is too short to equilibrate temperatures, particularly at greater depths, which may significantly affect the HYDRUS-predicted ALTs. In order to eliminate this problem, the initial conditions should be created (e.g. using one season as spin-up until steady-state conditions are reached) (e.g. Hipp *et al.*, 2014), at least in the uppermost part of the modelling domain, where maximum ALT is expected.

CLIMATE WARMING EXPLANATION?

Palmer Archipelago is the warmest in the Antarctic Peninsula region (Morris and Vaughan, 2003), with a rapid warming trend (e.g. Turner *et al.*, 2005) and permafrost temperatures close to 0 °C (Bockheim *et al.*, 2013; Wilhelm *et al.*, 2015). Because climate is a first-order control on ALT (Bonnaventure and Lamoureux, 2013), thicker active layers on Amsler Island are expected. However, their exceptional thickness in comparison to other ALTs reported from the region is hard to explain by regional climate warming alone. Positive temperature trends have been detected throughout the whole Antarctic Peninsula over the past few decades, with the lowest spatial variability during the summer months (e.g. Turner *et al.*, 2005). This climate signal would undoubtedly thicken active layers in a similar magnitude at other locations affected by climate warming, even though the importance of mean annual ground surface temperatures, ground temperatures during the freezing season and/or precipitation rates for active-layer dynamics has also been highlighted recently (Bonnaventure and Lamoureux, 2013). Nevertheless, such thick active layers as those inferred by Wilhelm *et al.* (2015) have not been observed

elsewhere in the region, even in a similar climate and geological setting (see Vieira *et al*., 2010; Bockheim *et al*., 2013).

Reports prior to 1980 mention ALTs of 0.25–0.35 m below moss beds in the Palmer Station area, located approximately 1 km from Amsler Island (Everett, 1976, and Smith, 1982, cited in Bockheim *et al*., 2013). Observations from maritime Antarctica show that moss-covered sites have active layers approximately two to four times thinner than bare ground locations (Cannone *et al*., 2006; Guglielmin *et al*., 2012). Accordingly, it can be estimated that over 35 years ago, the approximate ALT at bare ground sites ranged between 0.5–0.7 and 1–1.4 m in the Palmer Station area. Unfortunately, because permafrost temperature and ALT monitoring started no earlier than in 2000 throughout most of the Antarctic Peninsula, with most monitoring starting during the International Polar Year 2007–2009 (Vieira *et al*., 2010), it is difficult to quantify reliably the climate change impact on ALT at most of the monitoring sites. The rare long-term ALT observations on Signy Island, in the South Orkney Islands, however, show that active-layer thickening rates are slow, averaging 1 $cm.yr^{-1}$ (Cannone *et al*., 2006). The same or even slower rates were reported from Victoria Land, in continental Antarctica (Guglielmin and Cannone, 2012; Guglielmin *et al*., 2014a). In this context, the extremely thick active layers predicted by Wilhelm *et al*. (2015) appear to be unlikely.

Further, the Western Antarctic Peninsula area has smaller ranges of temperature than other parts of the Peninsula, owing to its more maritime climate. This should generate smaller ALTs, assuming that the mean annual ground surface temperatures and ground material properties are equal. However, the ALTs predicted by Wilhelm *et al*. (2015) show the opposite tendency when compared to those of other locations with larger temperature amplitudes and similar mean annual ground surface temperatures (e.g. Guglielmin *et al*., 2012, 2014b), which is hard to explain by differences in ground material properties. In fact, the surface thawing degree-days are substantially lower on Amsler Island than at other sites within the Antarctic Peninsula (e.g. Guglielmin *et al*., 2012, 2014b; Hrbáček *et al*., 2015) or the northern hemisphere (e.g. Christiansen *et al*., 2010), where thinner active layers have been reported.

CONCLUSIONS

Palmer Archipelago is the warmest area in the Antarctic Peninsula region, with permafrost temperatures close to 0 °C. In this context, the ground temperature data presented by Wilhelm *et al*. (2015) are of great interest, particularly with respect to ongoing climate change in the region.

Nevertheless, extremely thick active layers predicted by the Stefan and Kudryavtsev equations represent the upper limits of ALT and assume that little or no latent heat of phase change is absorbed during thawing. The predictive equations overestimate ALTs in this situation and therefore, the ALTs predicted by Wilhelm *et al*. (2015) are significantly overestimated and misleading. This is all the more serious as the region is an important climate change hotspot and the ALT predictions presented by Wilhelm *et al*. (2015) bring noise into the debate on climate change and its quantification.

Unfortunately, the Wilhelm *et al*. (2015) study lacks any reference ground temperature records from depths exceeding the predicted ALTs (except at the bedrock summit site) and so cannot validate the predicted values of ALT. As a result the study is unable to properly answer the main research question, which was to examine the ability of the Stefan and Kudryavtsev equations and the HYDRUS model to predict ALTs on Amsler Island.

ACKNOWLEDGEMENTS

Here, I wish to sincerely thank Peter Mida of the Charles University in Prague for encouraging me to submit this paper and his helpful comments on its earlier version. I would also like to thank two anonymous reviewers and the Associate Editor, Prof. Kenneth M. Hinkel, for their useful comments and review of the paper. A special thanks goes to the Editor, Prof. Julian B. Murton, for his assistance in the final editing of the article and in improving the English.

REFERENCES

Andersland OB, Ladanyi B. 2004. *Frozen Ground Engineering*. John Wiley & Sons, Ltd: Hoboken, New Jersey; 384.

Bockheim J, Vieira G, Ramos M, López-Martínez J, Serrano E, Guglielmin M, Wilhelm K, Nieuwendam A. 2013. Climate warming and permafrost dynamics in the Antarctic Peninsula region. *Global and Planetary Change* **100**: 215–223. DOI:10.1016/j.gloplacha.2012.10.018.

Bonnaventure PP, Lamoureux SF. 2013. The active layer: A conceptual review of monitoring, modelling techniques and changes in a warming climate. *Progress in Physical Geography* **37**: 352–376. DOI:10.1177/0309133313478314.

Cannone N, Ellis Evans JC, Strachan R, Guglielmin M. 2006. Interactions between climate, vegetation and the active layer in soils at two Maritime Antarctic sites. *Antarctic Science* **18**: 323–333. DOI:10.1017/S095410200600037X.

Christiansen HH, Etzelmüller B, Isaksen K, Juliussen H, Farbrot H, Humlum O, Johansson M, Ingeman-Nielsen T, Kristensen L, Hjort J, Holmlund P, Sannel ABK, Sigsgaard C, Åkerman HJ, Foged N, Blikra LH, Pernosky MA, Ødegård RS. 2010. The Thermal State of Permafrost in the Nordic Area during the International Polar Year 2007–2009. *Permafrost and Periglacial Processes* **21**: 156–181. DOI:10.1002/ppp.687.

De Pablo MA, Ramos M, Molina A. 2014. Thermal characterization of the active layer

at the Limnopolar Lake CALM-S site on Byers Peninsula (Livingston Island), Antarctica. *Solid Earth* **5**: 721–739. DOI: 10.5194/se-5-721-2014.

French HM. 2007. *The Periglacial Environment*. John Wiley & Sons, Ltd: Chichester, England; 458.

Gubler S, Fiddes J, Keller M, Gruber S. 2011. Scale-dependent measurement and analysis of ground surface temperature variability in alpine terrain. *The Cryosphere* **5**: 431–443. DOI:10.5194/tc-5-431-2011.

Guglielmin M, Cannone N. 2012. A permafrost warming in a cooling Antarctica? *Climate Change* **111**: 177–195. DOI:10.1007/s10584-011-0137-2.

Guglielmin M, Worland MR, Cannone N. 2012. Spatial and temporal variability of ground surface temperature and active layer thickness at the margin of maritime Antarctica, Signy Island. *Geomorphology* **155-156**: 20–33. DOI:10.1016/j.geomorph.2011.12.016.

Guglielmin M, Dalle Fratte M, Cannone N. 2014a. Permafrost warming and vegetation changes in continental Antarctica. *Environmental Research Letters* **9**: 1–14. DOI:10.1088/1748-9326/9/4/045001.

Guglielmin M, Worland MR, Baio F, Convey P. 2014b. Permafrost and snow monitoring at Rothera Point (Adelaide Island, Maritime Antarctica): Implications for rock weathering in cryotic conditions. *Geomorphology* **225**: 47–56. DOI:10.1016/j.geomorph.2014.03.051.

Heggem ESF, Etzelmüller B, Anarmaa S, Sharkhuu N, Goulden CE, Nandinsetseg B. 2006. Spatial Distribution of Ground Surface Temperatures and Active Layer Depths in the Hövsgöl Area, Northern Mongolia. *Permafrost and Periglacial Processes* **17**: 357–369. DOI:10.1002/ppp.568.

Hipp T, Etzelmüller B, Westermann S. 2014. Permafrost in Alpine Rock Faces from Jotunheimen and Hurrungane, Southern Norway. *Permafrost and Periglacial Processes* **25**: 1–13. DOI:10.1002/ppp.1799.

Hrbáček F, Láska K, Engel Z, 2015. Effect of Snow Cover on the Active-Layer Thermal Regime – A Case Study from James Ross Island, Antarctic Peninsula. *Permafrost and Periglacial Processes*, DOI:10.1002/ppp.1871.

Klene AE, Nelson FE, Shiklomanov NI, Hinkel KM. 2001. The N-Factor in Natural Landscapes: Variability of Air and Soil-Surface Temperatures, Kuparuk River Basin, Alaska, U.S.A. *Arctic, Antarctic, and Alpine Research* **33**: 140–148. DOI:10.2307/1552214.

Kurylyk BL. 2015. Discussion of 'A Simple Thaw-Freeze Algorithm for a Multi-Layered Soil using the Stefan Equation' by Xie and Gough (2013). *Permafrost and Periglacial Processes* **26**: 200–206. DOI: 10.1002/ppp.1834.

Matsuoka N. 2008. Frost weathering and rockwall erosion in the southeastern Swiss Alps: Long-term (1994−2006) observations. *Geomorphology* **99**: 353–368. DOI: 10.1016/j.geomorph.2007.11.013.

Michel RFM, Schaefer CEGR, Poelking EL, Simas FNB, Fernandes Filho EI, Bockheim JG. 2012. Active layer temperature in two Cryosols from King George Island, Maritime Antarctica. *Geomorphology* **155**−**156**: 12–19. DOI:10.1016/j.geomorph.2011.12.013.

Miller DL. 2004. Temperature monitoring/ground thermometry. In *Thermal Analysis, Construction, and Monitoring Methods for Frozen Ground*, Esch DC (ed). American Society of Civil Engineers: Reston, Virginia; 57–75.

Minasny B, Hartemink AE. 2011. Predicting soil properties in the tropics. *Earth-Science Reviews* **106**: 52–62. DOI:10.1016/j.earscirev.2011.01.005.

Morris EM, Vaughan DG. 2003. Spatial and temporal variation of surface temperature on the antarctic peninsula and the limit of viability of ice shelves. In *Antarctic Peninsula Climate Variability: Historical and Paleoenvironmental Perspectives*, Domack E, Levente A, Burnet A, Bindschadler R, Convey P, Kirby M (eds). American Geophysical Union: Washington, DC; 61–68. DOI: 10.1029/AR079p0061

Ramos M, Hasler A, Vieira G, Hauck C, Gruber S. 2009. Drilling and Installation of Boreholes for Permafrost Thermal Monitoring on Livingston Island in the Maritime Antarctic. *Permafrost and Periglacial Processes* **20**: 57–64. DOI:10.1002/ppp.635.

Romanovsky VE, Osterkamp TE. 1997. Thawing of the Active Layer on the Coastal Plain of the Alaskan Arctic. *Permafrost and Periglacial Processes* **8**: 1–22. DOI:10.1002/(SICI)1099-1530(199701)8:1<1::AID-PPP243>3.0.CO;2-U.

Schoeneich P. 2011. Ground surface temperature. *PermaNET – Guide lines for monitoring* Version 3 – 2.2.2011.

Shur Y, Hinkel KM, Nelson FE. 2005. The Transient Layer: Implications for Geocryology and Climate-Change Science. *Permafrost and Periglacial Processes* **16**: 5–17. DOI:10.1002/ppp.518.

Turner J, Colwell SR, Marshall GJ, Lachlan-Cope TA, Carleton AM, Jones PD, Lagun V, Reid PA, Iagovkina S. 2005. Antarctic climate change during the last 50 years. *International Journal of Climatology* **25**: 279–294. DOI:10.1002/joc.1130.

Vieira G, Bockheim J, Guglielmin M, Balks M, Abramov AA, Boelhouwers J, Cannone N, Ganzert L, Gilichinsky DA, Goryachkin S, López-Martínez J, Meiklejohn I, Raffi R, Ramos M, Schaefer C, Serrano E, Simas F, Sletten R, Wagner D. 2010. Thermal State of Permafrost and Active-Layer Monitoring in the Antarctic: Advances During the International Polar Year 2007–2009. *Permafrost and Periglacial Processes* **21**: 182–197. DOI:10.1002/ppp.685.

Wilhelm KR, Bockheim JG, Kung S. 2015. Active Layer Thickness Prediction on the Western Antarctic Peninsula. *Permafrost and Periglacial Processes* **26**: 188–199. DOI:10.1002/ppp.1845.

7.7 Paper VII

Hrbáček, F., **Uxa, T.** (2020). The evolution of a near-surface ground thermal regime and modeled active-layer thickness on James Ross Island, Eastern Antarctic Peninsula, in 2006–2016. *Permafrost and Periglacial Processes*, 31(1), 141–155. https://doi.org/10.1002/ppp.2018

Journal Citation Reports 2018: Impact factor 3.000, Q2(22/50) in Geography Physical, Q1(6/47) in Geology.

Citations as of 9 June 2020: Web of Science=1, Scopus=0, Google Scholar=2, ResearchGate=3.

Received: 6 March 2019 | Revised: 24 May 2019 | Accepted: 1 July 2019

DOI: 10.1002/ppp.2018

RESEARCH ARTICLE

WILEY

The evolution of a near-surface ground thermal regime and modeled active-layer thickness on James Ross Island, Eastern Antarctic Peninsula, in 2006–2016

Filip Hrbáček[1] | Tomáš Uxa[2,3]

[1] Department of Geography, Faculty of Science, Masaryk University, Brno, Czech Republic

[2] Department of Geothermics, Institute of Geophysics, Czech Academy of Sciences, Prague, Czech Republic

[3] Department of Physical Geography and Geoecology, Faculty of Science, Charles University, Prague, Czech Republic

Correspondence
Filip Hrbáček, Department of Geography, Faculty of Science, Masaryk University, Brno, Czech Republic.
Email: hrbacekfilip@gmail.com

Funding information
Ministry of Education, Youth and Sports of the Czech Republic, Grant/Award Numbers: LM2015078, LM2015079, Z.02.1.01/0.0/0.0/16_013/0001708

Abstract

Thermal regime and thickness of the active layer respond rapidly to climate variations, and thus they are important measures of cryosphere changes in polar environments. We monitored air temperature and ground temperature at a depth of 5 cm and modeled active-layer thickness using the Stefan and Kudryavtsev models at the Abernethy Flats site, James Ross Island, Eastern Antarctic Peninsula, in the period March 2006 to February 2016. The decadal average of air and ground temperature was −7.3 and −6.1°C, respectively, and the average modeled active-layer thickness reached 60 cm. Mean annual air temperature increased by 0.10°C y^{-1} over the study period, while mean annual ground temperature showed the opposite tendency of −0.05°C y^{-1}. The cooling took place mainly in summer and caused thawing season shortening and active-layer thinning of 1.6 cm y^{-1}. However, these trends need to be taken carefully because all were non-significant at $p < 0.05$. The Stefan and Kudryavtsev models reproduced the active-layer thickness with mean absolute errors of 2.6 cm (5.0%) and 3.4 cm (5.9%), respectively, which is better than in most previous studies, making them promising tools for active-layer modeling over Antarctica.

KEYWORDS

climate change, ground physical properties, ground temperature, modeling, permafrost, validation

1 | INTRODUCTION

The active layer is the top layer of the ground underlain by permafrost, which thaws in summer and freezes again in autumn. It reacts sensitively to the variability of climate parameters such as air temperature, global radiation or snow cover, and therefore it represents one of the key parameters of the cryosphere, which indicate climate change in polar regions (e.g. [1-3]). Unlike the Arctic, where permafrost areas occupy more than 25 million km^2, these environments are very rare in Antarctica as they cover only about 32 000 km^2, representing around 0.2% of the continent.[4,5] The active layer has been most intensively investigated in Victoria Land, where research started as early as the 1960s,[6] and recently in the Antarctic Peninsula (AP) region.[5,7] The AP is the warmest area in Antarctica and it has been considered to be among the most rapidly warming regions on Earth in the second half of the 20th century.[8] However, recent studies have shown that summer air temperature has been decreasing since around 2000,[9] which has impacted some cryospheric components including the thermal regime and thickness of the active layer.[10]

Nonetheless, temporal analyses of the active layer state in the AP region remain limited (e.g. [5,11,12]) as the majority of monitoring sites were established after the International Polar Year (IPY) 2007–2009.[13] Moreover, most observations are made through manual probing at the Circumpolar Active Layer Monitoring – South sites or in shallow boreholes (< 2 m) that frequently do not reach below the permafrost table[5,7,13] and, as such, they might be unrepresentative of the

Filip Hrbáček and Tomáš Uxa contributed equally to this paper.

full active-layer thickness (*ALT*). In the latter cases, the *ALT* has been mostly established as the depth of the 0°C isotherm by extrapolating the temperature gradient determined by continuous data-logger tracking of maximum annual ground temperatures (e.g. [11,14,15]) or by one-at-a-time probing using portable thermometers.[2,16] In particular, the former approach has been widely used across the AP region, with only slight modifications in the number and depth of temperature sensors and curve-fitting methods.[17-21] However, it may deviate substantially at places where the distance between the deepest temperature sensor and the permafrost table is large because the temperature gradient decreases non-linearly with depth, and thus it can be very small, (e.g. [18,20,21]) requiring highly accurate measurements.

Valuable insights into the dynamics of the thermal regime and thickness of the active layer can provide diverse thermal modeling techniques (e.g. [22,23]). Beside complex numerical models that account for many of the processes involved in surface and subsurface energy exchange and are capable of capturing the transient evolution of the active layer and permafrost conditions, (e.g. [24-26]) there also exist so-called equilibrium models which can define simple climate–permafrost relationships on an annual basis and evaluate such parameters as permafrost presence or absence, mean annual ground temperature or *ALT*.[22] Of these models, the Stefan[27] and Kudryavtsev[28] equations have been most widely used to calculate the *ALT*.[22] Simplicity and low requirements for input parameters have made these analytical solutions popular, particularly in modeling *ALT* over larger spatial scales or in situations where insufficient data were available to drive more sophisticated numerical models.[22,29] Despite their simplicity and several simplifying assumptions, which may be restricting in specific settings (e.g. [30,31]), these models have been extensively validated to provide thawing or freezing depth estimates with a reasonable degree of accuracy (e.g. [1,30,32-37]). Nonetheless, they have been used inexplicably rarely in Antarctica (e.g. [38,39]) compared to their long-term and widespread use in polar and alpine areas of the northern hemisphere.

In this study, we describe a 10-year period (March 2006 to February 2016) of air and ground surface temperature monitoring at the Abernethy Flats site, James Ross Island (JRI), Eastern AP, and we apply two equilibrium thermal models, the Stefan and Kudryavtsev equations, to assess the interannual variability of *ALT*. Our aims in bridging the gaps in active layer and permafrost research in Antarctica are twofold. First, we analyse the behavior of air and ground surface temperature and *ALT* over one decade (including the pre-IPY 2007–2009 period), which is unique within the region. Second, we use simple modeling tools to predict the *ALT*, which have been used only sporadically in this area before now. We further compare our results with observations from other parts of Antarctica and general climate patterns.

2 | REGIONAL SETTING

JRI is ~2,600 km^2 in area and is located on the northeastern coast of the AP (Figure 1). Glaciers cover about 75% of the island, but only a few occur in its northern part, the Ulu Peninsula, where the study area

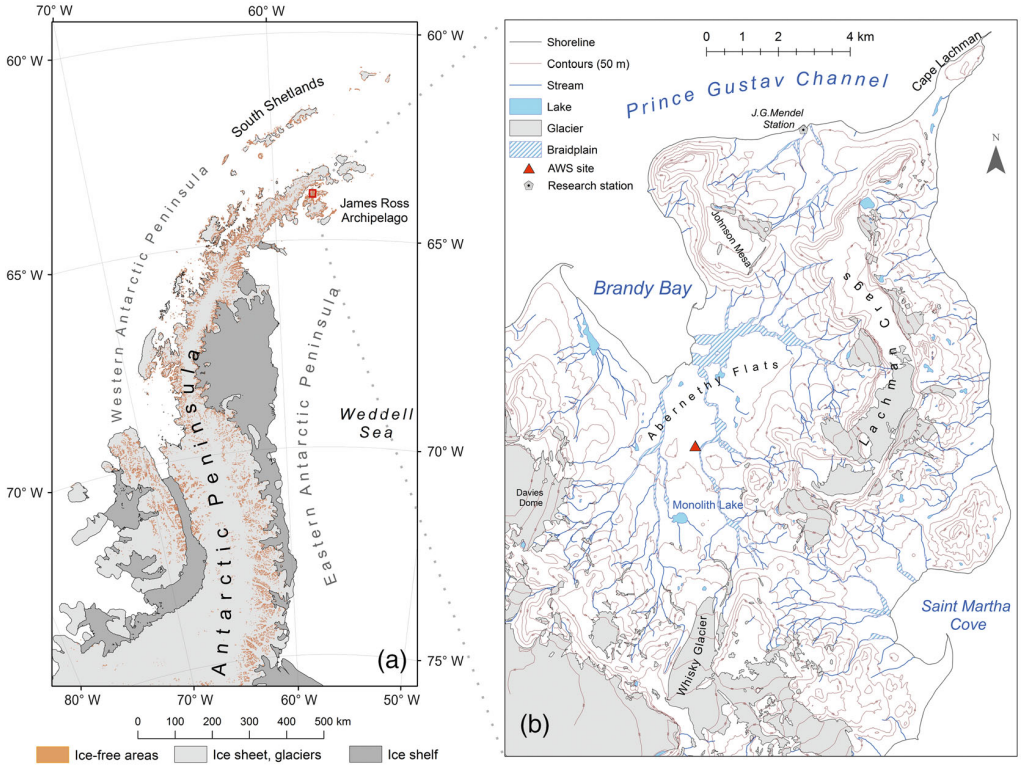

FIGURE 1 Regional setting (a) and location of the study site (b) [Colour figure can be viewed at wileyonlinelibrary.com]

is located.[40] Deglaciation of the Ulu Peninsula started 12.9 ± 1.2 ka[41] and resulted in exposure of more than 300 km^2 of land that represents one of the largest glacier-free areas within the AP region.[42] The geology of the Ulu Peninsula consists mostly of Neogene volcanic rocks, which built volcanic mesas, and Cretaceous sedimentary rocks in the lowlands, partially covered by Quaternary sediments.[43]

The climate of the Ulu Peninsula has a semi-arid polar-continental character,[44] with a mean annual air temperature (*MAAT*) around −7.0°C at sea level near the Johann Gregor Mendel Station[5] and estimated annual precipitation as low as 300–500 mm of water equivalent[45] because of a rain-shadow effect caused by the mountain ranges of the Northern AP.[44] Precipitation occurs largely as snow, but high wind speeds cause intense snow drifting and very irregular, topography-controlled snow deposition.[46,47]

The glacier-free surfaces are underlain by continuous permafrost,[7] the thickness of which reaches from around 3.4 m on coastal marine terraces to more than 67 m in lower-lying inland areas.[48,49] *ALT* depends strongly on local lithology, and usually ranges between approximately 50 and 145 cm.[5,42,49,50] Vegetation cover is sparse and is mostly concentrated in moist and nutrient-rich areas.[46]

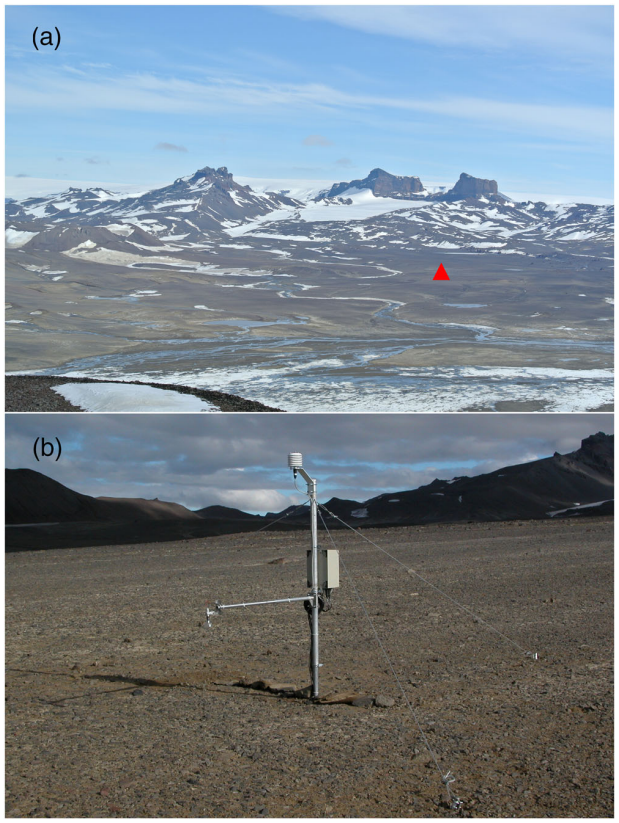

FIGURE 2 The Abernethy flats area (a) and a detailed photo of the study site (b). The red triangle indicates the position of the automatic weather station [Colour figure can be viewed at wileyonlinelibrary.com]

3 | METHODS

3.1 | Measurement setting and data processing

The study site is located in the Abernethy Flats area (63°52′53″S, 57°56′5″W; 41 m a.s.l.), which is a flat lowland of the Ulu Peninsula with a slope of up to 5° (Figures 1 and 2). It is built of fine-grained calcareous sandstones and siltstones of the Alpha Member, Santa Marta Formation,[43,51] partially covered by Holocene glacigenic sediments,[40,43] and it is completely vegetation-free (Figure 2).

Air temperature and ground temperature were monitored from March 2006 to February 2016. Air temperature was measured using an EMS33 sensor (EMS Brno) equipped with a Pt100/A resistance temperature detector (accuracy of ±0.15°C at 0°C) placed in a solar radiation shield 2 m above the ground surface. Ground temperature was measured with A-class Pt100/8 resistance temperature detectors (EMS Brno; accuracy of ±0.15°C at 0°C) placed directly into the ground at depths of 5, 10, 20, 30, 40 and 50 cm, and from February 2012 also at 75 cm. All the detectors were connected to an EdgeBox V12 data logger (EMS Brno) set to measure and record the temperature every 30 min.

Daily, monthly, seasonal and annual means of air temperature and ground temperature at a depth of 5 cm were calculated from the half-hour temperature data. A period from March 1 to February 28 or 29 of the following year was set to calculate the annual means in order to cover a 12-month period from the active-layer freezeback to the maximum thaw depth of the next year. Missing air and ground temperature data due to data logger malfunction in the period from September 17, 2011 to February 6, 2012 were complemented in a monthly or seasonal resolution using multiple regression based on data from two equally instrumented stations located at a distance of 5 and 7 km that have similar topography and bare surface, which ensured high accuracy of the regression models (R^2 > 0.9 in all cases). The temporal trends of selected characteristics were assessed using the non-parametric Mann–Kendall trend test[52,53] and Sen's slope estimator.[54] Relations between *ALT* (section 3.2) and selected air and ground temperature attributes were examined using the Pearson correlation coefficient. All statistics were tested at $p < 0.05$.

Thawing and freezing seasons were defined based on the continuous persistence of positive and negative mean daily temperatures, respectively, at a depth of 5 cm. For air temperature, the seasons were set to be equal to those at a depth of 5 cm. Subsequently, thawing and freezing degree-days for air (TDD_a and FDD_a) and ground at a depth of 5 cm (TDD_5 and FDD_5) were calculated as sums of all positive and negative mean daily temperatures (°C days) during the thawing and freezing seasons, respectively. The degree-days were further used to calculate the dimensionless thawing (n_t) and freezing (n_f) *n*-factors, which summarize the energy balance between air and ground surface at the end of the thawing and freezing seasons, respectively:[55]

$$n_t = \frac{TDD_5}{TDD_a} = \frac{\sum_{i=1}^{L_t} T_5(i)\ [\,T_5 > 0°C]}{\sum_{i=1}^{L_t} T_a(i)\ [\,T_a > 0°C]} \quad (1)$$

$$n_f = \frac{FDD_5}{FDD_a} = \frac{\sum_{i=1}^{L_f} T_5(i)\ [\,T_5 < 0°C]}{\sum_{i=1}^{L_f} T_a(i)\ [\,T_a < 0°C]} \quad (2)$$

where T_a and T_5 are the mean daily air temperature and ground temperature at a depth of 5 cm, respectively, during the thawing or freezing season, and L_t and L_f refer to the number of days in the thawing and freezing seasons, respectively.

Data from deeper parts of the profile were used only to determine the temperature-based *ALT* (hereafter referred to as observed *ALT*), which was used to validate the outputs of *ALT* modeling (section 3.2). It was defined as the maximum depth of the 0°C isotherm during the particular thawing season calculated by linear interpolation between the maximum temperature of the deepest sensor with at least one measurement >0°C and the maximum temperature of the shallowest sensor with all measurements ≤0°C. The observed *ALT* was available from a very cold season 2009/10 and from the period 2012/13 to 2015/16 when the measurement profile already reached a depth of 75 cm.

3.2 | Active-layer thickness modeling

The *ALT* over the period March 2006 to February 2016 was modeled via the Stefan[27] and Kudryavtsev[28] models. Both models were forced with ground temperature data from a depth of 5 cm and two sets of time-invariant ground physical properties based on ground samples from depths of 10 and 30 cm that were considered homogeneous across the entire ground profile for each model run. The outputs of the Stefan model are therefore hereafter called scenarios S_{10} and S_{30}, while the products of the Kudryavtsev model are termed scenarios K_{10} and K_{30}.

3.2.1 | Stefan model

The Stefan model[27] was applied on TDD_5 to predict the *ALT* (m) as follows:

$$ALT = z_5 + \lambda\sqrt{\frac{2k_t TDD_5 SF}{Q_L}} \quad (3)$$

where z_5 (m) is the depth of the ground temperature measurement, k_t is the thawed thermal conductivity (W m^{-1} K^{-1}), *SF* is the scaling factor of 86,400 seconds per day, and Q_L is the volumetric latent heat of fusion of water-ice (J m^{-3}) expressed as:

$$Q_L = L\rho\omega \quad (4)$$

where L is the specific latent heat of fusion of water-ice (334,000 J kg^{-1}), ρ is the dry bulk density (kg m^{-3}), and ω is the gravimetric water content (dimensionless). Because the Stefan model tends to overestimate the *ALT* due to errors arising from disregarding sensible heat or due to low ground temperatures at the onset of thawing,[30,56] we adopted a polynomial correction factor for ground thawing with sub-zero initial temperature (λ) in Equation (3) in order to improve its performance:[56]

$$\lambda = \left[1 + 0.147S_{te}\left(\kappa\frac{T_{init}}{MGTS_5}\right)^2 + 0.535\sqrt{S_{te}}\kappa\frac{T_{init}}{MGTS_5}\right] \times \left(1 - 0.16S_{te} + 0.038{S_{te}}^2\right) \quad (5)$$

with

$$S_{te} = \frac{C_t MGTS_5}{Q_L} \quad (6)$$

$$\kappa = \sqrt{\frac{k_f C_f}{k_t C_t}} \quad (7)$$

where S_{te} is the dimensionless Stefan number, which is proportional to the ratio of sensible heat to latent heat absorbed during thawing,[57,58] κ is a dimensionless parameter accounting for different thermal properties of the thawed and frozen zones within the ground profile,[56] T_{init} is the initial temperature corresponding to the mean ground temperature across the seasonally thawing layer at the onset of thawing (°C), $MGTS_5$ is the mean ground temperature of the thawing season at depth z_5 (°C), k_f is the frozen thermal conductivity (W m^{-1} K^{-1}), and C_f and C_t are the frozen and thawed volumetric heat capacity, respectively (J m^{-3} K^{-1}).

We calculated the sub-zero initial temperature by logarithmic fitting of the mean daily ground temperature profile one day before the start of thawing and then integrating this function across the depth range defined by z_5 and initial *ALT* estimate (ALT_{init}) based on the uncorrected Stefan model:

$$T_{init} = \frac{1}{ALT_{init} - z_5}\int_{z_5}^{ALT_{init}} a\ln z + b\,dz \quad (8)$$

where a and b are empirical constants. The initial temperature was determined for seasons 2012/13 to 2015/16, and the resulting average value of −3°C was subsequently used in the final *ALT* estimates in each thawing season.

3.2.2 | Kudryavtsev model

The Kudryavtsev model[28] was applied to ground temperature data at a depth of 5 cm to predict the *ALT* analogously to the Stefan model:

$$ALT = z_5 + \frac{2(A_5 - |T_{TOP}|)\sqrt{\frac{k_t C_t P_5}{\pi}} + \frac{(2A_{TOP}C_t Z_c + Q_L(ALT - z_5))Q_L\sqrt{\frac{k_t P_5}{\pi C_t}}}{2A_{TOP}C_t Z_c + Q_L(ALT - z_5) + \sqrt{\frac{k_t P_5}{\pi C_t}}(2A_{TOP}C_t + Q_L)}}{2A_{TOP}C_t + Q_L} \quad (9)$$

with

$$A_{TOP} = \frac{A_5 - |T_{TOP}| - \frac{Q_L}{2C_t}}{\ln\frac{A_5 + \frac{Q_L}{2C_t}}{|T_{TOP}| + \frac{Q_L}{2C_t}}} \quad (10)$$

$$Z_c = \frac{2(A_5 - |T_{TOP}|)\sqrt{\frac{k_t C_t P_5}{\pi}}}{2A_{TOP}C_t + Q_L} \quad (11)$$

Equation (9) can, however, be solved only numerically, and thus we used the modified Kudryavtsev model,[30] which is more convenient as it allows an analytical solution:

$$ALT = z_5 + ALT^* \sqrt{\frac{k_t P_5}{\pi C_t}} \tag{12}$$

with

$$ALT^* = B + \sqrt{B^2 + D} \tag{13}$$

$$B = \delta + \frac{\delta}{2\gamma} - \frac{\gamma}{2\delta} - \frac{\gamma}{2} \tag{14}$$

$$D = \delta + \delta\gamma + \gamma - \delta^2 - \frac{\delta^2}{\gamma} \tag{15}$$

$$\gamma = \alpha - \beta \tag{16}$$

$$\delta = \ln\frac{\alpha + 1}{\beta + 1} \tag{17}$$

$$\alpha = \frac{2C_t A_5}{Q_L} \tag{18}$$

$$\beta = \frac{2C_t |T_{TOP}|}{Q_L} \tag{19}$$

where P_5 is the period at depth z_5 calculated as the sum of the lengths of the thawing season for which the *ALT* is modeled and the preceding freezing season (s), A_5 is the physical amplitude (i.e. half range) of the annual ground temperature oscillations at depth z_5 (°C) and T_{TOP} is the mean annual ground temperature at the top of the permafrost (°C).

Previous studies have expressed the annual amplitude of ground temperature oscillations as half the annual range in the mean daily or mean monthly air or ground temperature (e.g. [33,37,59-62]) or as the difference between the maximum mean monthly ground surface temperature and the mean annual ground surface temperature.[30] However, daily or monthly temperatures might overestimate or underestimate, respectively, the annual ground temperature amplitude. Moreover, they might be unrepresentative of variously long thawing and freezing seasons whose summary length does not match the period of one year exactly. Accordingly, we calculated A_5 as the difference between the annual maximum of the 31-day moving average of ground temperature at depth z_5 and the mean annual ground temperature at depth z_5 ($MAGT_5$). We believe that this design is more representative of the *ALT* dynamics because it prefers the thawing season when calculating the amplitude and, as such, it emphasizes its utmost importance for active-layer formation. By contrast, it suppresses the freezing season, and thus it eliminates the potential attenuation of ground temperature amplitude caused by snow cover insulation.

The T_{TOP} for permafrost conditions ($T_{TOP} \leq 0$°C) was calculated using a semi-empirical equation after Garagulya:[63]

$$T_{TOP} = \frac{\frac{MAGT_5}{2}(k_f + k_t) + A_5\frac{k_t - k_f}{\pi}\left(\frac{MAGT_5}{A_5}\arcsin\frac{MAGT_5}{A_5} + \sqrt{1 - \frac{MAGT_5{}^2}{A_5{}^2}}\right)}{k_f} \tag{20}$$

If a sinusoidal temperature wave is assumed, Equation (20) produces identical results to the thermal offset equation,[64] which has been extensively employed in the T_{TOP} model.[65,66] However, for consistency of the calculations, we preferably use the former approach because it incorporates A_5 as an input parameter, like both forms of the Kudryavtsev model (Equations 9 and 12).

3.3 | Ground physical properties

Ground physical parameters (Table 1) are based on analyses of intact ground samples collected in duplicate from depths of 10 and 30 cm into 400-cm^3 plastic cylinders in February 2017 near the temperature measurement site. The ground samples were weighed twice before and after oven-drying for 24 h at 105°C. Afterwards, the dry bulk density was calculated as the ratio of the mass of dry ground to the total volume of the sample, the gravimetric water content was determined as the ratio of the mass of water to the mass of dry ground, and the volumetric water content (ϕ) was computed as the product of the above parameters (dimensionless). Ground texture characteristics were acquired by wet sieving of particles >63 μm and X-ray sedimentation of the finest fractions ≤63 μm (Sedigraph III Plus, Micrometrics).

In addition, seven replicate measurements on intact thawed samples were made with an ISOMET 104 device (Applied Precision Ltd) to determine the average thawed thermal conductivity and thawed volumetric heat capacity. The frozen thermal conductivity and frozen volumetric heat capacity were subsequently estimated based on the thermal properties of the thawed samples and their volumetric water contents, neglecting volume changes due to phase transitions. For the frozen thermal conductivity, we assumed a geometric mean

TABLE 1 Selected ground physical properties at the Abernethy flats site

Depth	ω (%)	ϕ (%)	ρ (kg m^{-3})	k_t (W m^{-1} K^{-1})	k_f (W m^{-1} K^{-1})	C_t (J m^{-3} K^{-1})	C_f (J m^{-3} K^{-1})	Sand (%)	Silt (%)	Clay (%)
10 cm	18.0	23.4	1,302	0.45	0.62	1.38	0.83	50	22	28
30 cm	18.2	26.5	1,457	0.61	0.87	1.68	1.06	53	20	27

ω (gravimetric water content); ϕ (volumetric water content); ρ (dry bulk density); k_t (thawed thermal conductivity); k_f (frozen thermal conductivity); C_t (thawed volumetric heat capacity); C_f (frozen volumetric heat capacity).

equation based on the thermal conductivity of the ground constituents and their volume fractions:[67]

$$k_f = k_t \left(\frac{k_i}{k_w}\right)^{\phi} \quad (21)$$

where k_i is the thermal conductivity of ice (2.22 W m^{-1} K^{-1}) and k_w is the thermal conductivity of water (0.57 W m^{-1} K^{-1}). Calculation of the frozen volumetric heat capacity builds on a weighted average of volumetric heat capacity of the ground constituents and their volume fractions:[66]

$$C_f = C_t - \phi(C_w - C_i) \quad (22)$$

where C_w is the volumetric heat capacity of water (4.21 MJ m^{-3} K^{-1}) and C_i is the volumetric heat capacity of ice (2.05 MJ m^{-3} K^{-1}).

4 | RESULTS

4.1 | Air and ground temperature regimes

MAAT at Abernethy Flats was −7.3°C in the period March 2006 to February 2016 and ranged from −5.1°C (2006/07) to −8.9°C (2009/10) (Figure 3). The warmest season was summer (DJF) with a mean seasonal air temperature (*MSAT*) average of 0.4°C, which varied between 2.0°C (2007/08) and −1.0°C (2009/10). The coldest season was winter (JJA) with *MSAT* average of −14.8°C. Winter *MSAT* varied between −9.9°C in 2010/11 and −18.3°C in 2009/10 (Table 2). The highest mean monthly air temperature was mostly recorded in January and averaged 1.2°C with a range between 2.7°C (2007 and 2009) and −0.6°C (2010). The coldest month was usually July with an average of −15.5°C and substantially higher temperature variability compared to the warmest month of between −9.8°C (2006) and −21.9°C (2007). The highest mean daily temperatures slightly exceeded 5°C and occasionally even 10°C during the summer months, while the minimum mean daily temperatures usually dropped below −25°C and rarely decreased even below −30°C (Figure 3). The *MAAT* tended to increase on average by +0.10°C y^{-1} over the entire period of March 2006 to February 2016. The major warming of +0.31°C y^{-1} was observed for the autumn months (MAM), while cooling of −0.16°C y^{-1} was found for the winter months (JJA). However, in all cases the trends were non-significant at $p < 0.05$.

MAGT$_5$ was −6.1°C in the period March 2006 to February 2016 and ranged from −3.3°C (2008/09) to −8.2°C (2007/08 and 2009/10) (Figure 3). Mean seasonal ground temperature at 5 cm (*MSGT*$_5$) in the summer months averaged 3.3°C and varied between 5.1°C (2007/08 and 2008/09) and 0.4°C (2009/10). The coldest season was winter when *MSGT*$_5$ decreased on average to −14.7°C, with a range between −9.6°C in 2008/09 and −18.9°C in 2007/08 (Table 2). The highest mean monthly ground temperature at a depth of 5 cm was mostly recorded in January and averaged 4.8°C, with variations between 7.1°C (2009) and 2.7°C (2010). The coldest months were July and

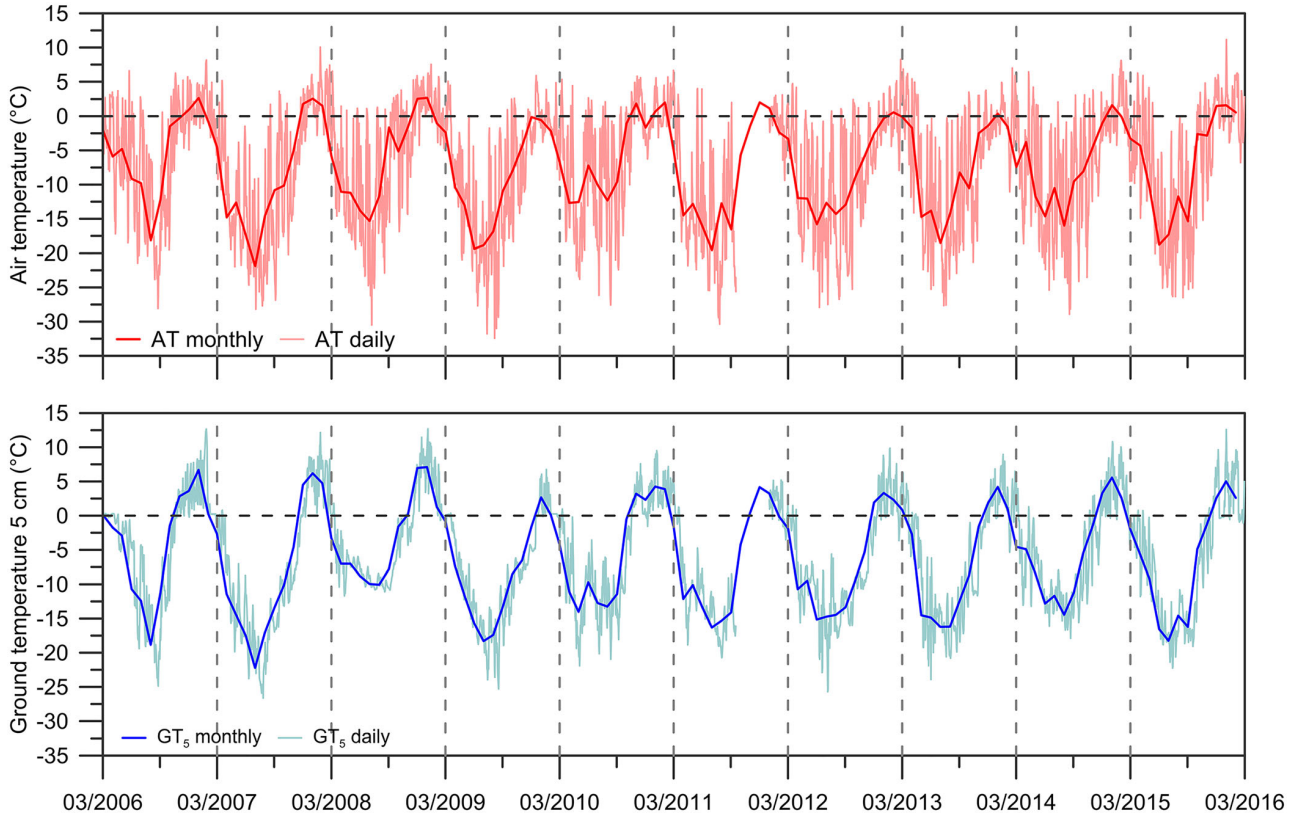

FIGURE 3 Daily and monthly air temperature (*AT*) and ground temperature at a depth of 5 cm (*GT*$_5$) [Colour figure can be viewed at wileyonlinelibrary.com]

TABLE 2 Annual and seasonal means of air temperature (*AT*) and ground temperature at a depth of 5 cm (GT_5) and the temperature trends for the period March 2006 to February 2016

	Annual		MAM		JJA		SON		DJF	
Period	*AT*	GT_5	*AT*	GT_5	*AT*	GT_5	*AT*	GT_5	*AT*	GT_5
2006/07	−5.1	−3.8	−4.2	−1.5	−12.4	−14.0	−4.6	−3.3	0.9	3.5
2007/08	−8.8	−8.2	−10.7	−9.5	−18.0	−18.9	−8.6	−9.4	2.0	5.1
2008/09	−6.1	−3.3	−9.4	−5.8	−13.6	−9.6	−2.8	−3.1	1.4	5.1
2009/10	−8.9	−8.2	−8.6	−6.6	−18.3	−17.1	−7.8	−9.4	−1.0	0.4
2010/11	−5.8	−5.3	−10.6	−9.7	−9.9	−11.9	−2.9	−2.9	0.3	3.5
2011/12	−8.6	−6.6	−10.8	−8.0	−16.1	−15.0	−7.7	−5.6	0.5	3.0
2012/13	−8.3	−7.3	−9.1	−7.4	−14.3	−14.8	−9.3	−9.4	−0.8	2.5
2013/14	−7.2	−6.6	−5.5	−5.4	−15.5	−15.8	−7.1	−7.6	−0.8	2.4
2014/15	−7.1	−5.3	−7.6	−6.0	−13.7	−13.0	−7.3	−6.0	0.2	3.8
2015/16	−6.9	−6.5	−6.0	−5.6	−15.9	−16.5	−6.9	−7.5	1.2	3.4
2006/16	**−7.3**	**−6.1**	**−8.3**	**−6.5**	**−14.8**	**−14.7**	**−6.5**	**−6.4**	**0.4**	**3.3**
Trend	0.10	−0.05	0.31	0.13	−0.16	−0.20	−0.08	−0.13	−0.09	−0.16

August, both having identical average of −15.2°C. The mean ground temperature of these two months varied considerably, between −10.0°C (2008) and −22.2°C (2007) (Figure 3). The highest mean daily ground temperatures at a depth of 5 cm usually reached around 10°C and occasionally even exceeded 15°C during summer months, while the minimum daily means usually dropped below −20°C and rarely even below −25°C (Figure 3). A negative trend of −0.05°C y^{-1} was detected on an annual basis. Seasonally, ground temperature increased by 0.13°C y^{-1} in autumn months (MAM), while a negative trend of −0.20°C y^{-1} was found for the winter months (JJA). However, all the trends were non-significant at $p < 0.05$.

Thawing seasons started between October 18 (2011/12) and December 20 (2010/11), while they ended between February 13 (2013/14) and March 19 (2011/12). These days also delimit the freezing seasons. The thawing seasons lasted for 153 days (2010/11) to 64 days (2009/10) with an average length of 105 days (Table 3). The thawing seasons shortened by an average of 1.5 days per year. Mean air temperature during the thawing season averaged 0.7°C, with the warmest thawing season in 2008/09 (2.0°C) and the coldest in 2013/14 (−0.8°C). The average TDD_a was 169°C days and varied between 242°C days (2015/16) and 37°C days (2009/10). Relatively high FDD_a values were observed during thawing seasons as well, averaging −92°C days, with a maximum of −41°C days (2008/09) and minimum of −162°C days (2013/14). Mean ground temperature during the thawing season at a depth of 5 cm was on average 3.4°C and varied between 5.3°C (2008/2009) and 1.7°C (2009/10). Similarly to seasonal ground temperature, TDD_5 reached a maximum of 520°C days in 2008/09 and minimum of 107°C days in 2009/10. The average TDD_5 was 368°C days. Summer FDD_5 was very low, with an average of −8°C days. The FDD_5 was zero in 2009/10, whereas it reached −32°C days in 2013/14. The average n_t was 2.35, with a maximum of 3.21 in 2013/14 and minimum of 1.59 in 2015/16 (Table 3).

TABLE 3 Characteristics of mean seasonal air temperature ($MATS_a$) and ground temperature at a depth of 5 cm ($MGTS_5$), thawing (*TDD*) and freezing (*FDD*) degree-days, thawing *n*-factor (n_t) and duration of thawing seasons in the period 2006/07–2015/16

Period	$MATS_a$ (°C)	$MGTS_5$ (°C)	TDD_a (°C days)	TDD_5 (°C days)	FDD_a (°C days)	FDD_5 (°C days)	n_t (–)	Duration (days)
2006/07	0.8	3.3	190	432	−84	−1	2.27	129
2007/08	1.6	4.4	236	475	−70	−1	2.01	107
2008/09	2.0	5.3	233	520	−41	−1	2.23	97
2009/10	−0.6	1.7	37	107	−77	0	2.89	64
2010/11	0.6	3.0	225	461	−131	−6	2.05	153
2011/12	–	*3.0**	–	*347**	–	–	–	–
2012/13	0.4	2.9	145	311	−106	−13	2.14	100
2013/14	−0.8	2.3	84	270	−162	−32	3.21	103
2014/15	0.6	4.2	132	370	−81	−2	2.80	88
2015/16	1.6	3.5	242	386	−74	−13	1.59	108
2006/16	0.7	3.4	169	370	−92	−8	2.35	105

*Value calculated by regression; it is not used to compute the period average.

Freezing seasons were substantially longer than thawing seasons, with an average length of 262 days and range between 302 days (2012/13) and 214 days (2006/07) (Table 4). Their duration was prolonged by an average of 3.8 days per year during the study period. Mean air temperature during freezing seasons dropped on average to −10.2°C. The warmest freezing season was in 2006/07 (−8.8°C), while the coldest was in 2007/08 (−12.5°C). Likewise, FDD_a also reached its maximum of −1,973°C days in 2006/07 and minimum of −3,448°C days in 2007/08. The average FDD_a was −2,757°C days. The positive air temperature events during winter (Figure 3) resulted in the occurrence of TDD_a in the freezing season, the average of which was 60°C days and it ranged from 87°C days in 2015/16 to 29°C days in 2007/08. Mean ground temperature during freezing seasons at a depth of 5 cm was −9.8°C and varied between −7.0°C in 2008/09 and −12.7°C in 2007/08. The average FDD_5 was −2,586°C days and reached a maximum of −1,745°C days in 2008/09 and minimum of −3,477°C days in 2007/08. Unlike TDD_a, TDD_5 was very limited during the freezing seasons. The average was as low as 3°C days, and the maximum reached 12°C days in 2014/15, while only 1°C day was detected in the freezing seasons 2008/09 and 2013/14. The average n_f was 0.93, with a maximum of 1.03 in 2010/11 and minimum of 0.71 in 2008/09 (Table 4).

4.2 | Active-layer thickness

The average *ALT* modeled for the S_{10} scenario was 58 cm and ranged from 33 cm (2009/10) to 70 cm (2008/09). Model outputs for scenario S_{30} exhibited 2–5 cm thicker *ALT* (Figure 4) with an average of 62 cm and range between 35 cm (2009/10) and 75 cm (2008/09). Both scenarios showed non-significant *ALT* thinning at a rate of 1.1 cm y^{-1}.

ALT modeled for scenario K_{10} achieved an average of 57 cm and ranged from 35 cm (2009/10) to 79 cm (2008/09). The Kudryavtsev model also tended to provide 2–6 cm thicker active layer for the K_{30} scenario compared to K_{10} (Figure 4). The average *ALT* modeled for the K_{30} scenario was 62 cm and it varied between 37 cm (2009/10) and 86 cm (2008/09). Likewise, scenarios K_{10} and K_{30} modeled non-significant *ALT* thinning at rates of 1.5 and 2.0 cm y^{-1}, respectively.

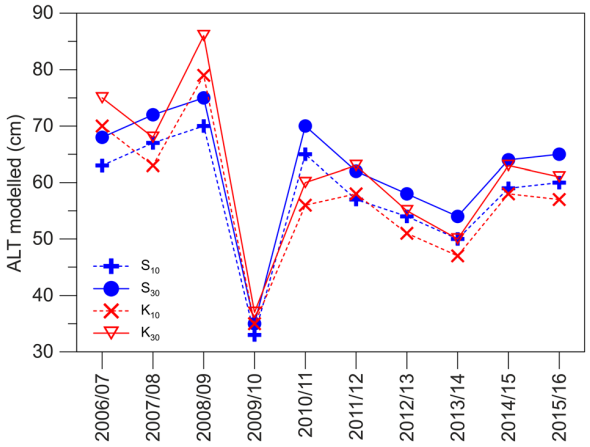

FIGURE 4 Interannual variability of the active-layer thickness (*ALT*) modeled by the Stefan (S_{10}, S_{30}) and Kudryavtsev (K_{10}, K_{30}) models [Colour figure can be viewed at wileyonlinelibrary.com]

The average *ALT* of all four scenarios reached 60 cm, ranging from 35 cm (2009/10) to 78 cm (2008/09). The average annual range of all four model scenarios was 9 cm. The annual range also positively correlated with the *ALT*, as the smallest model range of 4 cm was achieved when the mean modeled *ALT* reached its minimum, while the largest model range of 15 cm corresponded to its maximum (Figure 4). The thinning rate of the mean *ALT* was 1.6 cm y^{-1}, but it was also non-significant at $p < 0.05$.

The mean *ALT* modeled by the Stefan and Kudryavtsev models was controlled in particular by the summer ground temperature (r = 0.95 and 0.89, respectively), but it correlated highly significantly with the summer air temperature as well (r = 0.81 and 0.80, respectively; Figure 5). The influence of annual as well as winter air and ground temperatures was usually moderate (r = 0.43 to 0.61), with the only significant relationship (r = 0.75) found between the mean *ALT* modeled by the Kudryavtsev model and $MAGT_5$ (Figure 5).

TABLE 4 Characteristics of mean seasonal air temperature ($MAFS_a$) and ground temperature at a depth of 5 cm ($MGFS_5$), freezing (*FDD*) and thawing (*TDD*) degree-days, freezing *n*-factor (n_f) and duration of freezing seasons in the period 2006/07–2015/16

Period	$MAFS_a$ (°C)	$MGFS_5$ (°C)	FDD_a (°C days)	FDD_5 (°C days)	TDD_a (°C days)	TDD_5 (°C days)	n_f (–)	Duration (days)
2006/07	−8.8	−8.6	−1,973	−1,836	81	3	0.93	214
2007/08	−12.5	−12.7	−3,448	−3,477	29	2	1.01	273
2008/09	−9.6	−7.0	−2,449	−1,745	44	1	0.71	251
2009/10	−10.7	−10.4	−3,291	−3,116	75	2	0.95	300
2010/11	−9.5	−10.0	−2,307	−2,384	45	2	1.03	238
2011/12	–	*−12.7**	–	*−3,126**	–	–	–	–
2012/13	−10.3	−9.7	−3,146	−2,925	49	3	0.93	302
2013/14	−10.7	−10.9	−2,712	−2,706	72	1	0.99	247
2014/15	−10.0	−8.9	−2,691	−2,332	54	12	0.87	263
2015/16	−10.0	−10.2	−2,799	−2,757	87	5	0.98	271
2006/16	−10.2	−9.8	−2,757	−2,586	60	3	0.93	262

*Value calculated by regression; it is not used to compute the period average.

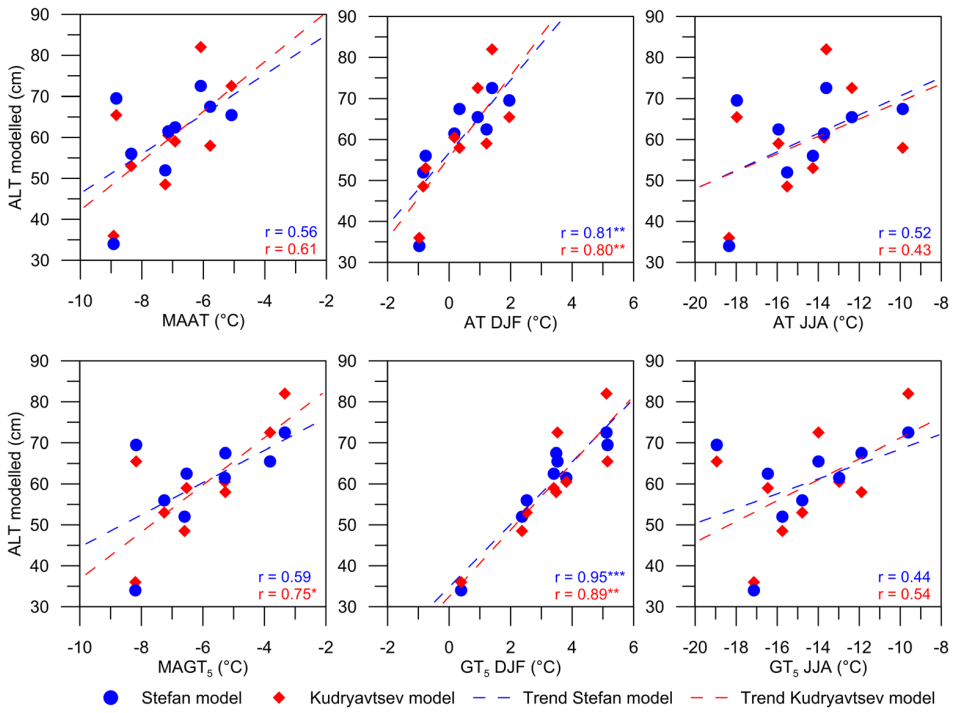

FIGURE 5 Correlations between mean active-layer thickness (*ALT*) modeled by the Stefan and Kudryavtsev models and mean annual air temperature (*MAAT*), mean annual ground temperature at a depth of 5 cm ($MAGT_5$), and mean seasonal air temperature (*AT*) and ground temperature at a depth of 5 cm (GT_5) in summer (DJF) and winter (JJA). Statistical significance is expressed as ***$p < 0.001$, **$p < 0.01$, *$p < 0.05$ [Colour figure can be viewed at wileyonlinelibrary.com]

The differences between the modeled and observed *ALT* reached on average −4.2 cm (−7.9%) and −5.8 cm (−10.3%) for scenarios S_{10} and K_{10}, respectively (Figure 6), with deviations from −1 to −8 cm (−1.1 to −15.4%) and −2 to −11 cm (−3.3 to −16.2%), respectively. Because both scenarios underestimated the *ALT* in all cases, the corresponding mean absolute errors were 4.2 cm (7.9%) and 5.8 cm (10.3%), respectively.

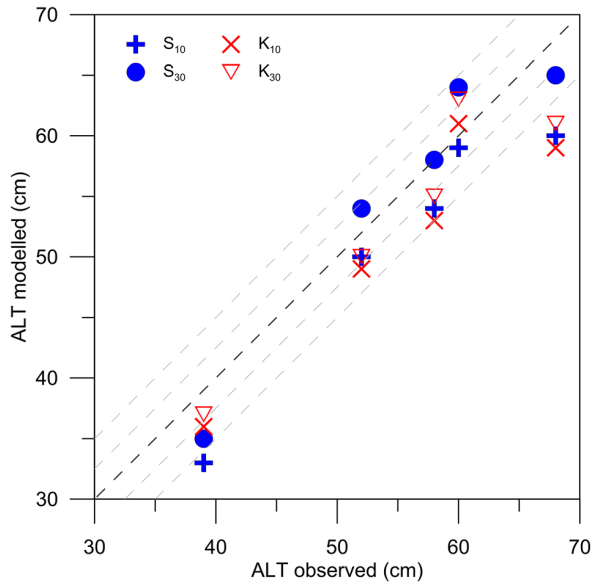

FIGURE 6 Validation of modeled active-layer thickness (*ALT*) by the Stefan (S_{10}, S_{30}) and Kudryavtsev (K_{10}, K_{30}) models with observed *ALT*. A dark dashed line indicates a 1:1 relationship between the observed and modeled *ALT*, and grey dashed lines indicate the error bands of 2.5 and 5.0 cm [Colour figure can be viewed at wileyonlinelibrary.com]

More accurate *ALT* was modeled for scenarios S_{30} and K_{30}, which deviated on average by −0.2 cm (−0.8%) and −2.2 cm (−3.9%), with variations from −4 to 4 cm (−10.3 to 6.7%) and from −7 to 3 cm (−10.3 to 5.0%), respectively (Figure 6). Because the scenarios both underestimated and overestimated the *ALT*, the corresponding mean absolute errors were 2.6 cm (5.0%) and 3.4 cm (5.9%) for S_{30} and K_{30}, respectively.

5 | DISCUSSION

5.1 | Climate and active-layer thickness

The climate on the Eastern AP, where JRI is located, has a prevailing continental character but also some patterns of an oceanic climate (e.g. [44,68]). In contrast to the Western AP where an oceanic climate is dominant, the *MAAT* at the same latitudes of the Eastern AP is about 4 to 6°C lower[69] and the annual amplitude of air temperature is almost two times larger.[70] Yet, the area of JRI is among the warmest parts of Antarctica as *MAAT* in the coastal areas of Eastern Antarctica is typically between −10 and −15°C and decreases to about −15 to −20°C in the southernmost coastal areas in the region of the McMurdo Dry Valleys.[71]

Active-layer formation is mainly controlled by summer temperatures (Figure 5), as has also been reported from numerous sites in polar and subpolar as well as mountain regions (e.g. [72-75]). The mean

DJF air temperature on JRI reached 0.4°C in the period March 2006 to February 2016, which was 0.2–0.8°C lower than at sites along the Western AP in the same period.[10] The mean DJF ground temperature on JRI differed from those on some sites on the South Shetlands, usually by −1 to +1°C.[11,76] Higher ground temperature differences in contrast to that of air temperature might be attributed to the specific conditions of each study site, such as snow cover presence, vegetation coverage, moisture content, topography or lithological properties.[77]

Despite lower summer air temperature and more variable summer ground temperature differences, the near-surface thawing degree-days were usually higher on the Abernethy Flats than on the South Shetlands (e.g. [11,20,70]). This can be explained by the almost two times higher mean daily global radiation during the summer months on JRI (~240 W m^{-2})[78] than on the South Shetlands (~130 W m^{-2})[79] associated with a prevailing oceanic climate causing higher cloudiness on the Shetlands. The eminent role of global radiation on ground temperature can be mainly exemplified on Victoria Land where its mean summer value can exceed 240 W m^{-2} and cause over 700°C days, despite mean summer air temperature being around −2°C.[80]

A significant air temperature decrease started around 2000 along most of the Western AP. The cooling triggered by natural variability of cyclonic activity and increasing sea-ice concentrations near coastlines caused *MAAT* trends of −0.16 to 0.05°C y^{-1} in the period 2006–2015.[9,10] In contrast, the *MAAT* on JRI was increasing at a non-significant rate of 0.10°C y^{-1}, which corresponds to observations from other sites of the north-eastern AP where positive, but non-significant, trends between 0.02 and 0.08°C y^{-1} have been reported.[10] Unlike *MAAT*, there was a non-significant negative trend of −0.05°C y^{-1} for $MAGT_5$. Interestingly, the *MSAT* and $MSGT_5$ trends were positive only in autumn (MAM), at 0.30 and 0.13°C y^{-1}, respectively, while they were negative in the other three seasons. Yet, the north-eastern AP region exhibited a *MAAT* more than 1°C lower in the period 2006–2015 compared to 1996–2005, and autumn (MAM) air temperature was even about 1.5°C lower.[10]

Among JRI sites of similar altitude, the average modeled *ALT* on Abernethy Flats of 60 cm was comparable to that at the site near the Johann Gregor Mendel station, where about 20% higher TDD_5 was observed, but *ALT* was reduced by lower thermal conductivity of around 0.30 W m^{-1} K^{-1} (see [42,50]), while about 20–30 cm higher *ALT* was reported at two other sites, mostly because of their higher thermal conductivity >0.7 W m^{-1} K^{-1} and slightly higher TDD_5.[42,50]

Despite similar summer ground surface temperatures, the *ALT* on Abernethy Flats was lower than in the Western AP, where it usually exceeds 80 cm (e.g. [5,7,13]) and sub-Antarctica with *ALT* > 100 cm.[19] In these areas, permafrost is much warmer as the temperature at the top of the permafrost table is about 4–5°C higher than on JRI.[70] Therefore, thaw propagation during summer can be more rapid because less heat is needed for active-layer thawing. Moreover, thawing can be accelerated by higher input of liquid precipitation, which frequently occurs in the Western AP in the summer months. Slightly higher *ALT* values (~65 to 100 cm) were also observed in the coastal parts of Enderby Land and Princess Elizabeth Land in eastern Antarctica. *MAAT* in these regions is about 3°C lower than on JRI, but summer air temperature is only about 1.0°C lower.[81,82] The difference might therefore be caused by contrasting ground physical properties as well as the slightly higher temperature amplitude of these areas. Lower *ALT* (< 50 cm) values were typical for cold areas with *MAAT* < −15°C such as northern Victoria Land,[2,5,16,75] McMurdo Dry Valleys,[5,83] and the mountainous areas in Dronning Maud Land[5,84] or the Ellsworth Mountains.[85] Mean monthly air temperatures during the summer only rarely exceeded −2°C in these areas, which probably enhanced the role of solar radiation in active-layer formation.[75,80]

Although the *MAAT* trend on JRI was positive, $MAGT_5$ decreased slightly, and the mean modeled *ALT* thinned by 1.6 cm y^{-1} during the study period. The thinning can be mainly related to the decreasing DJF temperatures (Figure 5) and shortening of the thawing seasons, which occurred across the whole AP region[10] and caused similar active-layer thinning of 1.5 cm y^{-1} on Deception Island during the period 2006–2014[12] as well as a thaw depth reduction of 1.6 cm y^{-1} on the South Shetlands in the period 2009–2016.[86] The long-term *ALT* observations from other regions of Antarctica are sparse, but show that *ALT* remained stable in the McMurdo Dry Valley region,[5,83] while even slight thickening of 0.3 cm y^{-1} was reported from northern Victoria Land in the period 1997–2012.[16] Generally, the summer season is the most important part of the year for active-layer development, while the effect of annual temperature is of lesser significance. Besides temperature, incoming solar radiation might become an important factor governing active-layer thawing in regions where no trend of summer air temperature was detected.[16,75]

5.2 | Model suitability

The Stefan and Kudryavtsev models have been widely used in different parts of the northern hemisphere for local *ALT* prediction based on *in situ* ground surface or subsurface measurements (e.g. [30,32,60,61]) as well as for regional or global *ALT* modeling (e.g. [1,33,34,59,62,87-89]), but until now they have been applied only twice in Antarctica.[38,39] The *ALT* values modeled in these two cases are, however, thought to be overestimated by up to hundreds of percent.[90] The present study is therefore the first one which provides validated *ALT* estimates based on the Stefan and Kudryavtsev models in Antarctica because their outputs based on ground physical parameters at a depth of 30 cm differ from the observed *ALT* on average by 2.6 and 3.4 cm or 5.0 and 5.9%, respectively (Table 5). Such accuracy is substantially better than in most previous studies, which showed average mean absolute errors of 3.6–58.8 cm and 2.8–65.7 cm for the Stefan and Kudryavtsev models, respectively, while their average mean absolute percentage errors were 6.0–26.1% and 5.8–24.7%, respectively (Table 5). Only two of these investigations reached an average mean absolute percentage error less than 10% for both the Stefan[60,86] and the Kudryavtsev models.[30,88] Romanovsky and Osterkamp[30] even achieved slightly better relative accuracy than this study, 5.8%, but on the other hand, they reached it by adapting the initially measured ground thermal properties through numerical modeling. The majority of studies have, however, reported average mean percentage errors

TABLE 5 Overview of the accuracy of the Stefan and Kudryavtsev models for selected studies from across the Earth

Model	Solution	*ALT* observed (cm)	*ALT* modeled (cm)	Mean error (cm)	Mean absolute error (cm)	Mean percentage error (%)	Mean absolute percentage error (%)	Source
Stefan	Classic	50.2 (35.5 to 62.0)	62.3 (44.5 to 79.3)	12.2 (9.0 to 17.3)	12.3 (9.3 to 17.3)	25.7 (20.4 to 28.6)	26.1 (20.4 to 29.6)	Romanovsky and Osterkamp (1997)
		46.8 (40.2 to 60.3)	49.9 (37.9 to 66.7)	3.1 (−8.7 to 12.8)	6.7 (3.6 to 12.8)	7.3 (−16.1 to 31.8)	14.9 (8.5 to 31.8)	Klene et al. (2001)
		328.8 (100.0 to 480.0)	295.0 (130.0 to 410.0)	−33.8 (−100.0 to 70.0)	58.8 (20.0 to 100.0)	−1.5 (−25.0 to 50.0)	21.5 (6.3 to 50.0)	Heggem et al. (2006)
		284.3 (150.0 to 480.0)	281.4 (160.0 to 460.0)	−2.9 (−90.0 to 60.0)	37.1 (0.0 to 90.0)	2.9 (−25.0 to 33.3)	13.8 (0 to 33.3)	Zorigt et al. (2016)
	Semi-empirical	39.7 (37.3 to 44.8)	40.9 (37.7 to 42.8)	1.2 (−2.0 to 4.8)	3.6 (2.0 to 4.8)	4.3 (−4.9 to 13.6)	9.8 (5.1 to 13.6)	Nelson et al. (1997)
		43.3 (29.0 to 56.0)	44.1 (35.0 to 59.0)	0.8 (−10.0 to 14.0)	4.4 (0.0 to 14.0)	2.1 (−18.5 to 46.7)	10.4 (0.0 to 46.7)	Shiklomanov and Nelson (2002)
	Corrected	217.4 (170.0 to 261.2)	218.2 (176.8 to 277.5)	0.8 (−10.5 to 16.3)	13.6 (6.8 to 22.3)	0.4 (−5.0 to 6.4)	6.0 (4.0 to 8.7)	Yin et al. (2016)
		55.4	51.2/55.2[a]	−4.2/ −0.2[a]	4.2/2.6[a]	−7.9/ −0.8[a]	7.9/5.0[a]	This study
Kudryavtsev		172.5 (29.3 to 298.9)	173.3 (39.2 to 272.5)	0.7 (−44.1 to 52.5)	—	6.6 (−15.8 to 43.1)	—	Anisimov et al. (1997)
		50.2 (35.5 to 62.0)	51.9 (33.5 to 68.0) /51.6 (36.3 to 63.0)[a]	1.7 (−2.0 to 6.0) /1.4 (0.8 to 2.5)[a]	5.4 (3.5 to 7.7) /2.8 (2.2 to 3.7)[a]	2.0 (−4.8 to 9.4) /2.8 (1.3 to 5.1)[a]	11.5 (6.8 to 15.4) /5.8 (5.1 to 6.4)[a]	Romanovsky and Osterkamp (1997)
		49.6 (43.0 to 55.0)	49.4 (41.0 to 58.0)	−0.2 (−8.0 to 6.0)	4.6 (2.0 to 8.0)	−0.4 (−16.3 to 14.0)	9.6 (3.6 to 16.3)	Shiklomanov and Nelson (1999)
		51.6 (33.0 to 65.0)	49.0 (26.0 to 67.0)	−2.6 (−16.0 to 15.0)	—	−4.8 (−27.1 to 34.1)	—	Sazonova and Romanovsky (2003)
		237.1 (159.9 to 379.7)	228 (181.7 to 269.4)	−9.0 (−110.3 to 80.3)	38.4 (5.7 to 110.3)	−0.3 (−29.0 to 47.1)	16.0 (2.7 to 47.1)	Pang et al. (2012)
		43.8 (37.0 to 56.0)	44.3 (31.0 to 59.0)	0.5 (−10.0 to 3.0)	—	1.0 (−24.4 to 8.1)	—	Streletskiy et al. (2012)
		217.4 (170.0 to 261.2)	236.5 (216.7 to 254.0)	19.1 (−7.3 to 46.7)	22.7 (7.3 to 46.7)	10.5 (−2.7 to 27.5)	11.9 (2.7 to 27.5)	Yin et al. (2016)
		284.3 (150.0 to 480.0)	275.7 (160.0 to 390.0)	−8.6 (−170.0 to 90.0)	65.7 (10.0 to 170.0)	4.6 (−51.5 to 40.9)	24.7 (2.8 to 51.5)	Zorigt et al. (2016)
		55.4	49.6/53.2[a]	−5.8/ −2.2[a]	5.8/3.4[a]	−10.3/ −3.9[a]	10.3/5.9[a]	This study

[a]Based on two sets of ground thermal properties.

mostly well below ±10% (Table 5). This probably relates to the fact that equilibrium models assume stationary conditions,[22] and thus they well represent multi-year or multi-site averages that moderate the energy imbalances introduced by short-term and/or long-term climate variations, while they tend to fail to capture interannual transient departures from the equilibrium state.[91] Yet, this and other studies[30,60] have shown that equilibrium models can perform reasonably well even on an annual basis regardless of their limitations.

Theoretical studies have shown that the Stefan model tends to overestimate *ALT* by up to tens of percent.[30,56,92] This drawback is nicely illustrated by the *ALT* modeled through the basic form of the solution, which deviated on average by 13.8–26.1% from the observed *ALT* and exhibited the highest mean absolute percentage errors of up to 50% as well (Table 5). Somewhat better accuracy, with average mean absolute percentage errors of 9.8–10.4%, but at the same time with maximum deviations of up to 46.7%, was achieved if the ground physical parameters were substituted by the single empirically estimated edaphic parameter (Table 5). The latter approach simply overcomes the main model shortcomings and even coarse temperature data alone are needed to force the model successfully,[87,89] but despite the range of the edaphic parameter is relatively low,[93] it has limited transferability because it is valid only where observed *ALT* is available for model calibration.[94] The most accurate *ALT* estimates utilizing the Stefan model have been achieved by this study and by Yin et al[60] which both employed correction factors accommodating sensible heat and ground temperature prior to thawing,[56] resulting in average mean absolute percentage errors as low as 5.0–6.0%. Likewise, the annual ground surface temperature amplitude calculated from the difference between the maximum of the 31-day moving average ground temperature at a depth of 5 cm and $MAGT_5$ and usage of the actual length of the freezing and thawing seasons instead of the standard annual period of 365 days probably better represent the ground surface temperature behavior, which is reflected in the lower bias of the Kudryavtsev model than in most previous studies (Table 5). However, note that these comparisons need to be taken with caution because the validation data as well as the length of the validation periods in Table 5 differ, which prevents precise assessment of the modeling accuracy.

Both models also benefited greatly from adding the depth of the driving ground temperature measurements to their outputs,[95] which reduced the mean absolute percentage error of the Stefan and Kudryavtsev models by 5.1 and 7.3%, respectively. However, it has not yet been used in other investigations utilizing the ground temperature to run the models for ground thawing.[30,32,34,60] Undoubtedly, driving temperature data measured directly in the ground might also significantly contribute to the high accuracy of the models compared to the case of air temperature forcing; the earlier studies are, however, inconclusive in this regard for both the Stefan and the Kudryavtsev models. Nonetheless, the model adjustments proved to be highly useful, but at the same time, they require more input data. Furthermore, it is unclear to what extent the high accuracy of the models is due to their modifications alone and what is the role of ground surface and subsurface characteristics.

Because ground physical parameters enter the models as constants, the accuracy of the models depends on how the parameters are representative of the entire profile, which inherently relates to their temporal variability. Besides meteorological conditions, the main drivers of their changes are such factors as vegetation, snow cover or ground texture, which significantly alter air–ground fluxes and hence the moisture content or thermal properties of the ground.[22] However, the study site is vegetation-free and winter snow cover, which comprises most of the total precipitation, is believed to be low and rather episodic[96] as the freezing *n*-factor mostly ranged between 0.93 and 1.03 (Table 4).[42,50] Likewise, ground texture and moisture are homogeneous at least in the upper half of the active layer (Table 1).[42] In contrast, bulk density tends to increase with depth, being about 12% higher at 30 cm than at 10 cm, which also led to about 22–40% higher values of ground thermal conductivity and volumetric heat capacity at this depth (Table 1), probably due to enhanced particle contact caused by a reduction in porosity.[67,97] The *ALT* modeled based on ground physical properties at a depth of 30 cm was more accurate, on average by about 2.9 and 4.4% for the Stefan and Kudryavtsev models, respectively, than those based on the characteristics at 10 cm. Ground physical parameters at a depth of 30 cm are therefore more representative of the entire profile, probably because they are closer to half the depth between the ground surface and the base of the active layer and, as such, they are close to their optimal values. Naturally, this applies for uniform profiles such as in this study, but would be invalid for multilayer systems, especially those consisting of materials in high contrast to soil such as a surface layer of peat or shallow bedrock.

The higher accuracy of the Stefan and Kudryavtsev models on JRI than in most other regions might therefore be attributed both to the application of recent model enhancements[56] and other modifications improving their performance as well as to comparably lower temporal variability of ground surface and subsurface parameters and to their relatively homogeneous distribution across the profile. High model accuracy can also be assumed especially in other cold and dry regions of Antarctica where ground physical properties, particularly water content, remain stable over the years. They might therefore help to better understand the spatial variability of *ALT* as well as its sensitivity to climate changes there. Further testing of the models is, however, highly desirable in more temperate and humid regions of maritime Antarctica.

6 | CONCLUSIONS

Study of the active-layer thermal regime and thickness on Abernethy Flats, James Ross Island, Eastern Antarctic Peninsula, in the period March 2006 to February 2016 led to the following main conclusions:

1. Decadal *MAAT* and $MAGT_5$ values were −7.3 and −6.1°C, respectively, and the average modeled *ALT* reached 60 cm.
2. The *MAAT* increased on average by 0.10°C y^{-1}, but a negative trend of −0.05°C y^{-1} was detected for $MAGT_5$. The modeled *ALT* thinned on average by 1.6 cm y^{-1}, which mainly related to a decrease in summer temperatures and to shortening of the thawing seasons. However, all the trends were statistically non-significant at $p < 0.05$.

3. The modeled *ALT* strongly and significantly correlated with summer air and ground temperature. It also showed moderate, but mostly non-significant, positive correlations with annual as well as winter air and ground temperatures.
4. The modeled *ALT* based on ground physical parameters at a depth of 30 cm showed a mean absolute error of 2.6 cm (5.0%) and 3.4 cm (5.9%) for the Stefan and Kudryavtsev models, respectively. This is therefore the first validated outcome of these analytical models in Antarctica. Their accuracy was, moreover, better than in most previous studies from the northern hemisphere, which is probably linked to the model modifications, rather low temporal variations of ground surface and subsurface characteristics, and homogeneous distribution of ground physical parameters within the active layer.

Our 10-year series is one of the longest datasets of simultaneous air temperature, ground temperature and *ALT* observations ever published in the Antarctic Peninsula region as well as throughout the Antarctica and it documents the short- to medium-term climate variations in the area. However, any trends should be taken carefully because the time series remains too short to capture a reliable climate signal.

The Stefan and Kudryavtsev models have been demonstrated to be simple tools that require a small amount of input data, while maintaining high accuracy of *ALT* estimates. They have considerable potential for reliable reconstructions of *ALT* at a local scale as well as its spatial modeling over Antarctica.

ACKNOWLEDGEMENTS

This research was supported by the Ministry of Education, Youth and Sports of the Czech Republic projects LM2015078, LM2015079 and Z.02.1.01/0.0/0.0/16_013/0001708. The authors thank Kamil Láska for maintenance of the meteorological station and providing meteorological data, Carsten W. Mueller for ground texture analysis, and Barret L. Kurylyk for discussing the calculation of the Stefan correction factors.

ORCID

Filip Hrbáček https://orcid.org/0000-0001-5032-9216
Tomáš Uxa https://orcid.org/0000-0001-9911-6529

REFERENCES

1. Anisimov OA, Shiklomanov N, Nelson FE. Global warming and active-layer thickness: results from transient general circulation models. *Global Planet Change*. 1997;15(3-4):61-77.
2. Guglielmin M. Ground surface temperature (GST), active layer, and permafrost monitoring in continental Antarctica. *Permafr Periglac Process*. 2006;17:133-143.
3. Romanovsky VE, Smith SL, Christiansen HH. Permafrost thermal state in the polar northern hemisphere during the international polar year 2007–2009: a synthesis. *Permafr Periglac Process*. 2010;21(2):106-116.
4. Burton-Johnson A, Black M, Fretwell PT, Kaluza-Gilbert J. An automated methodology for differentiating rock from snow, clouds and sea in Antarctica from Landsat 8 imagery: a new rock outcrop map and area estimation for the entire Antarctic continent. *Cryosphere*. 2010;10:1665-1677.
5. Hrbáček F, Vieira G, Oliva M, et al. Active layer monitoring in Antarctica: an overview of results from 2006 to 2015. *Polar Geogr*. 2019;n/a. https://doi.org/10.1080/1088937X.2017.14201056
6. Campbell IB, Claridge GGC. Permafrost properties, patterns and processes in the Transantarctic Mountains region. *Permafr Periglac Process*. 2006;17(3):215-2327.
7. Bockheim J, Vieira G, Ramos M, et al. Climate warming and permafrost dynamics in the Antarctic peninsula region. *Global Planet Change*. 2013;100:215-223.
8. Turner J, Colwell SR, Marshall GJ, et al. Antarctic climate change during last 50 years. *Int J Climatol*. 2005;25(3):279-294.
9. Turner J, Lu H, White I, et al. Absence of 21st century warming on Antarctic peninsula consistent with natural variability. *Nature*. 2016;535(7612):411-415.
10. Oliva M, Navarro F, Hrbáček F, et al. Recent regional climate cooling on the Antarctic peninsula and associated impacts on the cryosphere. *Sci Total Environ*. 2017;580:210-223.
11. Almeida ICC, Schaefer CEGR, Michel RFM, et al. Long term active layer monitoring at a warm-based glacier front from maritime Antarctica. *Catena*. 2016;149(2):572-581.
12. Ramos M, Vieira G, de Pablo MA, Molina A, Abramov A, Goyanes G. Recent shallowing of the thaw depth at Crater Lake, Deception Island, Antarctica (2006–2014). *Catena*. 2017;149(2):519-528.
13. Vieira G, Bockheim J, Guglielmin M, et al. Thermal state of permafrost and active-layer monitoring in the Antarctic: advances during the international polar year 2007–2008. *Permafr Periglac Process*. 2010;21(2):182-197.
14. Cannone N, Ellis Evans JC, Strachan R, Guglielmin M. Interactions between climate, vegetation and the active layer in soils at two maritime Antarctic sites. *Antarct Sci*. 2006;18(3):323-333.
15. Michel RFM, Schaefer CEGR, Poelking EL, Simas, Filho, Bockheim JG. Active layer temperature in two Cryosols from King George Island, Maritime Antarctica. *Geomorphology*. 2012;155–156:12-19.
16. Guglielmin M, Dalle Fratte M, Cannone N. Permafrost warming and vegetation changes in continental Antarctica. *Environ Res Lett*. 2014;9. https://doi.org/10.1088/1748-9326/9/4/045001
17. Guglielmin M, Evans CJE, Cannone N. Active layer thermal regime under different vegetation conditions in permafrost areas. A case study at Signy Island (maritime Antarctica). *Geoderma*. 2008;144(1-2):73-85.
18. Ramos M, Vieira G. Evaluation of the ground surface enthalpy balance from bedrock temperatures (Livingston Island, maritime Antarctic). *The Cryosphere*. 2009;3(1):133-145.
19. Guglielmin M, Worland MR, Cannone N. Spatial and temporal variability of ground surface temperature and active layer thickness at the margin of maritime Antarctica, Signy Island. *Geomorphology*. 2012;155:20-33.
20. De Pablo MA, Ramos M, Molina A. Thermal characterization of the active layer at the Limnopolar Lake CALM-S site on byers peninsula (Livingston Island), Antarctica. *Solid Earth*. 2014;5(2):721-739.
21. Oliva M, Hrbáček F, Ruiz-Fernandéz J, et al. Active layer dynamics in three topographically distinct lake catchments in byers peninsula (Livingston Island, Antarctica). *Catena*. 2017;149(2):548-559.
22. Riseborough D, Shiklomanov N, Etzelmüller B, Gruber S, Marchenko S. Recent advances in permafrost modelling. *Permafr Periglac Process*. 2008;19:137-156.
23. Bonnaventure PP, Lamoreaux SF. The active layer: a conceptual review of monitoring, modelling techniques and changes in a warming climate. *Prog Phys Geog*. 2013;37(3):352-376.
24. Weismüller J, Wollschläger U, Boike J, Pan X, Yu Q, Roth K. Modeling the thermal dynamics of the active layer at two contrasting permafrost

sites on Svalbard and on the Tibetan plateau. *The Cryosphere*. 2011;5(3):741-757.

25. Jafarov EE, Marchenko SS, Romanovsky VE. Numerical modeling of permafrost dynamics in Alaska using a high spatial resolution dataset. *The Cryosphere*. 2012;6(3):613-624.
26. Westermann S, Langer M, Boike J, et al. Simulating the thermal regime and thaw processes of ice-rich permafrost ground with the land-surface model CryoGrid 3. *Geosci Model Dev*. 2016;9(2):523-546. https://doi.org/10.5194/gmd-9-523-20162
27. Stefan J. Über die Theorie der Eisbildung, insbesondere über die Eisbildung im Polarmee. *Ann Phys*. 1891;278(2):269-286. https://doi.org/10.1002/andp.18912780206
28. Kudryavtsev VA, Garagulya LS, Kondrat'yeva KA, Melamed VG. *Fundamentals of frost forecasting in geological engineering investigations. Draft Translation 606*. U.S. Army Cold Regions Research and Engineering Laboratory: Hanover, NH; 1977.
29. Shiklomanov NI, Nelson F. Active Layer Processes. In: Elias SA, ed. *Encyclopedia of Quaternary Science*. Vol.3 Oxford, UK: Elsevier; 2007:138-2147.
30. Romanovsky VE, Osterkamp TE. Thawing of the active layer on the coastal plain of the Alaskan Arctic. *Permafr Periglac Process*. 1997;8(1):1-22.
31. Kurylyk BL. Discussion of 'a simple thaw-freeze algorithm for a multi-layered soil using the Stefan equation' by Xie and Gough (2013). *Permafr Periglac Process*. 2015;26(2):200-206.
32. Klene A, Nelson FE, Shiklomanov NI, Hinkel KM. The N-factor in natural landscapes: variability of air and soil-surface temperatures, Kuparuk River basin, Alaska, USA. *Arct Antarct Alp Res*. 2001;33(2):140-148.
33. Sazonova TS, Romanovsky VE. A model for regional-scale estimation of temporal and spatial variability of active layer thickness and mean annual ground temperatures. *Permafr Periglac Process*. 2003;14(2):125-139.
34. Heggem ESF, Etzelmüller B, Anarmaa S, Sharkhuu N, Goulden CE, Nandinsetseg B. Spatial distribution of ground surface temperatures and active layer depths in the Hövsgöl area, northern Mongolia. *Permafr Periglac Process*. 2006;17(4):357-369.
35. Shiklomanov NI, Anisimov OA, Zhang T, Marchenko S, Nelson FE, Oelke C. Comparison of model-produced active layer fields: results for northern Alaska. *J Geophys Res: Earth Surface*. 2007;112. https://doi.org/10.1029/2006JF000571
36. Smith SL, Wolfe SA, Riseborough DW, Nixon FM. Active-layer characteristics and summer climate indices, Mackenzie Valley, Northwest Territories, Canada. *Permafr Periglac Process*. 2009;20(2):201-220.
37. Peng X, Zhang T, Frauenfeld OW, et al. Response of seasonal soil freeze depth to climate change across China. *The Cryosphere*. 2017;11(3):1059-1073.
38. Wilhelm KR, Bockheim JG, Kung S. Active layer thickness prediction on the Western Antarctic peninsula. *Permafr Periglac Proces*. 2015;26(2):188-199.
39. Wilhelm KR, Bockheim JG. Influence of soil properties on active layer thermal propagation along the western Antarctic peninsula. *Earth Surf Process Landf*. 2016;41(11):1550-1563.
40. Davies BJ, Glasser NF, Carrivick JL, Hambrey MJ, Smellie JL, Nývlt D. Landscape evolution and ice-sheet behaviour in a semi-arid polar environment: James Ross Island, NE Antarctic Peninsula. In: Hambrey MJ, Barker PF, Barrett PJ, et al., eds. *Antarctic Palaeoenvironments and Earth-Surface Processes*. Vol.381 London, UK: Geological Society, Special Publications; 2013:353-395.
41. Nývlt D, Braucher R, Engel Z, Mlčoch B. ASTER team. Timing of the northern Prince Gustav ice stream retreat and the deglaciation of northern James Ross island, Antarctic peninsula during the last glacial–interglacial transition. *Quatern Res*. 2014;82(2):441-449.
42. Hrbáček F, Kňažková M, Nývlt D, Láska K, Mueller CW, Ondruch J. Active layer monitoring at CALM-S site near J.G.Mendel Station, James Ross Island, Eastern Antarctic Peninsula. *Sci Total Environ*. 2017;601–602:987-997.
43. Mlčoch B, Nývlt D, Mixa P, et al. *Geological map of James Ross Island – Northern part 1: 25,000*. Praha, Czech Republic: Czech Geological Survey; 2019.
44. Martin PJ, Peel DA. The spatial distribution of 10 m temperatures in the Antarctic peninsula. *J Glaciol*. 1978;20(83):311-317.
45. Van Lipzig NPM, King JC, Lachlan-Cope TA, van der Broeke MR. Precipitation, sublimation and snow drift in the Antarctic peninsula region from a regional atmospheric model. *J Geophys Res*. 2004;109(D24):D24106.
46. Nývlt D, Nývltová FM, Barták M, et al. Death age, seasonality, taphonomy and colonization of seal carcasses from ulu peninsula, James Ross island, Antarctic Peninsula. *Antarct Sci*. 2016;28(1):3-16.
47. Kňažková M, Hrbáček F, Nývlt D, Kavan J. Effect of hyaloclastite breccia boulders on meso-scale periglacial-aeolian landsystem in semi-arid Antarctic environment, James Ross Island, Antarctic Peninsula. Cuadernos de Investigacion Geografica. 2019; online first. https://doi.org/10.18172/cig.3800
48. Fukuda M, Shimokawa K, Takahashi N, Sone T. Permafrost in Seymour Island and James Ross island, Antarctic peninsula region. *Geogr Rev Jpn Ser a*. 1992;65(2):124-131.
49. Borzotta E, Trombotto D. Correlation between frozen ground thickness measured in Antarctica and permafrost thickness estimated on the basis of the heat flow obtained from magnetotelluric soundings. *Cold Reg Sci Technol*. 2004;40(1-2):81-96.
50. Hrbáček F, Nývlt D, Láska K, Kňažková M, Kampová B, Engel Z, Oliva M, Müller CW. Permafrost and active layer research on James Ross Island: An overview. *Czech Polar Reports*. 2019;9(1):20-36.
51. Olivero E, Scasso RA, Rinaldi CA. Revision of the Marambio Group, James Ross Island, Antarctica. Instituto Antártico Argentino, Contribución. 1986;331:28.
52. Mann HB. Non-parametric tests against trend. *Econometrica*. 1945;13:163-171.
53. Kendal MG. *Rank Correlation Methods*. 4th ed. London, UK: Charles Griffin; 1975 XX pp.
54. Sen PK. Estimates of the regression coefficient based on Kendall's tau. *J Am Stat Assoc*. 1968;63(324):1379-1389.
55. Lunardini VJ. Theory of N-factors and correlation of data. In: *Proceedings of the Third International Conference on Permafrost*. Vol.1 National Council of Canada: Ottawa; 1978:40-46.
56. Kurylyk BL, Hayashi M. Improved Stefan equation correction factors to accommodate sensible heat storage during soil freezing or thawing. *Permafr Periglac Process*. 2016;27(2):189-203.
57. Lunardini VJ. *Heat transfer in cold climate*. New York: Van Nostrand Reinhold; 1981.
58. Kurylyk BL, McKenzie JM, MacQuarrie KTB, Voss CI. Analytical solutions for benchmarking cold regions subsurface water flow and energy transport models: one-dimensional soil thaw with conduction and advection. *Adv Water Resour*. 2014;70:172-184.
59. Streletskiy DA, Shiklomanov NI, Nelson FE. Spatial variability of permafrost active-layer thickness under contemporary and projected climate in northern Alaska. *Polar Geogr*. 2012;35(2):95-116.

60. Yin G, Niu F, Lin Z, Luo J, Liu M. Performance comparison of permafrost models in Wudaoliang Basin, Qinghai-Tibet plateau, China. *J Mt Sci*. 2016;13(7):1162-1173.
61. Zorigt M, Kwadijk J, Van Beek E, Kenner S. Estimating thawing depths and mean annual ground temperatures in the Khuvsgul region of Mongolia. *Environ Earth Sci*. 2016;75(10):897.
62. Pang Q, Zhao L, Li S, Ding Y. Active layer thickness variations on the Qinghai–Tibet plateau under the scenarios of climate change. *Environ Earth Sci*. 2012;66(3):849-857.
63. Garagulya LS. *Application of Mathematical Methods and Computers in Investigations of Geocryological Processes*. Moscow, Russia: Moscow University Press; 1990.
64. Romanovsky VE, Osterkamp TE. Interannual variations of the thermal regime of the active layer and near-surface permafrost in northern Alaska. *Permafr Periglac Process*. 1995;6(4):313-335.
65. Smith MW, Riseborough DW. Permafrost monitoring and detection of climate change. *Permafr Periglac Process*. 1996;7(4):301-309.
66. Smith S, Riseborough D. Climate and the limits of permafrost: a zonal analysis. *Permafr Periglac Process*. 2002;13(1):1-15.
67. Farouki OT. Thermal Properties of Soils. U.S. Army Cold Regions Research and Engineering Laboratory Monograph. 1981: 81–1.
68. King JC, Comiso JC. The spatial coherence of interannual temperature variations in the Antarctic peninsula. *Geophys Res Lett*. 2003;30(2):1040.
69. Cook AJ, Vaughan DG. Overview of areal changes of the ice shelves on the Antarctic peninsula over the past 50 years. *The Cryosphere*. 2010;4(1):77-98.
70. Hrbáček F, Oliva M, Láska K, et al. Active layer thermal regime in two climatically contrasted sites of the Antarctic peninsula region. *Cuadernos de Investigacion Geografica*. 2016;42(2):457-474.
71. Comiso JC. Variability and trends in Antarctic surface temperatures from in situ and satellite infrared measurements. *J Climate*. 1999;13:1674-1696.
72. Kennedy AD. Water as a limiting factor in the Antarctic terrestrial environment: a biogeographical synthesis. *Arct Antarct Alp Res*. 1993;25(4):308-315.
73. Smith S, Romanovsky V, Lewkowicz A, et al. Thermal state of permafrost in North America: a contribution to the in-ternational polar year. *Permafr Periglac Process*. 2010;21(2):117-135.
74. Wu Q, Zhang T. Recent permafrost warming on the Qinghai-Tibetan Plateau. *J Geophys Res: Atmos*. 2008;113:D13. https://doi.org/10.1029/2007JD009539
75. Guglielmin M, Cannone N. A permafrost warming in a cooling Antarctica? *Clim Change*. 2012;111(2):177-195. https://doi.org/10.1007/s10584-011-0137-2
76. Arazny A, Kejna M, Sobota I. Ground temperature at the Henryk Arctowski station (King George Island, Antarctic) – case study from the period January 2012 to February 2013. *Bull Geogr Phys Geogr Ser*. 2013;6(1):59-80.
77. French H. *The periglacial environment* (p. 458). 3rd ed. England: John Wiley & Sons Ltd.; 2007.
78. Láska K, Budík L, Budíková M, Prošek P. Method of estimating solar UV radiation in high-latitude location based on satellite ozone retrieval with an improved algorithm. *Int J Remote Sens*. 2011;32(11):3165-3177.
79. Banon M, Justel A, Velazquez D, Queasada A. Regional weather survey on byers peninsula, Livingston Island, South Shetland Islands, Antarctica. *Antarct Sci*. 2013;25(2):146-156.
80. Cannone N, Guglielmin M. Influence of vegetation on the ground thermal regime in continental Antarctica. *Geoderma*. 2009;151(3-4):215-223.
81. Mergelov NS. Soils of wet valleys in the Larsemann Hills and Vestfold Hills oases (Princess Elizabeth land, East Antarctica). *Eurasian Soil Sci*. 2014;47(9):845-862.
82. Bockheim JG. *The soils of Antarctica*. Cham, Switzerland: Springer International; 2015:332.
83. Adlam LS, Balks MR, Seybold CA, Campbell DI. Temporal and spatial variation in active layer depth in the McMurdo Sound region, Antarctica. *Antarct Sci*. 2010;22(1):45-52.
84. Kotzé C, Meiklejohn I. Temporal variability of ground thermal regimes on the northern buttress of the Vesleskarvet nunatak, western Dronning Maud land, Antarctica. *Antarct Sci*. 2016;29(1):73-81.
85. Schaefer CEGR, Michel RFM, Delpupo C, Senra CO, Bremer UF, Bockheim JG. Active layer thermal monitoring of a Dry Valley of the Ellsworth Mountains, Continental Antarctica. *Antarctica Catena*. 2017;149(2):603-615.
86. De Pablo MA, Ramos M, Molina A, Prieto M. Thaw depth spatial and temporal variability at the Limnopolar Lake CALM-S site, byers peninsula, Livingston Island, Antarctica. *Sci Total Environ*. 2018;615:814-827.
87. Nelson FE, Shiklomanov NI, Mueller GR, Hinkel KM, Walker DA, Bockheim JG. Estimating active-layer thickness over a large region: Kuparuk river basin, Alaska, USA. *Arctc Antarc Alp Res*. 1997;29(4):367-378.
88. Shiklomanov NI, Nelson FE. Analytic representation of the active layer thickness field, Kuparuk River basin, Alaska. *Ecol Modell*. 1999;123(2-3):105-125.
89. Shiklomanov NI, Nelson FE. Active-layer mapping at regional scales: a 13-year spatial time series for the Kuparuk region, north-Central Alaska. *Permafr Periglac Process*. 2002;13(3):219-230.
90. Uxa T. Discussion on, 'active layer thickness prediction on the Western Antarctic peninsula' by Wilhelm et al. 2015. *Permafr Periglac Process*. 2016;28:493-498.
91. Riseborough DW. The effect of transient conditions on an equilibrium permafrost-climate model. *Permafr Periglac Process*. 2007;18(1):21-32.
92. Aldrich HP, Paynter HM. *Analytical Studies of Freezing and Thawing of Soils*. U.S. Army Arctic Construction and Frost Effects Laboratory: Boston, MA; 1953.
93. McRoberts EC. Field observations of thawing in soils. *Can Geotech J*. 1975;12(1):126-130. https://doi.org/10.1139/t75-011
94. Zhang Y, Carey SK, Quinton WL. Evaluation of the algorithms and parameterizations for ground thawing and freezing simulation in permafrost regions. *J Geophys Res*. 2008;113(D17):D17116. https://doi.org/10.1029/2007JD009343
95. Hayashi M, Goeller N, Quinton WL, Wright N. A simple heat-conduction method for simulating the frost-table depth in hydrological models. *Hydrol Process*. 2007;21(19):2610-2622. https://doi.org/10.1002/hyp.6792
96. Hrbáček F, Láska K, Engel Z. Effect of snow cover on the active-layer thermal regime – a case study from James Ross island, Antarctic Peninsula. *Permafr Periglac Process*. 2016;27(3):307-315.
97. Abu-Hamdeh NH, Reeder R. Soil thermal conductivity: effects of density, moisture, salt concentration, and organic matter. *Soil Sci Soc Am J*. 2000;64(4):1285-1290.

How to cite this article: Hrbáček F, Uxa T. The evolution of a near-surface ground thermal regime and modeled active-layer thickness on James Ross island, eastern Antarctic peninsula, in 2006–2016. *Permafrost and Periglac Process*. 2020;31:141-155. https://doi.org/10.1002/ppp.2018